

Scientifica
2020

MARIA DI ROSA

**Tectono-metamorphic
evolution of the
continental units along
the edge between Alpine
and Hercynian Corsica**

Constraints for the exhumation
models in the continental collision
setting

PREMIO TESI DOTTORATO
FIRENZE UNIVERSITY PRESS – UNIVERSITÀ DEGLI STUDI DI FIRENZE



Scientifica
2020

MARIA DI ROSA

**Tectono-metamorphic
evolution of the
continental units along
the edge between Alpine
and Hercynian Corsica**

Constraints for the exhumation
models in the continental collision
setting

P R E M I O T E S I D O T T O R A T O
F I R E N Z E U N I V E R S I T Y P R E S S — U N I V E R S I T À D E G L I S T U D I D I F I R E N Z E



PREMIO TESI DI DOTTORATO

ISSN 2612-8039 (PRINT) | ISSN 2612-8020 (ONLINE)

PREMIO TESI DI DOTTORATO
Commissione giudicatrice, anno 2020

Vincenzo Varano, *Presidente della commissione*

Aldo Bompani, *Area Scienze Sociali*

Mario Caciagli, *Area Scienze Sociali*

Franco Cambi, *Area Umanistica*

Giancarlo Garfagnini, *Area Umanistica*

Roberto Genesio, *Area Tecnologica*

Flavio Moroni, *Area Biomedica*

Adolfo Pazzagli, *Area Biomedica*

Giuliano Pinto, *Area Umanistica*

Vincenzo Schettino, *Area Scientifica*

Maria Chiara Torricelli, *Area Tecnologica*

Luca Uzielli, *Area Tecnologica*

Graziella Vescovini, *Area Umanistica*

Maria Di Rosa

Tectono-metamorphic evolution of the
continental units along the edge between
Alpine and Hercynian Corsica

Constraints for the exhumation models
in the continental collision setting

FIRENZE UNIVERSITY PRESS

2021

Tectono-metamorphic evolution of the continental units along the edge between Alpine and Hercynian Corsica : constraints for the exhumation models in the continental collision setting / Maria Di Rosa. – Firenze : Firenze University Press, 2021.
(Premio Tesi di Dottorato; 92)

<https://www.fupress.com/isbn/9788855184205>

ISSN 2612-8039 (print)
ISSN 2612-8020 (online)
ISBN 978-88-5518-419-9 (Print)
ISBN 978-88-5518-420-5 (PDF)
ISBN 978-88-5518-421-2 (XML)
DOI 10.36253/978-88-5518-420-5


Front cover: Microphotograph related to the deformation within the Metabreccia Fm. (Piedigriggio-Prato Unit, Lower Unit, Alpine Corsica).

FUP Best Practice in Scholarly Publishing (DOI https://doi.org/10.36253/fup_best_practice)

All publications are submitted to an external refereeing process under the responsibility of the FUP Editorial Board and the Scientific Boards of the series. The works published are evaluated and approved by the Editorial Board of the publishing house, and must be compliant with the Peer review policy, the Open Access, Copyright and Licensing policy and the Publication Ethics and Complaint policy.

Firenze University Press Editorial Board

M. Garzaniti (Editor-in-Chief), M.E. Alberti, F. Vittorio Arrigoni, E. Castellani, F. Ciampi, D. D'Andrea, A. Dolfi, R. Ferrise, A. Lambertini, R. Lanfredini, D. Lippi, G. Mari, A. Mariani, P.M. Mariano, S. Marinai, R. Minuti, P. Nanni, A. Orlandi, I. Palchetti, A. Perulli, G. Pratesi, S. Scaramuzzi, I. Stolzi.

 The online digital edition is published in Open Access on www.fupress.com.

Content license: except where otherwise noted, the present work is released under Creative Commons Attribution 4.0 International license (CC BY 4.0: <http://creativecommons.org/licenses/by/4.0/legalcode>). This license allows you to share any part of the work by any means and format, modify it for any purpose, including commercial, as long as appropriate credit is given to the author, any changes made to the work are indicated and a URL link is provided to the license.

Metadata license: all the metadata are released under the Public Domain Dedication license (CC0 1.0 Universal: <https://creativecommons.org/publicdomain/zero/1.0/legalcode>).

© 2021 Author(s)

Published by Firenze University Press
Firenze University Press
Università degli Studi di Firenze
via Cittadella, 7, 50144 Firenze, Italy
www.fupress.com

*This book is printed on acid-free paper
Printed in Italy*

Table of contents

SECTION 1. INTRODUCTION

Chapter 1.1 The continental crust's involvement in the orogenic processes	9
Chapter 1.2 Studying the Alpine Orogeny in Corsica	10
Chapter 1.3 Thesis outline	12

SECTION 2. THE CORSICA ISLAND AND THE WESTERN MEDITERRANEAN SEA

Chapter 2.1 The Corsica Island within the Alpine Orogeny setting	15
Chapter 2.2 The syn- to post-orogenic extension in the western Mediterranean Sea	20

SECTION 3. THE ARCHITECTURE OF THE EUROPEAN MARGIN AND THE PIEDMONT-LIGURIA OCEAN IN CORSICA

Chapter 3.1 Lithostratigraphic framework	23
3.1.1 The Hercynian Corsica	23
3.1.2 The Lower Units: the European-derived metamorphic units of the Alpine Corsica	25
3.1.3 Other groups of units of the Alpine Corsica: from the ocean-continent transition to the Piemont-Liguria Ocean	27
Chapter 3.2 The state of art	29
3.2.1 Overview of the tectono-metamorphic data	29
3.2.2 Geochronological constraints	30

FUP Best Practice in Scholarly Publishing (DOI 10.36253/fup_best_practice)

Maria Di Rosa, *Tectono-metamorphic evolution of the continental units along the edge between Alpine and Hercynian Corsica. Constraints for the exhumation models in the continental collision setting*, © 2021 Author(s), content CC BY 4.0 International, metadata CC0 1.0 Universal, published by Firenze University Press (www.fupress.com), ISSN 2705-0297 (online), ISBN 978-88-5518-420-5 (PDF), DOI 10.36253/978-88-5518-420-5

SECTION 4. GEOLOGICAL OVERVIEW OF THE STUDY AREAS

Chapter 4.1 Cima Pedani area	35
Chapter 4.2 Corte area	40
Chapter 4.3 Venaco area	46
Chapter 4.4 Noceta and Ghisoni areas	49

SECTION 5. THE ALPINE OROGENY IN CORSICA: INSIGHTS FROM THE LOWER UNITS, THE HERCYNIAN CORSICA AND THE SCHISTES LUSTRÉS COMPLEX

Chapter 5.1 Pre-subduction deformation of the lower plate: middle to late Eocene forebulge's formation	51
Chapter 5.2 The Lower Units deformation history: from map- to microscale	54
5.2.1 Cima Pedani	56
5.2.2 Corte	62
5.2.3 Venaco	74
5.2.4 Noceta and Ghisoni	76
Chapter 5.3 The metamorphic history of the Lower Units: evidence from the Permo-Carboniferous metagranitoids and the metagabbros and from the Permian and Tertiary metapelites	80
5.3.1 Cima Pedani	81
5.3.2 Corte	85
5.3.3 Noceta and Ghisoni	92
Chapter 5.4 The Alpine ductile deformation and the metamorphic imprint in the foreland: insights from Asco-Castirla, Razzo Bianco and Noceta-Ghisoni shear zones	93
5.4.1 Asco-Castirla shear zones	93
5.4.2 Razzo Bianco shear zones	97
5.4.3 Noceta-Ghisoni shear zones	100
Chapter 5.5 Tectono-metamorphic history of the tectonic slices belonging to the Schistes Lustrés Complex associated to the studied Lower Units	104
5.5.1 Cima Pedani and LEU	105
5.5.2 Corte and IZU	105
5.5.3 Noceta-Ghisoni and IZU	109
Chapter 5.6 The post-D3 deformation	109

SECTION 6. AGE CONSTRAINTS: MAGMATIC AGES AND THE PERMO-
TRIASSIC HEATING EPISODE

Chapter 6.1 Petrographic features of the metagranitoids and the epidote-bearing metagabbros	115
Chapter 6.2 U-Pb geochronology on zircons	117
6.2.1 Zircon texture	117
6.2.2 The magmatic ages of metagranitoids and metagabbros: petrological implications on the batholith's intrusion	120
Chapter 6.3 U-Pb geochronology on allanites	122
6.3.1 Allanite texture	122
6.3.2 Zircons vs. allanite ages: pre-Alpine rifting	124

SECTION 7. GEODYNAMIC IMPLICATIONS

	127
Chapter 7.1 Middle to late Eocene history of the European margin: insights from the stratigraphy	128
Chapter 7.2 Tectono-metamorphic history of the Lower Units, the Alpine shear zones of the Hercynian Corsica and of the associated tectonic slices belonging to the Schistes Lustrés Complex	131
7.2.1 Exhumation during compression: the D1 and D2 phases of the Lower Units	131
7.2.2 Syn-convergence deformation of the Hercynian Corsica	137
7.2.3 The post-D2 coupling with the Schistes Lustrés Complex	139
7.2.4 The D3 phase: extrusion vs. backthrusting	143
Chapter 7.3 The post-D3 phase: further exhumation during transtension?	144
Chapter 7.4 From data to model: extrusion tectonics	147
7.4.1 The perturbation of the geothermal field as consequence of the involvement of cold lithosphere into the subduction zone	147
7.4.2 From subduction to the wedge: toward a new geothermic equilibrium	149
7.4.3 Extrusion vs. erosion	151

SECTION 8. CONCLUSIONS

	157
--	-----

SECTION 9. SUPPLEMENTARY MATERIALS

Chapter 9.1 Thermobarometry on metapelites	161
9.1.1 Chlorite	163
9.1.2 Phengite	164
Chapter 9.2 P estimates based on sodic amphibole	170
Chapter 9.3 Calcite twins	174
Chapter 9.4 LA.ICP.MS dating	175
9.4.1 U-Pb zircon dating on separates	175
9.4.2 U-Pb allanite in-situ dating	180
References	185

Chapter 1

Introduction

1.1 The continental crust's involvement in the orogenic processes

The reconstruction of the collisional belt history includes the study of different steps of the convergence between two tectonic plates. After the subduction of the oceanic lithosphere, the progressive underthrusting of the passive margin beneath the wedge occurs simultaneously with the evolution of the foreland basins. Foreland basins represent a first-order tectonic element in the framework of collisional belts (e.g., Allen et al. 1986). They originate during the first stage of the collision when a passive margin collides with an active continental margin after the closure of an oceanic basin by subduction/obduction processes. The foreland basins continue to develop in front of the advancing wedge also during the mature stage of the collision and progressively become incorporated within it (e.g. Beaumont 1981).

Regarding the underthrusting of continental crust, several modeling studies have shown the various conditions that can make continental crust prone to subduction (Cloos 1982; Chemenda et al. 1995; 1996; Ernst 2001; Burov et al. 2014), and several evidences from exhumed orogens show that continental crust can be underthrust down to depths > 50 km so that they deform under eclogite facies, giving rise to high-pressure and ultra high-pressure (HP and UHP, respectively) units (Chopin 1984; Dewey et al. 1993; Chemenda et al. 1996; Compagnoni and Rolfo 2003; Ernst 2001; 2005; Guillot et al. 2009; Lanari et al. 2012). The exhumation of HP and UHP rocks is a transient process occurring during continental subduction and continental collision (Ernst 2001; Agard et al. 2009; Strzeczynski et al. 2012; Schmalholz et al. 2014). As for HP oceanic units, the vertical movement of continental slices from depth up to the surface is far to

be clearly understood, and different mechanisms have been proposed for the exhumation of HP and UHP units in orogenic belts, including the “classic”, but worthy to note models such as channel flow (Cloos, 1982), corner flow (Platt 1986), extensional collapse (Dewey et al. 1993), thrusting onto the foreland (Steck et al., 1998), buoyancy through erosion and tectonic processes (Chemenda et al. 1995), ductile extrusion (Chemenda et al. 1996; Gerya et al. 2002, 2008), compression of a soft zone between two rigid blocks (Thompson et al. 1997), serpentinite channel (Guillot et al. 2001), and coaxial extension associated with a decoupling fault (Jolivet et al. 2003). The development of different tectonic regimes during continental subduction depends on factors such as the pull force, the plate convergent rate and the geothermic gradient, that can change dramatically when continental crust enters the subduction zone and, progressively, during the proceeding of continental subduction. Consequently, the style of deformation, the metamorphic conditions and the exhumation mechanisms of HP continental rocks can change with time even in a single margin. The diverse possible mechanisms of exhumation developed through different thermomechanical processes testify the critical role of deciphering the kinematic evolution and dating the metamorphic history of HP continental units in orogenic belts (e.g. Guillot et al. 2009).

In this framework, the interaction of the subducting continental crust with the oceanic units already accreted to the wedge must be take into account. Although the underthrusting and the subsequent underplating of the oceanic lithosphere predates the continental subduction, a common exhumation path of the continental and oceanic units from the shallow depths to the surface could not be excluded.

1.2 Studying the Alpine Orogeny in Corsica

The Alps are a collisional belt where the foreland basin and the paired thrust wedge migrated for ~150–200 km in an approximately stable manner over the lower continental plate, leading to an inversion of a foreland basin, and its deformation by out-of-sequence thrusts (Sinclair 1997). This picture can be extended also to the Corsica island, where the southern continuation of the Alpine collisional belt has been recognized since long time (e.g. Mattauer et al. 1981).

From the geological point of view, the Corsica Island is divided into two domains, known as Hercynian and Alpine Corsica (e.g. Durand-Delga 1984), which extend in the south–west and north–east areas, respectively. The tectonic boundary between these two domains runs across the island with NNW–SSE strike along which the tectonic units of Alpine Corsica are thrust onto Hercynian Corsica. Hercynian Corsica is representative of a continental domain of the European plate whose eastern border played the role of the foreland domain during the continental collision. It consists of metamorphic basement with

Panafrican and Variscan metamorphic imprint and intruded by magmatic rocks of Permo–Carboniferous age (Ménot 1990; Laporte et al. 1991; Paquette et al., 2003; Rossi et al. 2009). This basement is covered along its eastern border by Mesozoic carbonates unconformably topped by siliciclastic turbidites of Tertiary age. In contrast, the Alpine Corsica consists of a complex stack of continental and oceanic units of a variable degree of metamorphism from very low-grade to blueschist-eclogite facies (e.g. Mattauer et al. 1981; Durand-Delga 1984). As in the Western Alps, the units with continental affinity are overthrust by oceanic and transitional units, referred to as the Schistes Lustrés Complex (Gibbons et al. 1986; Caron 1994; Levi et al. 2007; Vitale Brovarone et al. 2012).

The continental units (i.e. the Lower Units) crop out along a north-south trending strip at the western border of the Alpine Corsica, and are regarded as fragments of the thinned European margin (Durand-Delga 1984; Caron 1994; Malasoma et al. 2006; Molli et al. 2006; Di Rosa et al. 2017a) that underwent Early Tertiary continental subduction, and subsequent syn-convergent exhumation, as a result of the closure of western Tethys (Amaudric Du Chaffaut and Saliot 1979; Bezert and Caby 1988; Caron 1994; Tribuzio and Giacomini 2002; Malasoma and Marroni 2007; Molli 2008).

However, differently from Western and Central Alps where the continental collision tectonics is still active in the Quaternary, the advance of the Alpine wedge in Corsica is frozen at the Oligocene-Miocene boundary (Rehault et al. 1984; Jolivet et al. 1990; Fournier et al. 1991; Brunet et al. 2000), when the opening of the Liguro-Provençal and the Tyrrhenian Basins isolated the Alpine Corsica from the neighboring domains of the Alpine collisional belt with consequent stop of the collisional shortening (Doglioni et al. 1998; Mauffret et al. 1999; Fellin et al. 2005).

In a general view, the Hercynian Corsica is regarded as a single area unaffected by deformation and metamorphism during the Alpine tectonics, thus representing a foreland domain never underthrust by the orogenic wedge (Durand-Delga 1984), whereas the Alpine Corsica is considered the rest of the convergence between Europe and Africa, formed between the Late Cretaceous and the Miocene time lapse. In this framework, the exhumation of the Lower Units led the authors to apply the models proposed for the Alps to the Corsica Island. First, the local/lithospheric-scale extension in a thrust wedge setting (Platt 1986; England and Houseman 1989) has been proposed (Jolivet et al. 1990; 1991; Fournier et al. 1991; Daniel et al. 1996). Subsequently, the “nappe intrusion mechanism” of Escher and Beaumont (1997) was adopted by Malavieille et al. (1998). In this model, the continental crust involved in the subduction zone were detached from the downgoing slab because of the buoyancy forces and shearing. These supra-crustal rocks, lighter than the surrounding mantle, went up while the denser lower crust continued to be subducted. The syn-subduction rise of slices of upper crust leads the rapid exhumation of HP/LT rocks and the development of normal faulting zone along the upper surface of the rising body.

Deepening the study of some transects between the Hercynian and the Alpine

Corsica, several problems to the general model arise. The presence of Alpine deformation and metamorphism which locally affects the Hercynian Corsica has been observed. As regards the Alpine Corsica, the simultaneous exhumation of oceanic and continental units from shallow depths to the surface has been verified. Although local studies on the deformation of the Hercynian Corsica occur (e.g. Amaudric du Chaffaut 1980), its interpretation in the geodynamic evolution of the Alps is missing, as well as a comparison between the tectono-metamorphic history of the continental and oceanic units, so far studied separately (e.g. Malasoma and Marroni 2007; Vitale Brovarone et al. 2012).

1.3 Thesis outline

At the state of art, the study of the orogenic processes consists in connecting a wide range of data in order to constrain the behavior of the continental crust during the different stages of convergence. This thesis is aimed to reconstruct the Alpine cycle evolution of the European margin located in Corsica, focusing on (1) the effects of the orogeny on the foreland, (2) the behaviour of the portion of the continental margin involved in subduction and (3) the complex exhumation of the continental units that followed independent paths until the late stage, when the coupling with the oceanic units occur. The work is subdivided into two stages that describe the pre-collision setting, i.e. the stratigraphic features of the continental units, and the orogeny itself, i.e. the Middle to Late Eocene deposition of the forebulge deposits, the Late Eocene subduction and syn-convergent exhumation of part of the European-derived units, the simultaneous localization of deformation within the European margin and the Early Oligocene switching from compression to (transpression)/extension.

The study area is located in the western side of the Alpine Corsica between Asco and Fium'Orbo Valleys, and roughly covers the rim between the Hercynian and Alpine Corsica. Within this wide area, which has an extension of about 1200 km², six sites have been studied in detail (Asco, Cima Pedani, Corte, Venaco, Noceta and Ghisoni), in order to characterize the lithostratigraphy, the deformation mechanisms and the tectono-metamorphic history of the rocks belonging to the Hercynian and Alpine Corsica. Particular attention was paid to the Lower Units, that represent the portion of the European plate involved in the processes of subduction and exhumation during the Alpine Orogeny. The stratigraphic relations of the Lower Units with the foreland (i.e. the Hercynian Corsica), as well as the comparison of the tectono-metamorphic data of the Lower Units with those related to other units belonging to the Alpine Corsica (i.e. Schistes Lustrés Complex) are also discussed.

The results of a detailed map- to microstructural analysis and tectono-metamorphic studies conducted on the Lower Units and on the Schistes Lustrés Complex and the Hercynian Corsica in proximity of the Lower Units are

collected for this thesis. The field activity is summarized in the structural maps and integrated with estimation of the P-T conditions associated to the Lower Units deformation, of the age of the emplacement of magmatic rock and the age of the rifting, obtained through different laboratory techniques (all the methods are described in the supplementary materials).

Chapter 2

The Corsica Island and the western Mediterranean Sea

2.1 The Corsica Island within the Alpine Orogeny setting

From the geological point of view, the Corsica Island is divided into two domains known as Hercynian and Alpine Corsica that are cropping out in the south-west and north-east areas, respectively (Fig 1). The tectonic boundary between these two domains runs across the Corsica Island with NNW-SSE strike along which the tectonic units of the Alpine Corsica are thrust onto the Hercynian domain (e.g. Durand Delga 1984). The Hercynian Corsica is representative of a continental crust of the European plate; it consists of metamorphic rocks with Panafrican and Variscan deformation imprints that are intruded by magmatic rocks of Permo-Carboniferous age (Cabanis et al. 1990; Ménot 1990; Ménot and Orsini 1990; Laporte et al. 1991; Rossi et al. 1994; Paquette et al. 2003; Rossi et al. 2009). This basement is covered by unmetamorphosed sedimentary successions consisting of Mesozoic sedimentary rocks (mainly carbonates) unconformably covered by siliciclastic turbidites of Tertiary age (Durand-Delga 1984; Rossi et al. 1994; Michard and Martinotti 2002). The Alpine Corsica consists in a tectonic stack made of continental and oceanic units affected by a metamorphism that varies from blueschists-eclogite to prehnite-pumpellyite facies (e.g. Boccaletti et al. 1971; Durand-Delga 1974; 1978; 1984; Mattauer and Proust 1975; 1976; Amaudric du Chaffaut and Saliot 1979; Mattauer et al. 1981; Dallon and Nardi 1984; Gibbons and Horak 1984; Bezert and Caby 1988; Malavieille et al. 1998; Marroni and Pandolfi 2003; Malasoma et al. 2006; Levi et al. 2007; Vitale Brovarone et al. 2012). The present-day architecture of the Corsica Island derives from the different configu-

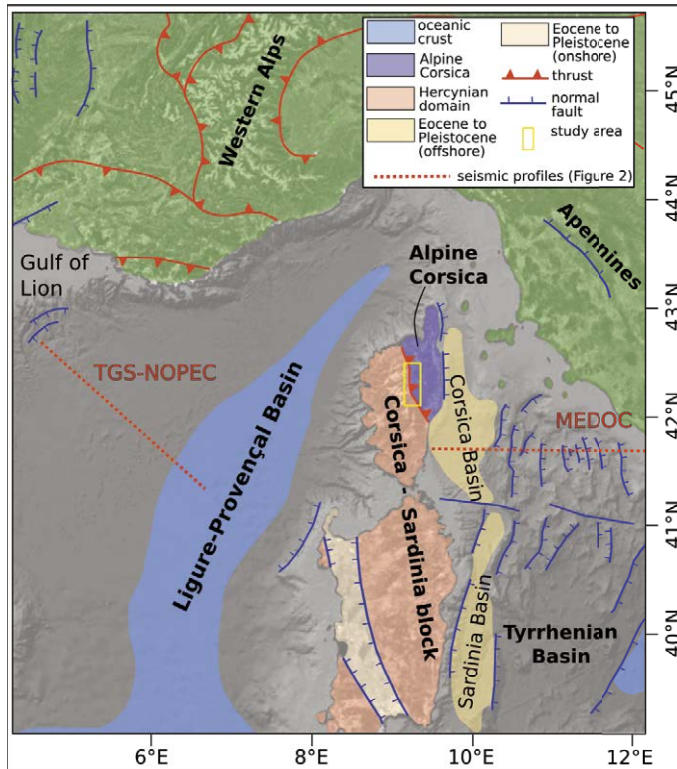
Maria Di Rosa, University of Pisa, Italy, maria.dirosa.scaglia@gmail.com, 0000-0002-1154-7429
FUP Best Practice in Scholarly Publishing (DOI 10.36253/fup_best_practice)

Maria Di Rosa, *Tectono-metamorphic evolution of the continental units along the edge between Alpine and Hercynian Corsica. Constraints for the exhumation models in the continental collision setting*, © 2021 Author(s), content CC BY 4.0 International, metadata CC0 1.0 Universal, published by Firenze University Press (www.fupress.com), ISSN 2705-0297 (online), ISBN 978-88-5518-420-5 (PDF), DOI 10.36253/978-88-5518-420-5

rations produced by the displacements of the Europe and Africa-Adria plates since the opening of the Piemont-Liguria Ocean (i.e. the western Tethys) in the Middle Jurassic (Favre and Stampfli 1992; Manatschal 1995; Froitzheim and Manatschal 1996; Bill et al. 1997; Marroni and Pandolfi 2007). The opening of the Piemont-Liguria Ocean was characterized by Early Jurassic rifting phase dominated by pure shear and by a Middle to Late Jurassic asymmetric extension dominated by simple shear (Marroni et al. 1998; 2001). The asymmetric non-volcanic rifting in the Piemont-Liguria Ocean evolved in spreading in the Bajocian age (Handy et al. 2010). From Middle Cretaceous, convergence affected the Piemont-Liguria Ocean resulting in the intra-oceanic subduction of the Piemont-Liguria Ocean first (Elter and Pertusati 1973; Lagabrielle and Polino 1988; Schmid et al. 1996; Michard et al. 2002; Molli 2008; Handy et al. 2010) and the subduction of continental lithosphere after (Malavieille et al. 1998). Shortly thereafter, the geodynamic scenario dramatically changed: in the post-35 Ma the convergence direction of the Adria-Africa plate turned from NW-SE to WNW-ESE (Handy et al. 2010). The ESE-dipping subduction of European continental margin beneath Adria provoked the WNW-directed thrusting (Schmid and Kissling 2000; Ceriani et al. 2001); toward SW, the not yet subducted Piemont-Liguria Ocean that moved with Adria-Africa plate until that moment, began to subduct to the west beneath Iberia-Europe in the Early Oligocene (Rosenbaum et al. 2002; Faccenna et al. 2004). This change of the subduction polarity, that led the onset of the Adria subduction, marked the onset of the Apenninic Orogeny (R hault et al. 1984; Doglioni 1991; Gueguen et al. 1998). Although the change in the subduction's polarity is accepted by many authors, the formation of the Alpine Corsica with an Apenninic-vergent subduction active since the Late Cretaceous time with the European plate as backstop is supported by others (Principi and Treves 1984; Lahond re 1996; Jolivet et al. 1998; Brunet et al. 2000).

Since the intuition of Argand (1924) and Staub (1924), the Alpine Corsica has been regarded as the prosecution of the Western Alps arc (e.g. Mattauer et al. 1981; Durand-Delga 1984; Marroni and Pandolfi 2003; Faccenna et al. 2004; Molli and Tribuzio 2004; Molli et al. 2006; Molli and Malavieille 2011; Handy et al. 2010; Gueydan et al. 2017), whose history is common until the Early Oligocene turnover. Witnesses of the aforementioned SE-dipping intra-oceanic and continental stages of subduction that provoked the closure of the Piemont-Liguria Ocean before and the subduction of the European continental margin after are verifiable through the tectono-metamorphic history of the Alpine Corsica (Decandia and Elter 1969; Zarki-Jakni et al. 2004). This tectonic stack consists of several units, that are generally divided in three groups according their stratigraphic and structural features (e.g., Durand-Delga 1984; Abbate et al. 1980; Savostin et al. 1986; Stampfli et al. 2004, Di Rosa et al. 2017a; 2018a; 2018b). Since the Late Cretaceous an accretionary wedge consisting of a pile of oceanic units showing deformations associated with high-pressure (HP) metamorphism has been developed (e.g. Mattauer et al. 1977; Caron and Delcey

Figure 1. Tectonic sketch of the Central Mediterranean Sea showing the Corsica Island and its offshore.



1979; Caron et al. 1981; Faure and Malavieille 1981; Lahondère 1983; Harris 1985; Warburton 1986; Waters 1990; Fournier et al. 1991; Jolivet et al. 1991; Caron 1994; Guieu et al. 1994; Lahondère and Guerrot 1997; Malavieille et al. 1998; Tribuzio and Giacomini 2002; Levi et al. 2007; Chopin et al. 2008; Ravna et al. 2010; Vitale Brovarone et al. 2012; 2014; Meresse et al. 2012). With the onset of the subduction of the European plate, occurred not before the Late Eocene, slices of continental crust detached from the downgoing plate were annexed to the wedge (e.g. Gibbons and Horak 1984; Bezert and Caby 1988; Egal 1992; Chemenda et al. 1995; Daniel et al. 1996; Brunet et al. 2000; Tribuzio and Giacomini 2002; Gueydan et al. 2003; Malasoma et al. 2006; Molli et al. 2006; Malasoma and Marroni 2007; Garfagnoli et al. 2009; Molli and Malavieille 2011; Maggi et al. 2012). In the Early Oligocene time, with the change of the subduction polarity that moved the convergent margin E of the island, the compressional tectonics in Corsica was followed by large-scale extension, connected to the W-dipping Apennine subduction (Jolivet et al. 1991; Fournier et al. 1991; Daniel et al. 1996), leading the collapse of the previously thickened orogenic wedge (Fournier et al. 1991; Jolivet et al. 1991; 1998; Daniel

et al. 1996; Brunet et al. 2000; Jakni et al. 1984; Jolivet et al. 1990; Malavieille et al. 1998; Marroni and Pandolfi 2003; Molli 2008). From bottom to the top, these groups are the Lower Units (also known as “Parautochthonous” or “Prépiémontais Units”), the Schistes Lustrés Complex and the Upper Units (also known as “Nappe Supérieure”).

The Lower Units are interpreted as fragments of the thinned European continental margin accreted to the Alpine orogenic wedge in the Tertiary time (Amaudric du Chaffaut 1975; Amaudric du Chaffaut et al. 1976; Amaudric du Chaffaut and Saliot 1979; Bezert and Caby 1988; 1989; Egal and Caron 1988; Egal 1992; Tribuzio and Giacomini 2002; Molli and Tribuzio, 2004; Molli et al. 2006; Malasoma and Marroni 2007; Di Rosa et al. 2017a). These continental-derived tectonic units (i.e. Caporalino Unit, Palasca-Moltifao Unit, Fuata-Pedanu Unit, Castiglione-Popolasca Unit, Croce d’Arbitro Unit, Piedigriggio-Prato Unit, Canavaggia Unit, Pedani Unit, Scoltola Unit, Ghisoni Unit, Annunciata Unit and Tenda Massif) mainly consist of slices of Variscan basement and its Late Carboniferous- Middle Eocene sedimentary covers. Generally, these units are characterized by polyphase deformation associated to Alpine metamorphism ranging from very low-grade to blueschist facies conditions (Bezert and Caby 1988; Molli et al. 2006; Malasoma and Marroni 2007; Moll 2008; Di Rosa et al. 2017a; 2017b; 2018a). The Schistes Lustrés Complex includes oceanic and continental units whose paleogeographic domain correspond to Piedmont-Liguria Ocean and the ocean/continent transition (Caron and Delcey 1979; Mattauer et al. 1981; Faure and Malavieille 1981; Pèguinot and Potdevin 1984; Jolivet et al. 1990; Fournier et al. 1991; Lahondère et al. 1999). They represent a fragment of oceanic and ocean-continent transition lithosphere (Agard et al. 2011; Rosenbaum et al. 2002; Mohn et al. 2009; Vitale Brovarone et al. 2014; Deseta et al. 2014), deformed from the Late Cretaceous and exhumed in the Tertiary (Jolivet 1993). Given the complex stratigraphy and the wide range of metamorphism that characterize the Schistes Lustrés Complex, several classifications have been proposed (e.g. Caron and Delcey 1979; Caron et al. 1979; Padoa 1999; Rossi et al. 2001; Marroni et al. 2004; Levi et al. 2007; Vitale Brovarone et al. 2012; Vitale Brovarone and Hewartz 2013). In this thesis the Schistes Lustrés Complex has been classified on the base of the lithostratigraphy and metamorphism into five groups of units: the Castagniccia Unit, the Morteda-Farinole-Volpajola Unit, the Serra di Pigno, Campitello, Oletta, Morosaglia and Zuccarello Units, the Bagliaccone-Riventosa Unit and the Lento and Inzecca Units. The HP peak metamorphic conditions range from blueschist-eclogite to low-blueschists facies with variable degrees of retrogression under blueschist and greenschist facies conditions (Tab 1, Dal Piaz and Zirpoli 1979; Cohen et al. 1981; Caron et al. 1981; Peguignot et al. 1984; Harris 1985; Gibbons et al. 1986; Warburton 1986; Waters 1990; Jolivet et al. 1991; Fournier et al. 1991; Lahondère 1991; Rossi et al. 1994; Caron 1994; Daniel et al. 1996; Lahondère and Guerrot 1997; Molli et al. 2006; Vitale Brovarone et al. 2012; 2014; Vitale Brovarone and Hewartz 2013). According to the available data, the age of the HP/LT metamorphism ranges from Late

Cretaceous to Late Eocene (Maluski 1977; Lahondere and Guerrot 1997; Brunet et al. 2000; Maggi et al. 2012; Martin et al. 2011; Brovarone and Herwatz 2013). The Upper Units (including Balagne, Nebbio, Macinaggio, Rio Magno, Bas Ostriconi, Serra Debbione and Pineto Units) consist of oceanic and continental units affected by a very low-grade metamorphism (e.g. Mattauer et al. 1981; Dallon and Nardi 1984; Durand-Delga 1984; Waters 1990; Fournier et al. 1991; Dallon and Puccinelli 1995; Daniel et al. 1996; Malavieille et al. 1998; Marroni and Pandolfi 2003; Molli and Malavieille 2011). Lastly, the Santa Lucia Unit is made of a metamorphic basement and Late Cretaceous unmetamorphosed conglomerates (Durand-Delga 1984; Zibra 2006). Given its peculiar stratigraphy and its position in the tectonic stack, it could not be inserted in none of the previous group and thus it will be described separately.

The tectonic stack made of Lower Units, Schistes Lustrés Complex and Upper Units is locally deformed by an important fault system called Central Corsica Shear Zone (CCSZ). The main fault has a sinistral strike-slip kinematics and roughly follow the direction of the boundary between the Alpine and Hercynian Corsica (Lacombe and Jolivet 2005; Di Rosa et al. 2017a; 2017b). To the main fault, sinistral synthetic and dextral antithetic systems are associated that cut and juxtapose the tectonic units of the different groups. The age of the CCSZ activity is poorly constrained: the only reference data for the authors, constrain its activity from Eocene (Maluski et al. 1973) to Early Miocene (Waters 1990). Being Late Eocene the age of the younger formation involved in the subduction (e.g. Di Rosa et al. 2017a), at least the CCSZ activity must necessarily be postponed. However, the CCSZ developed in response to the Late Oligocene - Early Miocene counter-clockwise rotation of the Corsica-Sardinia block (§ Cap 3.2). The relations between Lower Units, Schistes Lustrés Complex and Upper Units are sealed by the Burdigalian deposits cropping out in the Saint Florent and Francardo basins and the Aleria Plain (Dallon and Puccinelli 1995; Ferrandini et al. 1998; Cavazza et al. 2001; Gueydan et al. 2017), opened during the extensional regime that affected the Corsica Island in the post-collisional phase. The interaction of the Miocene deposits with the activity of the CCSZ is unclear: if a late extensional component of the CCSZ with the deposition in the Burdigalian could explain the sedimentation in the Saint-Florent Basin and Aleria Plain (Gueydan et al. 2017), no clear evidence of extension related to the Francardo Basin are found. The final deformation event in the Alpine Corsica is associated with the map-scale folds, characterized by N-S trend axes and sub-vertical axial plain (e.g. Gueydan et al. 2017). These structures, i.e. Cap Corse and Castagniccia antiforms and Centuri, Saint Florent and Aleria synforms, postdate the Miocene sealing deposits of Saint-Florent, Francardo and Aleria (Durand-Delga 1978; Faure and Malavieille 1981), but are however related to the Miocene tectonic extension (Jolivet et al. 1990; 1991; Fournier et al. 1991; Egal 1992; Marroni and Pandolfi 2003).

2.2 The syn- to post-orogenic extension in the western Mediterranean Sea

It is of primary importance to contextualize the geodynamic evolution of the Corsica Island with that of the Western Mediterranean in the Oligocene time. Although it is not easy to determinate the exact time of the tectonic switch from compressive to extensional regimes basing on data related to the onshore, we must take into account of some information about the island's offshore. The change in the polarity of the subduction from ENE-dipping (i.e. Alpine) to W-dipping (i.e. Apenninic) in fact implied the regional-scale shift from compressive to extensive regime, which caused the opening of the Ligure-Provençal and Tyrrhenian back-arc Basins starting from the Oligocene. The extension led the rotation of the Corsica-Sardinia block, separating it permanently from the neighboring domains of the Alpine collisional belt (Réhault et al. 1984; Vigliotti and Kent 1990; Jolivet et al. 1991; 1998; Vigliotti and Lagenheim 1995; Faccenna et al. 1997; Doglioni et al. 1997; 1999; Gueguen et al. 1998; Chamot-Rooke et al. 1999; Mauffret et al. 1999; Brunet et al. 2000; Speranza et al. 2002; Barruol and Granet 2002; Fellin et al. 2005; Lucente et al. 2006).

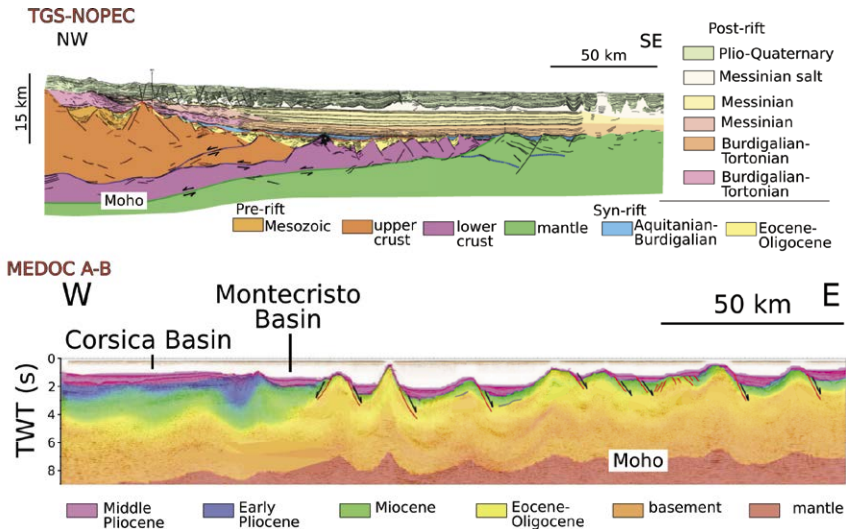
The Ligure-Provençal Basin extends westward of the island, from the Gulf of Lion to the Algerian Basin; the extension in this basin occurred through an early rifting phase (from 30 to 23 Ma) followed by the sea-floor spreading (from 23 to 14 Ma, Chamot-Rooke et al. 1999; Faccenna et al. 2001). A recent interpretation of the TGS- NOPEC seismic profile (Jolivet et al., 2015) highlights that the asymmetry of the rift, due to the activation of a NW-dipping detachment, produced the thinning of the upper plate and the exhumation of the lower crust (Fig 2). The age of this event is constrained by the syn-rift sedimentation (Oligocene-Aquitainian), occurred concurrently with steep normal faults dipping toward east (Gorini et al. 1994; Chamot-Rooke et al. 1999; Séranne 1999). Above an erosional surface that testifies a subaerial erosion during the rifting stage, a thick sequence of post-rift deposits occurs that suggests a fast post-rift subsidence in the Burdigalian-Messinian time span (Bache et al. 2010).

Given the lack of rotation in the paleomagnetic data between 30 and 23 Ma (i.e. the rifting phase), most of the counter-clockwise rotation of the Corsica-Sardinia block (Westphal et al. 1976) of about 30° with respect to a rotation pole located in the Gulf of Genoa (De Jong et al. 1969; Alvarez 1972; Edel and Lortsher 1977; Montigny and Edel 1981; Rehault et al. 1984.; Burrus 1984; van der Voo 1993; Speranza et al. 1999; Deino et al. 2001; Speranza et al. 2002; Carmignani et al. 2004; Moeller et al. 2013) was thus achieved during the spreading phase (Bellon et al. 1977; Burrus 1984; Chamot-Rooke et al. 1999) and ended with the collision with the Adriatic foreland (Moeller et al. 2014). This event marked the onset of the Apenninic Orogeny through the development of NW-SE striking fold-and-thrust belt (D'Agostino et al. 2008).

The migration toward NE of the trench allowed the extension in the West Mediterranean to concentrate in the eastern offshore of the Corsica island, i.e.

led the opening of the Tyrrhenian Sea (Malinverno and Ryan 1986; Kastens et al. 1987; Rosenbaum et al. 2002). The study of the seismic profiles highlights

Figure 2. Interpretation of the TGS-NOPEC (modified after Jolivet et al. 2015) and MEDOC A-B (modified after Moeller et al. 2014) seismic profiles.



that the Tyrrhenian Sea is composed by two domains: the Corsica and Montecristo Basins, between the Corsica and the Tuscan archipelago, characterized by smooth topography, and, to the east, a domain characterized by N-S striking horst and graben structures (Moeller et al. 2014) (Fig 2). The rifting stage in the Tyrrhenian basin is constrained between the Late Tortonian (9-8 Ma) to the Early Pliocene (5 Ma) by two regional unconformities (Trincardi and Zitellini 1987; Sartori 1990; Rosenbaum et al. 2002; Moeller et al. 2013), that confine the syn-rift deposits in the half-graben of the eastern domain. The younger age of the syn-rift deposits in the Corsica Basin (from pre-Langhian to Messinian) implies an older (Oligocene) rift-phase in the western Tyrrhenian, subsequently buried by the Early-Pliocene to Quaternary post-tectonic sedimentation (Moeller et al. 2013).

Chapter 3

The Architecture of the European margin and the Piedmont-Liguria Ocean in Corsica

3.1 Lithostratigraphic framework

The study area is located in the central position of the Corsica Island, along the boundary between the Hercynian and Alpine domains, where the relationships between these two domains and the features of the Alpine stack are observable. Unlike the monotonic lithostratigraphy of the Hercynian Corsica, the geology of the Alpine Corsica is extremely variable and complex, and over time its units have been classified in different ways. Therefore, a classification based on lithological, structural and metamorphic features of the Lower Units, the Schistes Lustrés Complex and the Upper Units is here proposed.

3.1.1 The Hercynian Corsica

The Hercynian Corsica represents the foreland of the Alpine belt (“autochthonous” domain) (Fig 3). The “Hercynian” appellative was attributed to this domain to distinguish it from the Alpine one, because on it, except for its eastern rim (Ménot and Orsini 1990), no evidence of post-Variscan deformation was found. The Hercynian Corsica consists of a Paleozoic basement intruded by Permo-Carboniferous granitoids, above which lies the Permian volcanics and volcanoclastics, the Mesozoic carbonates and the Tertiary polygenic deposits. The Paleozoic basement represents the south-western portion of the Variscan belt formed by the collision between Armorica microplate and Gondwana plate

Maria Di Rosa, University of Pisa, Italy, maria.dirosa.scaglia@gmail.com, 0000-0002-1154-7429
FUP Best Practice in Scholarly Publishing (DOI 10.36253/fup_best_practice)

Maria Di Rosa, *Tectono-metamorphic evolution of the continental units along the edge between Alpine and Hercynian Corsica. Constraints for the exhumation models in the continental collision setting*, © 2021 Author(s), content CC BY 4.0 International, metadata CC0 1.0 Universal, published by Firenze University Press (www.fupress.com), ISSN 2705-0297 (online), ISBN 978-88-5518-420-5 (PDF), DOI 10.36253/978-88-5518-420-5

in the Early Devonian-Carboniferous time span (e.g. Rossi et al. 2009; Casini et al. 2015; Massonne et al. 2017). This basement, made of paragneiss, amphibolites, micaschists, and quartzites and characterized by the Panafrican and Variscan metamorphic and deformation imprints, takes the name of Roches Brunes Fm. (Termier and Maury 1928) Based on the tectono-metamorphic features (Ménot and Orsini 1990) they have been distinguished in meso- to infra-crustal rocks (i.e. Belgodere, Zicavo, Solenzara-Fautéa, Porto Vecchio and Vico-Cargèse), supra-crustal rocks (i.e. Argentella-Galéria) and post-orogenic sequences (east of Monte Cinto). From here on, the more general term Roches Brunes Fm. will be used to define the Paleozoic basement. The change in composition of the batholith's magma with time, which requires an increasingly abundant mantle component, reflects the geodynamic evolution toward the pre-Alpine rifting (Paquette et al. 2003; Malasoma 2006).

Episodes of effusive activity are associated to the Permo-Carboniferous batholith, like those of Monte Cinto which is characterized by alkaline rhyolites and pyroclastic rhyodacites (Rossi et al. 2015 and references therein). On the eastern rim of the Hercynian Corsica, the Permian period is represented by a set of lithotypes (ignimbrites, rhyolitic tufs, volcanic breccias, arkoses with clasts of rhyolites and granitoids) which locally takes the name of Pajanello Fm. (Aicard et al. 1962; Amaudric du Chaffaut 1980) and hereafter called Volcanic and Volcaniclastic Fm..

Spread along the eastern rim of the Hercynian Corsica are the Mesozoic and Tertiary covers. The Mesozoic succession occurs only in three sites (Razzo Bianco, Roc de Gunzoli and Punta di Calcina, Amaudric du Chaffaut 1980) and mainly consists of dolomitic limestones and thin-grained limestones with ooides-bearing layers. The dolostones are attributed to Dogger for correlation with those found in Sardinia and described by Dieni et al. (1966), whereas the limestones are associated to the Kimmeridgian for the fossil content (foraminifera, cf. *Urgonia caelinensis*, *Kurnubia palestiniensis* and algae, cf. *Cayeuxia moldavica*, *Thaumatoporella sp.*, Amaudric du Chaffaut 1980).

The Tertiary succession outcrops in Cima Bondomo and in the widespread areas of Venaco (Monte Cardo, Monte Latiniccia, Punta di Capezzolo) and Prunelli-Solaro (Punta di Calcina, Monte Santo, Col de Prè d'Agnello, Col de Salto, Punta del Fornello). These series lie in angular unconformity above the Permo-Carboniferous batholith, the Volcanic and Volcaniclastic Fm. and the Mesozoic succession. The Tertiary succession includes, from bottom to top, carbonatic breccias, polygenic breccias and an alternation of sandstone and pelites. Only at the base of the Solaro series a Nummulitic limestones ("*calcaires de base*" of Amaudric du Chaffaut 1980) attributed to the Paleocene (e.g. *Planorbulina antiqua*) occur. The rest of the Tertiary succession is attributable to the Middle to Late Eocene (post-Lutetian), basing on the microfauna (cf. *Nummulites gallensi*, *Nummulites leupoldi*, *Turborotalia cerroazulensis*), that characterized the lithotypes (Rossi et al. 1994; Ferrandini et al. 2010).

3.1.2 The Lower Units: the European-derived metamorphic units of the Alpine Corsica

The Lower Units are interpreted as fragments of the European margin affected by Early Tertiary HP-LT metamorphism acquired during their subduction below the Adria margin (Bezert and Caby 1988; Molli et al. 2006; Malasoma and Marroni 2007; Molli 2008; Maggi et al. 2012; Di Rosa et al. 2017a). Because of their European derivation, the lithostratigraphy of the Lower Units is similar to those of the Hercynian Corsica. It consists of Paleozoic metamorphic rocks (i.e. Roches Brunes Fm. *Auctt.*) intruded by Permo-Carboniferous metagranitoids and unconformably covered by Permian metavolcanics and metavolcaniclastics. Above these Paleozoic lithotypes, there are two stratigraphic sequences, separated by an angular unconformity: an older sequence of Mesozoic platform-type metacarbonates, mainly made of Triassic metalimestones and metadolostones, Jurassic metacarbonates, and a Middle to Late Eocene (from Lutetian to Bartonian by Bezert and Caby 1988) sequence made of metabreccias and metasandstones, unconformably lying on both Variscan basement and Permo-Mesozoic sedimentary sequence.

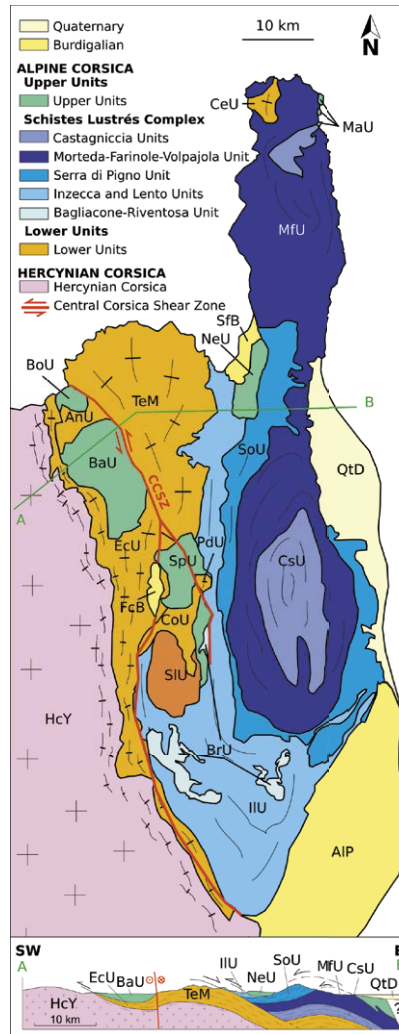
Differences in the lithostratigraphy among the units are mainly due to (1) the presence/lack of the Variscan basement and the Permian metasediments, (2) the presence/lack of the Mesozoic sequence, (3) if present, the thickness of the Mesozoic sequence (4) if present, the thickness of the Middle to Late Eocene covers and the position of the angular unconformity at its base.

Because of the variability of their metamorphism, the European-derived metamorphic units have been classified by the authors in different ways (e.g. Malasoma 2006). In the light of the data related to the metamorphism collected in the last decade (include those of this thesis), the term Lower Units will be used from here on to refer to all the units and groups of units which have as common features the continental affinity (i.e. the European derivation) and the structural position at the base of the Alpine stack, but characterized by different metamorphic degrees. Therefore, belong to the Lower Units:

- the Tenda Massif, characterized by a metamorphism of HP-LT (0.9-1.1 GPa, 400-500°C, Tribuzio and Giacomini 2002; Molli and Tribuzio 2004) reached between 45 and 32 Ma (Brunet et al. 2000; Maggi et al. 2012). Centuri Unit presents the same metamorphic degree;
- the External Continental Units (i.e. Popolasca, Corte, Pedani), which reached the geobaric peak in the blueschist facies with P-T values that change for each unit, and after retrocessed in the greenschist facies (e.g. Bezert and Caby 1988; Malasoma et al. 2006; Di Rosa et al. 2017a);
- the “parautochthonous” (Caporalino-Sant’Angelo and Annunciata Units), characterized by a weak deformation and the lack of metamorphic imprint (Nardi et al. 1978; Malasoma 2006).

Usually the Lower Units occur in groups of units (e.g. Corte, Pedani areas) or alone (e.g. Ghisoni area), they override the Hercynian Corsica and are overthrust by the Schistes Lustrés Complex.

Figure 3. Tectonic map of the NE Corsica (modified after Vitale Brovarone et al. 2012) and schematic cross section (not in scale, after Di Rosa et al. 2017a). QtD: Quaternary deposits, SfB: Saint-Florent Basin, FcB: Francardo Basin, AIP: Aleria Plain, MaU: Macinaggio Unit, BoU: Bas-Ostriconi Unit, BaU: Balagne Unit, NeU: Nebbio Unit, SpU: Serra Debbione and Pineto Units, SIU: Santa Lucia Unit, CsU: Castagniccia Unit, MfU: Morteda-Farinole-Volpajola Unit, SoU: Serra di Pigno and Oletta Units, IIU: Inzecca and Lento Units, BrU: Bagliaccone-Riventosa Unit, CeU: Centuri Unit, TeM: Tenda Massif, AnU: Annunciata Unit, EcU: External Continental Units, PdU: Cima Pedani Units, CoU: Caporalino Unit, HcY: Hercynian Corsica.



3.1.3 Other groups of units of the Alpine Corsica: from the ocean-continent transition to the Piemonte-Liguria Ocean

Schistes Lustrés Complex

The Schistes Lustrés Complex constitutes about half of the Alpine Corsica and includes unit of both continental and oceanic affinities. Its paleogeography is a first-order issues which is still unclear and needs to be improved. In this thesis we propose a classification based on those proposed by Vitale Brovarone et al. (2012) because it highlights the metamorphic degree of the units (§ Cap 2.2):

- The Castagniccia Unit (i.e. Castagniccia Fm. of Delcey 1974; Caron and Delcey 1979) occupies a low structural position of the Schistes Lustrés Complex stack (e.g. the Lower ophiolitic units of Rossi et al. 2001), and consists of metasediment-rich sequence (Brando, Olmo, Porri-Ortale, Vescovato Units). It is interpreted as the cover of a detached ophiolitic basement (Caron and Delcey 1979), and therefore representative of the oceanic crust. They are characterized by the eclogitic facies, after retrocessed in the greenschist;
- The Morteda-Farinole-Volpajola Unit (Lahondère 1988; Lahondère and Lahondère 1988; Lahondère and Caby 1989; Paperini 2004) and the Campitello, Morosaglia, Serra di Pigno, Oletta and Zuccarello Units (Lahondère and Caby 1989; Lahondère 1996; Paperini 2004; Vitale Brovarone et al. 2014) occupies an intermediate position in the Schistes Lustrés Complex stack (e.g. the continental and oceanic-derived units of Rossi et al. 2001), and include slivers of meta-ophiolites, continental basement rocks and associated metasediments. Because of the presence of both continental and oceanic material, they are interpreted as the ocean-continent transition (Vitale Brovarone and Hewartz 2013). The Morteda-Farinole-Volpajola Unit, which reached the metamorphic peak at the eclogitic facies conditions, differs from the others that registered the peak conditions in the lawsonite-blueschist facies;
- The Lento and Inzecca Units (Lahondère et al. 1999; Paperini 2004; Levi et al. 2007) crop out in the area around the Golo Valley (i.e. Lento Unit) and in the southernmost sector of the Alpine Corsica (i.e. Inzecca Unit). They overlap the Lower Units (§ Cap 4.1, 4.2, 4.4) or the Hercynian Corsica (§ Cap 4.3, Amaudric du Chaffaut et al. 1985). Lento and Inzecca Units are made of an ophiolitic basement covered by supra-ophiolitic sedimentary sequence (Amaudric du Chaffaut et al. 1972; Lagabrielle and Lemoine 1997), and the primary relationships between the ophiolitic basement and the covers are well preserved. Because of their oceanic affinity, these units are considered as representative of the Piemonte-Liguria oceanic lithosphere. The metamorphism of Lento and Inzecca Units varies from blueschist facies to the very low grade (e.g. Padoa 1999). Rossi et al. (2001) considered Lento and Inzecca Units in the upper position of the Schistes Lustrés Complex;
- The Bagliacone-Riventosa Unit (Caron 1977; Amaudric du Chaffaut et al.

1985; Egal 1992) occupies the lowest structural position of the Schistes Lustrés Complex and, being made of a succession typical of the continental covers, it is interpreted as the thinned continental margin (Caron 1979; Durand-Delga 1978; 1984). This unit is characterized by a complex deformation and metamorphic history, but its paleogeographic location is still unclear.

What does not properly fit into any of these classes is the Santo Pietro di Tenda Unit (Delcey 1974; Caron 1979; Caron and Delcey 1979; Durand-Delga 1984). It is made of a thin and continuous rim of meta-ophiolites and continental rocks, usually associated to important ophiolitic masses (Cap Corse and east of Nebbio) but also interlayered to the Castagniccia Unit (Caron and Delcey 1979). The Santo Pietro di Tenda Unit occupies the highest position in the Schistes Lustrés Complex stack and is generally referred to an ocean-continent transition paleogeographic domain (Caron and Delcey 1979; Vitale Brovarone et al. 2014). It. Although it is interpreted by some authors as the basement of the Castagniccia Unit (Caron and Delcey 1979), its metamorphism in the blueschist facies allows to associate it to the Lento and Inzecca Units.

Upper Units

The uppermost position of the Alpine Corsica stack is occupied by the Upper Units (i.e. “nappes supérieures”), a group of units of both continental and oceanic affinity, characterized by a weak deformation and a very low-grade metamorphism (Mattauer et al. 1981; Dallon and Nardi 1984; Durand-Delga 1984; Waters 1990; Fournier et al. 1991; Dallon and Puccinelli 1995; Daniel et al. 1996; Malavieille et al. 1998; Marroni and Pandolfi 2003; Levi et al. 2007; Malasoma 2006; Molli and Malavieille 2011; Maggi et al. 2012). The Upper Units have been recognized as klippen cropping out in different position of the Alpine Corsica and are mainly represented by Jurassic ophiolites and related Upper Jurassic-Upper Cretaceous covers (Balagne, Nebbio, Rio Magno, Serra Debbione and Pineto Units, Durand-Delga et al., 1997; Saccani et al. 2000; Marroni and Pandolfi 2003), even if units made of Cretaceous turbidites (Bas-Ostriconi and Macinaggio Units) also occur (Dallon and Nardi 1984; Malasoma 2006).

Balagne, Nebbio, Serra Debbione and Pineto Units are ophiolitic units consisting of a Jurassic ophiolitic sequence and related Late Jurassic-Late Cretaceous sedimentary cover (Dallon and Nardi 1984; Durand-Delga 1984; Saggi et al. 1982; Durand-Delga et al. 1997; Saccani et al. 2000; Padoa et al. 2001; Rossi et al. 2002; Marroni and Pandolfi 2003). The Balagne and Nebbio Units are generally associated to the Macinaggio and Bas-Ostriconi Units, in turn consisting of Late Cretaceous carbonate turbidites (Nardi 1968; Dallon and Nardi 1984; Durand-Delga 1984; Marroni and Pandolfi 2003). While the Balagne Unit is found in an external position directly overriding the Lower Units (Marroni and Pandolfi 2003 and references therein), Nebbio and Macinaggio Units occupy a more internal position, resting above the Schistes Lustrés Complex (Molli 2008).

Some authors (e.g. Durand-Delga 1984; Dallon and Puccinelli 1995; Lahondère 1996; Malavieille et al. 1998; Molli 2008) interpreted Nebbio Unit as remnants of the Alkapeca continental block (Boullin et al. 1986; Guerrero et al. 1993) a microcontinent similar to Adria in lithostratigraphy, drifted away from it during the rifting phase in the western Tethys (Michard et al. 2002).

A feature that characterizes the ophiolitic sequences is the presence of terrigenous debris of mixed composition (siliciclastic and carbonatic) interbedded along the whole stratigraphic log. Their source area is the near Hercynian Corsica, as testified by the composition of the clasts that includes the Variscan basement, the Permo-Carboniferous intrusions and the Permian-Jurassic covers (e.g. Pandolfi et al. 2016).

Santa Lucia Unit

The Santa Lucia Unit occurs in the south-western of the Alpine Corsica, above the Lower Units and below the Schistes Lustrés Complex (Rossi et al. 1994; Ferrandini et al. 2010). The Santa Lucia Unit consists of a continental crust basement (granulitic paragneiss with serpentinite and stratified mafic complex) characterized by Permo-Jurassic HT metamorphism, probably due to the lithospheric thinning of the Tethys margin (Rossi et al. 2006; Zibra 2006; Vitale Brovarone et al. 2012). This basement is covered by Late Cretaceous sedimentary succession, composed by the Tomboni Conglomerates and the Tralonca Flysch (Libourel 1988; Rossi et al. 1994; Zibra 2006; Zibra et al. 2010). The Alpine polyphasic history recorded by Santa Lucia Unit mainly develop under lower greenschist facies conditions (Libourel 1985).

The interpretation of the Santa Lucia Unit is debated: Rieuf (1980) and Durand-Delga (1984) correlated its Cretaceous covers with those of the Balagne Unit. Jolivet et al. (1998) and Gueydan et al. (2017) associated Santa Lucia Unit with the Upper Units, because of its continental affinity and low-grade metamorphism. Basing on their structural position, Levi et al. (2007) associated the Santa Lucia Unit to the Lower Units group. An alternative interpretation was given by Caby and Jacob (2000) who associated this unit to the Austroalpine units of the Central Alps. A correlation between Santa Lucia Unit and the Western Alps was given by Molli and Malavieille (2011), basing on its similarities with the Ivrea zone; in this case, Santa Lucia Unit represents Adria, and thus is considered as relics of the Alpine indentation system, or the upper plate of the Alpine subduction.

3.2 The state of art

3.2.1 Overview of the tectono-metamorphic data

The first studies about the tectono-metamorphic history of the Alpine Corsica go back to the '70s with the scientific production of Amaudric du Chaffaut

(Amaudric du Chahattaut 1975; Amaudric du Chaffaut and Saliot 1979; Amaudric du Chaffaut 1980), devoted to the description of the relationships between the Lower Units (i.e. “*Ecailles Cortenais*”) and the Hercynian Corsica (i.e. “*Massif cristalline Corse*”), and those of Caron (1977) focused on the tectonic setting of the Schistes Lustrés Complex. Shortly after, Durand-Delga (1984) made a connection between the Alpine Corsica and the Western Alps, defining the Lower Units as “*domain cortenais prépiémontais*”. The Late Eocene HP metamorphism of the Lower Units was estimated for the first time by Bezert and Caby (1988); subsequently, several studies have deepened this theme, basing on the detailed structural analysis of selected areas (Marroni et al. 2001; Marroni and Pandolfi 2003; Molli and Tribuzio 2004; Malasoma et al. 2006; Molli et al. 2006; Malasoma and Marroni 2007; Levi et al. 2007). The elaboration of the geodynamic evolution model for the Alpine Corsica was treated in the pioneering paper of Malavieille et al. (1998) and, after the intense production of data overmentioned, updated in the review paper of Molli (2008). In the last ten years several data about the metamorphism of the Schistes Lustrés Complex (Vitale Brovarone et al. 2012; 2014; Vitale Brovarone and Hewartz 2013) and the Lower Units (Di Rosa et al. 2017a; 2018a; 2018b; Molli et al. 2017) have been published. The study of the post-orogenic extension in the Alpine Corsica started with Jolivet et al. (1990; 1991; 1998) and is nowadays intensely treated (Maggi et al. 2012; Rossetti et al. 2015; Gueydan et al. 2017).

On the other hand, the Hercynian Corsica, classically described as a not deformed and not metamorphosed “autochthon” foreland, escaped from any Early Tertiary deformation and never buried at deep below the orogenic wedge (e.g. Durand-Delga 1984). Razzo Bianco was firstly studied by Amaudric du Chaffaut (1980), who recognized the deformation within the Mesozoic lithotypes (e.g. marbles etc.), but does not discuss it in terms of Alpine deformation. However, Ménot and Orsini (1990) attributed to the Alpine Orogeny the partitioned deformation observed on the eastern rim of the Hercynian Corsica, after reported in the official geological maps (Amaudric du Chaffaut et al. 1985; Rossi et al. 1994). The geochronological constraint was provided by Di Vincenzo et al. (2016), who associated the Early Tertiary age to these ductile (-brittle) shear zones, confirming the involvement of the Hercynian Corsica in the Alpine deformation processes. In addition, apatite- and zircon- fission tracks thermochronology evidenced a cooling history that interested the whole island from 35 to 15 Ma (Danisik 2005; Danisik et al. 2007; 2012).

3.2.2 Geochronological constraints

The geochronological data available for the Corsica Island regard the post-Variscan magmatism and the Alpine metamorphism. The post-collision magmatism has been long studied in terms of geochronology (Paquette et al. 2003; Giacomini et al. 2008), which allowed to recognize different magmatic pulse in the Permo-Carboniferous age. These granitoids represent the set of magmatic intrusions emplaced in the Carboniferous and the Permian which

together constitute the Corsica-Sardinia batholith (e.g. Ménot and Orsini 1990). It is formed between the Visean to the Artinskian by three main magmatic pulses alternated to periods of inactivity (e.g. Renna et al. 2007):

- At about 345-338 Ma, the earliest intrusions made of Mg-K rich granitoids with a shoshonitic affinity (Cocherie et al. 1994; Paquette et al. 2003);
- After 305 Ma, the calc-alkaline intrusions dominated by low-k hornblende granitoids (Cocherie et al. 1994; Tommasini et al. 1995; Paquette et al. 2003);
- Between 290 and 280 Ma, the last tholeiitic pulses and related dykes simultaneously with peralkaline to slightly peraluminous A-type granites (Paquette et al. 2003; Cocherie et al. 2005).

As regards the Alpine metamorphism, geochronological data are less abundant and their interpretation is subject to debate. The timing of the deformation, as well as that of the metamorphic peak, was different for each group of units and for each single unit. As in the Western Alps, the tectono-metamorphic history associated to the units belonging to the Alpine Corsica is polyphased (Lanari et al. 2012, Di Rosa et al. 2017a), and the exhumation of certain tectonic units occurred at the same time as others are buried (Strzeczynski et al. 2012). Therefore, a trend to younging moving from the oceanic and the ocean/continent transition units (i.e. the Schistes Lustrés Complex) to the continental units (i.e. the Lower Units) is expected. The most accepted age for the HP metamorphism is those of Lahondère and Guerrot (1997) who estimated the Late Cretaceous 83.8 ± 4.9 Ma for the Morteda-Farinole-Volpajola Unit of the Schistes Lustrés Complex. However, Ar-Ar and U-Pb estimations associate the same unit to the Middle/Late Eocene (40 ± 0.9 Ma in Monié in Lahondère 1996; 34.6 ± 0.6 Ma in Brunet et al. 2000; 34.4 ± 0.8 Ma in Martin et al. 2011; 34.4 ± 1 Ma in Maluski 1977; 34.2 ± 0.7 Ma in Vitale Brovarone et al. 2012). The metamorphism in the Serra di Pigno and Oletta Units seems roughly coeval (37.6 ± 1.4 Ma in Vitale Brovarone et al. 2012; 31.7 ± 0.3 Ma in Brunet et al. 2000). As regards the Lower Units, all the radiogenic data available are related to the Tenda Massif, which point to Middle/Late Eocene metamorphism: Brunet et al. (2000) estimated 39.4 ± 0.4 Ma for the phengites sampled in the inner position of the massif; data related to the East Tenda Shear Zones range between $54 \pm 8 - 48 \pm 18$ Ma (Maggi et al. 2012) and $37-34$ Ma (Mailhé 1982) and 34.4 ± 0.8 , 32.6 ± 0.8 Ma (Jourdan 1988). Only Amaudric du Chaffaut and Saliot (1979) reports a geochronological data related to the Corte area (40 ± 2 Ma) obtained on HP phengites. $37.3 - 34.9 \pm 0.3$ Ma is instead the age estimated by Di Vincenzo et al. (2016) for the shear zones occurring in the Hercynian Corsica granites in the Golo Valley and in the Razzo Bianco area, ~300 m west of the tectonic contact with the Alpine Corsica.

Apatite fission tracks ages were estimated by Danisik et al. (2007) on samples collected in the whole island (i.e. Hercynian Corsica, Lower Units, Schistes Lustrés Complex and Upper Units), in order to constrain the time in which the rock volumes reached temperatures of $110-70^\circ\text{C}$. These authors obtained for the

Table 1. Age constraints in Corsica: a review.

Magmatic age						
Unit	method	mineral	locality	Age (Ma)	authors	meaning
Hercynian Corsica	U-Pb	Zircon in granodiorite	Capo Cavallo	347.0 ±1.3	Paquette et al. 2003	Post-collisional magmatism
Hercynian Corsica	U-Pb	Zircon in calc-alkaline dykes	Capo Cavallo	305.5 ±1.6	Paquette et al. 2003	Post-collisional magmatism
Hercynian Corsica	U-Pb	Zircon in diorite	Santa Lucia di Mercurio	281.0 ±3.3	Paquette et al. 2003	Post-collisional magmatism
CPU	U-Pb	Zircon in metagranitoid	Venaco	285 ±3	Di Rosa et al. 2018*	Post-collisional magmatism
GHU	U-Pb	Zircon in metagranitoid	Sampolo (Fium'Orbo Valley)	283 ±3	Di Rosa et al. 2018*	Post-collisional magmatism
GHU	U-Pb	Zircon in epidote-bearing metagabbro	Sampolo (Fium'Orbo Valley)	275.8 ±0.9	Di Rosa et al. 2018*	Post-collisional magmatism
Rift-related age						
Unit	method	mineral	locality	Age (Ma)	authors	meaning
CPU	U-Pb	Allanite in metagranitoid	Venaco	224.9 ±7	Di Rosa et al. 2018*	Heating event associated to rifting
Biostratigraphic constraints						
Unit	method	fossil	locality	Age	authors	meaning
Lower Units	Fossil content	<i>Nummulites sp.</i>	Corte	Bartonian	Bezert and Caby 1988	Post-Bartonian deformation of the Lower Units
Hercynian Corsica	Fossil content	<i>Nummulites sp.</i>	Monte Cardo (Venaco)	Bartonian	Ferrandini et al. 2010	Youngest age found in the Eocene of the Hercynian Corsica

Caporalino Unit	Fossil content	<i>Globorotalia sp.</i>	Caporalino	Middle Eocene	Puccinelli et al. 2012	Post-Bartonian deformation of the Lower Units
Francardo Basin	Fossil content		Francardo	Burdigalian	Alessandri et al. 1977; Ferrandini et al. 2003	Oldest age found in the sealing deposits

Metamorphic constraints

Unit	method	mineral	locality	Age (Ma)	authors	meaning
MfU	Sm/Nd	Garnet-jadeite	Accendi Pipa (Golo Valley)	83 ±4.9	Lahondère and Guerrot 1997	Peak metamorphism
MfU	Ar/Ar	Phengite	Golo Valley	40±0.9	Monié in Lahondère 1996	HP metamorphism
MfU	Ar/Ar	Phengite	Barcolaccia	34.6 ±0.6	Brunet et al. 2000	Cooling/recrystallization
MfU	U-Pb	Zircon	Monte San Petrone	34.4 ±0.8	Martin et al. 2011	Peak metamorphism
MfU	Ar/Ar	Phengite	Sant'Andrea di Cotone	34.4±1	Maluski 1977	Peak metamorphism
MfU	Lu/Hf	Garnet	Castello di Rostino	34.2 ±1.6	Vitale Brovarone et al. 2013	Peak metamorphism
SoU	Lu/Hf	Lawsonite	Morosaglia	37.5±1.3	Brovarone et al. 2013	Peak metamorphism
SoU	Ar/Ar	Phengite	Santa Catilina	31.7±0.3	Brunet et al. 2000	Cooling/recrystallization
Tenda Massif	Ar/Ar	Phengite	Central Tenda	39.4±0.4	Brunet et al. 2000	Mixed age
Tenda Massif	U/Pb TIMS	Rutile and phengite	East Tenda Shear Zone	48-54	Maggi et al. 2012	Top-to-W HP metamorphism

Tenda Massif	Ar/Ar	Phengite	East Tenda Shear Zone	34-37	Mailhé et al. 1982	Peak metamorphism
Tenda Massif	Ar/Ar	Phengite	East Tenda Shear Zone	32.6-34	Jourdan 1988	Peak metamorphism
Lower Units	Ar/Ar	Phengite	Corte	40±2	Amaudric du Chaffaut and Saliot 1979	Peak metamorphism
Hercynian Corsica	Ar/Ar	Phengite	Venaco	37.3 to 34.9±0.3	Di Vincenzo et al. 2016	Top-to-W shearing phase

Final exhumation from shallow depth

Unit	method	mineral	locality	Age (Ma)	authors	meaning
Alpine Corsica	Fission track	Apatite - zircon	Asco-Pedani	15-25	Danisik et al. 2007	Post-collisional cooling
Hercynian Corsica	Fission track	Apatite - zircon	Calacuccia - Galeria	16-24	Danisik et al. 2007	Post-collisional cooling

* new data collected for this thesis (§ Cap 6).

central Corsica ages always younger than 25 Ma and recognized a trend of younging from W to E in the area between Asco (~25 Ma) and Cima Pedani (~15 Ma), and in the Hercynian Corsica an opposite trend of younging from E to W between Calacuccia (~24 Ma) and Galeria (~16 Ma).

Where radiogenic data are missing, the deformation of the Lower Units is constrained by the stratigraphic relationships, and thus bracketed between the age of the youngest rock involved in the deformation and the age of the older sediment that unconformably seal the tectonic stack of deformed units. Therefore, the Bartonian age (Middle Eocene) assigned through the occurrence of *Nummulites sp.* contained in metabreccias and metasandstones that top the Lower Units (Bezert and Cabay 1988, Ferrandini et al. 2010) predates their subduction. The Middle Eocene age is also proposed by Puccinelli et al. (2012) for the Caporalino Unit basing on the content of *Globorotalia sp.*. The upper limits for the deformation is instead provided by the continental sedimentary succession of Francardo (Ferrandini et al. 2003) that unconformably covers the Lower Units, in the Francardo area immediately west of the CCSZ (Cavazza et al. 2007). The Burdigalian age of the base of the Francardo's succession (Alessandri et al. 1977) postdate the deformation history of the Lower Units, which thus necessary occurred in the Priabonian-Aquitania (37.2-20.4 Ma, Gradstein et al. 2012).

Chapter 4

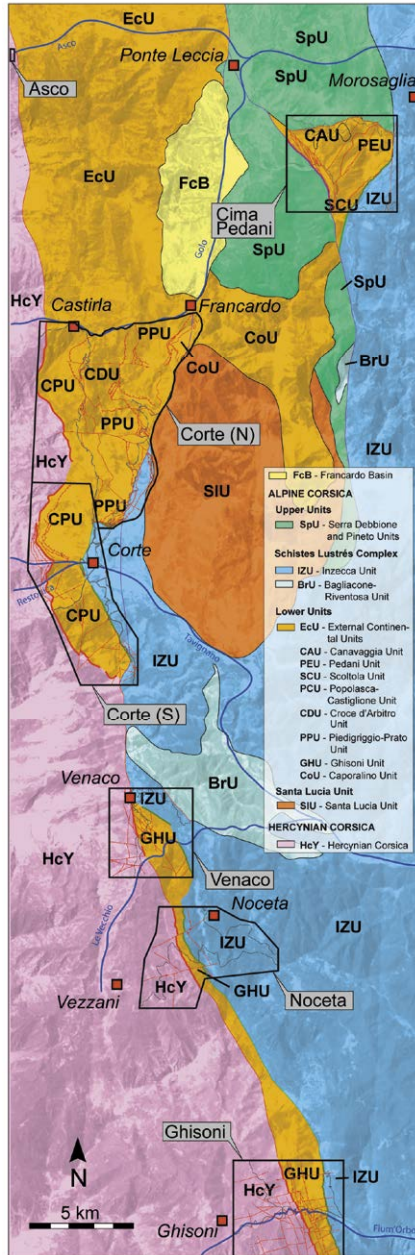
Geological overview of the study areas

The study areas are located in the western side of the Alpine Corsica between Asco and Fium'Orbo valleys, and roughly cover the rim between the Hercynian and Alpine Corsica. In the northern sector, from Asco to Corte, the Hercynian Corsica (HCY) is overthrust by a set of Lower Units, Schistes Lustrés Complex and Upper Units. In the southern sector, from Venaco to Ghisoni, the Alpine Corsica is almost totally made of the units belonging to the Schistes Lustrés Complex, whereas the Lower Units are reduced to one unit (i.e. the Ghisoni Unit) and the Upper Units disappear. In order to characterize, the lithostratigraphy of the Lower Units, the adjacent tectonic units of the Alpine Corsica and the portion of the HCY in contact with them, follows the description of five of sites studied for this thesis.

4.1 Cima Pedani area

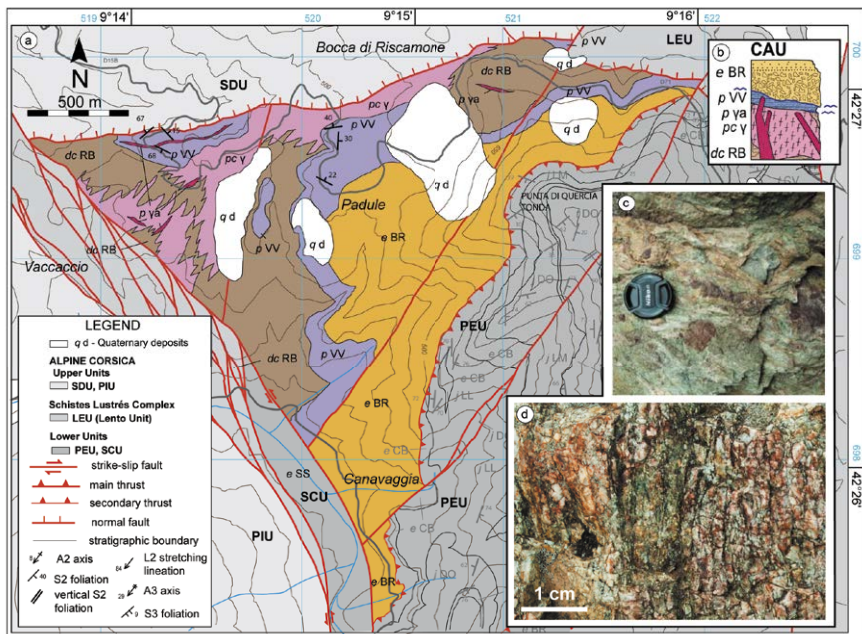
The study area is located ca. 5 km SW of the town of Ponte Leccia, and 2 km west of the little town of Morosaglia (Fig 4), around the 816 m high mountain of Cima Pedani (42°26'17.6"N 9°15'46.7"E). This region, which geologically belongs to the Alpine Corsica, is characterized by a tectonic window that exposes a stack of tectonic units of continental affinity. In the recent reviews for the Alpine Corsica, the units cropping out in this area are correlated with the Caporalino Unit and all together referred as a single tectonic body named Caporalino-Pedani Unit (e.g. Vitale Brovarone et al. 2012). However, differences in the stratigraphic setting already reported in literature (Rodriguez 1981; Puccinelli et al. 2012) and the tectono-metamorphic history reconstructed

Figure 4. Tectonic sketch map of the central Corsica. In the studied areas: thick lines indicate tectonic contact between HCY and the Lower Units and between the Lower Units and the Schistes Lustrés Complex. The Central Corsica Shear Zone fault system is also shown.



here clearly indicate that the units from the Pedani area must be separated from the Caporalino Unit, as also assessed in the past by Amaudric du Chaffaut (1980). These units can be correlated with the Lower Units as, according to their structural position, they are overlain by units belonging both to Schistes Lustrés Complex and Upper Units. The Lower Units in Cima Pedani are represented, from bottom to the top, by the Canavaggia, Pedani and Scoltola Units, whereas the Schistes Lustrés Complex and Upper Units are, respectively, represented by the Lento Unit (i.e. Inzecca Unit of Durand-Delga 1984) and the couple Serra Debbione and Pineto Units belonging to the Upper Units, with the latter at the top. The tectonic window is 6 km² wide and shows an about square shape with the Canavaggia, Pedani and Scoltola Units at the core and the Lento, Pineto and Serra Debbione Units at the top.

Figure 5. The Canavaggia Unit: (a) geological map (modified after Di Rosa et al. 2018a); (b) lithostratigraphic log: *dc RB*: Roches Brunes Fm., *pc* \blacksquare : metagranitoids, *p* \blacksquare : dykes complex, *p VV*: Metavolcanic and Metavolcaniclastic Fm., *e BR*: Metabreccia Fm.; (c) Metabreccia Fm., Middle to Late Eocene and (d) metagranitoids, Permo-Carboniferous.

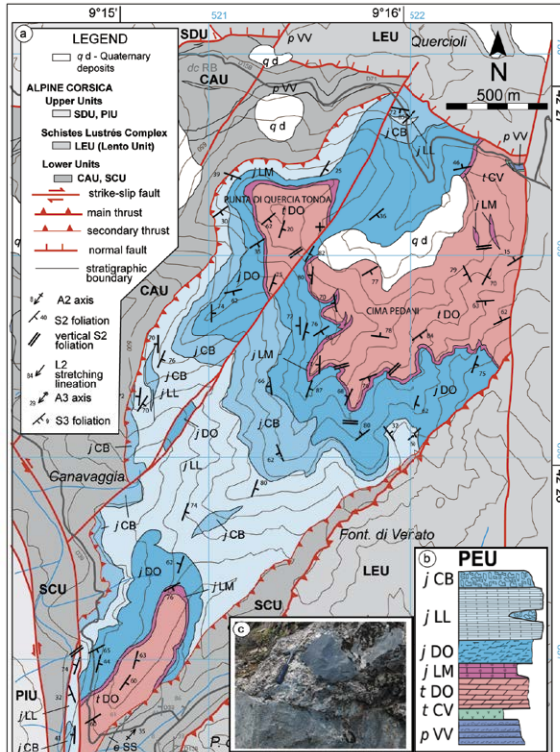


The Canavaggia, Pedani and Scoltola Units are metamorphic fragments of the European continental margin: their reconstructed typical succession includes a Paleozoic basement, made up of Carboniferous metagranitoids and the Roches Brunes Fm., both covered by a Permian Metavolcanic and Metavolcaniclastic Fm. that shows a transition to a Triassic-Jurassic, mainly carbonate, metamorphic sequence unconformably covered by metabreccias and siliciclastic metarenites of

Eocene age. Each unit includes only part of this succession.

In the Canavaggia Unit (CAU, Fig 5), the basement, made of Roches Brunes Fm. intruded by the metagranitoids (Fig 5d), is cut by felsic meta-dykes. The cover of this basement is represented by the Metavolcanic and Metavolcaniclastic Fm. made up of orthogneisses whose protoliths are represented by hyperalkaline volcanic products such as rhyolites and dacites of Permian age (Rossi et al. 1994). This sequence is unconformably covered by the Metabreccia Fm. (Rossi et al. 1994), a matrix supported polygenic meta-breccia where clasts of meta-limestone, meta-dolostone, meta-arenite, quartzite, metabasalt and meta-granite are set in a fine-grained recrystallized matrix (Fig 5c). Although Rossi et al. (1994) consider this formation as Jurassic in age, the occurrence of meta-limestone and meta-arenites suggest an Eocene age, as recognized in the neighboring areas of the Alpine Corsica (Bezert and Caby 1988; Malasoma and Marroni 2007; Di Rosa et al. 2017a).

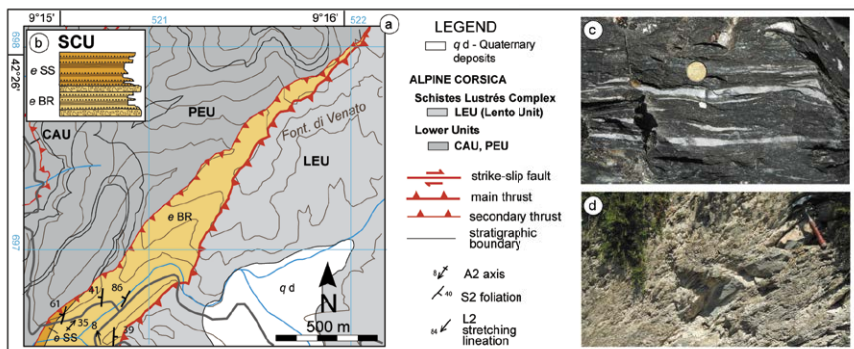
Figure 6. The Pedani Unit: (a) geological map (modified after Di Rosa et al. 2018a); (b) lithostratigraphic log: *p* VV: Metavolcanic and Metavolcaniclastic Fm., *t* CV: Cavernoso Metalimestone Fm., *t* DO: Lower Metadolostone Fm., *j* LM: Lumachella Metalimestone Fm., *j* DO: Upper Metalimestone Fm., *j* LL: Laminated Metalimestone Fm. and *e* CB: Metacarbonate Breccia; (c) Metacarbonate Breccia, Middle to Late Eocene.



In contrast, the Pedani Unit (PEU, Fig 6, Rodriguez 1981; Gelmini and Mantovani 1982; Rossi et al. 1994) lacks the Carboniferous basement and consists of a carbonate meta-sedimentary succession starting with a thin level of Metavolcanic and Metavolcaniclastic Fm. of Permian age in all similar to that cropping out in the Canavaggia Unit. The Metavolcanic and Metavolcaniclastic Fm. is topped by the Cavernoso Metalimestone Fm. (Middle Triassic; Rodriguez 1981) that shows a stratigraphic transition to the Lower Metadolostone Fm., attributed by Rodriguez (1981) to the Norian age, and Lumachella Metalimestone Fm. (Rethian; Rodriguez 1981). The succession continues with the Upper Metadolostone Fm., attributed to the Hettangian by comparison with the Liassic carbonates of the Saint-Florent region which contain *Gryphaea arcuate* (Ricour 1949) and Laminated Metalimestone Fm. (Sinemurian; Rossi et al. 1994), unconformably covered by the Meta-Carbonate Breccia of supposed Eocene age (Fig 6c).

The Scoltola Unit (SCU, Fig 7) only features the Eocene age, including the Metabreccia Fm. (Fig 7d) and Metasandstone Fm. (Fig 7c, Rossi et al. 1994). The Metabreccia Fm. of CAU as well as the Metabreccia and Metasandstone Fms. of the Scoltola Unit can be correlated with the metaturbidites of the Castiglione-Popolasca Unit (§ Cap 4.2, Bezert and Caby 1988; Di Rosa et al. 2017b) outcropping westward of Cima Pedani, where the occurrence of *Nummulites sp.* indicates a Bartonian age (Middle Eocene).

Figure 7. The Scoltola Unit: (a) geological map (modified after Di Rosa et al. 2018a); (b) lithostratigraphic log: e BR: Metabreccia Fm., and e SS: Metasandstone Fm.; (c) Metasandstone Fm., Middle to Late Eocene and (d) Metabreccia Fm., Middle to Late Eocene.



The Lower Units are topped by the ophiolitic Lento Unit (LEU, Figs 6-7), made up of meta-ophiolitic sequence and its metasedimentary cover (Levi et al. 2007). The meta-ophiolites are represented by a peridotite-gabbro basement, Middle to Late Jurassic in age. They are covered by a thin volcano-sedimentary complex followed by a thick sedimentary Late Jurassic–Early Cretaceous pelagic succession (Rossi et al. 1994; Levi et al. 2007). In the Cima Pedani tectonic

window the meta-sediments of the Lento Unit are represented by metaradiolarites and the Erbajolo Fm., a thick sequence of levels of marbles and schists.

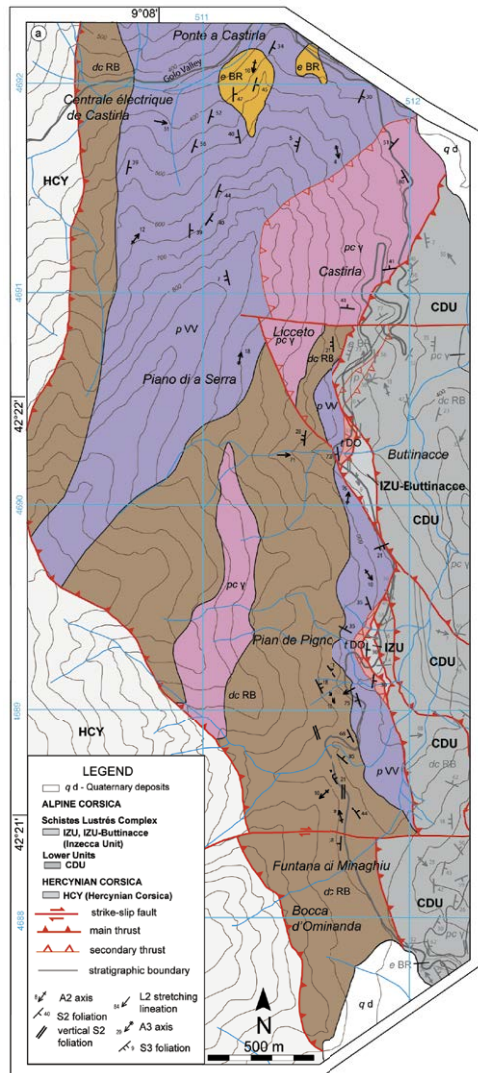
The Lento Unit is topped by the Serra Debbione and Pineto Units, both considered as belonging to the Upper Units. The Serra Debbione Unit, as described by Levi et al. (2007), is represented by peridotites cut by gabbroic bodies and basaltic dykes. In contrast, the Pineto Unit (Saccani et al. 2000; Sanfilippo and Tribuzio 2012) mainly consists of Jurassic gabbros cut by basaltic dykes (Fig 5).

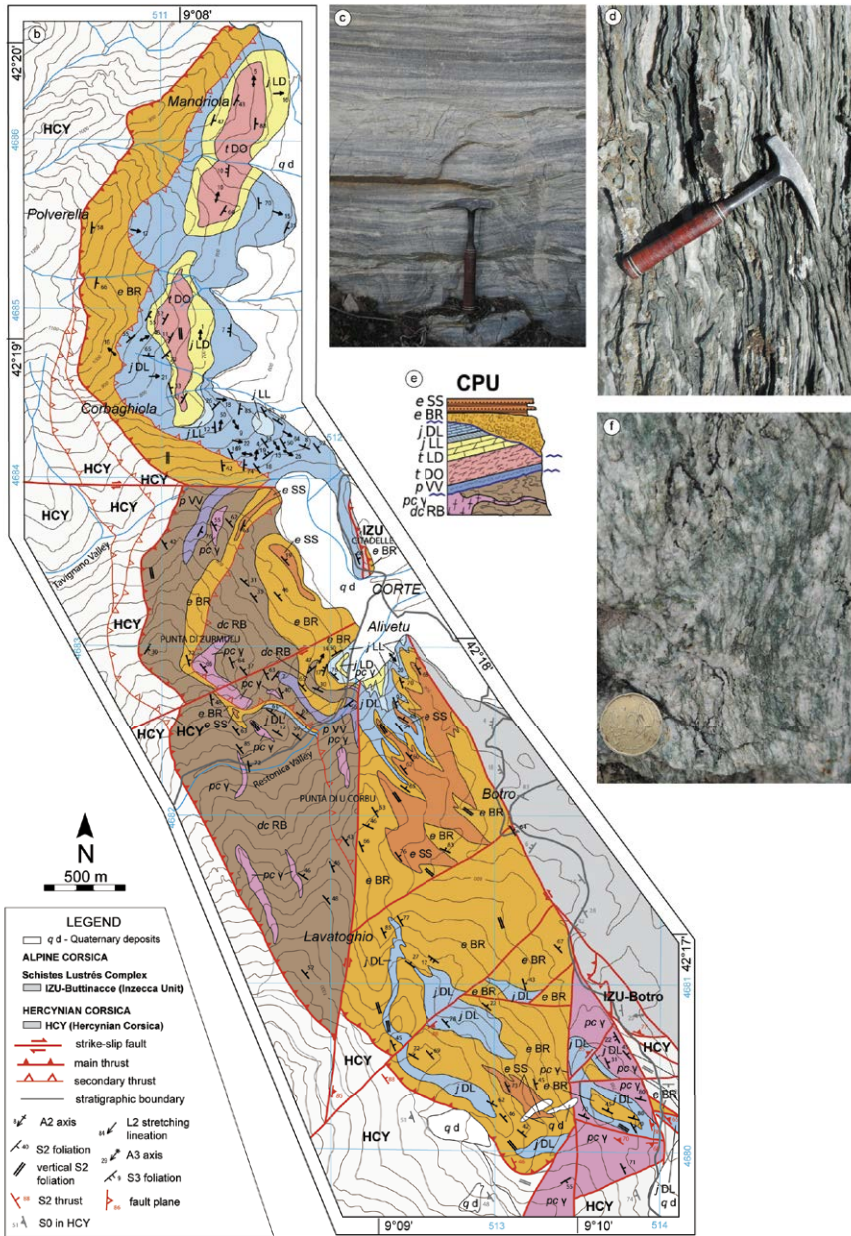
4.2 Corte area

The area between Ponte a Castirla and Corte (top-east: 42°38'45.35''N 9°12'28.66''E, bottom-west: 42°27'01.54''N 9°15'49.73''E) is characterized by a N-S trending stack of three continental metamorphic units (i.e. Castiglione-Popolasca, Croce d'Arbitro and Piedigriggio-Prato) belonging to the Lower Units, that are thrust onto HCY (Fig 4). The low-grade Caporalino Unit crop out NE of the area at the top of the Piedigriggio-Prato Unit, and its presence is strictly controlled by the CCSZ. Slices of the Schistes Lustrés Complex have been also mapped along the tectonic contacts between the Lower Units (Figs 8-10).

The Castiglione-Popolasca Unit (CPU, Fig 8) is constituted by a Permo-Carboniferous basement unconformably covered by a Mesozoic metasedimentary succession, which is in turn unconformably topped by a Tertiary siliciclastic metabreccias and metasandstones (Rossi et al. 1994). The basement consists of Roches Brunès Fm. (e.g. Funtana di Minaghiu, Fig 8a), intruded by metagranitoids of Permo-Carboniferous age (e.g. W of Pian de Pigno. Fig 8a,f) and covered by a thick package of Metavolcanic and Metavolcaniclastic Fm. of Permian age (e.g. Centrale électrique de Castirla, Fig 8a). The Mesozoic succession starts with the Norian Lower Metadolostone Fm. (e.g. E of Mandriola, Fig 8b), which consists of thick beds of grey metadolomites interspersed with levels of red pelites interpreted as paleosoils. The Lower Metadolostone Fm. is topped by the Hettangian-Sinemurian Metalimestone and Metadolostone Fm. (e.g. E of Corbaghiola, Fig 9b), represented by an alternance of thin to thick layer of grey metalimestones and light-grey metadolomites. At the top of the Metalimestone and Metadolostone Fm., a discontinuous layer of Laminated Metalimestone Fm. of Liassic age (e.g. E of Corbaghiola, Fig 8b) was found. The Mesozoic succession ends with the Detritic Metalimestone Fm. (e.g. E of Corbaghiola, Fig 8b,c), which consists of a matrix-supported polymict metabreccias, often characterized by well graded beds. The Mesozoic succession is unconformably covered by the Metabreccia Fm. (e.g. S of Castirla, Fig 8a,d), which shows a gradual transition to the Metasandstone Fm.. The metabreccias are represented by subrounded to subangular clasts of orthogneisses, paragneisses, micaschists, quartzites, marbles and metagranitoids enclosed in a fine-grain matrix. The Metasandstone Fm. tops the Metabreccia Fm. (W of

Figure 8. The Castiglione-Popolasca Unit: (a) geological map of the northern sector (modified after Di Rosa et al., 2017b): *dc* RB: Roches Brunes Fm., *pc* ■: metagranitoids, *p* VV: Metavolcanic and Metavolcaniclastic Fm., *t* DO: Lower Metadolostone Fm. and *e* BR: Metabreccia Fm.; (next page) (b) geological map of the southern sector; (c) Detritic Metalimestone Fm., Restonica Valley, Lias; (d) Metabreccia Fm., Punta di Zurmulu, Middle to Late Eocene; (e) lithostratigraphic log: *dc* RB: Roches Brunes Fm., *pc* ■: metagranitoids, *p* VV: Metavolcanic and Metavolcaniclastic Fm., *t* DO: Lower Metadolostone Fm., *j* LD: Metalimestone and Metadolostone Fm., *j* LL: Laminated Metalimestone Fm., *j* DL: Detritic Metalimestone Fm., *e* BR: Metabreccia Fm. and *e* SS: Metasandstone Fm. and (f) metagranitoids, Botro, Permo-Carboniferous.





Botro, Fig 8b) and consists of well bedded, medium layers of metapelites and metarenites, where the intervals of Bouma sequence are still preserved. These two formations are attributed to the Middle to Late Eocene, according to the occurrence of *Nummulites sp.* found in the Metasandstone Fm.

The Croce d'Arbitro Unit (CDU, Fig 9) shows a basement similar to that of the previous unit (e.g. Buttinacce, Fig 9a-c, Rossi et al. 1994), but includes metaconglomerates deposits of fluvial origin (Fonde-Fuata Metaconglomerates Fm., e.g. Fuata, Fig 9a,b) at the top of the Permian Metavolcanic and Metavolcaniclastic Fm. (e.g. Soveria, Fig 9a). The Mesozoic succession (Rossi et al. 1994) is reduced and consists of a thin level of Cavernoso Metalimestone Fm. (e.g W of Soveria, Fig 9a), a thick layer of Lower Metadolostone Fm.

Figure 9. The Croce d'Arbitro Unit: (a) geological map (modified after Di Rosa et al. 2017b); (b) lithostratigraphic log: *dc* RB: Roches Brunes Fm., *pc* □: metagranitoids, *p* VV: Metavolcanic and Metavolcaniclastic Fm., *p* CF: Fonde-Fuata Metaconglomerate Fm., *t* CV: Cavernoso Metalimestone Fm., *t* DO: Lower Metadolostone Fm., *j* LD: Metalimestone and Metadolostone Fm., *j* LL: Laminated Metalimestone Fm., *e* NM: Nummulite-bearing Metalimestone Fm., *e* BR: Metabreccia Fm. and *e* SS: Metasandstone Fm.; (c) Roches Brunes Fm., Devonian – Carboniferous and (d) Nummulite-bearing Metalimestone Fm., Middle to Late Eocene.

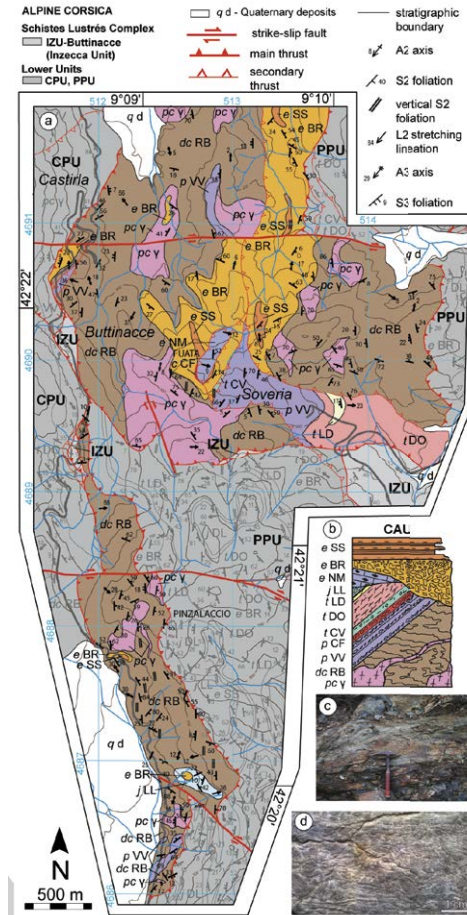
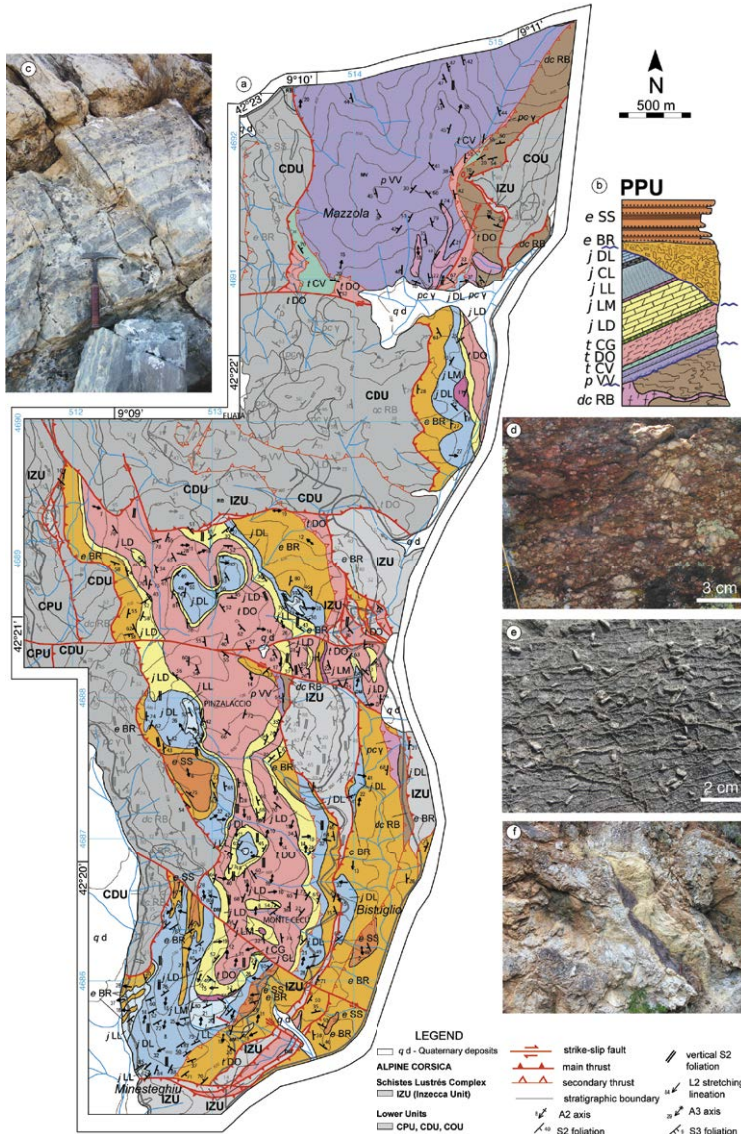


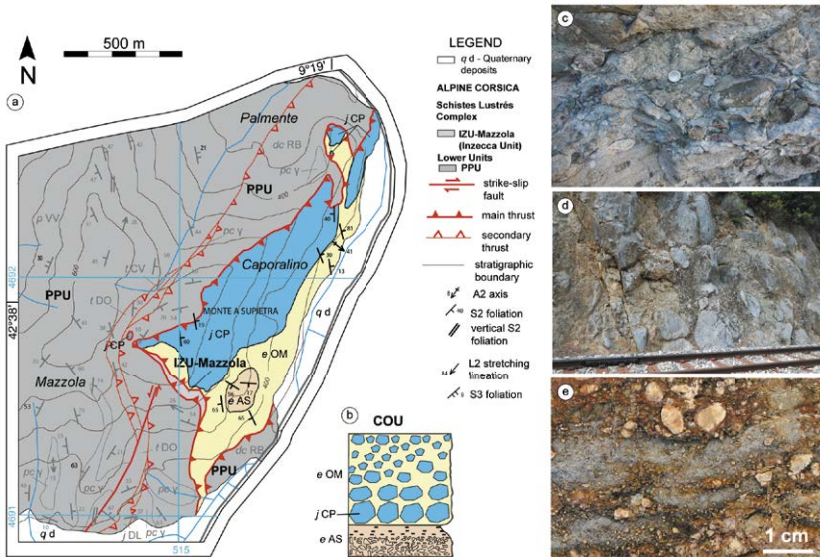
Figure 10. The Piedigriggio Unit: (a) geological map (modified after Di Rosa et al. 2017b); (b) lithostratigraphic log: *dc RB*: Roches Brunes Fm., *pc* \blacksquare : metagranitoids, *p VV*: Metavolcanic and Metavolcaniclastic Fm., *t CV*: Cavernoso Metalimestone Fm., *t DO*: Lower Metadolostone Fm., *t CG*: Metaconglomerate Fm., *j LD*: Metalimestone and Metadolostone Fm., *j LM*: Lumachella Metalimestone Fm., *j LL*: Laminated Metalimestone Fm., *j CM*: Cherty Metalimestone Fm., *j DL*: Detritic Metalimestone Fm., *e BR*: Metabreccia Fm. and *e SS*: Metasandstone Fm.; (c) Metalimestone and Metadolostone Fm., Jurassic; (d) Metabreccia Fm., Middle to Late Eocene; (e) Detritic Metalimestone Fm., Jurassic and (f) Lower Metadolostone Fm. Triassic.



alternated to Metalimestone and Metadolostone Fm. (e.g. E of Soveria, Fig 9a) and a thin discontinuous level of Laminated Metalimestone Fm. (e.g. S of Pinzalaccio, Fig 9a). The Tertiary succession is made of Nummulites-bearing Metalimestone Fm. (e.g. NW of Soveria, Fig 9a,d) of Middle Lutetian age and then by the Metabreccia and Metasandstone Fms. of Middle to Late Eocene age (e.g. N of Soveria, Fig 9a). The Tertiary formations unconformably cover the basement, the metavolcanics and metavolcaniclastics and the Fonde-Fuata Metaconglomerate Fms. (Di Rosa et al. 2017b).

Compared to the previous two units, the Piedigriggio-Prato Unit (PPU, Fig 10) is characterized by a more complete and thick Mesozoic succession (Rossi et al. 1994). The main differences (Di Rosa et al. 2017a) are the occurrence of the Cavernoso Metalimestone Fm. (e.g. W of Mazzola, Fig 10a) of Carnian age at the base of the Lower Metadolostone Fm. (Fig 10a,f, Durand-Delga 1984) and the presence of Norian Metaconglomerate Fm. (e.g. S of Monte Cecu, Fig 10a), consisting of fragments of metadolomites and metavolcanites in a carbonatic matrix, between the Lower Metadolostone and the Metalimestone and Metadolostone Fms. (Fig 10d). Another relevant difference is represented by the discontinuous levels of Lumachella Metalimestone Fm. (e.g. N of Minesteghio, Fig 10a) of Hettangian-Sinemurian age and Cherty Metalimestone Fm. (e.g. N of Minesteghio, Fig 10a) of Liassic age, that were found, respectively, at the base and at the top of the Laminated Metalimestones Fm.

Figure 11. The Caporalino Unit: (a) geological map (modified after Di Rosa et al. 2017b); (b) lithostratigraphic log; *e* AS: Setonia Sandstone Fm., *e* OM: Omessa Fm. *j* CP: slide-blocks of Jurassic limestones within the Omessa Fm.; (c) the Setonia Sandstone Fm., Middle to Late Eocene; (d) slide-blocks of Jurassic limestones in the Omessa Fm. and (e) the Setonia Sandstone Fm., Middle to Late Eocene.



The Caporalino-Sant'Angelo Unit (COU, Fig 11) crops out in the NE of the study area and consists of Setonia Sandstone (Fig 11e) and the Omessa Fms., both of the Middle to Late Eocene age (Puccinelli et al. 2012). In the study area, the Omessa Fm. is characterized by Middle Eocene clast-supported breccia made of huge slide-blocks of Middle to Late Jurassic carbonates (the so-called Caporalino Limestones; Fig 11d, Durand-Delga 1984); at the top of the Omessa Fm. the slide-blocks decrease in size until became rudites (Fig 11c).

The Schistes Lustrés Complex is made up of metaophiolites and related metasedimentary cover (Figs 8-10). In the mapping area they are represented by thin slices of metaserpentinites, metagabbros, metabasalts and calcschists (Rossi et al. 1994). Although the complete succession never occurs in the Corte area, on the base of the lithostratigraphy and the metamorphism these slices are attributed to the Inzecca Unit.

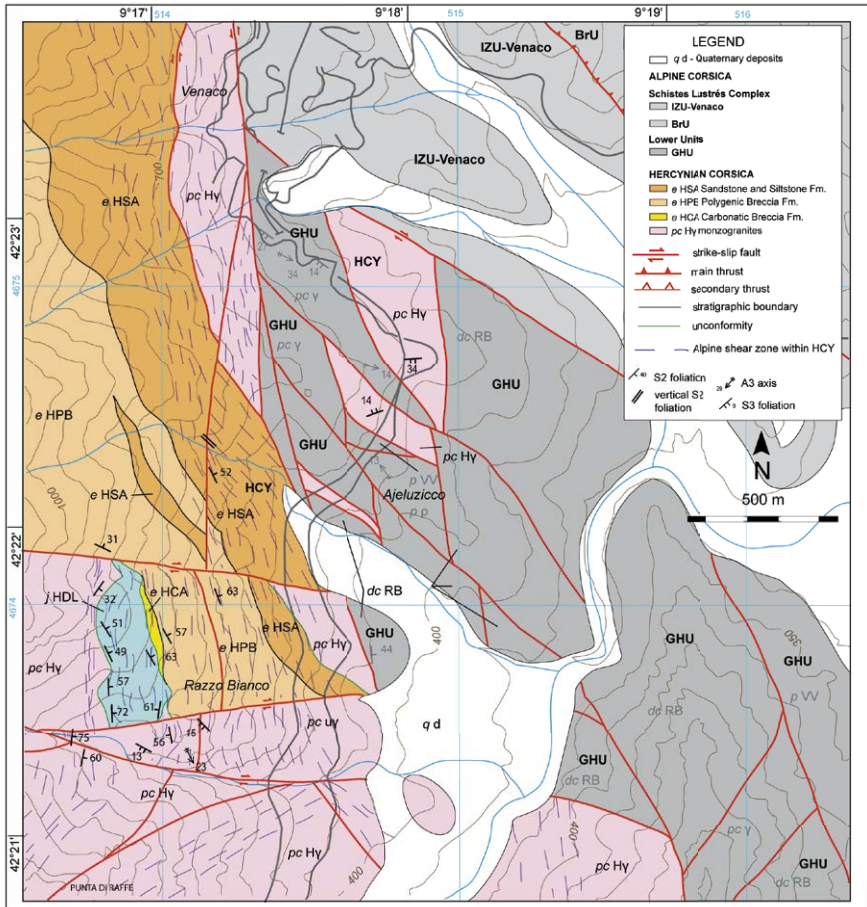
4.3 Venaco area

In the area between Venaco and Punta di Raffè (Fig 4), the HCY is overthrust to the north by the Schistes Lustrés Complex (i.e. Inzecca and Bagliaccone-Riventosa Units) and to the south by the Lower Units (i.e. Ghisoni Unit).

The HCY crops out in the western side of the area, and it includes Razzo Bianco (Figs 12-13), that is one of the rare sites where the primary relations between the Permo-Carboniferous granitoids and the Mesozoic and Tertiary covers are preserved (e.g. Amaudric du Chaffaut 1980). The Mesozoic covers consist of a 75 m thick sequence of metacarbonates, a fine-grained massive metalimestone alternated to layered metalimestones, mainly composed by calcite of metamorphic origin inside which rare cherts and clasts of quartz, pyrite and oxides are found. These detritus are more abundant at the bottom of the Detritic Limestone Fm., concurrent with the disconformity which separates it from the basement (Fig 13). The Tertiary covers consist of three formations: the older formation consists of a clast-supported metacarbonate breccia that unconformably tops the metagranitoids and the Detritic Limestone Fm.; the Carbonatic Breccia Fm., previously attributed to the Late Cretaceous (Amaudric du Chaffaut et al. 1985), is in this work assigned to the Middle to Late Eocene by correlation with the Metabreccias Fm. of the Monte Cecu area, that crops out about 15 km to the north of Razzo Bianco (Di Rosa et al. 2017a). The younger Tertiary formations consist in an alternation of matrix-supported polygenic metabreccias and metasandstones, also attributed to the Middle to Late Eocene by correlation with the Corte area (Di Rosa et al. 2017a; 2017b).

The Ghisoni Unit is the southernmost unit of the Lower Units. it extends from the Venaco town to Lugo di Nazza and is always sandwiched between the HCY and the Inzecca Unit of the Schistes Lustrés Complex. The Ghisoni Unit is made by Paleozoic lithotypes, including the Roches Brunès Fm., the Permo-Carboniferous metagranitoids, the Permian metarhyolites and the Metavolcanic

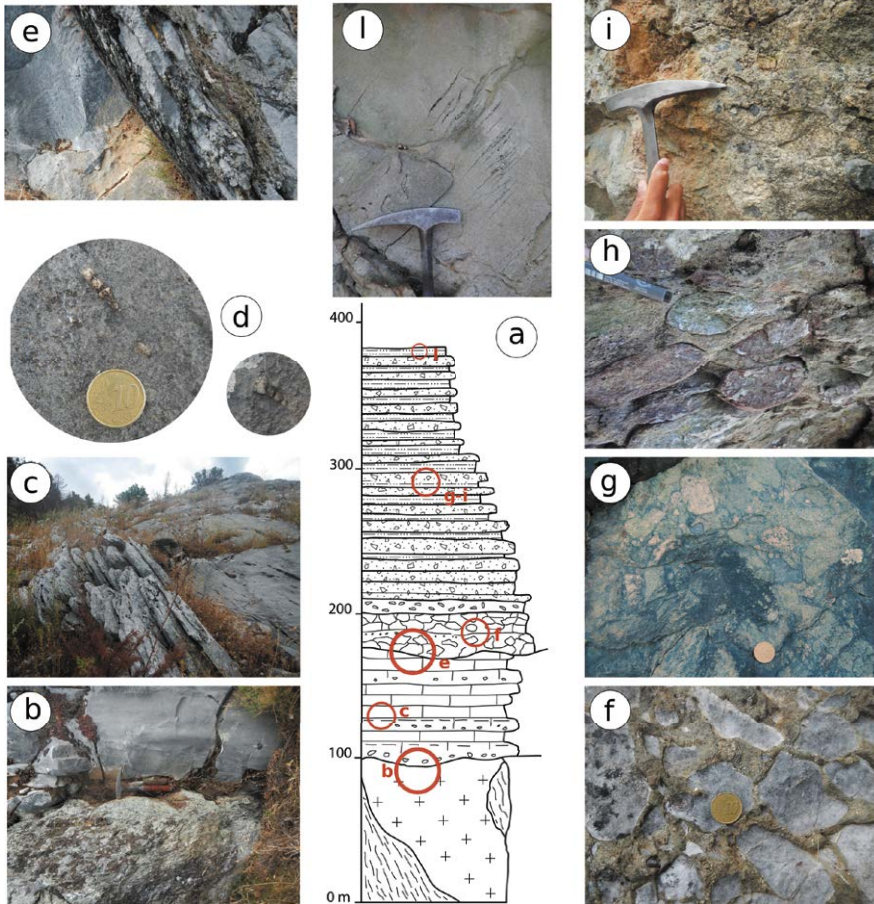
Figure 12. Geological map of the HCY in the Venaco area.



and Metavolcanoclastic Fm.. The Mesozoic and Tertiary covers do not occur in the study area, but probably crops out southward of Ghisoni area in Roc de Gunzoli, where a carbonatic succession is found (Amaudric du Chaffaut 1980). In the Venaco area all the Paleozoic lithotypes of the Ghisoni unit crop out (Amaudric du Chaffaut et al. 1985). The detailed study of the Venaco area made for this thesis allowed to collect new stratigraphic and structural data that are gathered in the geological map here presented. The main difference compared to the official 1:50.000 map (Feuille de Venaco, Amaudric du Chaffaut et al. 1985) is the identification of a fault system (i.e. the CCSZ) that splits and juxtaposes slices of the HCY, the Ghisoni Unit and the Schistes Lustrés Complex. Therefore, within the area where Amaudric du Chaffaut et al. (1985) reported the Roches Brunes Fm., several slices of Ghisoni Unit made of metagranitoids, Roches Brunes Fm. and Metavolcanic and Metavolcanoclastic Fm. are found alternate with slices of undeformed granitoids of the HCY.

The Schistes Lustrés Complex are represented by two units: the Inzecca Unit, that is thrust onto the Ghisoni Unit, and the Bagliaccone-Riventosa Unit at its top. The Inzecca Unit is mainly made of the Late Jurassic- Early Cretaceous covers (Amaudric du Chaffaut et al. 1985), whereas the Bagliaccone-Riventosa Unit is represented by calc-schists of unknown age.

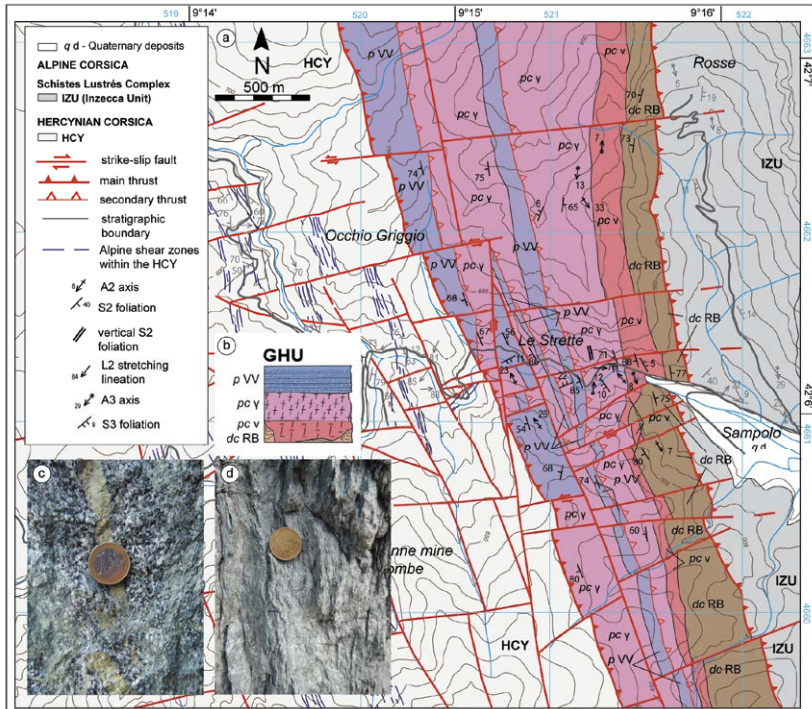
Figure 13. (a) Stratigraphic log of Razzo Bianco (modified after Amaudric du Chaffaut, 1980). The basement is made of *dc* HRB: Roches Brunes Fm. (Devonian-Carboniferous), intruded by *pc* Hy: monzogranites (Permo-Carboniferous); unconformity (b) separates this basement from the Mesozoic succession, made of (c) *j* HDL: Detritic Limestones Fm. (Lias), characterized by fossiliferous layers with reminds of (d) crinoid columnals. At the top of the carbonates, lies, in angular unconformity (e), the Tertiary deposits: (f) *e* HCA: Carbonatic Breccia Fm. (Late Eocene), (g-i) *e* PB: Polygenic Breccia Fm. (Late Eocene) and (l) *e* HSA: Sandstone and Siltstone Fm. (Late Eocene).



4.4 Noceta and Ghisoni areas

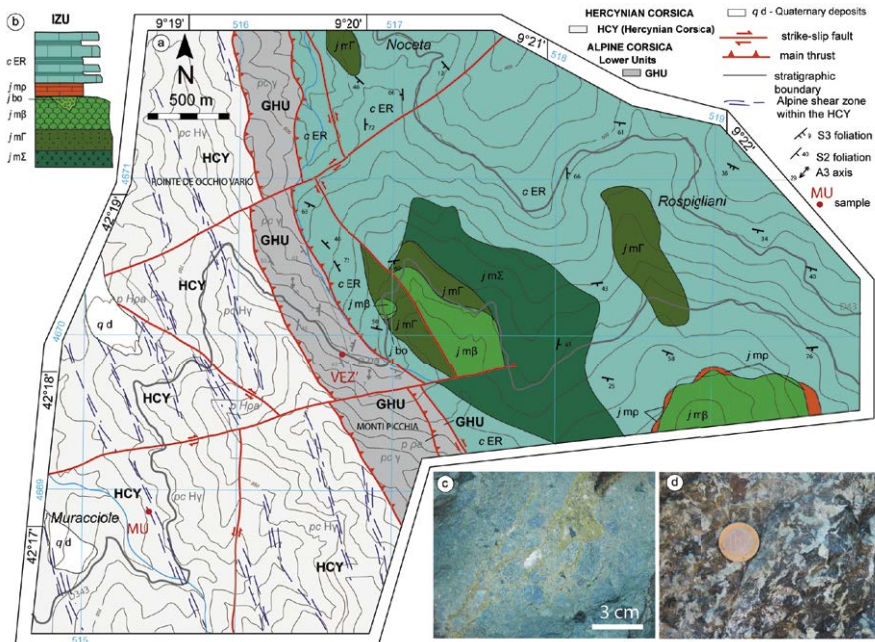
Despite the distance between these two sites, Noceta and Ghisoni areas have similar features (Figs 14-15). The Lower Units, represented by the Ghisoni Unit, crops out between the HCY and the Schistes Lustrés Complex (i.e. Inzecca Unit). The HCY is represented by granitoids intruded in Roches Brunes Fm. that rarely occurs; the granitoids, as well as the Permian rhyolites are cut by mafic dykes. The sedimentary covers are represented by the Permian Volcanic and Volcaniclastic Fm. and the Breccias of the Middle to Late Eocene. The Ghisoni Unit (Razzo Bianco-Sampolo Unit of Garfagnoli et al. 2009). consists of Roches Brunes Fm., metagranitoids, metarhyolites and the Metavolcanic and Metavolcanoclastic Fm. (Fig 14d). Only in the Ghisoni area, between the metagranitoids and the Roches Brunes Fm., a more felsic intrusive products (i.e. epidote-bearing metagabbros, Fig 14c) occurs. This rock type is a metagabbros mainly made of plagioclase, clinopyroxene and amphibole, and is characterized by 0.2-0.3 m thick boudinated mylonitic layers enriched in epidote and plagioclase. The epidote-bearing metagabbros are crosscut by 0.2 to 1 m thick

Figure 14. The Ghisoni Unit: (a) geological map of Ghisoni Unit in the Ghisoni area (modified after Di Rosa et al. 2018b); (b) lithostratigraphic log of the Ghisoni Unit: *dc* RB: Roches Brunes Fm., *pc* y: metagranitoids, *pc* ■: epidote-bearing metagabbros and *p* VV: Metavolcanic and Metavolcaniclastic Fm.; (c) epidote-bearing metagabbros, Permian and (d) Metavolcanic and Metavolcaniclastic Fm., Permian.



leucocratic bodies. The transition between the epidote-bearing metagabbros and the metagranitoids is developed in a band of about 20 m where bodies of epidote-bearing metagabbros are alternated to bodies of metagranitoids.

Figure 15. The Inzecca Unit in the Noceta area: (a) geological map; (b) lithostratigraphic log; *j mΣ* metaserpentinites; *j mΓ* metagabbros; *j mβ* metabasalts; *j bo* ophiolitic metabreccias; *mp*: metaradiolarites and *c ER* Erabajolo Fm; (c) ophiolitic metabreccias, Late Jurassic-Late Cretaceous, and (d) metagabbros, Late Jurassic-Late Cretaceous.



The Schistes Lustrés Complex are represented by the Inzecca Unit (Fig 15, Amaudric du Chaffaut et al. 1972; Caron et al. 1979; Padoa 1999). In the Noceta-Ghisoni area the succession is almost complete from the Late Jurassic – Late Cretaceous metaophillites (metaserpentinites, metagabbros, metabasalts and ophiolitic metabreccias) and related covers (i.e. metaradiolarites and the Erabajolo Fm.). The Erabajolo Fm. (Early to Late Cretaceous, Amaudric du Chaffaut et al. 1972; Marroni et al. 1992), cropping out in the Ghisoni area at the contact with GHU, consists in a thick succession of micaschists and marbles alternating with calcschists (Levi et al. 2007).

Chapter 5

The Alpine orogeny in Corsica: Insights from the Lower Units, the Hercynian Corsica and the Schistes Lustrés Complex

This chapter collects all the data that characterized the Alpine history of the study area, through the stratigraphic, deformation and metamorphic points of view. Because of the HCY, the Lower Units and the Schistes Lustrés Complex were interested by different processes and were involved in subduction at different times, the use of an “absolute” chronology might create confusion. Therefore, the order with which the groups of units will be presented is (1) the Lower Units, (2) the HCY and (3) the Schistes Lustrés Complex and only the order of the events within each group is chronological. Therefore, the first section is dedicated to the description of the Tertiary deposits related to the forebulge of the lower plate (§ Cap 5.1), that interests the HCY as well as the Lower Units. Follows the chapters related to the subduction of the oceanic crust and continental margin, through the analysis of the ductile deformation and related metamorphism of both the HCY and Alpine Corsica (§ Cap 5.2-5.5). The last section is dedicated to the brittle deformation that interest the whole area (§ Cap 5.6).

5.1 Pre-subduction deformation of the lower plate: middle to late Eocene forebulge's formation

A regional unconformity at the top of the Paleozoic basement and Mesozoic carbonates of the European plate has been recognized since the pioneering studies of Amaudric du Chaffaut (1975; Amaudric du Chaffaut and Villey 1979)

Maria Di Rosa, University of Pisa, Italy, maria.dirosa.scaglia@gmail.com, 0000-0002-1154-7429
FUP Best Practice in Scholarly Publishing (DOI 10.36253/fup_best_practice)

Maria Di Rosa, *Tectono-metamorphic evolution of the continental units along the edge between Alpine and Hercynian Corsica. Constraints for the exhumation models in the continental collision setting*, © 2021 Author(s), content CC BY 4.0 International, metadata CC0 1.0 Universal, published by Firenze University Press (www.fupress.com), ISSN 2705-0297 (online), ISBN 978-88-5518-420-5 (PDF), DOI 10.36253/978-88-5518-420-5

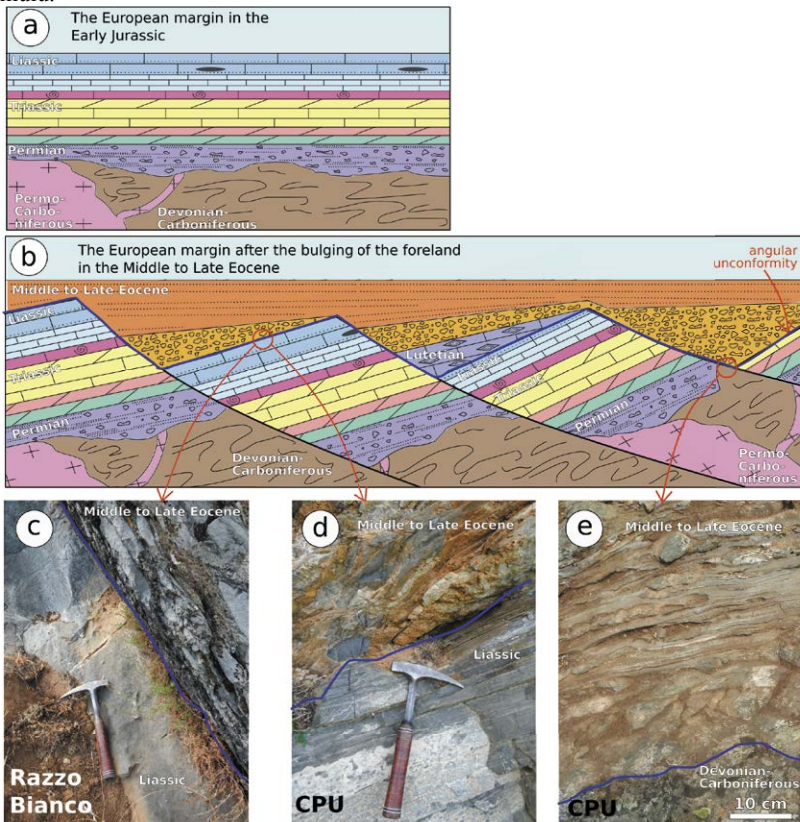
and Durand-Delga (1984). These authors associated the metabreccias lying at the top of the unconformity to the Late Cretaceous age, based on the presence of metacarbonatic clasts. Rossi et al. (1994) correlated the Metabreccia and Metasandstone Fms. with those of Caporalino, that at that time were associated to the Dogger age. Di Rosa et al. (2017a; 2017b) describe in the Corte area stratigraphic evidence allowing to attribute all the sedimentary covers above the unconformity to the Middle to Late Eocene age. Extending these observations to the other areas studied for this thesis, four different post-unconformity rock types were found at the top of the European margin (i.e. HCY) and the European derived units (i.e. Lower Units) that could be summarized as follow (from the older to the younger):

- Nummulite-bearing metalimestones, outcropping in the Soveria area (Nummulites-bearing Metalimestone Fm., Di Rosa et al. 2017b) that tops the CDU. They underlain the Metabreccia and the Metasandstone Fms.; the contact between them is marked by a shear zone, those s-c structures indicate a top-to-W sense of shear. Even if the primary contacts at its base (i.e. the Tertiary unconformity) and at its top with the Metabreccia Fm. are not preserved, the Nummulite-bearing Metalimestone Fm. was dated to the Middle Lutetian age (Maury 1910; Denizot 1952), and thus must be the youngest of the Eocenic succession.
- Carbonatic breccias/metabreccias, found in the Cima Pedani area (PEU, Rodriguez 1981; Rossi et al. 1994 and § Cap 4.1), in the Corte area (Monte Zurmulu and Corbaghiola, CPU, Amaudric du Chaffaut 1980 and § Cap 4.2) and in the Venaco area (i.e. Razzo Bianco, Amaudric du Chaffaut 1980 and § Cap 4.3). In Razzo Bianco, the angular unconformity between the underlying Mesozoic Limestone Fm. and the Carbonatic Breccia Fm. occurs, as well as its transition with the polygenic breccias at its top (Fig 16c).
- Polygenic breccias/metabreccias with rare carbonatic clasts, outcropping in Pedani (CAU and SCU, Rodriguez 1981; Rossi et al. 1994 and § Cap 4.1), in the Corte area (CPU, CDU and PPU, Rossi et al. 1994; Di Rosa et al. 2017a; 2017b and § Cap 4.2), in Venaco (Amaudric du Chaffaut 1980, Ferrandini et al. 2010 and § Cap 4.3) and in Ghisoni (Aicard et al. 1962; Durand-Delga 1978; Garfagnoli et al. 2009). The breccias was firstly dated, in the Ghisoni area, to the post-Berriasian age (Netelbeek 1951). Amaudric du Chaffaut et al. (1985), basing on the presence of carbonatic blocks, proposed the Cretaceous age for this rock type, outcropping in both the Lower Units (i.e. Pedani, Corte and Venaco areas) and the HCY (Venaco). Further step was done by Rossi et al. (1994), who assigned the polygenic breccias to the Dogger-Malm for correlation with those of Caporalino. These latter breccias were postdated to the Eocene by Puccinelli et al. (2012) because of the presence of Nummulites within the matrix between the clasts. Moreover, at the top of the breccias the stratigraphic transition with the metasandstone was found in the PPU (Di Rosa et al. 2017a).
- Sandstone/metasandstones, outcropping in Cima Pedani (SCU, Rodriguez 1981; Rossi et al. 1994 and § Cap 4.1), in Corte (CPU, CDU and PPU, Di

Rosa et al. 2017a; 2017b and § Cap 4.2) and in Venaco (Ferrandini et al. 2010 and § Cap 4.3). Within the pelitic layers of the sandstones of Venaco, Eocene shapes of planktonic foraminifera were described by Ferrandini et al. (2010). In addition, nummulites fossil were found in the Golo Valley (CDU, Di Rosa et al. 2017b). Therefore, this formation has been assigned to the Middle to Late Eocene.

It is important to underline that all the Tertiary deposits of the study area are made of clasts coming from the European margin (Paleozoic basement and Mesozoic covers); ophiolitic clasts (both deformed and undeformed) never occur in these lithotypes.

Figure 16. (a) sketch of the European margin at the Early Jurassic time; (b) reconstruction of the Middle to Late Eocene architecture of the European margin after the forebulge of the lower plate and the deposition of the Tertiary deposits; (c) angular unconformity between the Detritic Metalimestone Fm. and the Carbonatic Breccia Fm. of Razzo Bianco; (d) angular unconformity between the Detritic Metalimestone Fm. and the Metabreccia Fm. of CPU, quarry close the Campus Grimaldi di Corte and (e) angular unconformity between the Roches Brunes Fm. and the Metabreccia Fm. of CPU, Monte Zurmulu.



Although this succession does not occur complete in any site, and given the lack of fossils in many outcrops, the Middle to Late Eocene age is extended by all the carbonatic and polygenic breccias/metabreccias and sandstone/metasandstone by correlation (Fig 16). Basically, the Middle to Late Eocene is characterized by Nummulitic limestones followed by a fining-upward sequences of deposits made of clasts of materials ever more ancient from base (i.e. Liassic limestones) to the top (i.e. Permo-Carboniferous granitoids, Permian rhyolites and volcanics and volcanoclastics and lithotypes belonging to the Roches Brunes Fm.). The Middle to Late Eocene age thus proposed for the Tertiary deposits has first order implications in the geodynamic evolution of the European margin next to the subduction (§ Cap 7.1).

5.2 The Lower Units deformation history: from map- to microscale

The deformation history of the Lower Units regards the tectonic evolution of the European margin involved in the Alpine subduction. The Lower Units are affected by a polyphase ductile deformation of Tertiary age which can be divided into three phases, respectively, referred as D1, D2 and D3 (Bezert and Caby 1988; Malasoma et al. 2006; Malasoma and Marroni 2007; Di Rosa et al. 2017a). This pervasive deformation is observable from the map- to the micro-scale and concerns all the lithotypes that constitute the units belonging to the Lower Units (i.e. from the Paleozoic basement to the Tertiary metabreccias and metasandstone). Although the D1-D3 phases have similar features in all the Lower Units, the intensity of the deformation is different for each tectonic unit.

Generally, the D1 phase is almost totally transposed by the D2. Only in the F2 hinge zones is possible to distinguish the S1 foliation crenulated by the S2 foliation (Fig 17). Rare F1 non-cylindrical folds are observed in the Corte area (Fig 17d). At the microscale the S1 foliation is well preserved in the metapelites in the microlithons of the S2 foliation. To the D2 phase are associated the main structures observed on fields: F2 isoclinal folds (Fig 17e), an S2 foliation along which necking and boudinages are commonly observed and a L2 stretching lineation. Only in the Pedani area sheath folds associated to the D2 phase are found. Several top-to-W ductile shear zones, characterized by s-c fabric are developed during the D2 phase in all the areas studied. At the microscale the S2 foliation is recognizable in all the lithotypes, as well as F2 microfolds and sigma-type porphyroclasts (Fig 18). The D3 phase produce F3 open to close folds, everywhere characterized by a clear eastward/southeastward vergence and by a flat-lying S3 foliation (Fig 17 f). This last generation of folds is coaxial to the previous one, and thus type-3 interference pattern of Ramsay's classification is generated (Ramsay 1967). The morphology of the S3 foliation and the solely recrystallization of Cal suggest the development of the D3 phase at shallow structural level during the final stage of exhumation. The F3 folds not only fold the previous S1/S2 foliation, but also the tectonic contacts between the Lower Units and the Schistes Lustrés Complex. This evidence, considering also the

Figure 17. Sketch of the polyphasic deformation in the Lower Units at the macroscale. (a) D1, (b) D2 and (c) D3 phases; (d) F1 sheath folds in the Laminated Metalimestone Fm., PPU, Monte Cecu; (e) F2 isoclinal folds with S2 subvertical axial plane foliation, Metasandstone Fm., PPU, Bistuglio and (f) F3 open folds with S3 subhorizontal axial plane foliation in metagranitoids, GHU, Ghisoni.

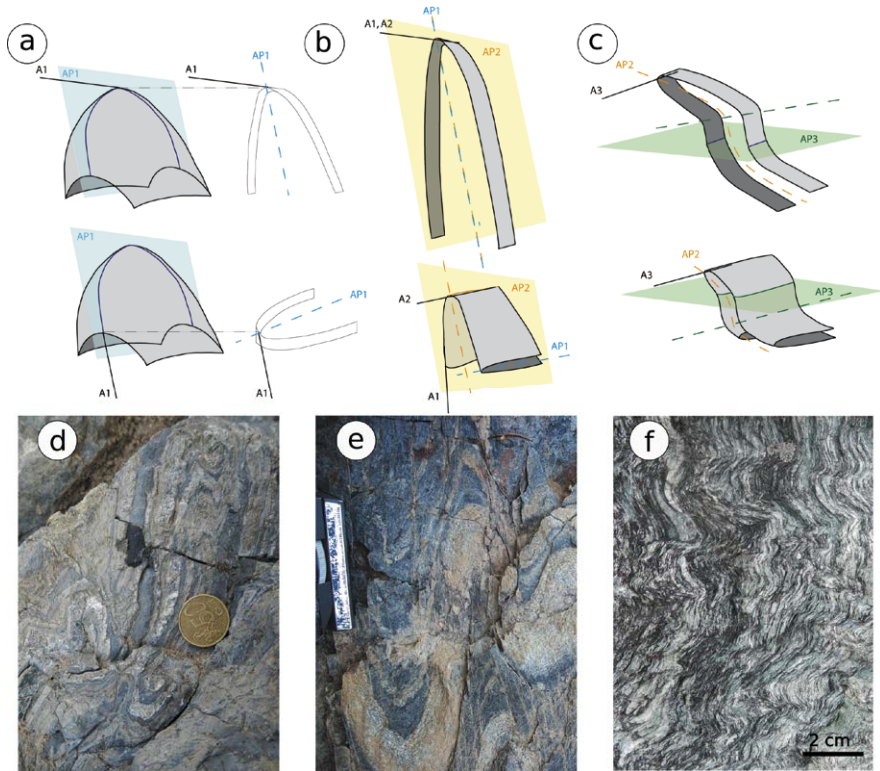
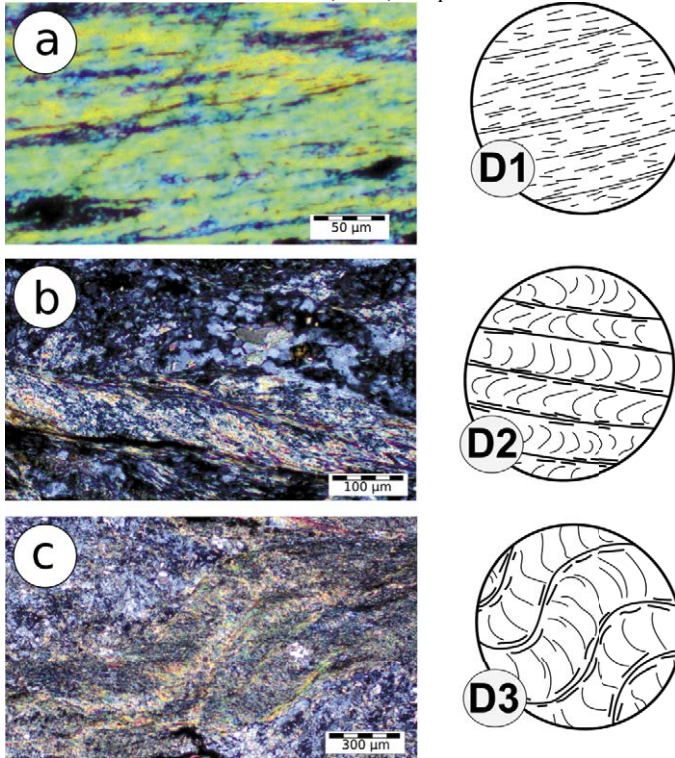


Table 2. Mineral abbreviations.

Abbr.	Mineral	Abbr.	Mineral	Abbr.	Mineral
Alb	Albite	Cl	Clinopyroxene	Na/Ca Amp	Sodic/calcic amphibole
All	Allanite	Da	Daphnite	Phg	Phengite
Am	Amesite	Epd	Epidote	Py	Pyrophyllite
Amp	Amphibole	Fds	Feldspar	Pyx	Pyroxene
Apt	Apatite	Hbl	Hornblende	Qtz	quartz
Bit	biotite	K Fds	K-feldspar	Rut	Rutile
Cal	Calcite	Lws	Lawsonite	Sud	Sudoite
Ce	Celadonite	Mnz	Monazite	wt	water
Chl	Chlorite	Mu	Muscovite	Zrc	Zircon

different P-T conditions at which the third generation of Chl-Phg were grown, implies that the coupling of the Lower Units, as well as the Lower Units with the Schistes Lustrés Complex, happened during the late D2 phase (Di Rosa et al. 2017b).

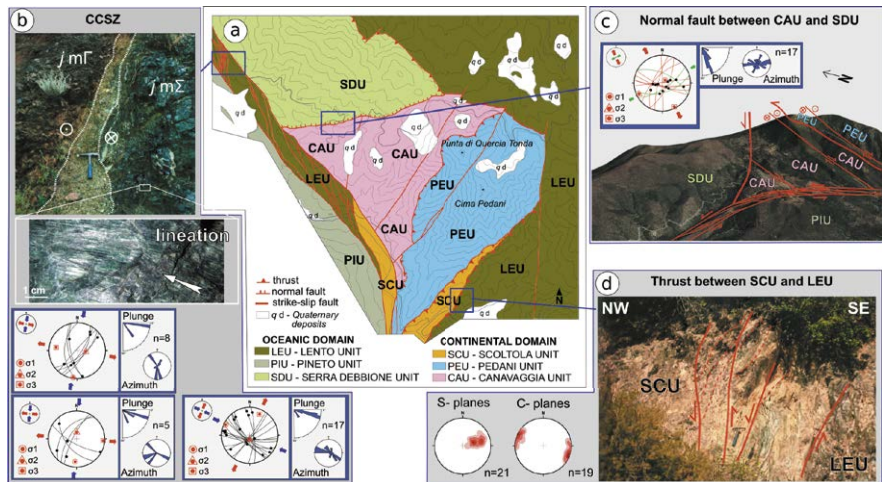
Figure 18. 2 Sketch of the polyphasic deformation in the Lower Units at the microscale. (a) S1 foliation in the metapelitic layer of the Metasandstone Fm., CPU, sample CM22B; (b) S1 and S2 foliations in the Metabreccia Fm., PPU, sample CM21 and (c) S1-S2-S3 foliation in the Metabreccia Fm., PPU, sample CM32C.



5.2.1 Cima Pedani

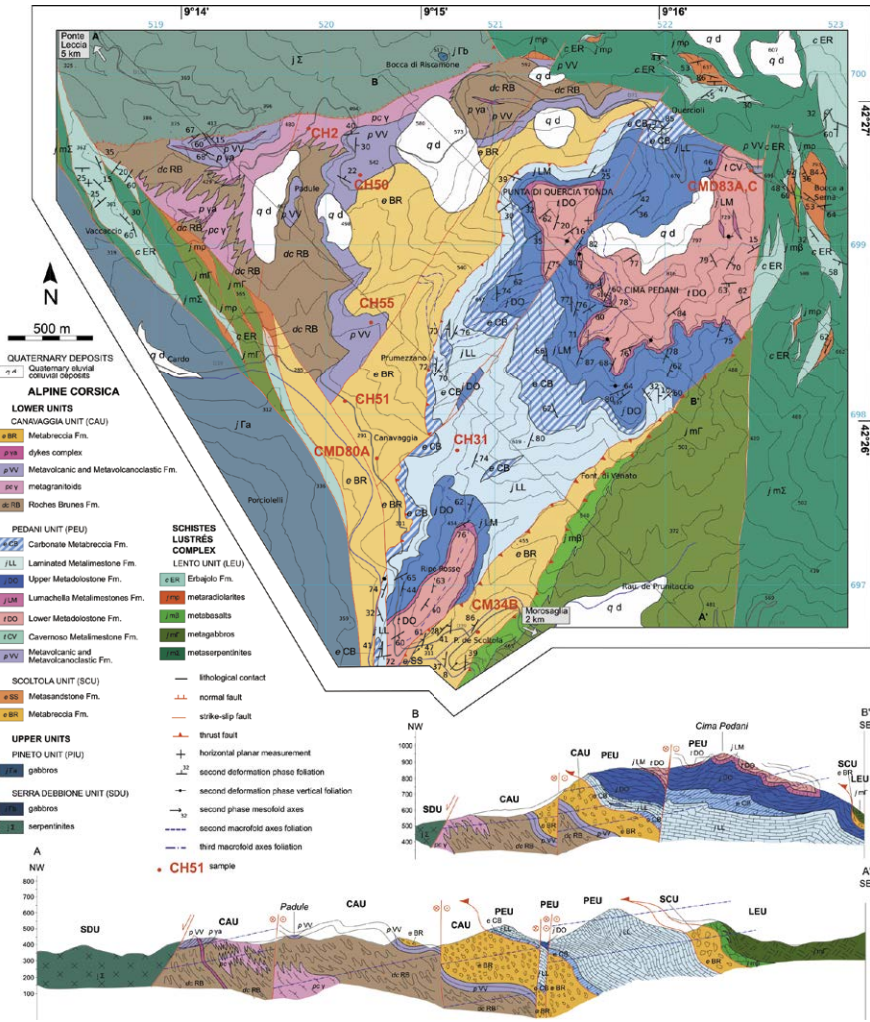
From the structural point of view, the core of the Cima Pedani tectonic window consists of a south-east dipping stack of tectonic units (Fig 19). Each unit is bounded by low-angle cataclastic shear zones, not dipping more than 40°, with top-to-NNW sense of shear. A well-exposed example of unit-bounding cataclastic shear zones has been identified between CAU and PEU, west of Punta di Quercia Tonda. The outcrop consists mainly of deformed Laminated Metalimestone Fm., showing well-developed s-c structures.

Figure 19. (a) tectonic sketch map of Cima Pedani area with stress analysis results (Wintensor software) of (b) the Central Corsica Shear Zone and (c) the normal fault between CAU and SDU; stereograms (Schmidt net, lower hemisphere) with traces of fault planes, observed slip lines and slip senses. The main stress axes (σ_1 , σ_2 , σ_3) and type of stress are reported. (d) s-c fabric on the thrust between SCU and LEU and related stereographic projections (the tectonic contact is inverted by the D3 folds). Modified after Di Rosa et al. 2018a.



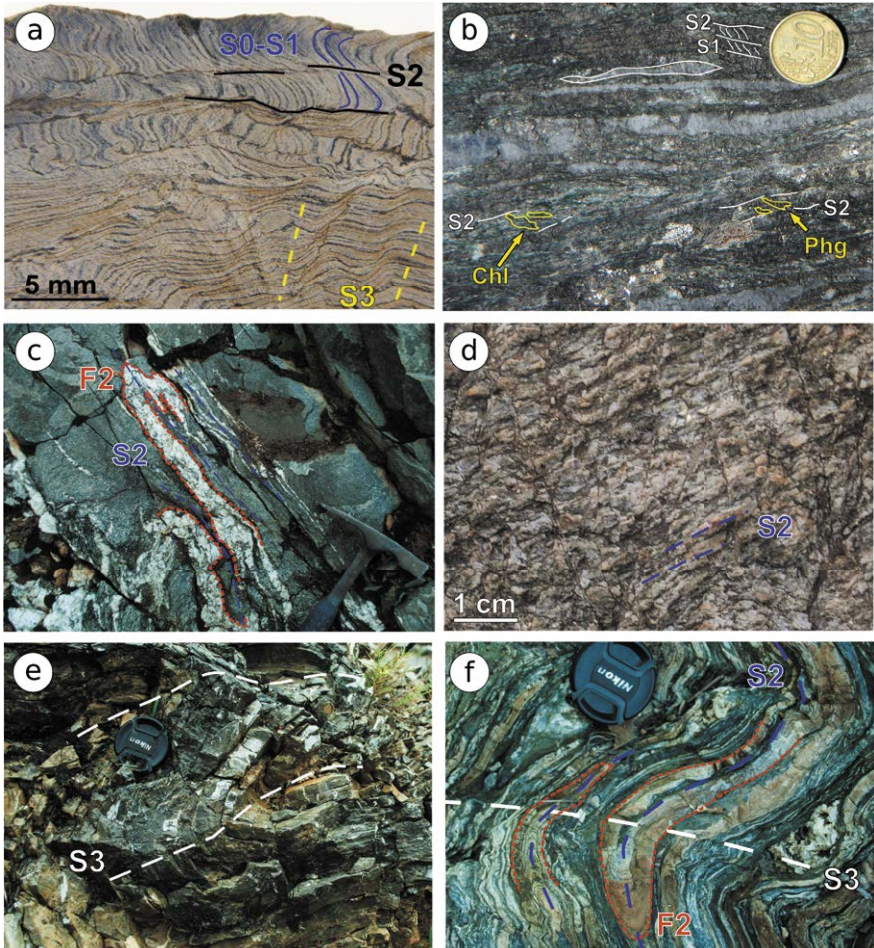
The boundaries of the Lower Units with LEU, SDU and PIU are different in the western, southern and north-eastern sides of the tectonic window. In the western side, the boundary between the Lower Units and the PIU is represented by a NNW-SSE trending strike-slip fault system, interpreted as one of the branches of the Central Corsica Shear Zone (CCSZ). It occurs as a 200-300 m wide fault zone made up of subvertical, lozenge shaped tectonic slices belonging to different units, mainly serpentinites from SDU, gabbros from PIU, meta-breccias from SCU and Roches Brunes Fm. from CAU (Fig 19b). Moreover, in the northern sector of the strike-slip fault system, slices of metabasalts, metagabbros, metacherts and Erbjolo Fm. referable to the Lento Unit, have been identified. The strike-slip fault system also produces up to two kilometers long conjugate faults where two dextral faults cutting the whole PEU and CAU can be recognized. A brittle, steep shear zone with transtensive sense of shear represents the northern limit of the tectonic window and juxtaposes the CAU and PEU with the couple SDU and LEU (Fig 19c). The fault shows an E-W trend at an angle of about 60° to the strike-slip fault system. According to this orientation, this fault can be interpreted as transtensional fault coeval to the strike-slip fault system. The southern border of the Cima Pedani tectonic window is defined by a high-angle, SW-dipping brittle shear zone through which the LEU overthrusts the SCU (Fig 19d). The shear zones feature well developed

Figure 20. Geological map of the Cima Pedani area and related cross sections (modified after Di Rosa et al. 2018a).



s-c structures, with the attitude of the s and c planes consistent with a top-to-NW sense of shear. Secondary, cataclastic shear zones are found parallel to the main boundary of the two in the Metabreccia Fm. of SCU, as well as in the metabasalts of the LEU. All these shear zones are deformed by open folds with sub-horizontal axial planes. At the map-scale it is observed that in the Pedani area the stacking of the continental units (CAU, PEU and SCU) as well as their coupling with LEU occurred before the last ductile phase (i.e. D3), because of the folding of the tectonic contacts that border the units (Fig 20). In the field, the

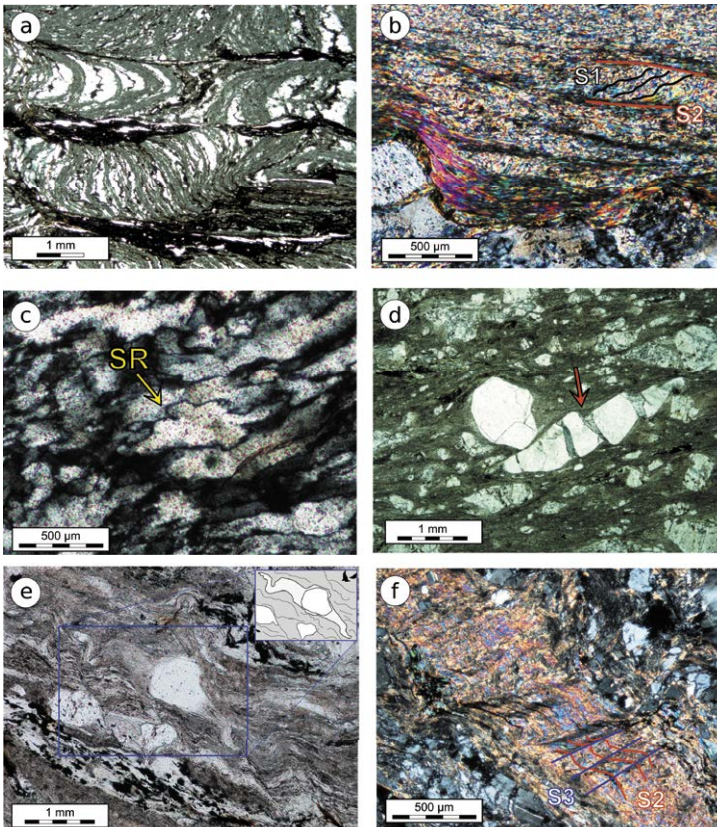
Figure 21. (a) S1-S2 foliation interference pattern in the Laminated Metalimestone Fm., PEU (b) S1-S2 foliations relationships in the Metabreccia Fm., CAU, Chlorite (Chl) and Phengite (Phg) minerals are found along the S1 foliation relics. An elongated clast of meta-limestone is also shown, (c) F2 isoclinal fold and S2 axial plain foliation in the Metasandstone Fm., SCU, (d) S2 foliation in the metagranitoids of CAU, (e) S3 foliation in the Laminated Metalimestone Fm. of PEU and (f) F2 folds re-folded by D3 folding phase (the S3 axial plain foliation is shown in white) in the Metabreccia Fm., SCU (modified after Di Rosa et al. 2018a).



structures of the D1 phase has been observed only west of Punta di Quercia Tonda, where the Laminated Metalimestone Fm. of the PEU preserves relics of the S1 foliation within the microlithons along the S2 foliation (Fig 21a). The S1 foliation is generally observed in the hinge zone of the F2 folds where the S1

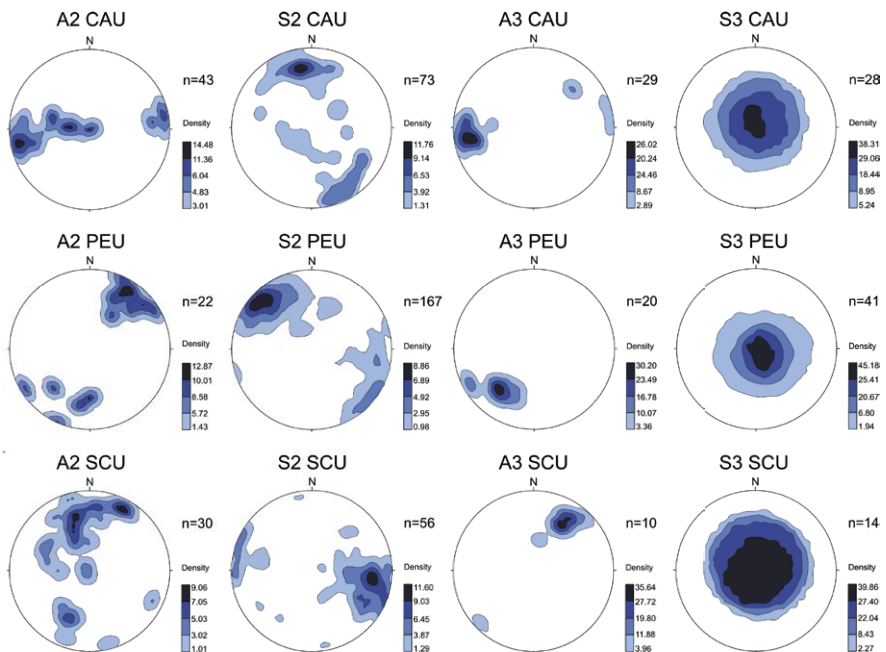
foliation occurs in the microlithons along the S2 foliation as coarse-grained, continuous schistosity. At the microscale, relics of the S1 foliation can be easily observed in the pelitic layers contained in the Metavolcanic and Metavolcaniclastic Fm., as well as in the Laminated Metalimestone fm. (Fig 21a), in the metabreccias and metasandstones. In the Metavolcanic and Metavolcaniclastic Fm. the pelitic fraction represents the matrix of the lithotype

Figure 22. (a) S1-S2 foliations in the Laminated Metalimestone Fm., PEU (close up view of Fig.5.6a), sample CH31, crossed Nicols; (b) S1-S2 relationships in the Metavolcanic and Metavolcanoclastic Fm. of PEU, sample CH55, crossed nicols, showing discrete to gradational transition, (c) subgrain rotation (indicated by yellow arrow) in the metagranitoids of CAU, sample CH2, crossed Nicols; (d) bookshelf structure in a quartz crystal (indicated by red arrow) in the pelitic matrix of the Metavolcanic and Metavolcanoclastic Fm. of PEU) sample CH50, parallel Nicols; (e) π -type porphyroblast within the S2 foliation of the Metabreccia Fm. of CAU, sample CH51, parallel Nicols; (f) S2-S3 interference pattern in a pelitic layer on the Metabreccia Fm. of CAU, sample CH51, crossed Nicols (modified after Di Rosa et al. 2018a).



where aggregates of Qtz, K Fds and Alb + Qtz + opaque oxides with rare Epd (i.e. pistacite), All and titanite (Fig 21b). The Laminated Metalimestone Fm. consists in an alternance of carbonatic and pelitic layers, whose composition is mainly made of Chl + Phg + opaque oxides. In the Metabreccia and Metasandstone Fms. the pelitic fraction represents the matrix of these lithotypes and is composed by abundant Chl, Phg, Alb, Qtz and K Fds with minor quantities of Cal, Epd, titanite and Mnz.

Figure 23. Sterographic plots of the structural data collected in the Cima Pedani area (Schmidt net, lower hemisphere). Modified after Di Rosa et al. 2018a.



The D2 phase produces the most evident structures at field-scale that consist of widespread F2 folds with an associated penetrative S2 axial plane foliation. Depending on lithology, F2 folds show variable geometries, but can be generally described as tight to isoclinal, non-cylindrical folds: as a result, the strikes of the A2 axes are relatively scattered (Fig 23). The axial plane S2 foliation in the metapelites and metasiltites can be defined as a spaced, pervasive anisotropy, commonly anastomosed. Although re-oriented by the subsequent deformation phase, the S2 foliation is generally NE-SW striking with a variable dip, but everywhere parallel to the boundaries between the different units. In the metabreccias, the D2 phase produces high-strained bands with stretched clasts with 7:1 R_{xz} ratio (S.D.=0,167, Dunnet 1969). The D2 phase also yield the

stretching of the fossil content in metalimestones, as recognized in the Lumachella Metalimestone Fm. of the PEU. At the microscale, the S2 foliation has been recognized mainly in the metapelites (i.e. metavolcanites, metabreccias and metasandstones) and metagranitoids and impure metalimestones (i.e. Laminated Metalimestone Fm., Fig.5.9). In the metapelites and metasandstones the S2 foliation is represented by a composite layering defined by the overprinting of S2 foliation, mainly made of Chl+Phg+Qtz+Alb, on the S1 (Fig 22). In the F2 hinge-zone, the S2 foliation can be classified as crenulation cleavage characterized by smooth cleavage domains showing a gradational to discrete transition to the microlithons where the S1 foliation is still preserved. The S2 foliation is made up of Chl+Phg+Qtz+Cal of smaller grain size compared to those that recrystallized during the D1 phase. . In the metagranitoids, the S2 foliation poorly developed protomylonitic fabrics and is marked by discontinuous layers of recrystallized Phg, wrapping cm-sized Fds and Qtz grains, aggregates of Qtz+Fds, and lenses of very fine-grained (less than 6 μm) recrystallized Qtz and Fds. Cm-sized Phg show undulatory extinction and kinking. In the metalimestones, the S2 foliation is defined by a fine-grained carbonates, settled in a granoblastic texture. Qtz and Fds crystals often show angular shape and reduction grain size produced by microcracking and microfaulting indicative of a late to post-foliation cataclastic event. In the metabreccias, pressure shadows that sometimes surround the larger crystals can be classified as σ -type porphyroclasts. The asymmetric tails of the sigma-type porphyroclasts systematically show a top-to-NW sense of shear, that well fit with the meso-scale kinematics deduced by the s-c structures at the boundary between the different continental units. In the field, the D3 phase is mainly represented by cylindrical, open to close F3 folds, commonly associated to sub-horizontal axial plane foliation. The interference pattern due to overprinting of the F2 folds by the F3 ones can be classified as Type 3 of Ramsay and Huber (1987). It is important to outline that the F3 folds deform also the boundaries between all the units of the Cima Pedani tectonic window. In the whole study area, the S3 foliation is always subhorizontal whereas the A3 axes are gently dip to NE and W-SW (Fig 23). At the microscale, a weak S3 foliation has been observed in the metapelites and metasandstones, metavolcanites and metavolcaniclastics, where it is classifiable as crenulation cleavage. Along the S3 foliation only minor metamorphic recrystallization of Qtz, Cal and Fe-oxides occurs. In the more competent lithotypes, as metagranitoids and metalimestones, the S3 foliation occurs as disjunctive cleavage.

5.2.2 Corte

The study area, about 60 km² wide, is characterized by a north-south trending stack of three continental metamorphic units (e.g. CPU, CDU and PPU, § Cap. 3.1 *Corte*) belonging to the Lower Units, that are thrust onto HCY Corsica (Fig 24). Slices of Schistes Lustrés Complex have been mapped along the shear zones at the boundaries of the Lower Units. Eastward, the CCSZ separates the

Lower Units from the not metamorphic Caporalino Unit and the Schistes Lustrés Complex (Fig 25). In the CPU, CDU and PPU the D1 phase is characterized by rarely preserved isoclinal F1 folds with acute to sub-acute hinges. Sheath folds have been observed in CPU and PPU (Fig 26).

Figure 24. (a) Tectonic sketch map and cross section of the area between Castirla, Caporalino and Corte; (b) landscape of the south side of the Restonica Valley and (c) landscape of the northern side of the Restonica Valley (modified after Di Rosa et al. 2017b).

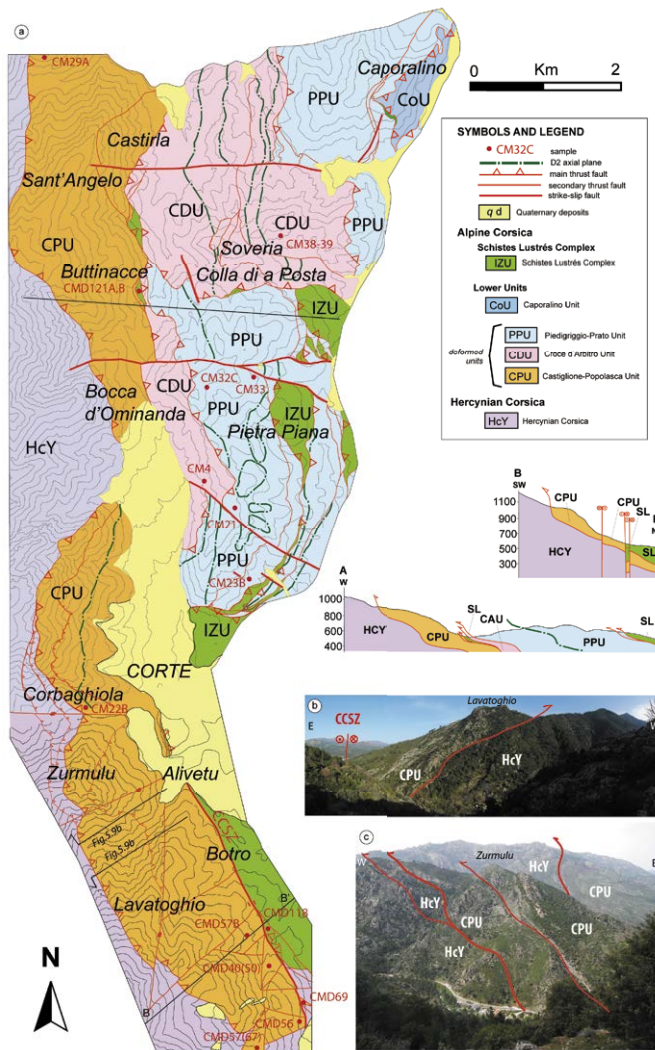
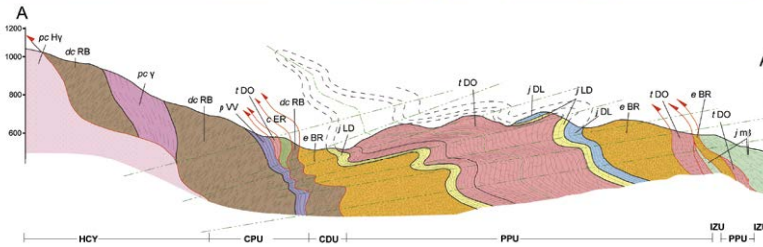
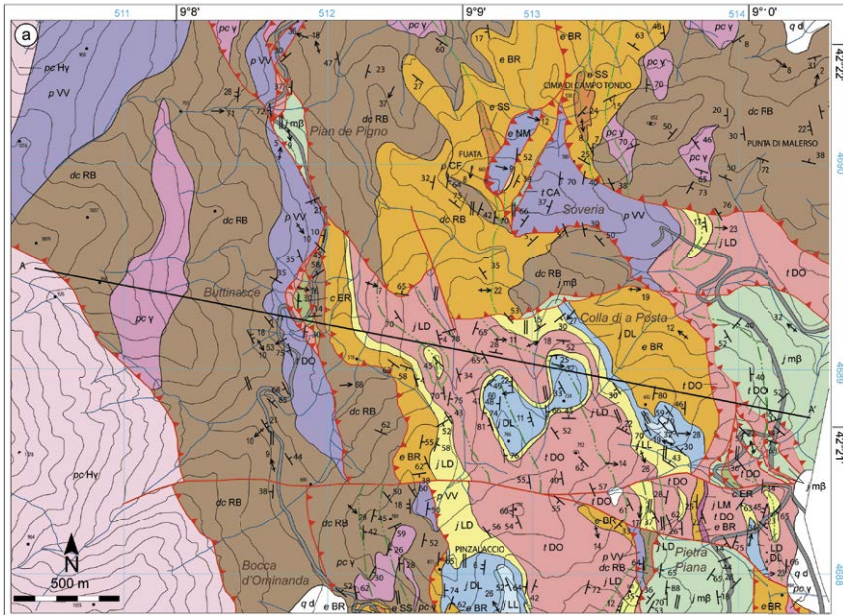


Figure 25. Geological map of the Castirla-Casanova area and related cross sections. (a) Castirla-Soveria, modified after Di Rosa et al. 2017b; (b) Soveria-Monte Cecu, Di Rosa et al. 2018b; (c) Botro and (d) cross sections of Botro: HCY: Hercynian Corsica, CPU: Castiglione-Popolasca Unit, BRU: Bagliacone-Riventosa Unit, *dc* HRB: Roches Brunes Fm. (not affected by the Alpine deformation), *pc* H□: granitoids, *p* HVV: Volcanic and Volcaniclastic Fm., *e* PB: Poligenic Breccia Fm., *e* SA: Sandstone and Siltstone Fm., *pc* *y*: metagranitoids, *dc* RB: Roches Brunes Fm., *p* VV: Metavolcanic and Metavolcaniclastic Fm., *t* DO: Lower Metadolostone Fm., *j* LD: Metalimestone and Metadolostone Fm., *j* LL: Laminated Metalimestone Fm., *j* DL: Detritic Metalimestone Fm., *e* BR: Metabreccia Fm., *e* SS: Metasandstone Fm..



LEGEND

□ q d - Quaternary deposits

ALPINE CORSICA

Schistes Lustrés Complex

IZU (Inzecca Unit)

■ c ER - Erbajolo Fm.

■ j mβ - metabasalts

Lower Units

PPU (Piedigriggio-Prato Unit)

■ e SS - Metasandstone Fm.

■ e BR - Metabreccia Fm.

■ j DL - Detritic Metalimestone Fm.

■ j LL - Laminated Metalimestone Fm.

■ j LM - Lumachella Metalimestone Fm.

■ j LD - Metalimestone and Metadolostone Fm.

■ t DO - Lower Metadolostone Fm.

■ p VV - Metavolcanic and Metavolcaniclastic Fm.

■ pc γ - metagranitoids

■ dc RB - Roches Brunes Fm.

CDU (Croce d'Arbitro Unit)

■ e SS - Metasandstone Fm.

■ e BR - Metabreccia Fm.

■ e BR - Nummulitite-bearing Metalimestone Fm.

■ j LD - Fonde-Fuata Metaconglomerate Fm.

■ j LD - Metalimestone and Metadolostone Fm.

■ t DO - Lower Metadolostone Fm.

■ t CA - Cavernoso Fm.

■ p VV - Metavolcanic and Metavolcaniclastic Fm.

■ pc γ - metagranitoids

■ dc RB - Roches Brunes Fm.

CPU (Castiglione-Popolasca Unit)

■ t DO - Lower Metadolostone Fm.

■ p VV - Metavolcanic and Metavolcaniclastic Fm.

■ pc γ - metagranitoids

■ dc RB - Roches Brunes Fm.

HERCYNIAN CORSICA

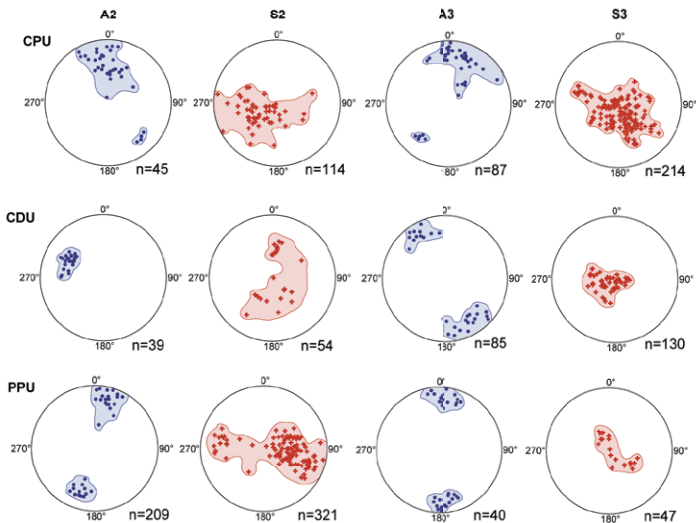
□ HCY - Hercynian Domain

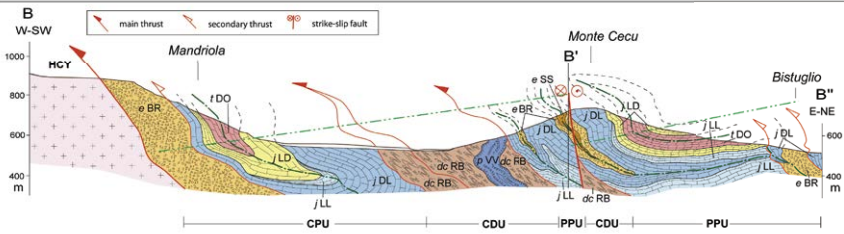
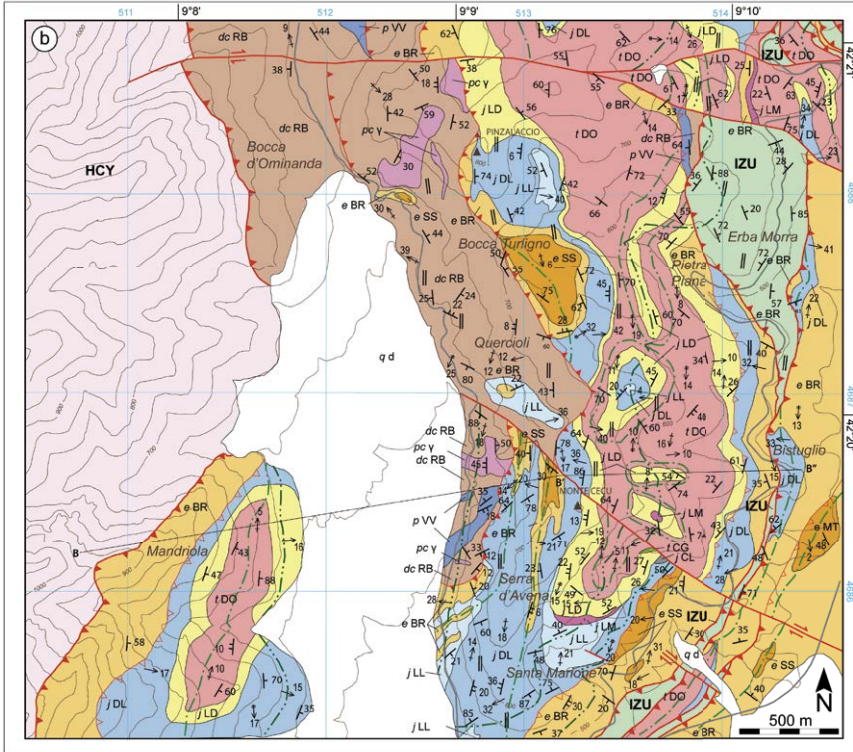
SYMBOLS

- strike-slip fault
- main thrust
- secondary thrust
- minor thrust
- stratigraphic boundary
- D2 axial plane trace
- D3 axial plane trace
- 8 / A2 axis
- 10 / S2 foliation
- 10 / vertical S2 foliation
- 84 / L2 mineral stretching lineation
- 29 / A3 axis
- 9 / S3 foliation
- A — A' trace of the geological cross-section

STEREOGRAPHIC PROJECTIONS

Schmidt





LEGEND

□ q d - Quaternary deposits

ALPINE CORSICA

Schistes Lustrés Complex

□ izu (Inzecca Unit)

Lower Units

PPU (Piedigriggio-Prato Unit)

■ e SS - Metasandstone Fm.

■ e BR - Metabreccia Fm.

■ j DL - Detritic Metalimestone Fm.

■ j CL - Cherty Metalimestone Fm.

■ j LL - Laminated Metalimestone Fm.

■ j LM - Lumachella Metalimestone Fm.

■ j LD - Metalimestone and Metadolostone Fm.

■ t CG - Metaconglomerate Fm.

■ t DO - Lower Metadolostone Fm.

■ p VV - Metavolcanic and Metavolcaniclastic Fm.

■ dc RB - Roches Brunes Fm.

CDU (Croce d'Arbitro Unit)

■ e SS - Metasandstone Fm.

■ e BR - Metabreccia Fm.

■ j LL - Laminated Metalimestone Fm.

■ p VV - Metavolcanic and Metavolcaniclastic Fm.

■ pc γ - metagranitoids

■ dc RB - Roches Brunes Fm.

CPU (Castiglione-Popolasca Unit)

■ e BR - Metabreccia Fm.

■ j DL - Detritic Metalimestone Fm.

■ j LD - Metalimestone and Metadolostone Fm.

■ t DO - Lower Metadolostone Fm.

■ dc RB - Roches Brunes Fm.

HERCYNIAN CORSICA

□ HCY - Hercynian Domain

SYMBOLS

— strike-slip fault

— main thrust

— secondary thrust

— minor thrust

— stratigraphic boundary

- - - D2 axial plane trace

- - - D3 axial plane trace

84° A2 axis

40° S2 foliation

∥ vertical S2 foliation

84° L2 mineral stretching lineation

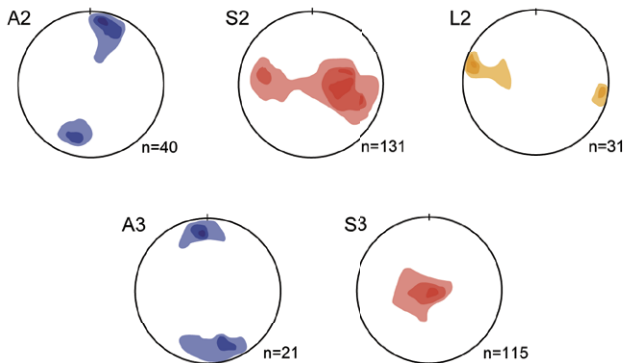
29° A3 axis

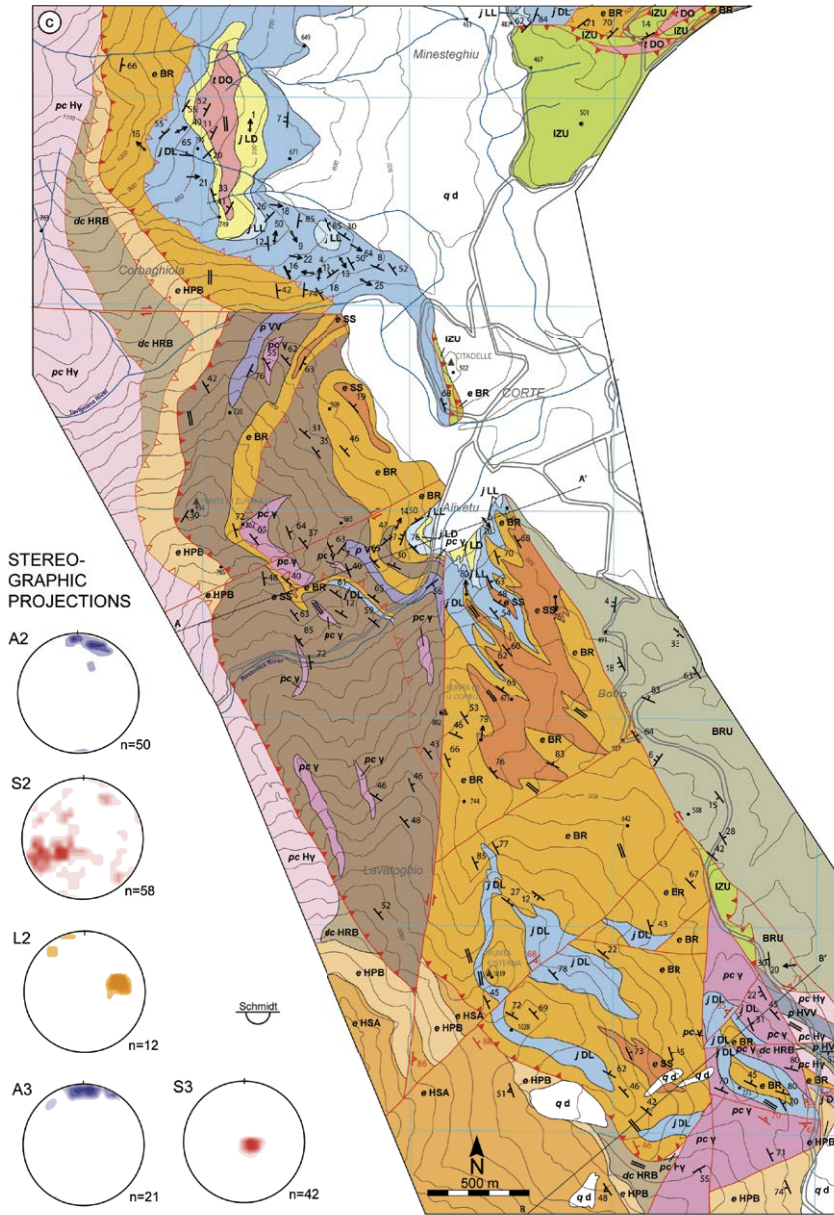
9° S3 foliation

B — B' trace of the geological cross-section

STEREOGRAPHIC PROJECTIONS

Schmidt





LEGEND

□ q d - Quaternary deposits

HERCYNIAN CORSICA

- e HSA - Sandstone and Siltstone Fm.
- e HPB - Polygenic Breccia Fm.
- p HVV - Volcanic and Volcaniclastic Fm.
- pc Hy - granitoids
- dc HRB - Roches Brunes Fm.

ALPINE CORSICA

Schistes Lustrés Complex

Inzecca Unit (IZU)

- IZU - Inzecca Unit (undiff.)
- BRU - Bagliacone-Riventosa Unit (undiff.)

Lower Units

Piedigriggio-Prato Unit (PPU)

- e BR - Metabreccia Fm.

■ j DL - Detritic Metalmestone Fm.

■ j LL - Laminated Metalmestone Fm.

■ f DO - Lower Metadolostone Fm.

Castiglione-Popolasca Unit (CPU)

■ e SS - Metasandstone Fm.

■ e BR - Metabreccia Fm.

■ j DL - Detritic Metalmestone Fm.

■ j LL - Laminated Metalmestone Fm.

■ j LD - Metalmestone and Metadolostone Fm.

■ f DO - Lower Metadolostone Fm.

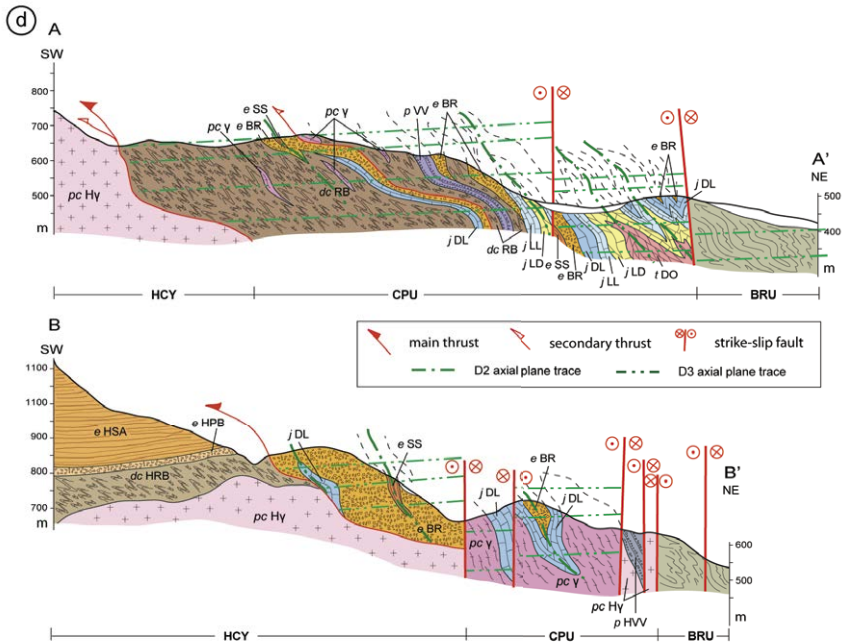
■ p VV - Metavolcanic and Metavolcaniclastic Fm.

■ pc γ - metagranitoids

■ dc RB - Roches Brunes Fm.

SYMBOLS

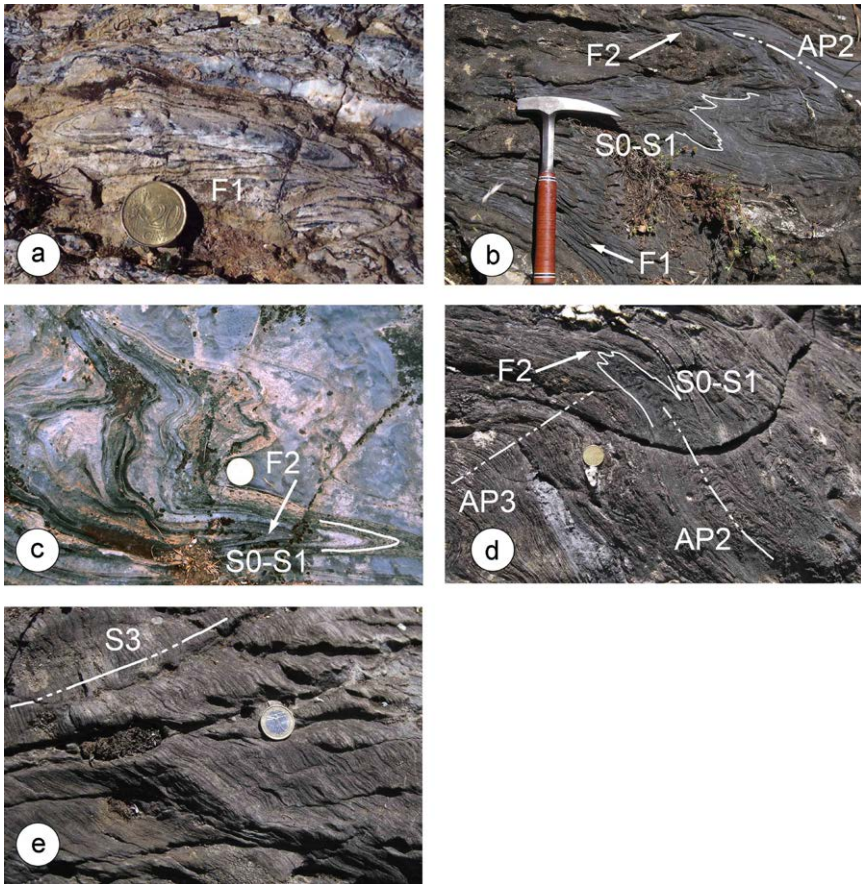
- strike-slip fault
- main thrust
- minor thrust
- stratigraphic boundary
- S₁ S0 primary contact in HCY
- 50 A1 axis
- 52 A2 axis
- 40 S2 foliation
- vertical S2 foliation
- 54 L2 mineral stretching lineation
- 88 D2 thrust
- 29 A3 axis
- 53 S3 foliation
- 88 fault plane
- B—B' trace of the geological cross-section



The F1 folds are associated with S1 foliation, seldom observed in the outcrops but well recognized in the thin sections of the metapelites (Fig 27). The S1 foliation is constituted by a Chl+Phg+Qtz+Cal assemblage of metamorphic origin and is observable in the microlithons along the S2 foliation (Figs 27-28).

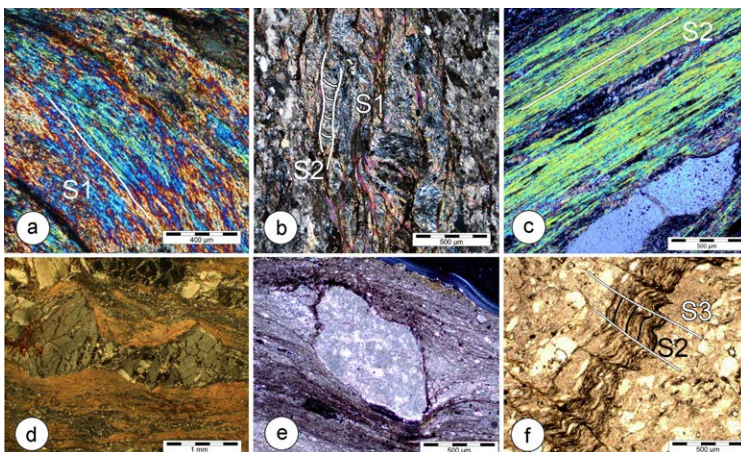
The D2 phase is characterized by W-verging, sub-isoclinal to isoclinal F2 folds with NNE-SSW trend of the A2 axes (Fig 29). At both meso- and map-scale, the F2 folds show limbs often affected by necking and boudinage. The F2 folds are associated with a well developed NNE-SSW striking S2 foliation that represents the main surface identified in the field (Figs 26-27). The only place where the S2 foliation changes its direction is southward of Soveria. There, the tectonic contact between the CDU and PPU has ENE-WSW direction and includes a slice of IZU within which the S2 main foliation (§ Cap 5.5.2) also has E-W trend. Following the tectonic contact toward NW, it changes its orientation and takes a N170 orientation in the Buttinacce area. Everywhere in the Corte

Figure 26. Deformation features in the Detritic Metalimestone Fm. (a) F1 sheath folds; (b) S0-S1 foliation folded by AP2 axial plane; (c) F2 isoclinal fold which folds the S0-S1 foliation and (d) F2 fold and AP3 axial plane interference pattern (modified after Di Rosa et al. 2017b).



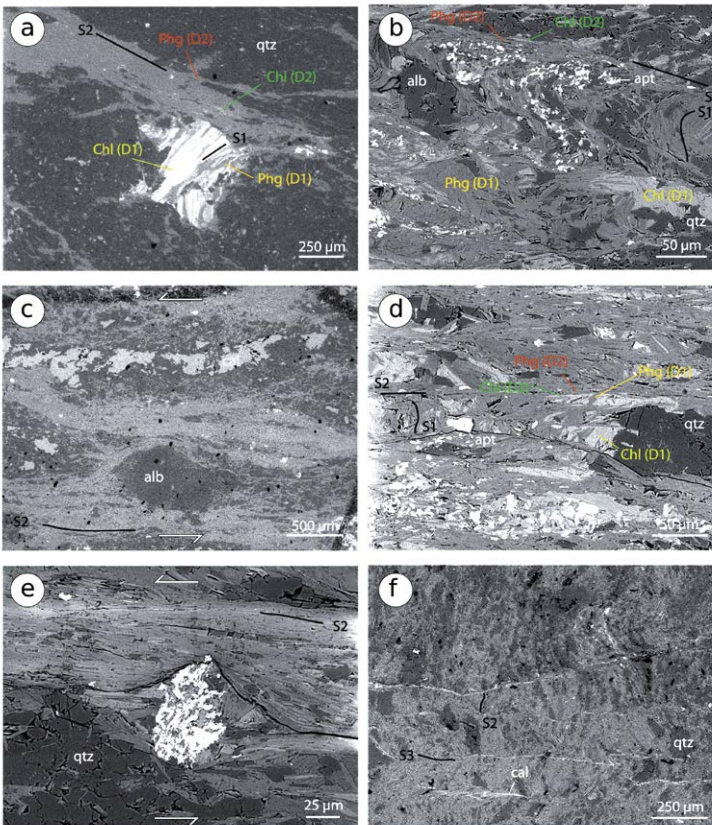
area the S2 foliation transposes the previous S1 and only in the F2 hinge zones the S1/S2 relationship is preserved. On the S2 foliation, the ESE-WNW trending L2 mineral and stretching lineations have been measured. In the metapelites, the L2 mineral lineation is represented by elongated Chl, Qtz and Phg grains, whereas in the metalimestones and in the metadolomites are prevailing the L2 stretching lineations represented by boudinaged millimetric pyrite and Qtz grains. At the microscale, the metagranitoids of CPU and PPU show protomylonitic to ultramylonitic foliation in which the foliation is marked by discontinuous layers of recrystallized Phg, Bit and granoblastic layers of fine-grained recrystallized Qtz and Plg wrapping weakly elongated Fds grains and Qtz crystals. S-c' fabric, σ -type porphyroclast of Fds and bookshelf structures (with synthetic and antithetic fractures) indicate a top-to-W sense of shear (Fig 26). Similar observations were done by De Giorgi (2016) on the metagranitoids of CDU (CM38, CM39). A dominant mylonitic foliation is defined by the planar distribution of mica and Chl and the shape-preferred orientation of Qtz and Fds. Deformation is heterogeneous: relics of the protholith and of older paragenesis are preserved in lens alterned by phyllosilicates layers in which s-c and s-c' domains are distinguishable. Relics of Qtz and Fds are characterized by cataclastic flow, and the fractures are filled by Phg, Chl and thin-grained Qtz. Mylonitic domains Qtz and Fds are characterized by bulging recrystallization and subgrain rotation. In the thin sections of metapelites, the S2 foliation is a crenulation cleavage characterized by a new generation of Chl+Phg+Qtz+Alb+Cal (Fig 27).

Figure 27. Pictures of the Metabreccia Fm. in thin section. (a) S1 foliation (sample CM21); (b) S1–S2 interference pattern (sample CM4); (c) S2 foliation (sample CM22B); (d) Boudinaged quartz level along the S2 foliation (sample CM33); (e) Rotated porphyroclast in the pelitic matrix (sample CM3) and (f) S2–S3 foliations interference pattern (sample CM23B). Modified after Di Rosa et al. 2017b.



At the boundary, but also inside the mapped units, top-to-W shear zones represented by cataclasites with well developed s-c structures have been identified. These shear zones have the same strike of the S2 foliation and are deformed by the F3 folds; thus, the stacking of the Lower Units is regarded as developed during the late stage of the D2 phase.

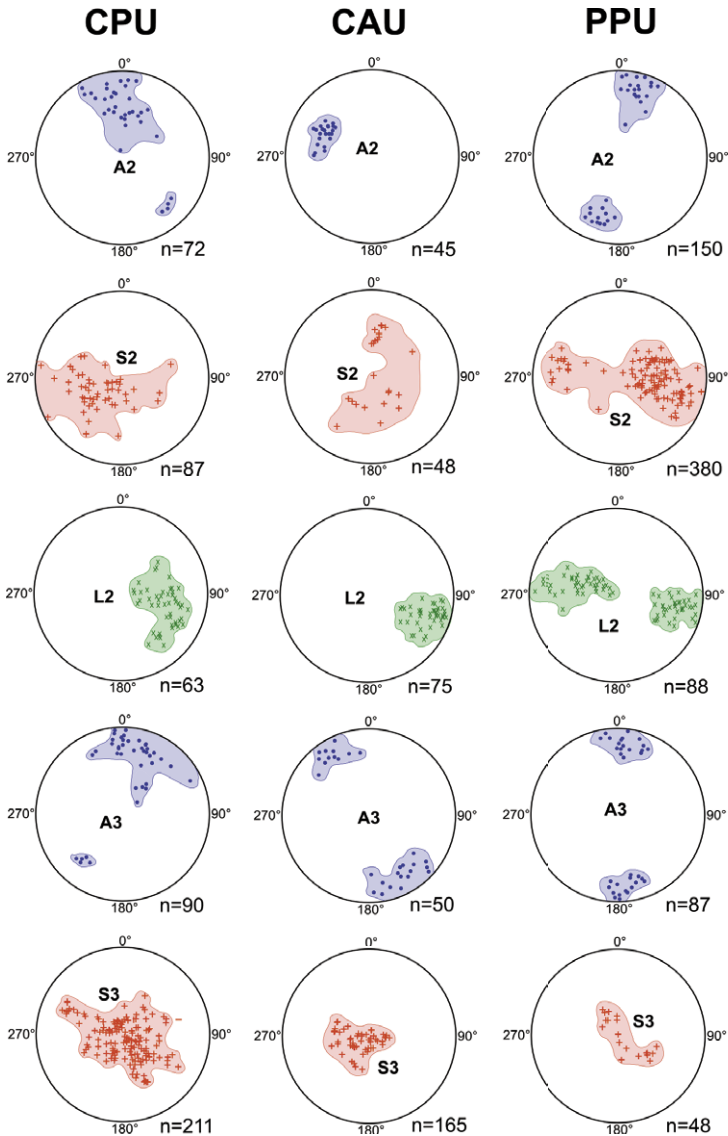
Figure 28. SEM pictures of the Metabreccia Fm. of CPU and PPU. (a) D1 chlorite and S1-S2 foliations made by thin crystals of chlorite and phengite, CPU sample CM29A; (b) S1 foliation crenulated by the S2 foliation, CPU, sample CM22B; (c) S2 mylonitic foliation, CPU, sample CM29A; (d) S1 foliation preserved in the pressure shadow of quartz porphyroclast, CPU, sample CM22B; (e) titanite porphyroclast in the S2 foliation, CPU, sample CM22B and (f) S2-S3 foliations interference pattern, PPU, sample CM23B.



The D3 phase produced E-verging, open to close F3 folds with NNE-SSW trend (Fig 26) and low-angle shear zones due to the vertical shortening of the tectonic stack. The associated S3 foliation can be classified as a disjunctive

cleavage. Only recrystallizations of Cal and Qtz associated to this foliation have been observed in thin section (Figs 28-29).

Figure 29. Stereographic plots of structural data collected in the Corte area (Schmidt net projection, lower hemisphere). Faults belonging to the CCSZ are shown (the length of the black sectors is proportional to the number of strike measures). Modified after Di Rosa et al. 2017b.



5.2.3 Venaco

South of the Venaco village, at the intersections of the roads N193 and D143, the Ghisoni Unit crops out. It is sandwiched between the portion of the HCY that is affected by Alpine deformation (i.e. Razzo Bianco, § Cap 5.4.2) and the Inzecca Unit belonging to the Schistes Lustrés Complex (§ Cap 4.3) and is characterized by a strong deformation over which an intense fracturing is imposed (Fig 30). This post-D3 brittle deformation reworked the tectonic contact between the Ghisoni Unit and the HCY; the pre-D3 coupling of the GHU with the IZU is preserved 3 km toward north along the N193, in the Casanova village, where the brittle deformation is less intense. The D1 phase has been observed only at the microscale in the hinge zone of the F2 folds within the metapelitic layer of the Metavolcanics and Metavolcaniclastic Fm., where relics of the S1 foliation has been found in the microlithons of the S2 foliation. In the mafic dykes intruded into the metagranitoids (e.g. sample CMD122C, Figs 30-31), some mylonitic bands has been found. These shear zones, the thickness of which varies from 1 to 3 mm, are folded by isoclinal folds whose axial planes are the S2 main foliation.

Figure 30. (a) Landscape of the Razzo Bianco and related tectonic sketch; (b) metagranitoids and mafic dykes of GHU in Venaco; (c) s-c' fabric in the Polygenic Breccia Fm. of Razzo Bianco and (d) S2-S3 interference pattern in the metagranitoids of GHU, sample CMD92, Venaco.

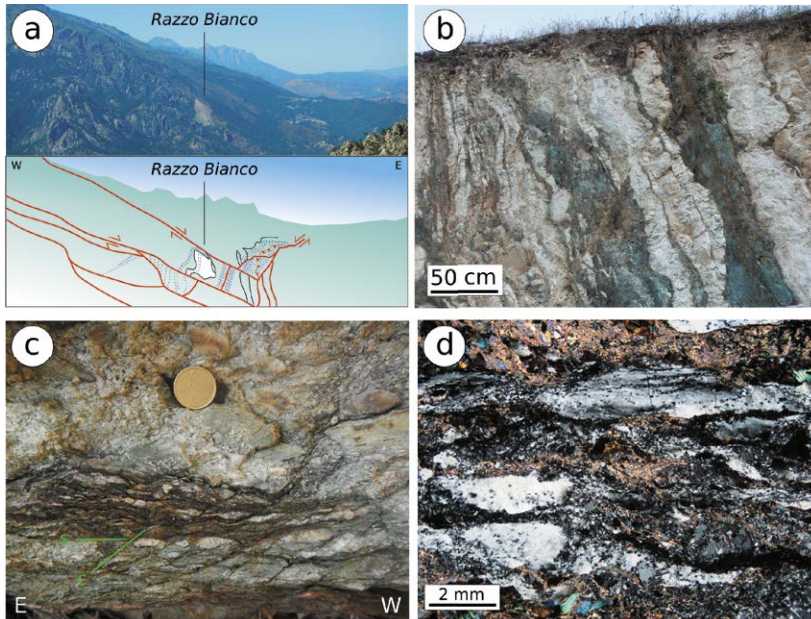
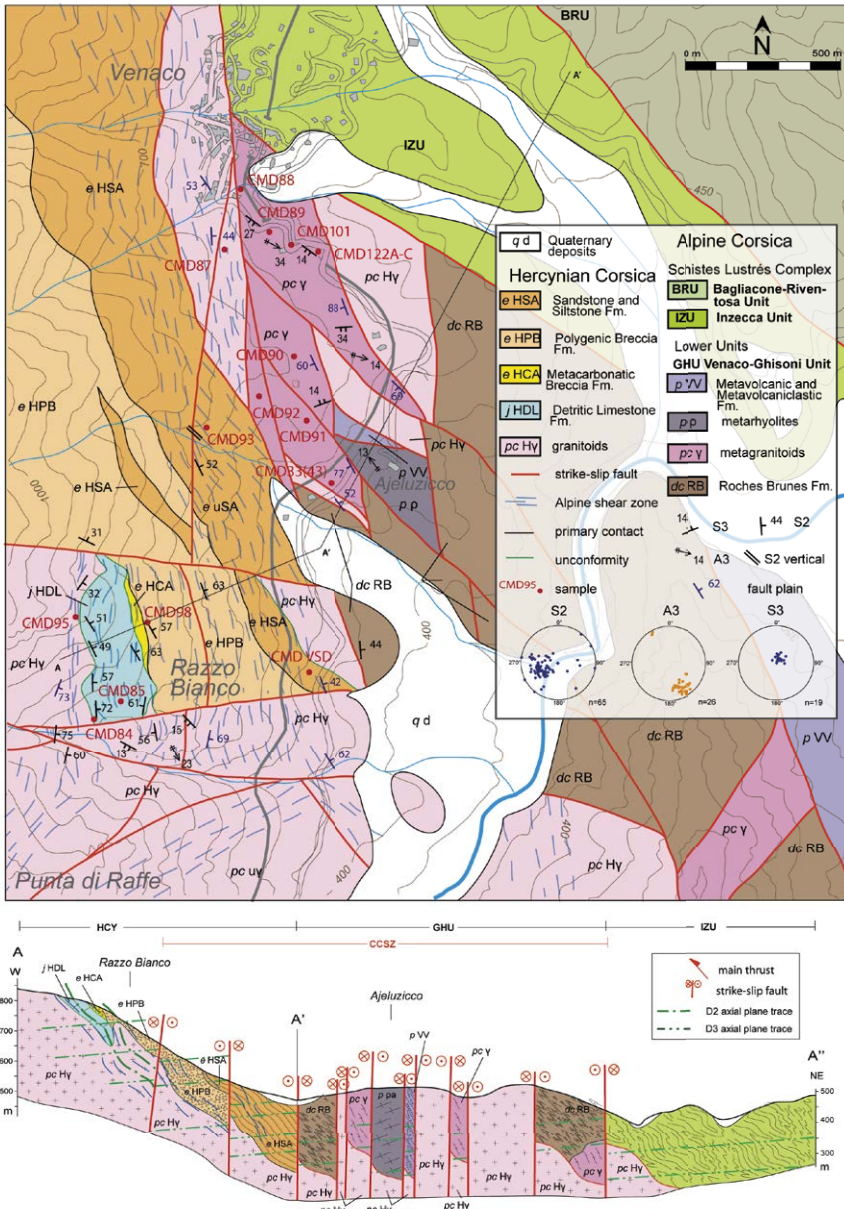


Figure 31 Geological map of the Venaco area and related cross section.



At the meso-scale, the D2 phase is represented by a sub-vertical S2 foliation, well preserved in all the lithotypes. In thin section, the Permo- Carboniferous metagranitoids the S2 foliation consists in a mylonitic foliation made at the

expense of Qtz, Alb, Chl and Phg (samples CMD122A, CMD92). Within this foliation, besides s-c structures made on the phyllosilicates layers, a top-to-W sense of shear is suggested by relics of Epd, All and Qtz aggregates. They behave as σ -type porphyroclasts, and around them Chl tails are commonly found. Along the rim between the mylonitic layers and the domains where the deformation is less intense, sometimes is clear that the mylonitic fabric is superimposed on a previous S2 foliation (i.e. CMD122a), but sometimes the growth of metamorphic white micas seems subsequent to the mylonitic fabric (i.e. CMD92). Qtz ribbons, within which bulging fabric is well preserved, are common in certain samples (i.e. CMD92) but are absent in others (i.e. CMD91), while the dynamic crystallization of Qtz is sometimes characterized by subgrain rotation fabric (i.e. CMD122A). The cm-sized Qtz crystals (CMD91) are affected by undulatory extinction and deformation lamellae, while Fds shows features typical of low-temperatures conditions such as microfaulting and boudinage.

The individuation of domains characterized by different degree of deformation within the same lithotypes (i.e. the metagranitoids) and in an area few km² extended, testifies that during the D2, in addition to the pervasive deformation observed everywhere in the Lower Units, the ductile deformation was concentrated in shear zones with top-to-W sense of shear, as observed in the Corte area (Di Rosa et al. 2017b). In the Permian mafic dykes (CMD122C, CMD122B) the S2 foliation is characterized by the reorientation of the relict minerals such as Cpx, Na Amp, Alb and Chl. σ -type porphyroclasts of Cpx and Alb whose tails are filled by Qtz aggregates are common. Local protomylonitic to mylonitic fabrics superimposed on the S2 foliation has been also observed; the s-c structures associated to these shear zones give a top-to-W sense of shear, coherent to those of the σ -type porphyroclasts (Fig 30c). To the D3 phase is associated the S3 sub-horizontal foliation related to the F3 open asymmetric folds. The best example of the type-3 interference pattern (Ramsay 1967) created by the D2-D3 phase is related to the primary contact between the metagranitoids and the mafic dykes intruded inside them (Fig 30b). At the microscale the S3 foliation has been observed in these two lithotypes (CMD122A, and CMD122C respectively): it is characterized by F3 open to close asymmetric folds that involve both the S2 shear zones and the layer where the deformation is less intense. No dynamic crystallization associated to the S3 foliation has been observed.

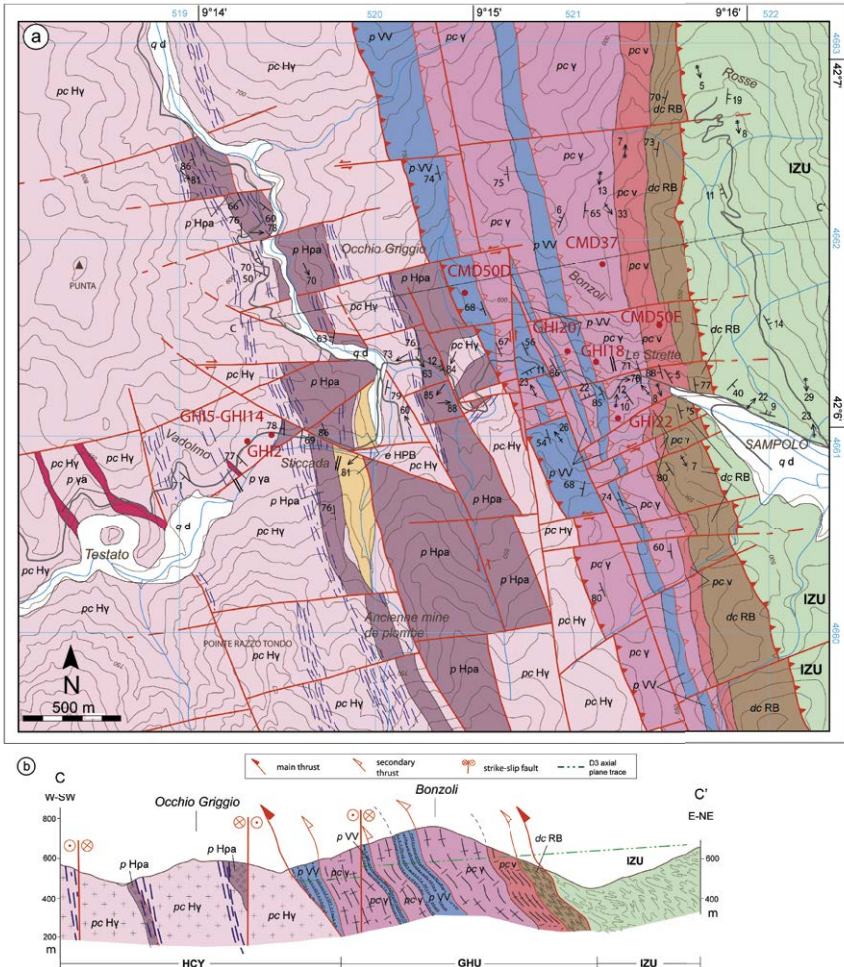
5.2.4 Noceta and Ghisoni

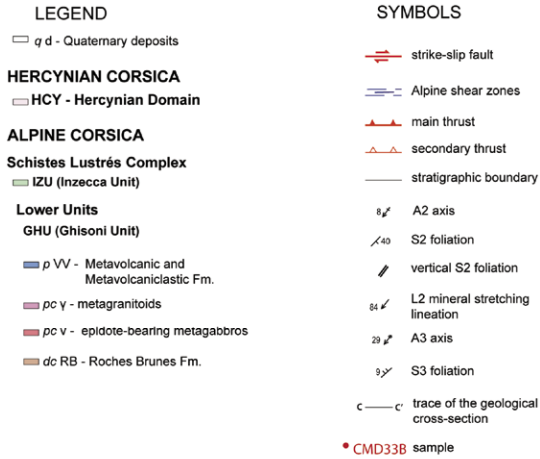
In the two transects of Vivario-Noceta (road D343) and Ghisoni-Sampolo (road D344), the tectonic structuration observed in the Venaco area preserves the same features. The stacking of the GHU (i.e. Lower Units) and the IZU (i.e.

Schistes Lustrés Complex) above the portion of the HCY locally affected by Alpine deformation is ruled by sub-vertical tectonic contacts that have a N170 direction and dip toward NE (Fig 32). Similar to Venaco, also in these two transects the post-D3 brittle deformation have an important role in the final setting of the Noceta-Ghisoni area: two main fault systems (N160 and N50 trends) create a puzzle of blocks that rework the primary contacts between the lithotypes of the three domains (HCY, GHU and IZU) as well as the tectonic contacts between them, deleting almost everywhere the original pre-D3 ductile structuration.

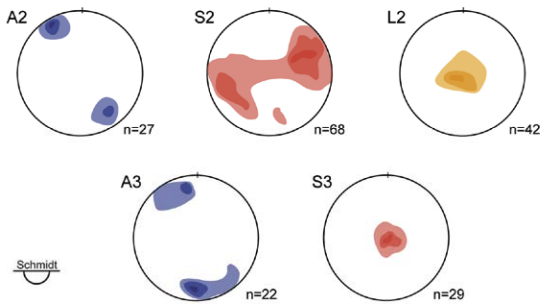
In the GHU the deformation framework described for the Lower Units in the

Figure 32. (a) Geological map and stereographic projections of the main structural elements documented in the Ghisoni area; (b) cross section of the Ghisoni area and (c) landscape of the Fium'Orbo Valley (modified after Di Rosa et al. 2018b).





STEREOGRAPHIC PROJECTIONS

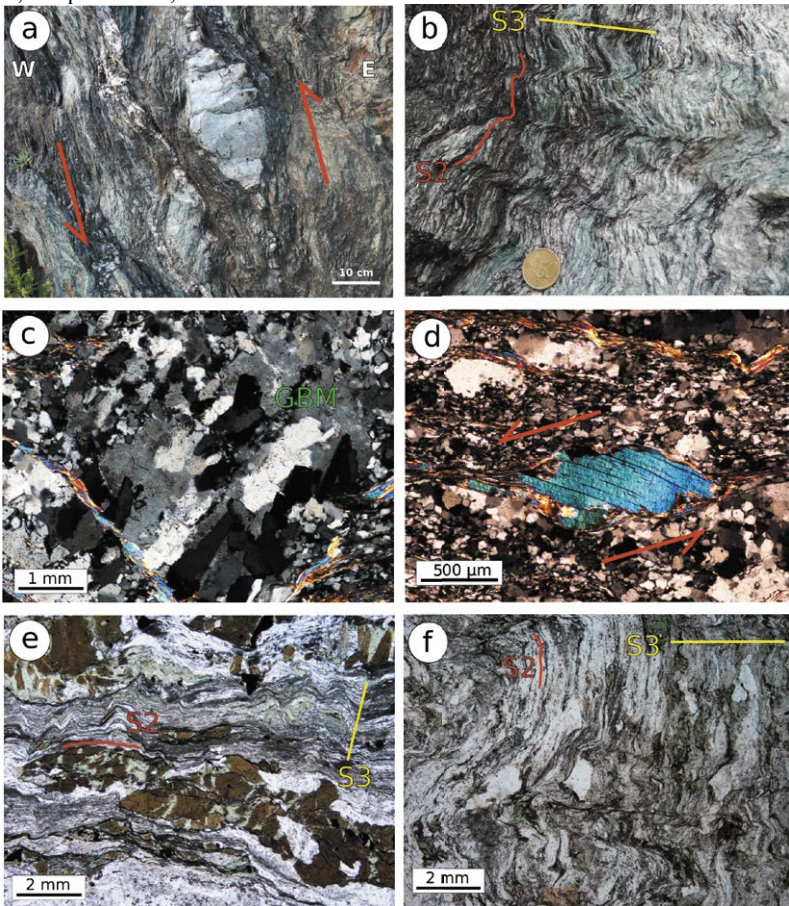


other localities occur (Figs 32-33). The D1 is completely transposed by the D2 phase, and thus at the outcrop scale no evidence of the oldest phase has been observed. In thin section a S1 foliation crenulated by the D2 phase is instead distinguishable in the metapelitic layer of the Permian metasediments.

The D2 phase is characterized by a pervasive S2 sub-vertical foliation, well recognizable in the metagranitoids, in the metagabbros and in the Permian

lithotypes (Fig 33a). In thin section the metagranitoids are made of Qtz, k Fds and Plg showing a protomylonitic to mylonitic fabrics. The main foliation (S2 foliation) is marked by elongated clasts of Fds (R_{xz} max = 9:3) and Qtz (R_{xz} max = 13:3) wrapped by a fine-grained recrystallized matrix of Qtz + Alb and by irregular thin layers of recrystallized Phg (up to 100 μ m). σ -type porphyroclasts

Figure 33. (a-b) Meso and (c-f) microphotographs of the GHU in the Noceta-Ghisoni area. (a) Φ -shaped clasts of quartz in the Metavolcanic and Metavolcaniclastic Fm. of GHU along the tectonic contact with the calc-schist of the IZU, Sampolo; (b) S2-S3 interference pattern in the Metavolcanic and Metavolcaniclastic Fm. of GHU, Ghisoni; (c) Grain boundary migration recrystallization in quartz, metagranitoids, GHU, sample GHI22, Ghisoni; (d) mica fish in the S2 mylonitic foliation, metagranitoids, GHU, sample GHI20, Ghisoni; (e) S2-S3 interference pattern in the epidote-bearing metagabbros, GHU, sample GHI18, Rosse, and (f) S3 folds in the Metavolcanic and Metavolcaniclastic Fm. of GHU, sample VEZ1', Noceta.



of Fds showing asymmetric tails of recrystallized Qtz and/or Phg, and bookshelf structures in Fds represent the main kinematic indicators pointing to a top-to-W sense of shear. The cm-sized Qtz crystals are affected by undulatory extinction, deformation lamellae, deformation bands (developing frequently as conjugate sets), bulging and by conjugate bands of recrystallized grains oriented at low- and at high-angle respect the main S2 foliation. Within these recrystallized bands, new- and sub-grains show the same grain size (4-8 μm). Crystal preferred orientation is weak and shape preferred orientation is limited to boudins, necks and to the asymmetric tails in σ - porphyroclasts. Locally, Qtz crystals are strongly elongated and partly recrystallized indicating that incipient grain boundary migration recrystallization mechanisms occurred. Fds shows features typical of low-temperatures conditions such as undulatory extension, microfaulting and boudinage. Rare deformation twins are also present. The epidote-bearing metagabbros are characterized by a well developed S2 mylonitic foliation (e.g. sample CMD50D, Fig 33a) made of Alb, k Fds, Chl and Qtz. Within this matrix, Epd-shaped crystals of pistacite commonly occur, as well as millimetric porphyroclasts of Pyx completely substituted by Epd aggregates. These latter are characterized by bookshelf structures, due to the fracturing of the crystals along the cleavage of the original Pyx. The S2 foliation is folded by F3 open to close asymmetric folds to which is associated a S3 sub-horizontal axial plain foliation classifiable as a spaced disjunctive cleavage. A sub-horizontal Qtz-vein system related to the S3 disjunctive cleavage occurs in the metagranitoids and in the Permian metasediments of the GHU. In the epidote-bearing metagabbros some Qtz veins parallel to the S3 foliation has been found (i.e. CMD50D).

5.3 The metamorphic history of the Lower Units: evidence from the Permo-Carboniferous metagranitoids and the metagabbros and from the Permian and Tertiary metapelites

The deformation history of the Lower Units controls the development of three metamorphic paragenesis that were in equilibrium at different P-T conditions. The first and the second paragenesis are associated to the D1 phase and have been detected on the metapelitic lithotypes (i.e. the Metavolcanic and Metavolcaniclastic Fm., the Metabreccia Fm. and the Metasandstone Fm.). They are made of Chl, Phg, Qtz, Alb, k Fds, Alb and mineral accessories like All, Mnz and Epd. These two paragenesis are differentiated by the composition of Phg and Chl. The third paragenesis constitutes the S2 foliation and is made of Chl, Phg and less Qtz, k Fds and Cal. Qtz and Cal veins are associated to both the D2 and D3 phases.

Having the microstructures as a constraint (§ Cap 5.2), a range of pressures and temperatures has been identified, in order to provide an estimation of the paths made by the Lower Units during their subduction and exhumation. Basing

on the lithotypes, different techniques have been chosen:

- The application of the classification proposed by Passchier and Throw (2005), in order to estimate the deformation conditions through the study of the Qtz and Alb microfabrics in the metagranitoids and metagabbros and thus to provide approximate values of the temperature reached during the LP-HT event;
- The classical thermobarometry (e.g. Massonne and Schreyer 1987; Cathelineau 1988), the Chl-Phg-Qtz-water multi-equilibrium approach (Vidal and Parra 2000) on the metapelites and the classical thermobarometry based on Ca and Na Amp (Leake et al. 1997) contained in the metagranitoidic clasts of the Metabreccia Fm., in order to constrain the geobaric and geothermic peaks, as well as the conditions of LP-LT registered during the D2 phase;
- The measurement of the Cal twins (Ferrill et al. 2004) in order to constrain the last HT event registered by the metalimestones, the metacarbonatic clasts of the Tertiary metabreccias and by the Cal veins contained in all the lithotypes.

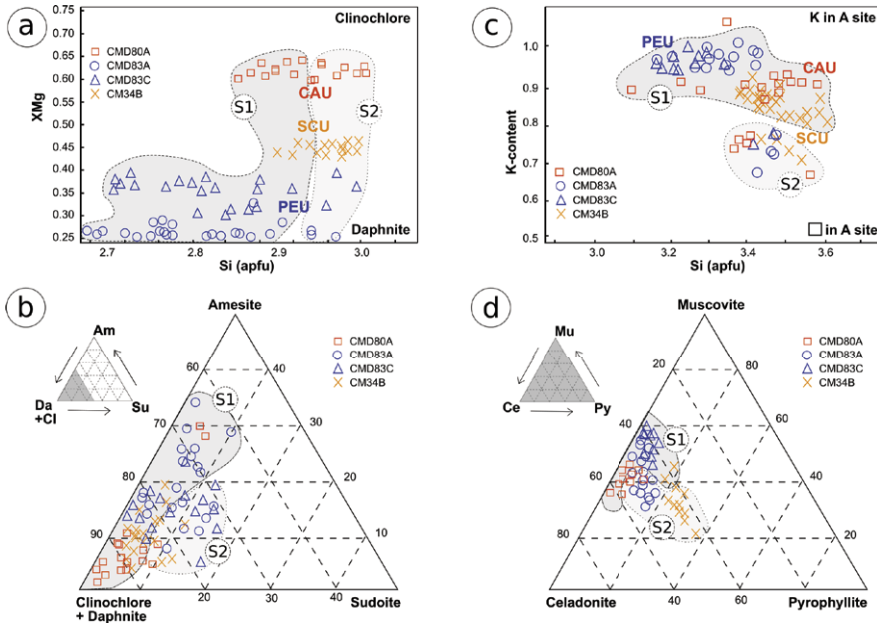
The detailed explanations of the methods employed are listed in the supplementary materials (§ Cap 9); only the data and the results obtained will be described in the following sections.

5.3.1 Cima Pedani

In the Pedani area, the metagranitoids occur only in the CAU. Qtz shows evidences of undulatory extinction and is generally bordered by subgrains as a result of bulging and subgrain rotation mechanisms. In turn, Fds is deformed in a brittle way, which suggests T conditions lower than 400°C (Passchier and Thruw 2005). Within the metagranitoids, Cal crystals filling syn-tectonic veins grown parallel to the S2 foliation show type IV deformation twins (Ferrill et al. 2004) indicative of deformation temperatures higher than 250°C. In the metabreccias, clasts of Qtz and Fds associated to the D2 phase are deformed in a brittle manner (i.e. bookshelf textures), suggesting T conditions lower than 400°C (Stipp et al. 2002).

Metapelites have been identified in each unit of Cima Pedani: in CAU they occur in layers of the Metabreccia Fm., in PEU they belong to the Permian Metavolcanic and Metavolcaniclastic Fm. while in SCU they constitute the Tertiary Metasandstone Fm.. These metapelites are characterized by three metamorphic paragenesis grew during the D1 and the D2 phases. The first and the second grew along the S1 foliation and are made of Chl, Phg, Qtz, Alb, Cal and Epd; some thin crystals of All and Mnz are also found. The third metamorphic paragenesis constitute the S2 foliation and is mainly made by Chl, Phg, Alb and Qtz and rare k Fds. Through the different compositions of Chl and Phg grew in the metapelites along the S1 and S2 foliations, it is possible to backtrack to the P-T equilibrium conditions existing during the D1 and D2 phases (§ Supplementary materials). The P-T conditions of CAU, PEU and SCU have been estimated using the Chl-Phg-Qtz-wt multiequilibrium approach proposed by

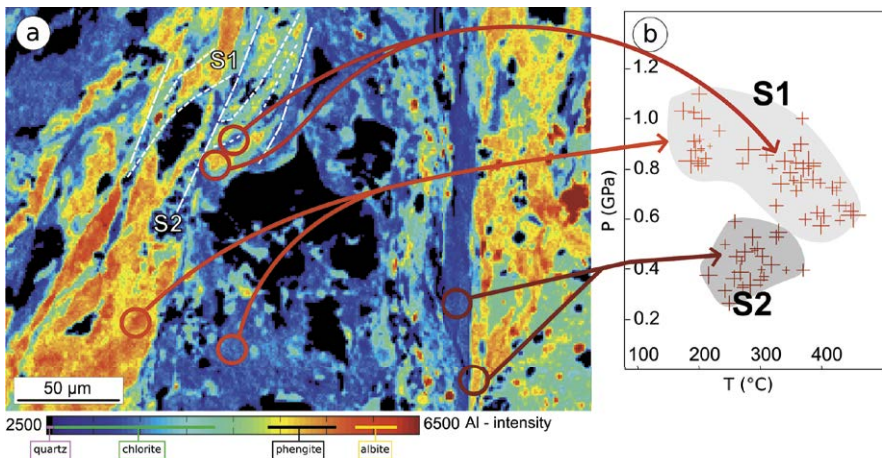
Figure 34. Geochemistry of the chlorite and phengite of the Cima Pedani area. (a) Si/XMg diagram of chlorites, (b) ternary diagram of the chlorite end-members, (c) Si/K diagram of phengites and (d) ternary diagram of the phengite end-members (modified after Di Rosa et al. 2018a).



Vidal and Parra (2000): no previous thermobarometric estimates are available in literature. Four samples have been selected in the study area: one from the Metabreccia Fm. of CAU (CMD80A), two from the Metavolcanic and Metavolcaniclastic Fm. of PEU (CMD83A and CMD83C) and from the Metabreccia Fm. of SCU (CM34B). The selected samples are characterized by the abundance and variability of the Chl-Phg end-members, the distribution of which is correlated to the microstructures. The relative proportions of Am, Cl, Da and Su end-members in Chl are highlighted in the Si/XMg diagram (Fig 34a) and the Am-(Cl+Da)-Su ternary diagrams (Fig 34b). Fig. 5.19a shows that the Si content varies from 2.67 to 3.01 a.p.f.u., whereas the XMg ranges between 0.25 and 0.65. A considerable contrast between the sample CMD80A, containing Mg-rich Chl (high Cl content), and the other three samples that are richer in the Da member is observed. The same analyses plotted in the ternary diagram of Fig 34b show that Chl in all samples has a Su content less than 20 mol%, and a (Cl+Da)-content above 60%. The samples CMD83A and CMD83C have the highest Am content, which reflects higher temperatures of crystallization (Worley et al. 1997; Vidal and Parra 2000; Vidal et al. 2001; 2005; 2006; 2016; Parra et al. 2002b; Dubacq et al. 2010; Lanari et al. 2014a; 2014b). Phg shows variable proportions

Ce, Mu and Py end-members. Phg in sample CM34B present a lower K content respect the other samples (Fig 34) due to a higher content of the Py end-member, while the average Si content is lower for the CMD83A and CMD83C samples.

Figure 35. (a) Al-intensity map acquired with EPMA and elaborated with XMapTools (sample CMD80A, CAU), four phases are distinguishable on the base of the Al content: quartz, chlorite, phengite and albite; (b) P-T equilibriums calculated with ChlMicaEqui software combining chlorite-phengite couples selected in the map (a) and indicated by circles. The three clusters of data correspond to the P-peak, T-peak and S2 P-T estimates for CAU (modified after Di Rosa et al. 2018a).

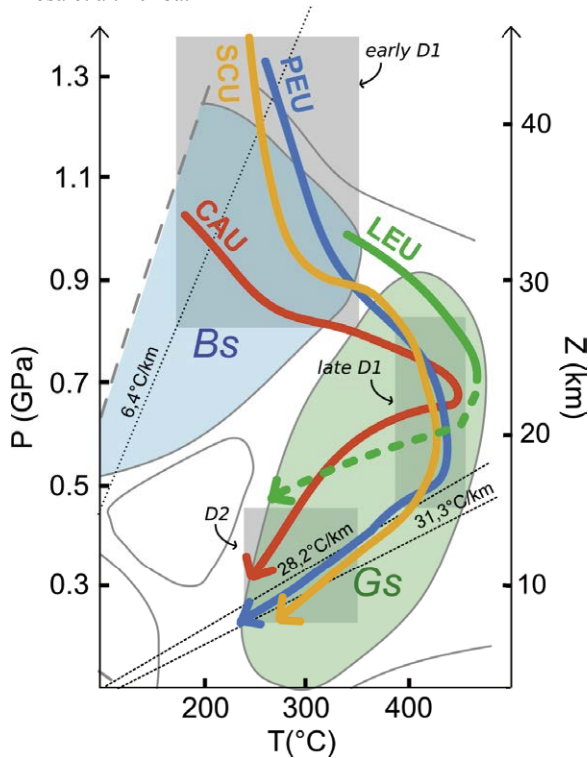


The Phg of the sample CM80A have a Ce content between 50 and 60% (Fig 34d) while in the samples CMD83A and CMD83C the proportion of the end-members is more variable, but always with a Py content less than 20%.

The compositional heterogeneity of Chl and Phg reflects the variations of the P-T conditions related to their crystallization. The compositional maps obtained with EPMA highlight the link between phyllosilicates composition and microstructures. The compositional map obtained for sample CMD80A (Fig 35) shows that 30 μm large Su- rich Chl and Py-rich Phg grains are located in the S2 foliation, whereas 30 to 60 μm Am-rich Chl and Py-poor Phg are located in the relicts of the older S1 foliation. This relationship between the composition of phyllosilicates and the microstructures suggests that the P-T condition related to S1 foliation are higher than those related to S2 foliation. Consequently, ca. 50 Chl-Phg couples have been selected along each S1 and S2 foliations observed in the microstructures of the different samples in order to apply the Chl-Phg-Qtz-wt multiequilibrium approach; repeating this calculation for each sample coming from the three tectonic units, a complex scenario has emerged (Fig 36). Plotting all P-T results in the same P-T diagram, the samples from each unit all cluster in three different groups: two of them are representative of phyllosilicates located in

the S1 foliation and represent the highest calculated P and T conditions, whereas the last group gathers all the analyses related to the Chl-Phg pairs located in the S2 foliation.

Figure 36. P-T paths obtained for the samples CMD80A (CAU), CMD83A (PEU) and CMD34B (SCU); the P-T path of LEU calculated by Levi et al. (2007) is also included (note that the arrows pass where the density of the measure-points are maximum). Modified after Di Rosa et al. 2018a.

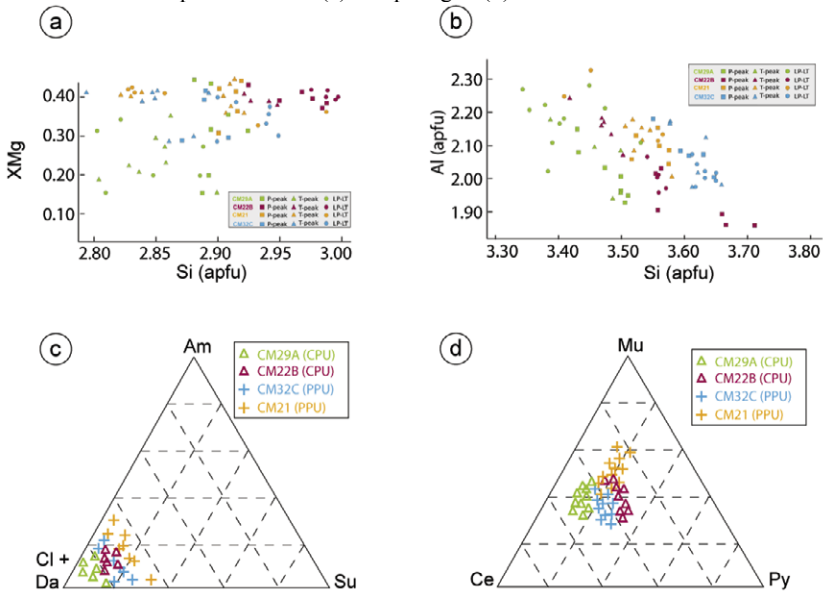


All the analyzed samples, representative of the three continental units exposed in the tectonic window, define the same P-T trend, that differ only for the P and T peak values attained (Fig 36). Similar P-peak conditions are estimated for PEU and SCU ($0.80-1.35 \pm 0.20$ GPa and $280-360 \pm 30^\circ\text{C}$ and $0.90-1.34 \pm 0.20$ GPa and $260-280 \pm 30^\circ\text{C}$ respectively). Lower temperature conditions of the P-peak are estimated for the CAU at lower pressures ($0.82-1.04 \pm 0.20$ GPa and $176-262 \pm 30^\circ\text{C}$). Similar peak temperatures are reached in the CAU, PEU and SCU, at $393-455^\circ\text{C}$ ($0.63-0.76 \pm 0.20$ GPa), $435-440 \pm 30^\circ\text{C}$ ($0.45-0.75 \pm 0.20$ GPa) and $388-435 \pm 30^\circ\text{C}$ ($0.51-0.83 \pm 0.20$ GPa), respectively. The last event is reached between $0.23-0.45 \pm 0.20$ GPa and $237-351 \pm 30^\circ\text{C}$ by all the units.

5.3.2 Corte

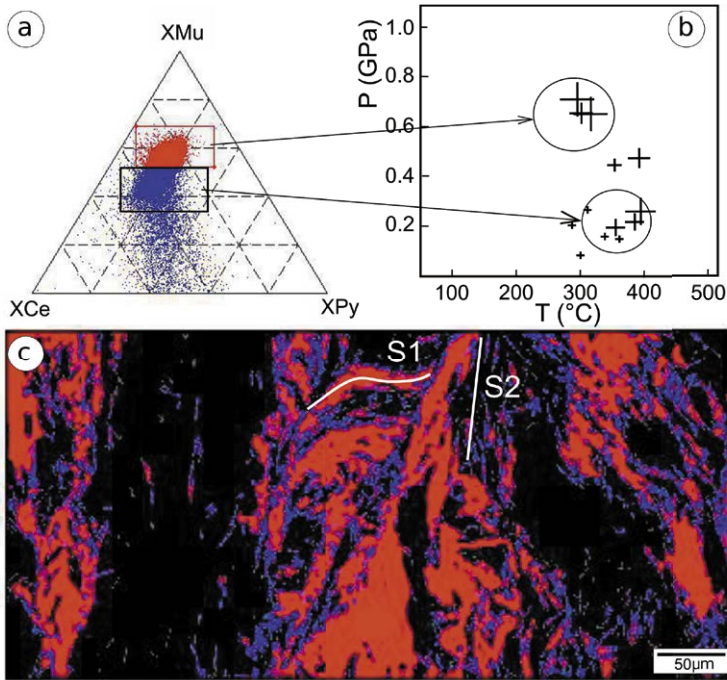
The geochronological data available for the Corsica Island regard the post-The deformation of the metagranitoids of CPU and CDU of the Corte area were studied in detail by Malasoma (2006), Malasoma et al. (2006) and by De Giorgi (2016). The deformation of CPU is coherent with a T of 300-370°C (Malasoma et al. 2006; Malasoma, 2006), whereas Qtz and Fds features indicate deformation temperatures in CDU of ca. 400°C (Passchier and Trouw 2005; De Giorgi 2016).

Figure 37. Binary diagrams related to (a) chlorite and (b) phengite compositions of the CPU and PPU samples. (c,d) ternary diagrams related to CPU and PPU, showing the proportion in each sample of chlorite (c) and phengite (d) end-members.



As regards the metapelites, four samples (CM22B and CM29A from CPU and CM21 and CM32C from PPU) were studied to calculate the P-T conditions of the D1 and D2 phases. All the samples show two metamorphic paragenesis related to the S1 and S2 foliations and made of Chl+Phg+Alb+Qtz±Cal±Epd±Kfd (Fig 37). In the sample CM22B (CPU), the presence of thin euhedral crystals of All (maximum length of <15 μm) grew parallel to the S2 foliation has been also verified. Chl are enriched in Cl and Da end-members while Phg compositions is intermediate between Ce and Mu end-members with a Py content always lower than 35%. The composition of the Phg grown along the S1 ranges between Ce and Mu end-members of 40-60% and 30-60% respectively, whereas those grown along the S2 foliation are characterized by an increasing Py content observable in all the units. Inside this general trend, several small-scale differences in end-members proportions can be recognized.

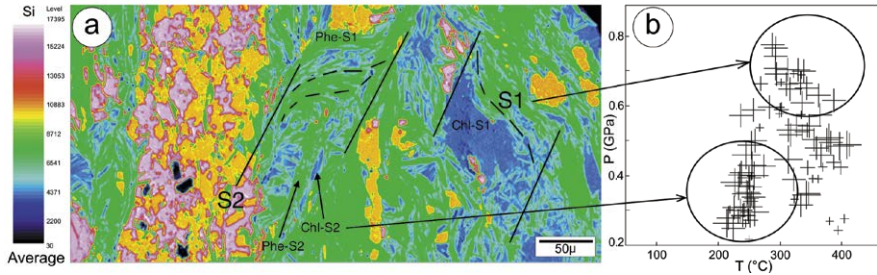
Figure 38. (a) Ternary diagram of phengite end-members for sample CM21 (XMu: muscovite, XCe: celadonite, XPy: pyrophyllite). Light coloured points: phengites more enriched in the muscovitic end-member grown along the S1 foliation. darker points: phengites enriched in the celadonitic end-member grown in the S2 foliation. (b) P–T equilibria conditions obtained for phengites plotted in (a). (c) Element map showing the phengites grew during the D1 phase (in light grey) and the D2 phase (in dark grey). Modified after Di Rosa et al. 2017a.



The P–T paths obtained with the Chl-Phg-Qtz-wt method describe the retrograde history of CPU and PPU during their moving from the deepest positions in the tectonic wedge to the surface (Fig 38). No trace of the older prograde history has been observed, thus the study is focused on the most significant stages of the exhumation history registered by the Lower Units after the geobaric peak conditions.

Through the dynamic recrystallization of Chl and Phg within the microstructures, three clusters of data have been recognized that are reached at pressures and temperatures slightly different between the two tectonic units. The P-peak is located at 1.00–1.22 GPa/250–300°C for the CPU and 0.75–1.04 GPa/200–240°C for the PPU (HP/LT), the T-peak at 0.80–0.56 GPa/320–350°C for the CPU and at 0.80–0.51 GPa/340–400°C for the PPU, whereas the LP/LT corresponds to the Chl-Phg in equilibrium at 0.36–0.25 GPa/310–230°C for the CPU and 0.30–0.23 GPa/240–300°C for the PPU.

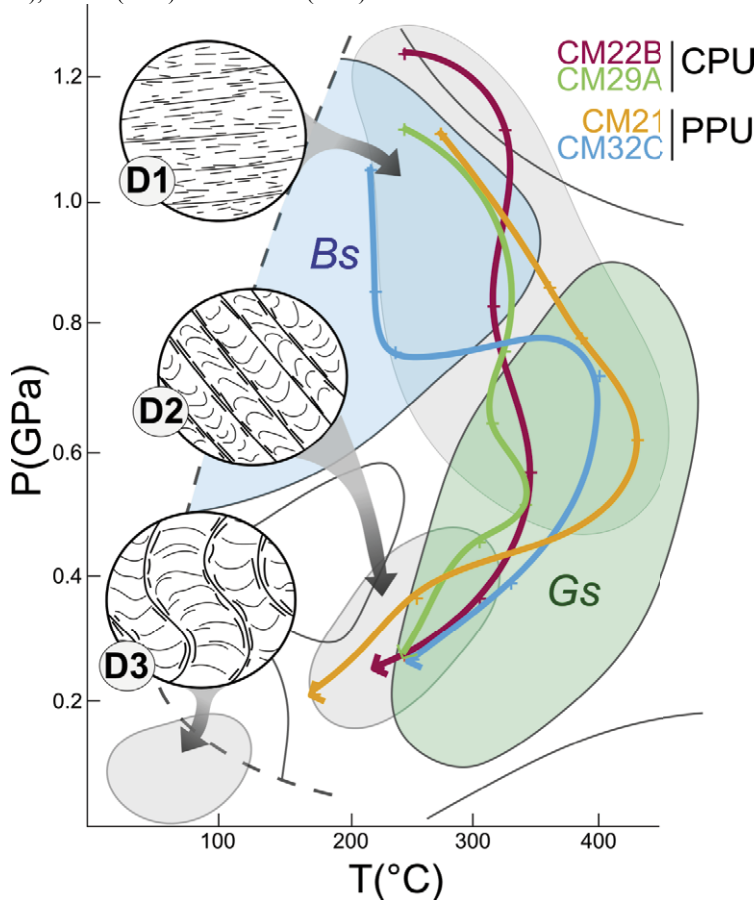
Figure 39. (a) Si-intensity map acquired with EPMA (sample CM21); five phases are identifiable: quartz (level17395-11968), feldspar (level11968-10000), phengite (level 10000-6500), chlorite (6500-3000). (b) P–T equilibria conditions of sample CM21. Arrows indicate the studied areas (modified after Di Rosa et al. 2017a).



Always regarding the Metabreccia Fm., the neoblastic Cal has been found, in addition to the one that replaces the metalimestones clasts, in the matrix within the S2 foliation. The grain size varies from 50 μm to 3 mm and show tabular thick twins, typical of temperatures between 200 and 300°C (Type II of Burkhard 1993). These values are similar to those estimated in the metagranitoids of the CDU (De Giorgi 2016). Concerning to the Qtz clasts of the Metabreccia Fm. of CPU and PPU, undulose extinction and subgrain rotation have been found in the crystals grew within the S2 foliation; although these textures depend not only by pressure and temperature, but also by differential stress, strain rate and water content (Stipp et al. 2002b), a greenschist facies is proposed for them, that is compatible with the temperatures around 250-300°C estimated for the D2 phase. The data obtained in this work for CPU and PPU are in agreement with those calculated by Malasoma et al. (2006) for CDU (0.40-0.85 GPa, 300-370°C).

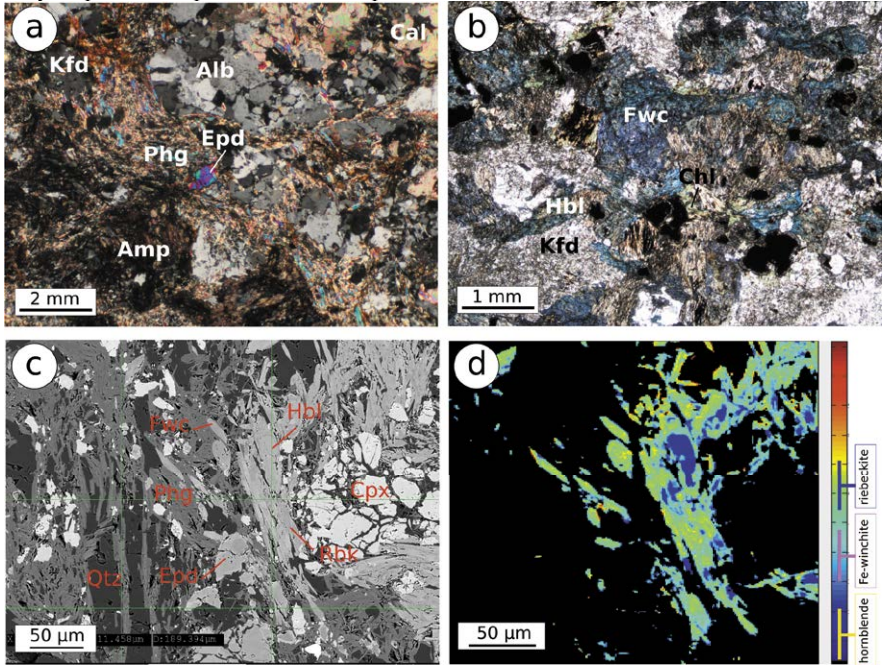
In the outcrop of Metabreccia Fm. located S of Botro (Lat:42°16'26.47"N; Long:9°10'11.27"E), clasts of metagabbros occur (samples CMD56, CMD69). They are made of Cpx (augite), Hbl, Plg and minor Rut, Chl and Fe-oxides and Chl and are characterized by a metamorphic paragenesis made of Na and Ca-Na Amp, Alb, Phg, Epd, Qtz and minor Cal and Apt (Fig 41). Amp were classified following Leake et al. (1997); structural formulae were calculated assuming 23 oxygens and ferric iron contents were calculated following Schumacher classification (Leake et al. 1997). The Na Amp (Fig 41) grew around relics of Hbl and is in turn almost completely substituted by the Ca-Na Amp, which is in equilibrium with the other phases that constitute the main foliation of the metagabbros (i.e. S2). In the Na Amp the $\text{Fe}^{3+}/(\text{Fe}^{3+}+\text{Al}^{\text{VI}})$ ratio ranges between 0.25 and 0.90, whereas $\text{Mg}/(\text{Mg}+\text{Fe}^{2+})$ between 0.25 and 0.75, and most of the data are thus included in the riebeckite field (Fig 42a). The Ca-Na Amp have $\text{Mg}/(\text{Mg}+\text{Fe}^{2+})$ always between 0.3 and 0.75; most of them have Si >7.5 a.p.f.u. and fall in the field of the winchite/richterite, while the others have lower Si content (but always higher than 6.5 a.p.f.u.) and are classifiable as barroisite/katophorite (Fig 42b).

Figure 40. Fig.5.25 P-T paths obtained for the samples CM29A (CPU), CM22B (CPU), CM21 (PPU) and CM32C (PPU).



Holland and Blundy (1994) and Lanari et al. (2014c) methods were applied to riebeckite and to Fe-winchite, in order to estimate the P-T condition taking into account the composition of the Amp and the presence/lack of other phases like plagioclase. The tectono-metamorphic history of the megabros clasts of the Metabreccia Fm. can be deduced correlating the results obtained on the metamorphism and the texture relationships of the two Amp analyzed. The multi-equilibrium method proposed by Lanari et al. (2014c) has been first applied on the riebeckite and Fe-winchite in order to estimate the maximum range in which these phases are in equilibrium. P condition were calculated using the geobarometer of Brown (1977, Fig 43) and then T were thus calculated with Holland and Blundy (1994) fixing P at 0.7 GPa for riebeckite and at 0.6 GPa for Fe-winchite. The results obtained with the different methods overlap, and thus the P-T conditions for riebeckite and Fe winchite are assumed to be 0.7 GPa and 380°C and 0.6 GPa and 450°C, respectively (Fig 43).

Figure 41. (a) texture and mineral assemblage of the metagabbros studied, CPU, sample CMD69, crossed Nicols; (b) texture and mineral assemblage of the metagabbros studied, CPU, sample CMD56; (c) SEM picture of the sample CMD69 and (d) Na intensity map of the amphibole of the sample CMD69.



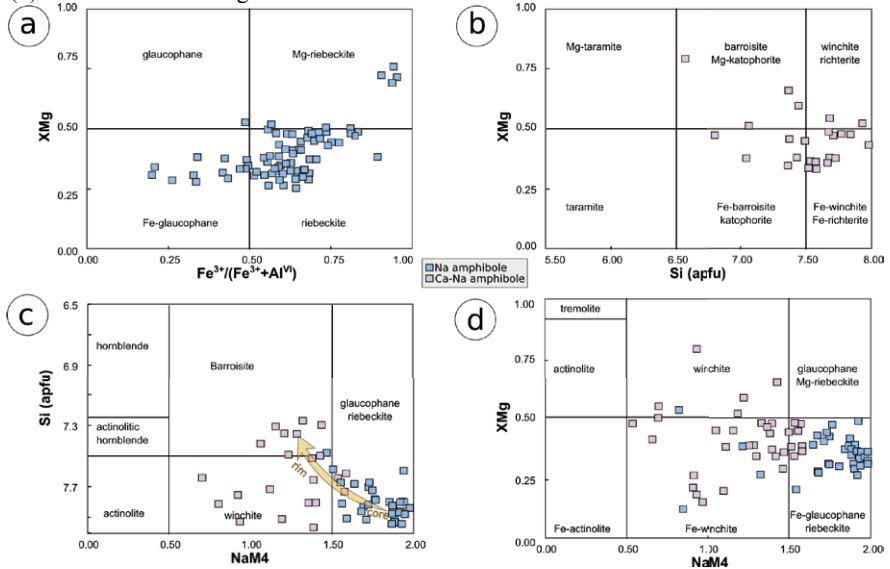
All the T range calculated are higher comparing with the results obtained for CPU with the Chl+Phg+Qtz+Wt multiequilibrium approach on metapelites (Vidal and Parra 2000), but are included within the errors of the methods ($\pm 30^{\circ}\text{C}$ for Vidal and Parra 2000; $\pm 50^{\circ}\text{C}$ for Holland and Blundy 1994 and Lanari et al. 2014c).

Table 3. Thermo-barometers based on amphibole (sample CMD69).

Method	Authors	Riebeckite	Fe-winchite
Amp-P-T (Amp+Plg)	Lanari et al. 2014c	0.65-0.71 GPa, 360- 400°C	0.55-0.68 GPa, 420- 450°C
Amp-T (Amp+Plg)	Holland and Blundy1994	0.7 GPa *, 400-450°C	0.6 GPa *, 400- 460°C

* input value chosen by the user.

Figure 42. Compositions of amphiboles of sample CMD69 (CPU) using the classification of Leake et al. (1997): (a) Na-amphiboles, (b) Na-Ca amphiboles. Plots showing amphibole chemistry, sample CMD69 (CPU): (c) Na in the M-site vs. Si (a.p.f.u.) and (d) Na in M-site vs XMg.

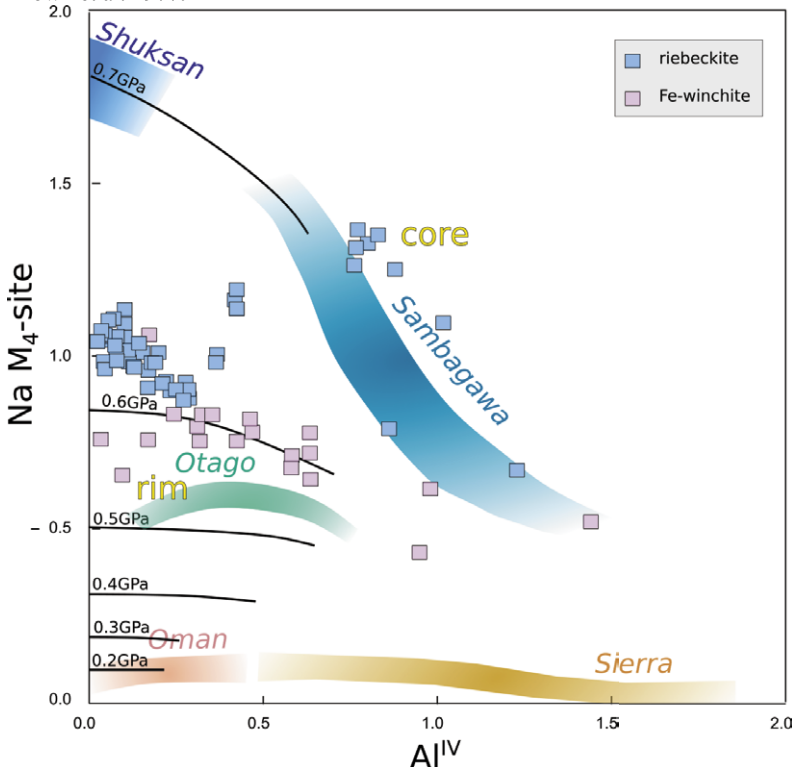


As regards the presence/lack of All observed in CPU, several observations could be done. Their presence has been verified, in this work, into two different rock types:

- In the metagranitoids and related mafic dykes of the CPU (CMD122A). They are not in equilibrium in the greenschist facies reached by the mylonitic foliation in which they occur, and their age correspond to the Triassic rifting (§ Cap 6.3 and 6.4);
- In the Metabreccia Fm. of CPU (CM22B) and of PPU (CMD28B). Very thin euhedral All crystals (<15 μm) nucleate within the S1 foliation. Although their abundance, it was not possible to date them because of their size.

Considering that the samples CMD122A and CM22B belong to the same tectonic unit, and thus they were evenly subducted and exhumed, an apparent discrepancy seems arise. The P-T values reached by the CPU, calculated from the sample CM22B, indicate that during the late D1 phase the unit reached the geothermic peak at about 0.82 GPa and 350°C. The All incipient nucleation found along the S1 foliation of the sample CM22B fit quite well with the window 0.8-1.5 GPa/420-450°C defined by Janots et al. (2006; 2008) in which Mnz (also found on the sample) is replaced by this LREE-rich mineral phase. They affirm that in Alpine metasediments, this reaction, previously constrained to the P-T conditions of the Bit isograd (Smith and Barreiro 1990; Wing et al. 2003), occurs at the lower metamorphic conditions of the chloritoid isograd. This

Figure 43. Geobarometry of amphiboles belonging to sample CMD69 (CPU), after Brown et al. 1977.



effect, maybe owing also by differences in fluid compositions, is probably due to the bulk composition of the rocks. On this topic, the authors obtain controversial data: some of them observed that for low Al and Ca bulk compositions Mnz is preserved (Wing et al. 2003; Krenn and Finger 2007) while others have the evidence that the Ca content is not a valid criterion to exclude All as the precursor of Mnz at HT conditions (Janots et al. 2008). Without going into too much detail, the bulk composition of the two rock types could explain the lack of All nucleated during the late D1 phase in metagranitoids. This rocks instead preserved big fractured crystals of All related to a previous history of heating, that clearly are not in equilibrium with the greenschist facies that characterizes the metamorphic conditions associated to the late S1 foliation. Another possible explanation for the lack of Alpine imprint on the All of the metagranitoids comes from the mechanical and chemical behaviour of this mineral during mylonitization. Cenki-Tok et al. (2011) observed that in the metagranodiorites of Monte Mucone, those shear zones experienced the eclogite facies during the Alpine Orogeny, the All preserved the Permian magmatic age. They attribute to a strong strain partitioning the fact that All, occurring as “eyes” within a thin-grained matrix made of Fds, did not registered the Alpine age in terms of U-Th-

Pb isotopic ratios. Given the texture features of the sample CMD122A, this behaviour as rigid clast in a thin-grained matrix of phyllosilicates, Qtz and Fds could be therefore postulated also for the All of the metagranitoids of CPU.

5.3.3 Noceta and Ghisoni

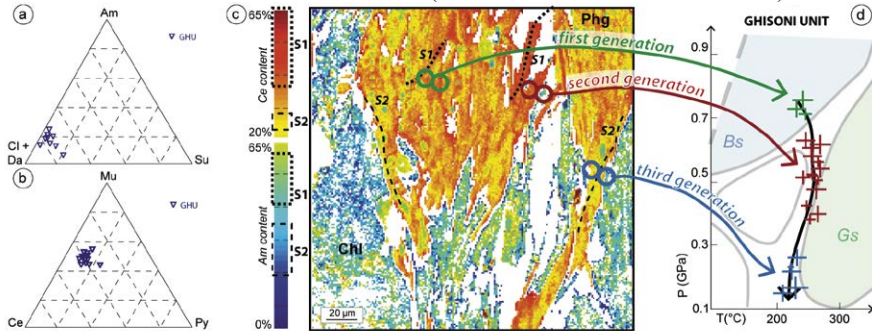
The selected samples from GHU are deformed metagranitoids consisting of Qtz, k Fds, Plg, Na Amp, Phg and Chl showing a protomylonite to mylonitic fabrics. The main foliation (S2 foliation) is marked by elongated clasts of Fds (R_{xz} max = 9:3) and Qtz (R_{xz} max = 13:3) wrapped by a fine-grained recrystallized matrix of Qtz + Alb and by irregular thin layers of recrystallized Phg (up to 100 µm). σ -type porphyroclasts of Fds showing asymmetric tails of recrystallized Qtz and/or Phg, and bookshelf structures in Fds represent the main kinematic indicators pointing to a top-to-W sense of shear.

The cm-sized Qtz crystals are affected by undulatory extinction, deformation lamellae, deformation bands (developing frequently as conjugate sets), bulging and conjugate bands of recrystallized grains oriented at low- and at high-angle respect the main S2 foliation. Within these recrystallized bands, new- and sub-grains show the same grain size (4-8 µm). Crystal preferred orientation is weak and shape preferred orientation is limited to boudins necks and to the asymmetric tails in sigma porphyroclasts. Locally, Qtz crystals are strongly elongated and partly recrystallized indicating that incipient subgrain rotation recrystallization mechanisms occurred. Fds shows features typical of low-temperatures conditions such as undulatory extension, microfaulting and boudinage. Rare deformation twins are also present. These microstructures indicate that dislocation creep represents the main deformation mechanism in Qtz during the development of the main foliation, suggesting deformation temperature comparable to those estimated for the Corte area (i.e. T c. 400°C).

The Chl-Phg-Qtz method has been applied on the metapelites belonging to the Metavolcanic and Metavolcaniclastic Fm. of GHU (i.e. sample CMD50E, Fig 44). The sample is composed by Chl enriched in Cl and Da end-members and by Phg poor of Py (less than 20%) and the same proportion of Mu and Ce. Three generations of Chl and Phg have been recognized: the first and the second generations grew along the S1 foliation and are in equilibrium at 0.81-0.72 GPa/245-250°C and 0.68-0.39 GPa/263-243°C respectively. The third generation of Chl-Phg couples are related to the S2 foliation and are in equilibrium at 0.36-0.25 GPa and 310-230°C.

Tension gashes systems have been found within the Metavolcanic and Metavolcaniclastic Fm. of GHU. They cut the D2 foliation, with which they do a low angle, and are clearly folded by F3 folds.

Figure 44. Ternary diagrams related to GHU, showing the proportion in the sample CMD50D of (a) chlorite and (b) phengite end-members. (c) Si-intensity map acquired with EPMA. (d) P-T equilibria conditions of the three generations of Chl-Phg couples (the error of each cross is ± 0.2 GPa and $\pm 30^\circ\text{C}$). Dots in the maps indicate the sampled microareas from which the P-T estimates were obtained (modified after Di Rosa et al. 2018b).



5.4 The Alpine ductile deformation and the metamorphic imprint in the foreland: insights from Asco-Castirla, Razzo Bianco and Noceta-Ghisoni shear zones

In this section, new structural and petrographic data from the shear zones set within the HCY are presented. In the Asco-Castirla and Noceta-Ghisoni areas they are set in the Permo-Carboniferous granitoids, while in Razzo Bianco area they involve the granitoids and the Mesozoic-Tertiary covers (Amaudric du Chaffaut 1980). We further provide the evidence that the HCY is affected by a polyphase deformation recognized at the meso- and microscale. Moreover, the study of the metamorphism performed on the metapelites of Razzo Bianco, indicating a deep burial below the Alpine Orogenic wedge. These data provide a new scenario for the Tertiary geodynamic history of the Corsica Island.

5.4.1 Asco-Castirla shear zones

Several ductile shear zones have been identified inside the Permo-Carboniferous granitoids of the HCY. Two of them are exposed along the roads that skirt the Asco (D147, lat: $42^\circ 28' 04.26''\text{N}$, long: $9^\circ 06' 25.07''\text{E}$) and the Golo rivers (D84, lat: $42^\circ 22' 18.07''\text{N}$, long: $9^\circ 06' 49.79''\text{E}$) which have a direction orthogonal to that of the shear zone.

The Asco-Castirla shear zones are the Alpine ductile structures located in the innermost position of the HCY. Respect to the other studied areas, in which these shear zones are located a few tens of meters from the boundary with the Alpine Corsica, in this sector the eastern rim of the HCY is 1,5 km away. The Asco shear

zone is 80 m extended shear zone striking roughly NNW-SSE. It is characterized by zones dominated by protomylonitic to mylonitic fabrics alternated with others where the cataclastic and ultracataclastic fabrics occur (Fig 45). The rock types are mainly granitoids, although mafic dykes and rocks characterized coarse-grained Qtz immersed in a pelitic matrix (probably the Permian Volcanic and Volcaniclastic Fm., widely outcropping W of the shear zone) also occur (Fig 46). The Asco shear zone display a well developed subvertical foliation, parasite folds and a stretching lineation, recognizable in both the granitoids and in the basaltic dykes emplaced inside them, that indicate a top-to-W sense of shear. Despite the intensity of the deformation, s-c and s-c' structures have been recognized within all the deformation domains, as well as mica and Fds fishes. In the place where AS3 was sampled, the mylonitic foliation is folded in close to subisoclinal folds having a subvertical axial plane foliation and axes going from S to N and dipping of $\sim 40^\circ$. Because of the different rheology of the mylonitic layers, dominated by phyllosilicates and small-grained Qtz, and the less deformed layers, along the flanks these folds S and Z parasite folds coherent with a N-vergence are observed.

To characterize the Asco shear zone, 9 samples representative of granitoids, Volcanic and Volcaniclastic Fm. and mafic dykes affected by deformation of different intensity have been collected. In thin section, Qtz and Fds crystals of the cataclastic/ultracataclastic domain (e.g. sample AS2, Fig 46a) show strong intracrystalline deformation (undulose extinction and deformation lamellae), indicating $T < 400^\circ\text{C}$ (Passchier and Trouw 2005). Increasing the strain rate, the samples show small-grained protomylonitic to mylonitic layers made of phyllosilicates, Qtz and Fds alternated to layers where the magmatic texture of the granitoids is roughly preserved (Fig 46b-f). In the latter, Qtz crystals are characterized by intracrystalline deformation; bulging recrystallization occur along parallel folded planes on Qtz (sample AS2, Fig 46c). Crystals and ribbons are made of Qtz aggregates where the transition between bulging and subgrain rotation is observed (sample AS5, Fig 46 d). Antitaxial (sample AS3a, Fig 46e) and blocky (sample AS9, Fig 46d,f) Qtz veins, found in all the lithotypes, are usually folded or parallel to the s- shear bands. Microscale observations on granitoids sampled in these two places highlight the presence of different microfabrics indicating different strain rates and thus a localized deformation that change in intensity within a few meters. Within the domains closer to the undeformed rock-volume, cataclastic flow is dominant: undulose extinction of the Qtz crystals and minor bulging recrystallization indicated that the crystal plasticity had a small contribution to total strain of these domains. Thus, the semibrittle behavior of the cataclastic domains develop under $280\text{-}300^\circ\text{C}$, above which recovery features become dominant (Hirt and Tullis 1994; Stipp et al. 2002b). Increasing shear strain, increase bulging recrystallization and subgrain rotation within the Qtz crystals, that suggest T range of $280\text{-}400^\circ\text{C}$ and $400\text{-}500^\circ\text{C}$ respectively (Stipp et al. 2002a).

In the Golo Valley, W of Castirla village, a similar scenario occurs, even if the shear zone is less extended (about 30 m in thickness) and less articulated.

Figure 45. The Asco shear zone from meso- to microscale. The transition from cataclasite to proto and mylonite fabrics is shown in the outcrop as well as in thin section. Stereographic projections indicate the mylonitic foliation (MF) and the axes of the folds (AP), the orientation of the fault system (FS) and the two groups of lineations (Ldd: down-dip lineation; Lss: strike-slip lineation).

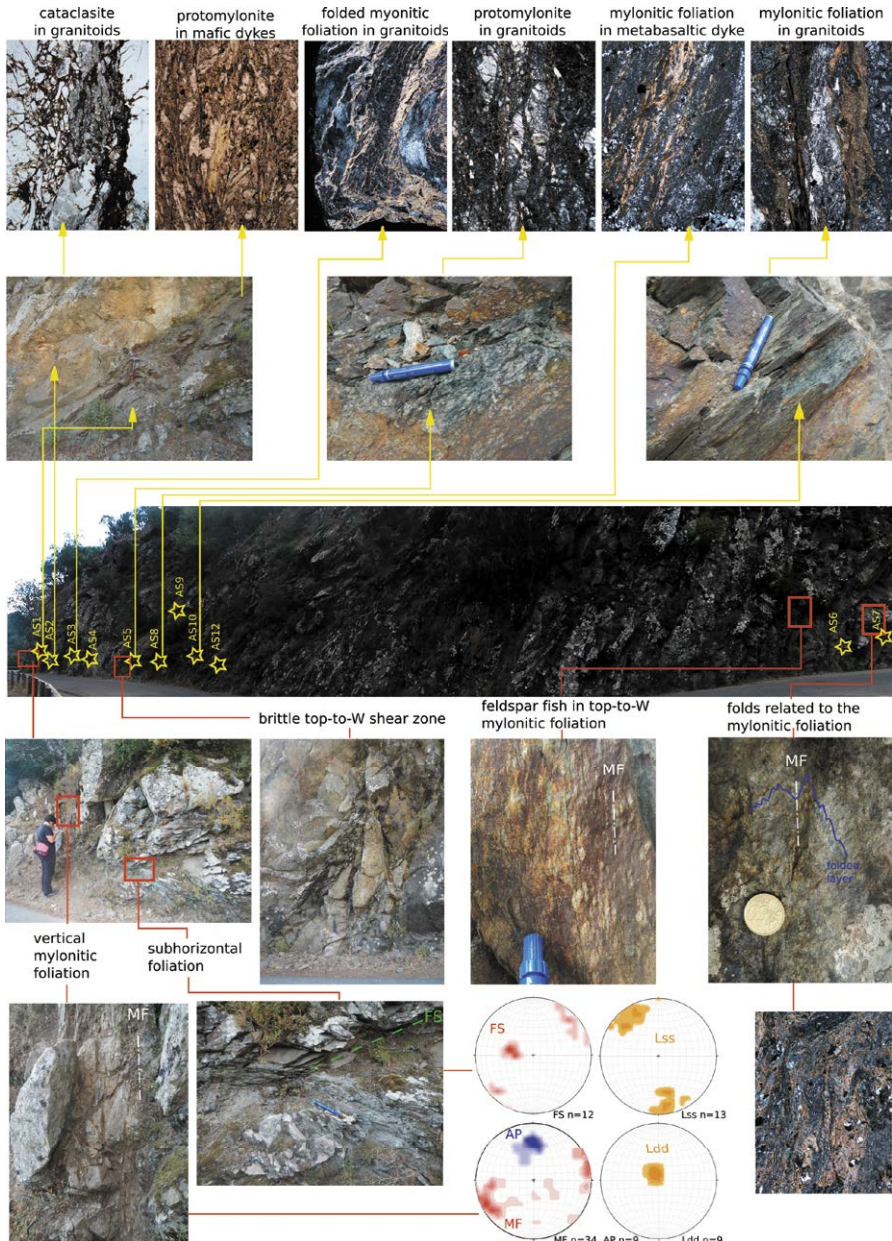
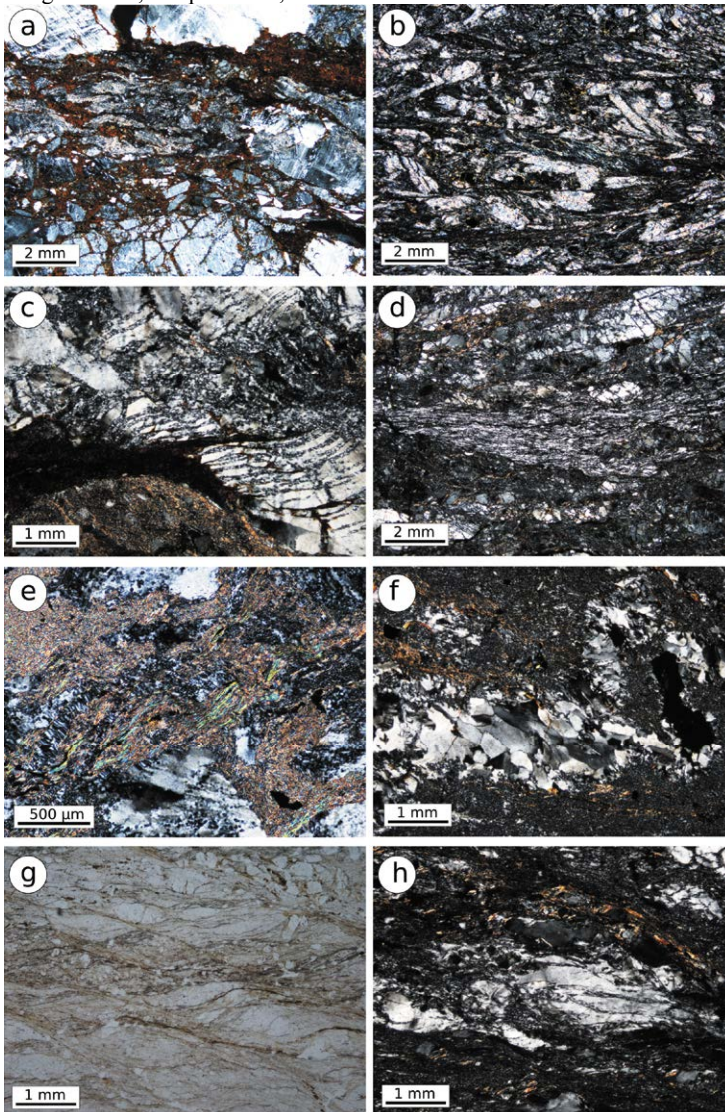


Figure 46. Microstructures related to Asco (a-f) and Castirla (g-h) shear zones. (a) undulose extinction of quartz and feldspar in cataclastic granitoids, sample AS2, cross nicols; (b) protomylonitic fabric in the mafic dykes, sample AS1, cross nicols; (c) bulging recrystallization in folded cracks and fractures filled by phyllosilicates in quartz crystals of granitoids, sample AS2, cross nicols; (d) bulging- subgrain rotation transition in a quartz ribbon, sample AS5, cross nicols; (e) s-c structures and folded antitaxial quartz veins in Volcanic and Volcaniclastic Fm., sample AS3a, cross nicols; subgrain rotation also occurs in quartz crystals; (f) blocky folded vein in basalt dyke, sample AS9, cross nicols; (g) s-c' structures and quartz and feldspar fishes in granitoids, sample AS12, parallel nicols and (h) s-c' fabric in granitoids, sample AS12, cross nicols.



The Castirla shear zone is developed in the granitoids and related mafic dykes, where a mylonitic foliation striking NE-SW occur. In both the lithotypes s-c' fabrics are found, as well as the stretching lineation indicating a top-to-NW sense of shear. In the two thin sections studied (AS12 and AS13, Fig 46g-h) the reorientation of phyllosilicates and the deformation of Qtz ribbons produce s-c' fabric, recognized within the granitoids also at the mesoscale. Necking and boudinage of the Qtz crystals, that show undulose extinction, is observed; bulging recrystallization is located in the squeezed areas between boudins in the Qtz ribbons and is set along planes parallel to the s- shear bands in single crystals of Qtz.

5.4.2 Razzo Bianco shear zones

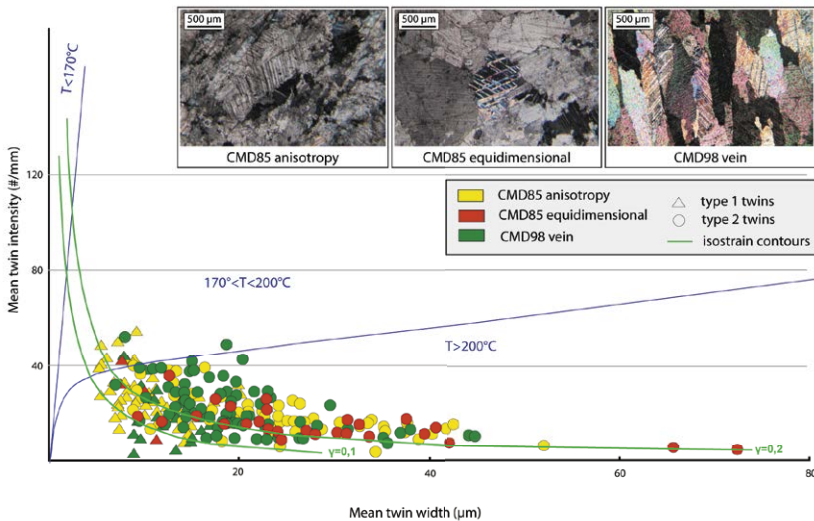
The area between Venaco village and the Punta di Raffè (D723, lat : 42°12'02.23''N, long : 9°9'20.75''E), west of the road N 193, is characterized by the presence of a shear zone involving the HCY that is overthrust by the Lower Units and the Schistes Lustrés Complex. The ductile deformation associated to the shearing of Razzo Bianco area is composed by three phases, whose structural elements were partially reworked during the subsequent brittle phase.

The D1 phase, almost completely transposed by the next D2 phase, has been detected only at the micro-scale in the metapelitic layer of the Eocene lithotypes; it consists of a relict S1 foliation made of Chl and Phg of metamorphic origin, to which are associated Alb and Qtz. The coexistence within the S1 foliation of Si-poor Chl and Al-poor Phg implies that the P-T conditions related to the D1 phase were typical of the low-grade blueschist to greenschist facies (Vidal and Parra 2000). The Chl that constitute the S1 foliation have a Si content between 2,45 and 2,65 a.p.f.u., with a XMg ranging from 0,53 and 0,65 (Fig.5.33); it has been also observed that the cores of the S1 Chl perform the highest values of XMg (Chl 1) while lower XMg values characterize their rims (Chl 2). The S1 Phg has a Si content between 2,90 and 3,40 a.p.f.u. and the Al content between 2 and 2,5 a.p.f.u.; from the cores to the rims of the crystals the Tschermak substitution is activated, consistent with a shift from Ce (Phg 1) to Mu (Phg 2) end-members (§ Cap 9). Using the Chl-Phg-Qtz-wt multi-equilibrium method (Vidal et al. 2009, § Cap 9), the P-T equilibrium range related to the D1 phase has been constrained between 0,97 and 1,26 ± 0.2 GPa and between 362 and 434 ± 30°C.

To the D2 phase is related the main foliation (S2) recognizable at the mesoscale in all the lithotypes; it is NNE-SSW oriented and generally dips toward ESE. At the thin section scale the granitoids show a main anisotropy (i.e. the S2 foliation) while no evidence of the relict D1 phase are preserved. Samples CMD84 and CMD95 show that a protomylonitic fabric is associated to the S2 foliation. In the CMD84, sampled close to the contact with the metalimestones, no intracrystalline deformation of Qtz occurs, while Fds clasts are affected by a weak intracrystalline deformation (patchy undulose extinction).

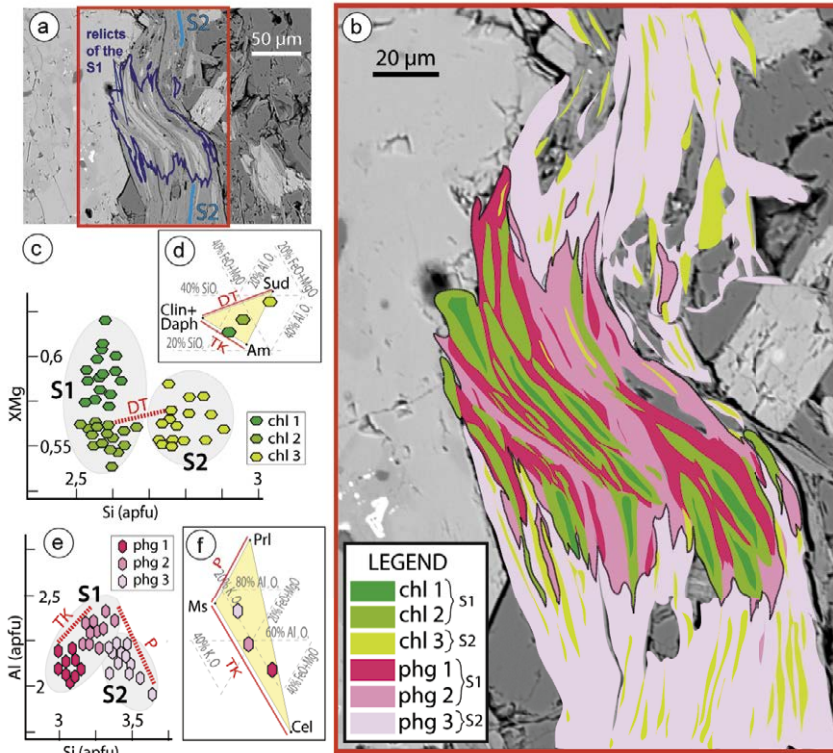
The granitoids of the CMD95, sampled west of the metalimestones, are characterized by a more intense deformation: Qtz shows sweeping undulose extinction and bulging intracrystalline deformation, to which are usually related temperatures of 300-400°C (Stipp et al. 2002a). The features of the Cal crystals in the metalimestones as well as in the carbonatic clasts of the Tertiary metabreccias (i.e. set of thick and thin twins cut by other set of thin twins, no grain boundary recrystallization, Fig 47) are typical of twinning that occur at $T > 200^\circ\text{C}$, followed by a cooling (Ferrill et al. 2004).

Figure 47. Mean twin width vs. mean twin intensity diagram (after Ferrill et al. 2004). The ratios have been measured on the Detritic Limestone Fm. (sample CMD85) and on the Carbonatic Breccia Fm. (CMD98) of Razzo Bianco.



The S2 foliation made of neo-formed Chl and Phg has been observed in the metapelites of the Tertiary Fms. In the hinge zone of the F2 folds it is observable the S2 foliation that crenulates the S1 foliation. The S2 Chl (Chl 3) have a Si content ranging between 2,70 and 2,90 a.p.f.u. and the XMg between 0,55 and 0,58 (Fig 48). The S2 Phg (Phg 3) have a Si and Al content ranging between 3,25 and 3,70 a.p.f.u. and between 1,90 and 2,25 a.p.f.u., respectively. The couples of Su-rich Chl and Py-rich Phg, grown along the S2 foliation, are in equilibrium in a P-T range of $0,84 - 0,26 \pm 0,2$ GPa and $293 - 169 \pm 30^\circ\text{C}$. Basically, the di-trioctahedral substitution in the Chl causes the change from a Da-rich Chl during the D1 phase to a progressively Su-rich Chl during the D2 phase, that implies a progressively decrease of the temperature conditions (Vidal and Parra 2000), whereas the activation of the pyrophyllite substitution observed in the Phg between the D1 and the D2 indicates a progressively decrease of the pressure conditions (Vidal and Parra 2000).

Figure 48. SEM picture of the Polygenic Breccia Fm., sample CMD98; relics of the S1 foliation are preserved in the S2 foliation; (b) zoom of the red box in (a); (c) Si vs. XMg content in the chlorite sampled in the foliation of the sample CMD98; (d) ternary diagram showing the proportion of the chlorite end-members of the sample CMD98; (e) Si vs. Al content in the phengite sampled in the foliation of the sample CMD98 and (f) ternary diagram showing the proportion of the phengite end-members of the sample CMD98.



The temperatures computed with the Chl geothermometer on the Chl3 ($293-169 \pm 30^\circ\text{C}$) are consistent with those obtained with the Cal twins: both the domains recognized (isotropic and stretched, Fig 47) present an high mean width/mean intensity width ratio, typical of Cal recrystallized at $T > 200^\circ$ (Ferrill et al. 2004). From the evaluation of the Qtz deformation in the shear zone within the granitoids arose slightly higher temperature values for the D2 phase ($400-500^\circ\text{C}$, Stipp et al. 2002a). This discrepancy could be explained considering the limits of the methods employed: it is necessary to take into account that the criteria used for the study of the Qtz deformation, despite being widely applied on granitoid rocks, it was created by studying rocks composed of 90% Qtz, and the temperatures are estimated with the help of pseudosections related to granitic rock; less influential but still present is the standard deviation associated to the Chl-Phg-Qtz-wt multiequilibrium method ($\pm 30^\circ\text{C}$). At the mesoscale, the D3 phase produces open to close asymmetric folds (F3) with an axial plane foliation

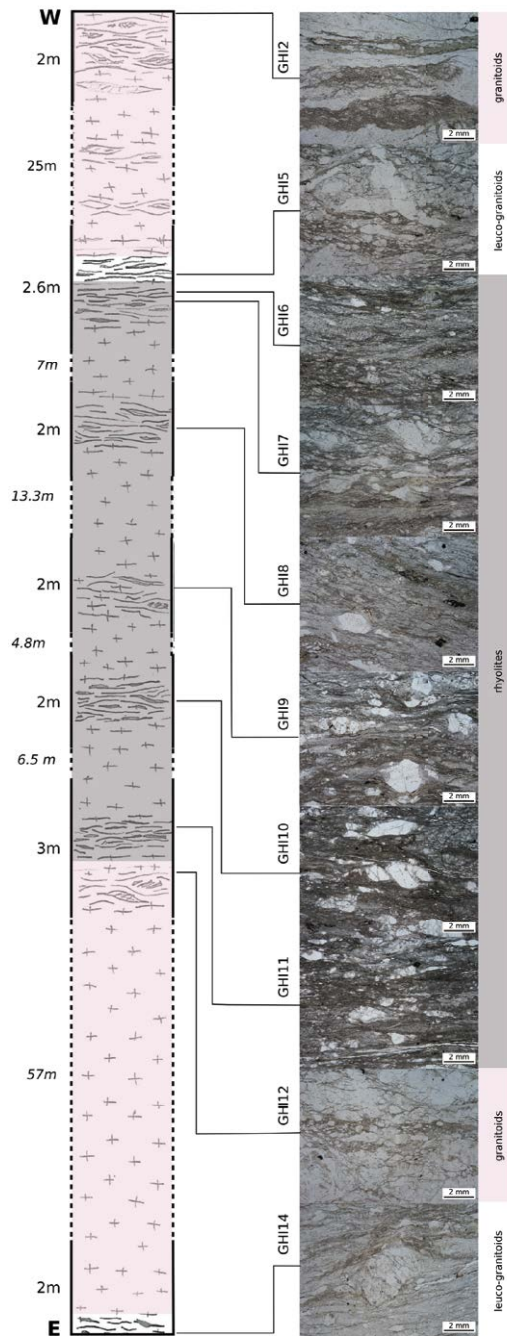
NNE-SSW oriented that dips of about 30° toward ESE. At the microscale the S3 foliation yields a spaced crenulation cleavage of the metapelitic layers of the Tertiary metabreccias and metasandstones, to which no phyllosilicates recrystallization is associated. The lack of a new generation of phyllosilicates associated to the D3 allowed to define a very shallow depths of Razzo Bianco during the last ductile phase. In terms of P-T conditions and microstructures, the resulting deformation history of Razzo Bianco is comparable to those of the Lower Units of the Alpine Corsica: as reported by Malasoma et al. (2006) and Di Rosa et al. (2017a ; 2017b ; 2018a ; 2018b), the tectonic units located between Popolasca and Corte are affected by a polyphased deformation history, to which are associated values of P and T that vary for each unit, but on average close to the values we calculated for Razzo Bianco in this work.

5.4.3 Noceta-Ghisoni shear zones

In the area between the Vezzani-Noceta (road D343) and Ghisoni-Sampolo (road D344) four structural domains has been recognized, limited by subvertical tectonic contacts that strike from N-S to NW-SE. These domains are (from west to east), (1) the Hercynian Corsica *sensu strictu* (W of Ghisoni), where no kind of deformation has been observed, (2) the HCY deformed by Alpine shear zones, where both ductile and brittle shear zones have been observed like those of Razzo Bianco, (3) the GHU, that represents the Lower Units group (§ Cap 4.4, 5.2.4) and (4) the IZU, representing the Schistes Lustrés Complex (§ Cap 4.4, 5.5.3). Given the post-last-ductile-phase (that corresponds to the post-D3 of the Lower Units) brittle deformation (i.e. the CCSZ) that strongly reworked the area and because of the thick vegetation, it was not possible to follow the structures between the two transects and thus to produce a detailed map of the whole area. However, since the attitude of the structures is similar along the two transects, here and in the next sections (§ Cap 5.5.3) they will be described together.

The shear zones have a NW-SE trend and are distributed in a 3-km thick area between the undeformed HCY and the GHU. 42 samples representative of all the lithotypes and of all the deformation degree were collected in Noceta and Ghisoni areas (Fig 49). The microstructures confirm the observation made at the mesoscale: the undeformed/cataclastic granitoids (Fig 50a) are cut by shear zones where the intensity of the deformation produces protomylonitic (Fig 50b,c) to ultramylonitic fabrics. S-c structures are well developed in the pelitic layer (Fig 50d,e), while Qtz and Fds show bulging recrystallization. In few cases has been observed that the main mylonitic foliation cut a previous mylonitic event (Fig 50e), rarely observed because these two foliations are parallel, and thus they are distinguishable only if the new “s” are set on the old “c” planes. The less deformed samples of rhyolites (GHI9) and granitoids (GHI12) show a protomylonitic fabric, to which \square -type porphyroclasts are associated; Fds show undulose extinction and cataclastic flow, typical of low metamorphic degree (<400°C). Increasing the deformation, the mylonitic fabric occurs in both

Figure 49. Sketch of the Ghisoni shear zones.



rhyolites (GHI7, GHI8) and granitoids (GHI5). Aggregates of Qtz and Fds constitute σ -type porphyroclasts in the rhyolites, whereas single crystals of Fds are fractured and present the bookshelf structure; subgrain rotation recrystallization occurs in the biggest Qtz clasts. These microstructures are associated to temperature of 400-500°C (Llyod and Freeman 1994; Passchier 1982). Further increasing of deformation, enhance the percentage of the matrix up to 85% in the rhyolites (e.g. GHI11) and up to 80% in the granitoids (GHI2). Qtz ribbons are almost completely recrystallized and affected by subgrain rotation in the granitoids, while rare σ -type porphyroclasts of Fds are preserved in the pelitic matrix of the rhyolites. Pinch and swell structures (Gardner et al. 2015) are also observed within the rhyolites. This deformation is associated to medium temperatures (>400°C, Passchier and Trouw 2005).

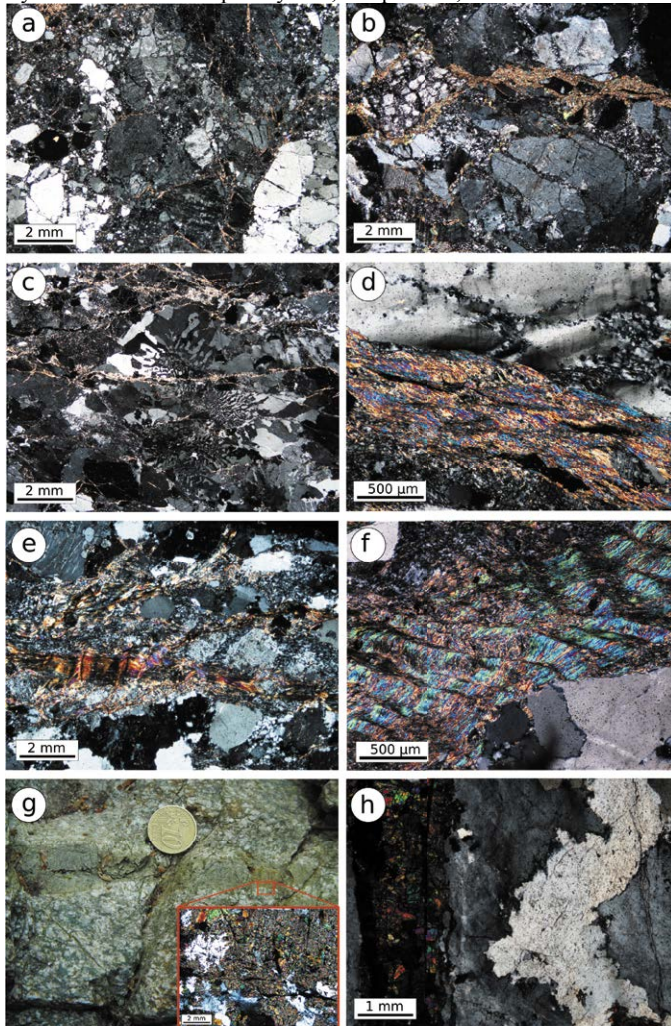
Near Muracciole village, the HCY, located west of GHU, is cut by several shear zones that range in thickness from 30 m to 350 m. The intensity of the ductile deformation varies from domains characterized by protomylonitic to ultramylonitic fabrics (Spry 1969; Sibson 1977; Shelley 1993; Passchier and Trouw 2005) to domains where the ductile deformation is very weak and dominate brittle structures. These shear zones are set on the Permo-Carboniferous granitoids and on the Permian rhyolites, and in small part also the Permo-Carboniferous basaltic dykes, leuco-granitoids and the Polygenic Breccia Fm..

These bands are characterized by a subvertical mylonitic foliation; s-c and s-c' fabrics, as well as σ -type porphyroclasts, indicate a top-to-W sense of shear. There is no an univoque correspondence between the thickness of the shear zone and the intensity of the deformation: for instance, in the shear zone related to the samples GHI5-GHI7 the mylonitic to ultramylonitic fabrics is extended in the rhyolites for about 3 m, while the shear zone related to the sample GHI14 is few cm thick and surrounded by undeformed granitoids. Sample GHI9 is instead representative of a protomylonitic shear zone few tens cm thick within the rhyolites. The contact with the undeformed granitoids/rhyolites tends to be a gradual fabric transition ending in a granular texture. Epidote veins are observed within the undeformed granitoids E of Muracciole (Fig 50g,h). They have the same orientation of the mylonitic foliation found few meters away, that is the same of the Ghisoni transect (~NS, subvertical).

Not everywhere open asymmetric folds have been observed within this domain of the HCY. They are equipped with subhorizontal axes and an axial plane foliation dipping of ~20° toward W and fold the mylonitic foliation.

The brittle deformation is widely developed in the whole area. It is usually set on the ductile shear planes where two systems of stretching lineation are found. The older one is down-dip and is coherent with a normal sense of shear; this lineation probably obliterated those associated with the top-to-W sense of shear given by the kinematic indicators of the mylonitic foliation. The younger stretching lineation is superimposed on the older one and indicates a strike-slip kinematics. Within the epidote veins of Muracciole, Qtz and Fds clasts coming from the host rock are affected by bulging recrystallization (Fig 50g,h).

Figure 50. Microstructures related to Ghisoni (a-f) and Noceta (g-h) shear zones. (a) granitoids affected by a weak cataclastic fabric, sample CMD33B, cross nicols; (b) protomylonitic fabric in granitoids, sample CMD31A, cross nicols; (c) myrmekitic texture in feldspar crystals of granitoids, sample GHI12, cross nicols; (d) incipient s-c' fabric in a metapelitic layer of rhyolites, sample GHI5, cross nicols; (e) incipient s-c fabric in the granitoids: parallel to the “s” bulging microfabric is set on the feldspar crystal. The mineral layering, as well as the previous foliation within the white mica layer suggest the presence of a previous event of ductile deformation, sample GHI13, cross nicols; (f) mylonitic foliation crenulated by the younger ductile event in a pelitic layer of the rhyolites, sample GHI7, cross nicols; (g) epidote vein within the granitoids at the meso and microscale. Undulose extinction of feldspar also occur, sample MU, cross nicols and (h) bulging recrystallization on feldspar crystals, sample MU, cross nicols.



5.5 Tectono-metamorphic history of the tectonic slices belonging to the Schistes Lustrés Complex associated to the studied Lower Units

The detailed study of the tectono-metamorphic history of the Schistes Lustrés Complex is out of the aim of this thesis. However, slices of rocks of oceanic affinity belonging to the LEU and the IZU interact with the Lower Units. Therefore, the study of the deformation history and of the metamorphic imprint localized to these slices coupled with the Lower Units has been carried out. To deepen the study of the Schistes Lustrés Complex at the regional scale, a wide bibliography is available (Mattaueer et al. 1977; Faure and Malavieille 1981; Malavieille 1983; Harris 1985; Warburton 1986; Malavieille et al. 1998; Levi et al. 2007; Vitale Brovarone et al. 2012).

In the Schistes Lustrés Complex a westward thrusting compatible with the Alpine E-dipping subduction has been recognized by several authors (e.g. Mattauer and Proust 1975; 1976; Mattauer et al. 1977; Cohen et al. 1981; Faure and Malavieille 1981; Malavieille 1983; Dallon and Nardi 1984; Harris 1985; Waters 1990; Jolivet et al. 1990; 1991; Fournier et al. 1991; Daniel et al. 1996; Malavieille et al. 1998). They include several groups of units for the lithostratigraphy and the metamorphic degree reached during the Alpine subduction (§ Cap 3.1.3). They usually occupy a position in the Alpine Corsica stack between the Lower and the Upper Units, but several slices of them have been found interspersed between the Lower Units or at the base of the tectonic stack, directly overthrusting the HCY.

The deformation history of the Schistes Lustrés Complex is difficult to outline: unlike the Lower Units, characterized by a polyphase deformation history that have similar features in all the units studied (§ Cap 5.2), the Schistes Lustrés Complex is composed by tectonic units having different deformation frameworks. The only common features observed in the areas studied in this thesis is that the last ductile event recognizable within the units of the Schistes Lustrés Complex is subsequent to their coupling with the Lower Units. In fact, the open asymmetric folds with subhorizontal axial plane foliation, that are related to the D3 phase in the Lower Units, also fold the units belonging to the Schistes Lustrés Complex, as well as the tectonic contacts between these two groups of units.

Regarding the metamorphism, as mentioned in the previous chapter (§ Cap 3.1.3) the P-T peaks conditions of the units belonging to the Schistes Lustrés Complex dramatically vary from the blueschist-eclogite of the Morteda-Farinole-Volpajola Unit to the very low grade of the Inzecca Unit (e.g. Vitale Brovarone et al. 2012 and references therein).

In order to constrain the geodynamic evolution of the Lower Units, the study of the deformation history and of the metamorphic conditions of the tectonic units belonging to the Schistes Lustrés Complex related to the Lower Units studied is here performed.

5.5.1 Cima Pedani and LEU

In the Cima Pedani tectonic window, the Schistes Lustrés Complex is represented by the Lento Unit (LEU) that overrides CAU, PEU and SCU Lower Units (§ Cap 4.1). According with the observations made by Levi et al. (2007) in the Golo Valley about the LEU, in the Cima Pedani area the deformation history of this unit is composed by four phases (D1-D4), developed during the intra-oceanic subduction, the annexion to the accretionary wedge and the exhumation during the Alpine Orogeny. Analogously to the Lower Units, the D1 of LEU is almost completely transposed by the D2 phase. Only in thin section the S1 foliation is distinguishable from the S2 foliation in the F2 hinges, preserved within the microlithons of the S2. In the metagabbros the S1 foliation consists of a metamorphic paragenesis made of Chl+Phg+Lws+Qtz. Basing on this metamorphic assemblage, Levi et al. (2007) estimated the P-T conditions (Vidal et al. 2001; Parra et al. 2002a) related to the D1 phase of the LEU (0.8 ± 0.2 GPa, $400\pm 50^\circ\text{C}$).

The D2 phase is characterized by F2 isoclinal folds having a S2 sub-vertical axial plane foliation that strikes N10 and dips toward SE with variable angles. The F2 are cylindrical with A2 sub-horizontal axis that trend from N-NE to S-SW. The F2 hinges range from sub-acute to rounded and the limbs are characterized by necking, boudinage and pinch and swell structures. At the microscale different textures are associated to the S2 foliation in the metapelites (i.e. Erbajolo Fm.). In the hinges of the F2 folds the S2, made of Chl and Phg, is classifiable as crenulation cleavage. On the limbs, where the S1 foliation is completely transposed by the S2, associated to the Chl and Phg grew along the S2, porphyroclasts with strain shadows have found and Qtz presents traces of a dynamic recrystallization variable from bulging to subgrain rotation (Hobbs 2014).

The D3 phase is characterized by F3 open to close folds with A3 sub-vertical axes going from N to S and a S3 sub-vertical spaced foliation. At the microscale, in the metapelites the S3 is classifiable as crenulation cleavage to which no recrystallization is associated.

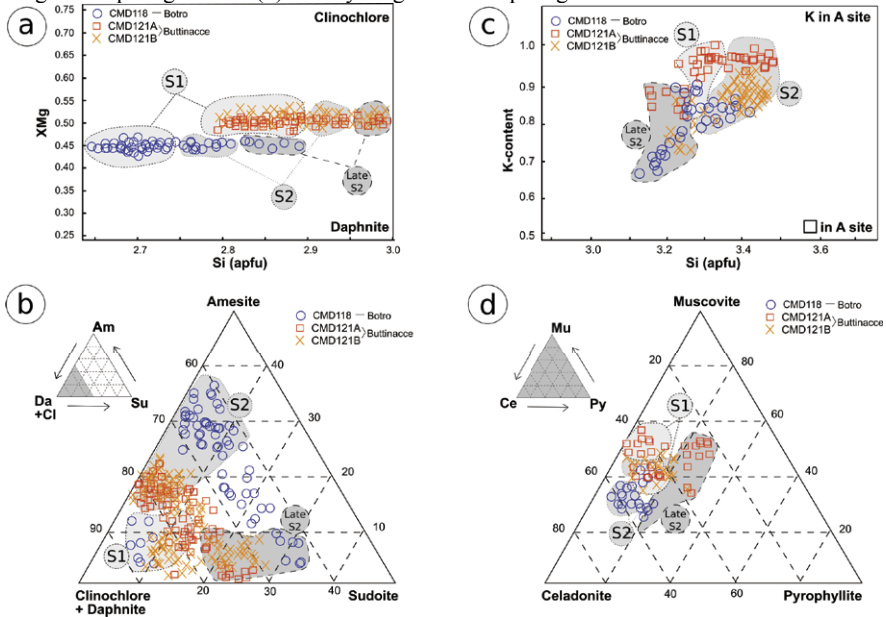
The D4 phase produces F4 open asymmetric folds with a S4 sub-horizontal axial plain foliation, classifiable as disjunctive cleavage. It has been observed that the S4 foliation folds also the tectonic contact between LEU and the SCU of the Lower Units; therefore, the S4 foliation corresponds to the S3 of the Lower Units. No evidence of the D4 has been observed at the microscale, as well as the presence of a new metamorphic assemblage.

5.5.2 Corte and IZU

The geochronological data available for the Corsica Island regard the post- In the Corte area, the Schistes Lustrés Complex (i.e. IZU) occur as tectonic slices whose extension varies from $0,1\text{ km}^2$ (i.e. Colla di a Posta, Fig.5.9) to $0,6\text{ km}^2$ (i.e. north of the intersection between the roads D18 and N193, Di Rosa et al.

2017b). The Schistes Lustrés Complex are located, respect to the Lower Units stacking, at the top (i.e. Pietra Piana slice), at the base (i.e. Botro slice) and also between the Lower Units (i.e. Sant'Angelo and Buttinacce slices, Fig 24). In the south-eastern side of the area, the relationships between the Lower Units and the IZU are obliterated by the CCSZ.

Figure 51. Geochemistry of the calc-schists of IZU-Botro and IZU-Buttinacce. (a) Si/XMg diagram of chlorites, (b) ternary diagram of the chlorite end-members, (c) Si/K diagram of phengites and (d) ternary diagram of the phengite end-members.



In each slice of the IZU, the main foliation recognizable at the mesoscale has similar features to the D2 of LEU: F2 isoclinal folds with a S2 axial plane foliation and A2 sub-horizontal axes trending from N to S. The S2 foliation has a N-S trend in all the tectonic slices of the area, except for the one of Colla di a Posta in which the S2 foliation has a WNW-ESE strike.

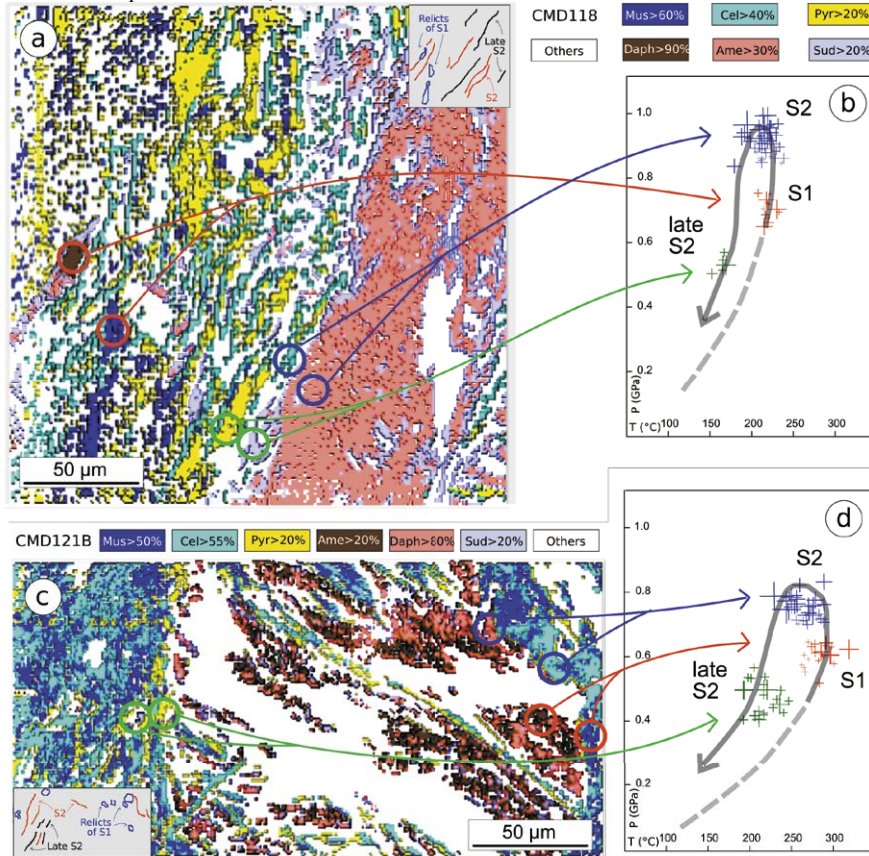
The D3 phase recognized everywhere in the IZU slices of the Corte area corresponds to the D3 phase of the Lower Units. The same F3 open to close asymmetric folds with subhorizontal axial plane foliation also fold the previous structures of the IZU, as well as the tectonic contact between them and the Lower Units.

In the thin section, an older foliation (S1) has been found in the hinge zones of the F2 folds. The study of the metamorphism performed on the calc-schists belonging to two of these slices (i.e. Botro and Buttinacce) revealed that the metapelitic layers are characterized by three paragenesis associated to two deformation phases (i.e. D1 and D2, Fig 51). The D1 phase is represented by

relics of Chl and Phg preserved within the microlithons of the S2 foliation; a late S2 foliation, arranged at low-angle respect to the S2, is also observed. Although these features characterize all the samples, the P-T values associated to the three steps change in all the samples.

Three samples of calc-schists were selected (CMD118 of IZU Botro slice, CMD121A and CMD121B of IZU Buttinacce slice) in order to study the thermobarometry of IZU Botro and IZU Buttinacce. The S1 and S2 foliations are made of Chl, Phg, Qtz, Alb and Cal that constitute two different metamorphic parageneses. In addition to them, a third generation of Chl and Phg grow along surfaces that made a low angle with those of the S2 foliation. This foliation is clearly subsequent to the S2 foliation, but, given the lack of mesoscale evidence of a foliation between the S2 and the S3, this anisotropy has been assigned to the late D2 phase. The thermodynamic equilibrium of these three different paragenesis allowed to estimate the P-T values of the D1, D2 and late-D2 phases. The Si content in the Chl ranges between 2.78 and 3.00 a.p.f.u. in the samples from Buttinacce and between 2.65 and 2.90 a.p.f.u. in the sample from Botro, whereas the XMg is higher in the samples of Buttinacce (0.48-0.54) than in the sample of Botro (0.42-0.46) (Fig.5.36). As regards the Phg, three clusters of data are recognizable in the binary diagrams: the first dataset is characterized by a Si content between 3.20 and 3.35 a.p.f.u. in all the sample and K-content always > 0.85 a.p.f.u.. The second dataset includes Phg with similar K content to the previous one, but higher Si content (3.35-3.50 a.p.f.u. for samples CMD121A and CMD121B and 3.25-3.40 a.p.f.u. for CMD118). The Phg belonging to the third dataset are characterized in all the sample by lower content of Si (3.10-3.25 a.p.f.u.), and K (0.65-0.90 a.p.f.u.). The Al_{tot} is basically higher in the sample of Botro (1.60-1.75 a.p.f.u.) than those of Buttinacce (1.40-1.55 a.p.f.u.). It has been observed that the first cluster of data, the chemistry of which indicates Phg enriched in the Mu end-member, is related to the crystals grew during the D1 phase, whereas the second cluster of data, suggesting a higher content of Ce end-member, is related to the crystals grew within the S2 foliation; the Phg grew along the late S2 foliation are instead enriched in the Py end-member. The older paragenesis (D1) is characterized by Chl with the highest content of Am end-members (20-40%), whereas those grew during the D2 phase have an Cl+Da content higher than 80% with a Su content always lower than 10%; the Chl grew along the late D2 phase are instead enriched in the Su end-members, that reach the proportion of 35%. Therefore, three areas in the P-T paths where the Chl-Phg couples are in equilibrium have been identified (Fig 52). For the Botro and Buttinacce slices, the Chl-Phg couples related to the S1 phase are in equilibrium at 0.65-0.75 GPa and 220-245°C and at 0.55-0.65 GPa and 265-310°C, respectively. During the D2 phase the slices of IZU reach the highest pressures condition, in particular the Botro slice at 0.85-1.00 GPa and 200-250°C, while the Buttinacce slice at 0.70-0.85 GPa and 240-275°C. These values change in the late D2 phase, as demonstrated by the P-T equilibrium of the Chl-Phg couples grew along the late-S2 foliation (0.5-0.6 GPa and 150-190°C for Botro, 0.4-0.6 GPa and 200-250°C for Buttinacce).

Figure 52. (a) EPMA micromaps of (a) IZU-Botro, sample CMD118 and (c) IZU-Buttinacce, sample CMD121B, highlighting the relationships between foliation and phases distribution. (c) IZU-Botro and (d) IZU-Buttinacce P-T equilibria obtained combining chlorite-phengite couples selected in the map and indicated by circles. The three clusters of data correspond to the S1, S2 and the late S2 foliations.



From these data emerges that the two slices studied (i.e. IZU Botro and IZU Buttinacce) had independent paths of subduction and exhumation until the end of the D2 phase. The P-T conditions estimated for the D1 phase do not coincide with those of the geobaric peak in all the samples studied. The P-peak is indeed reached during the D2 phase, as testified the P-T equilibrium of the Chl-Phg couples sampled along the S2 foliation. The transition between the S1 and the S2 occur in isothermic conditions for the Botro slices, while the temperature range between the D1 and the D2 phase is lower than 50°C for the Buttinacce slice. Similar values for all the samples are instead reached during the late D2 phase, to which is associated the late S2 foliation: the pressure values drastically decrease (from 1.0 GPa to 0.5 GPa for Botro and from 0.8 to 0.4 for Buttinacce), while the temperature conditions decrease 200° to 160°C in Botro and from 230° to 200°C

in Buttinacce.

As regards the D3 phase, F3 open folds and a S3 foliation classifiable as disjunctive cleavage are found in thin section of the calc-schists (e.g. CMD120). Commonly, microfractures, whose thick range from 300 μm to several mm, are superimposed on the S3 foliations. The recrystallization associated to this phase lacks, as well as the filling of these surfaces with Cal or Qtz.

5.5.3 Noceta-Ghisoni and IZU

The IZU unit is the easternmost domain recognized in the area between Vezzani-Noceta and Ghisoni-Sampolo. The attitude of the tectonic contact that brings IZU above GHU is similar in the two transects (N145 in the Vezzani-Noceta and N018 in Ghisoni-Sampolo), as well as the main foliation measured in the calc-schists, that correspond to the S2 foliation measured in the slices of IZU of Corte area. Associated to this foliation, F2 isoclinal folds with A2 subhorizontal axes have been found. A thick network of Cal veins not younger than the D2 phase are also observed. No evidence of the D2 deformation occur in the other rock-types of IZU (gabbros, breccias, pillow basalts) because of the weakness of the deformation typical of the IZU. At the microscale, the calc-schists appear as layered metacarbonates made of recrystallized Cal alternated with thin levels of metapelites. This lithological alternation, together with a younger generation of Cal veins, is folded by isoclinal folds. The Cal crystals of the metacarbonatic layers are different in shape, size and texture to those of the Cal veins:

The D3 phase produces in the calc-schists open folds with a S3 axial plane foliation that dips toward E of about 10°. Nice examples of F2 isoclinal folds folded by the S3 foliation have been found close to Sampolo lake. A new generation of Cal veins occurs parallel to the S3 foliation, that seem folded by tardive folds characterized by subvertical axial plane foliation.

Differently to the ductile deformation history, the post-D3 phase have been registered by all the rock types cropping out in the IZU of Noceta-Ghisoni area: the main fault system described in the HCY and in GHU domains has been recognized, in addition to the calc-schists, in the pillow basalts as well as in the gabbros.

5.6 The post-D3 deformation

After the D3 phase, the main deformation event that affects the Corsica Island consists in the brittle deformations related to the Central Corsica Shear Zone (i.e. CCSZ, Fig.5.38). It is an important regional-scale structure, widely described in Corsica as a sinistral strike slip fault zone (Maluski et al. 1973; Jourdan 1988; Waters 1990; Molli and Tribuzio 2004; Lacombe and Jolivet 2005). In the study area it mainly develops through a km-wide, north-south trending sinistral strike

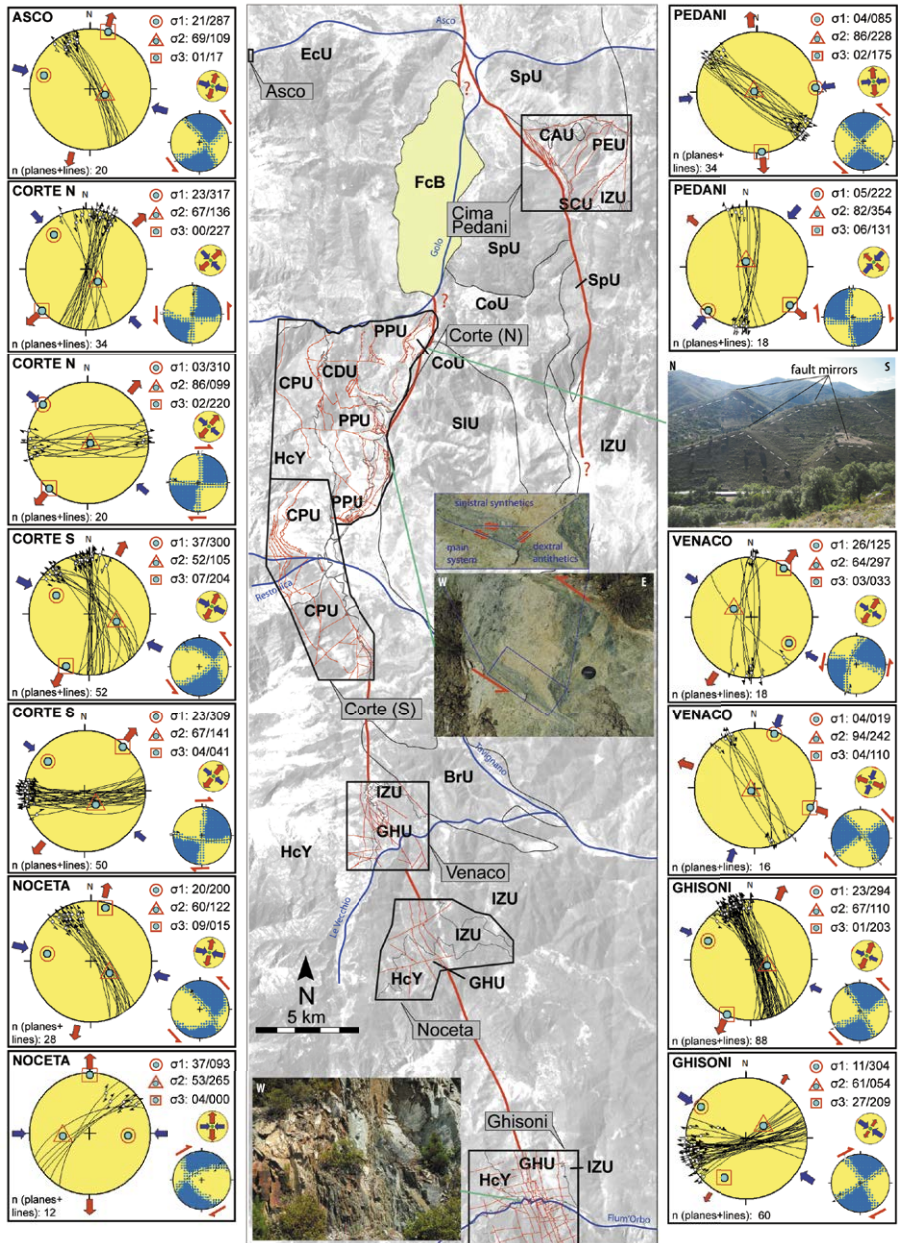
slip fault, associated with sinistral and dextral syntetic and dextral antthetic strike-slip faults (Di Rosa et al. 2017b). Brittle structures associated to this post-D3 phase are often superimposed on the pre-D3 tectonic contacts between HCY and Alpine Corsica, as well as between the groups of units of the Alpine Corsica (i.e. Lower Units, Schistes Lustrés Complex and Upper Units). At the map scale the sinistral sense of shear is observed in the NNW-SSE oriented structures and a dextral sense of shear in the antithetics faults, given by the displacement of the S2 foliation. Although the brittle structures of the CCSZ are commonly associated to the main tectonic contacts between the HCY and the Lower Units (e.g. Venaco and Noceta-Ghisoni areas) and between the Lower Units and the Schistes Lustrés Complex (e.g. Cima Pedani and Corte areas), at least in two cases structures associated to the CCSZ set within the HCY have been found (e.g. Asco and Ghisoni areas).

In the Cima Pedani area one of the main fault zone of the CCSZ occurs in the western side of the tectonic window (§ Cap 4.1), obliterating the original relationship between the Lower Units and the overlying Upper Units (Fig 53). The attitude of the NNW-SSE trending fault planes and the associated slikenlines have been measured in the serpentinites and gabbro, and the results from the elaboration of these collected data comply with a sinistral strike-slip fault kinematics. Associated to the main system, three dextral antithetic NE-SW striking strike slip faults that crosscut the Lower Units of the Cima Pedani tectonic window are found.

In the Corte area, the CCSZ is mainly represented by a complex network of brittle deformations, the cartographic expression of which draws the valley where the road N193 is located (Figs 53-54). In the Caporalino area, the CCSZ marks the contact between the Lower Units and the Santa Lucia Unit and it characterized by NNE-SSW trending splay thrusts along which the Caporalino Unit is carried over the PPU. In this fault zone several slices of metadolostones and metagranotids belonging to the PPU and metabasalts of the Schistes Lustrés Complex occur. Toward south, near San Quilico hill, the CCSZ is superimposed on the pre-D3 contact between the Lower Units and the Schistes Lustrés Complex (Fig 54b). In the adjacent area of Monte Cecu a well developed riedel system of strike-slip faults with NNE-SSW and SE-NW trend crosscuts the Monte Cecu antiform in several places (§ Cap 4.2). South of Corte town, the CCSZ develops a map-scale shear band similar to those of Cima Pedani. Along the road N193, south of Botro, slices of granitoids of the HCY and metamorphic rocks belonging to the Lower Units and to the Schistes Lustrés Complex are interposed between the CPU and the IZU, wiping out the original pre-D3 overthrusting of the Schistes Lustrés Complex above the Lower Units.

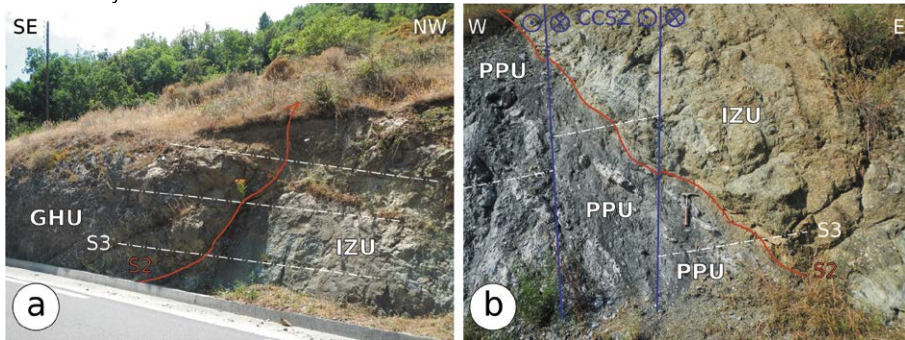
Between Casanova and Santo Pietro HCY and the Schistes Lustrés Complex, despite is characterized by the presence of slices probably belonging to the Lower Units, is preserved in the original pre-D3 setting. A nice example of a tectonic contact between IZU and slices of Roches Brunes Fm. folded by the D3 phase is exposed northern of Casanova along the road N193 (Fig 54 a). It is plausible that at this latitude the main branch of the CCSZ observed in the Corte area is

Figure 53. The CCSZ in the study area. Stereographic projections are made with Wintensor software. The main stress axes (σ_1 , σ_2 and σ_3) and types of stress are reported.



located toward west of this contact, within the HCY, where a 15 m thick cataclasites made at the expense of the granitoids and the Roches Brunes Fm. has been found. What is clear is that south of Venaco village the brittle deformation reworks again the tectonic contact between the HCY, the Lower Units and the Schistes Lustrés Complex (Fig 53). In addition to the main fault system, that has NNW-SSE trend, at least two other secondary systems occur that create a puzzle of tectonic slices made of granitoids, metagranitoids, rhyolites, Roches Brunes Fm. and Tertiary undeformed deposits.

Figure 54. (a) tectonic contact between GHU and IZU folded by the D3 phase, north of Venaco village and (b) tectonic contact between PPU and IZU folded by the D3 phase and reworked by the CCSZ in the San Quilico area.



In the area between Noceta and Ghisoni, the tectonic contacts at the base and top of the GHU are difficult to trace because the brittle deformation strongly reworked the previous structures. In the Fig.5.38 a simplified map is proposed, where only the main faults are reported. In the Noceta-Ghisoni area the post-D3 brittle deformation is not constrained within the GHU and the Schistes Lustrés Complex, but also interest the domain of the HCY between Ghisoni village and the tectonic contact with GHU, i.e. in the same sector where the D2 ductile shear zones are found (§ Cap 5.4.3). In this sector, differently from the ductile deformation that is localized in few bands, the brittle deformation is pervasive, leaving only few meters of undeformed rocks. Several measures of fault planes referable to three different systems are collected, compatible with a sinistral strike system NNW-SSE oriented with related syntethical and antithetical, the orientation of which make with the main system low and high angles, respectively. On the fault planes of the main fault system (~NNW-SSE) and on the dextral antithetical system (~ENE-WSW), two slickenlines systems are found: an older one (down-dip) and a younger one (strike-slip). The downdip slickenlines gives in both cases a normal sense of shear; in the NNW-SSE faults system, when these planes are superimposed on the c- planes of the D2 ductile shear zones, the older vertical slickenlines obliterated the L2 stretching lineation, deleting the original top-to-W sense of shear.

Another case in which the CCSZ crosscut the HCY is located in the Asco Valley, in the place where the ductile shear zone crops out (§ Cap 5.4.1). Above

the older L2 stretching lineation, also in this case partially reworked by down-dip slickenlines coherent with a normal sense of shear, a younger system, NW-SE trending and dipping of about 10° toward SE, is due to the strike-slip phase similar to those observed in Noceta-Ghisoni area.

Chapter 6

Age constraints: magmatic ages and the Permo-Triassic heating episode

The geochronological study of seven samples of magmatic products of the Permo-Carboniferous batholith and belonging to the Lower Units allowed to constrain the age of different magmatic bodies (i.e. the metagranitoids and the epidote-bearing metagabbros) and to detect the post-Variscan/pre-Alpine history of heating of the European margin. These data were obtained with the U-Pb dating of zircons (extracted crystals) and of allanites (*in situ*) of metagranitoids and epidote-bearing metagabbros specimens, sampled in different localities along the south-western rim of the Alpine Corsica.

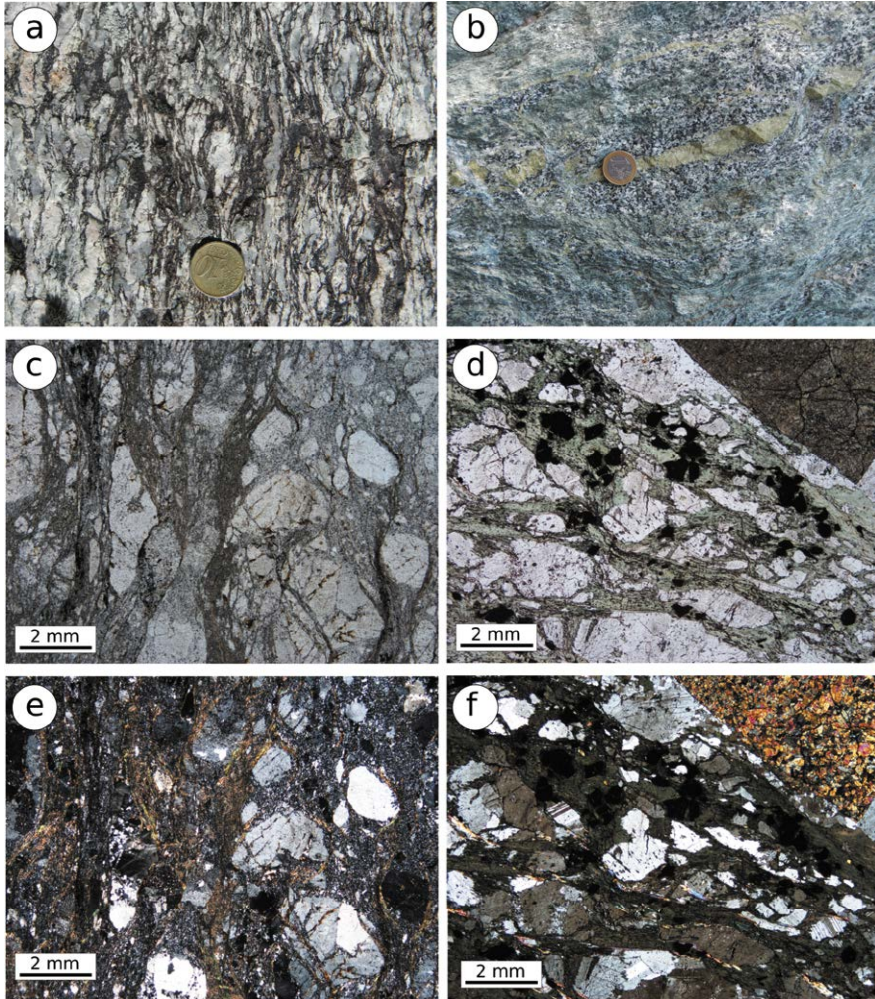
6.1 Petrographic features of the metagranitoids and the epidote-bearing metagabbros

The metagranitoids (e.g. samples CMD37, CMD33A, CMD33(43), CMD40(50), CMD57(67) and CMD57B) are metamorphic monzogranites made by 35% of Qtz, 30% of k Fds, 25% of Fds and 5% of Chl that probably replaces the magmatic Bit. The remaining 5% includes Phg, minor Epd and accessories phases like All, Mnz and Zrc (Fig 55a,c,e). The protholith of this rock was a peraluminous A-type granite (SIAM classification, Chappell and White 1974), typically found in collisional belt and originated by the melting of the continental crust. The metagranitoids are cut by mafic dykes, composed by Cpx, Plg, Amp, less abundant Qtz and accessories like Epd and All. The dykes swarms were

Maria Di Rosa, University of Pisa, Italy, maria.dirosa.scaglia@gmail.com, 0000-0002-1154-7429
FUP Best Practice in Scholarly Publishing (DOI 10.36253/fup_best_practice)

Maria Di Rosa, *Tectono-metamorphic evolution of the continental units along the edge between Alpine and Hercynian Corsica. Constraints for the exhumation models in the continental collision setting*, © 2021 Author(s), content CC BY 4.0 International, metadata CC0 1.0 Universal, published by Firenze University Press (www.fupress.com), ISSN 2705-0297 (online), ISBN 978-88-5518-420-5 (PDF), DOI 10.36253/978-88-5518-420-5

Figure 55. Fig.6.1 (a) Metagranitoids and (b) epidote-bearing metagabbros of GHU. The two lithotypes in thin section: metagranitoids, sample CMD37, (c) parallel and (e) crossed nicols; epidote-bearing metagabbros, sample CMD50E, (d) parallel and (f) crossed nicols.



deformed and metamorphosed together with the metagranitoids. The epidote-bearing metagabbros show a more complex composition and texture, nowadays made for the 35% by Plg, 10% by Plg, 10% by Amp, 5% by Fds, 10% by Epd, 10% by Chl, 10% by Qtz and 5% by Phg; the remaining 5% includes opaque oxides, Apt and Zrc (Fig 55b,d,f). The Cpx (augite in this case) occur as euhedral crystals in the mylonitic layers and are partially replaced by a mixture of Epd and Chl; the matrix of these layers is made of Plg, Chl and Qtz. SEM analysis show a considerable amount of Al, that probably substitutes Si in the tetrahedral site. Alb and Plg occur in subhedral crystals, while Qtz occurs in aggregates. The Epd

belongs to the metamorphic blastesis and occurs, other than associated to augite, in subrounded crystals with high relief and high interference colors. Evidence of deformation are found in both the lithotypes: an anisotropy to which is usually associated the mylonitic fabric is everywhere folded in open asymmetric folds.

6.2 U-Pb geochronology on zircons

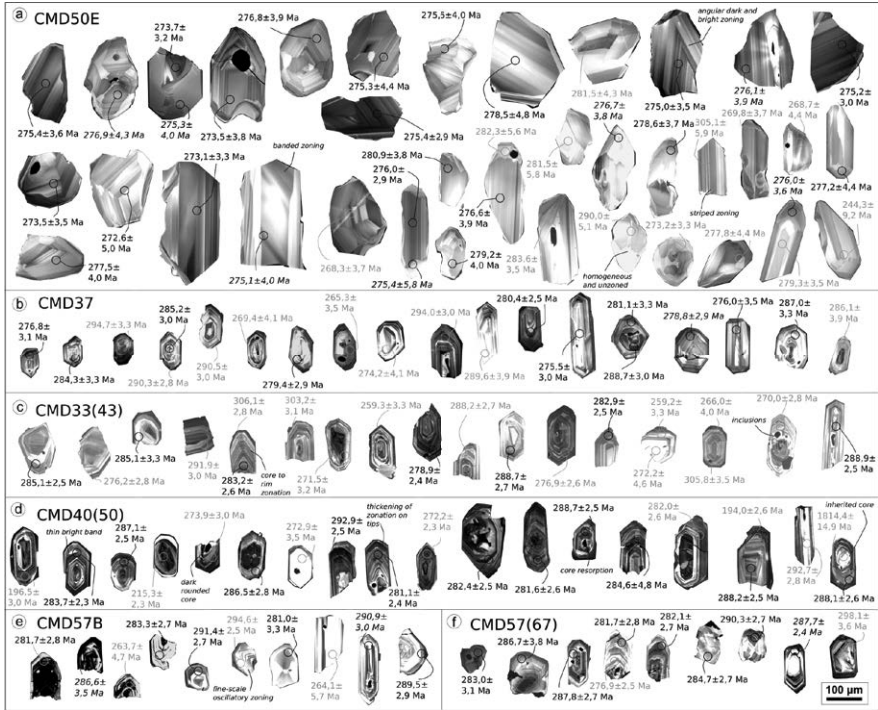
6.2.1 Zircon texture

Sixty-five zircon crystals have been separated from five samples of metagranitoids coming from the CPU and GHU and one sample of epidote-bearing metagabbros of GHU. Zircons of the metagranitoids (i.e. CMD 57(67), CMD40(50), CMD57B, CMD33(43) and CMD37) are 35-450 μm in size, they appear colourless and present the typical euhedral shape, range from stumpy (e.g. CMD57(67), CMD37) to elongate (e.g. CMD33(43)), sometimes broken by microcracks. Under cathodoluminescence (CL), the grains are characterized by a homogeneous or faintly zoned centres surrounded by fine-scale oscillatory zoned rims (e.g. CMD57B) sometimes thickened towards the tips (e.g. CMD40(50)) and seldom exhibit complex core-to-rim growth zoning with common local intermediate resorption (e.g. CMD40(50), Fig 56). Usually a core-to-rim zonation is observed; only in few cases inherited cores have been detected. In other cases, the cores are rounded and composites, usually dark, without evidence of zonation. The presence of inclusions varies for each sample: in some samples are abundant and are placed in the core (e.g. CMD33(43), CMD40(50)), in some samples are present only along the rims (e.g. CMD57B) and in others are rare (e.g. CMD57(67), CMD37). Few crystals are metamictic (e.g. CMD33(43), CMD40(50)) and these, located in both cores and rims, are black. Thin bright bands are common (CMD40(50)), and in some case a polyphase internal structures have been observed (e.g. CMD40(50)).

Zircons of the epidote-bearing metagabbros (i.e. CMD50E) are transparent to translucent and bigger than those of metagranitoids (95-580 μm). They are subhedral to anhedral, and the original prismatic shape is badly preserved. The crystals are tendentially elongated, but almost all of them are broken by irregular fracturation. Under CL, zircons show banded zoning typical of mafic rocks. Very often the crystals show angular dark and high luminescence domains, but some of them are homogeneous and unzoned. Dark patches due to metamictization are common, in some case associated to microfractures. The cores, when visible, are either bright or dark, angular and zoned and without evidences of resorption. Inclusions, rarely observed, are located on both the core and the rim of the crystals. In a few cases, striped zoning is observed.

Although in some cases thin bright rims have been observed (e.g. CMD37, CMD40(50)), evidence of metamorphic rims on the zircon crystals belonging to both rock types attributable to a metamorphic recrystallization are missing.

Figure 56. Zircon CL images and analysis points of the samples a) CMD50E b) CMD37, c) CMD33(43), d) CMD40(50), e) CMD57B and f) CMD57(67). In black are indicated the spots whose value has been used to calculate the weighted average age of the samples; italics has been used for the spots whose value is included within the error of the sample age. In grey are marked the spots whose age has not been considered for the age calculation.

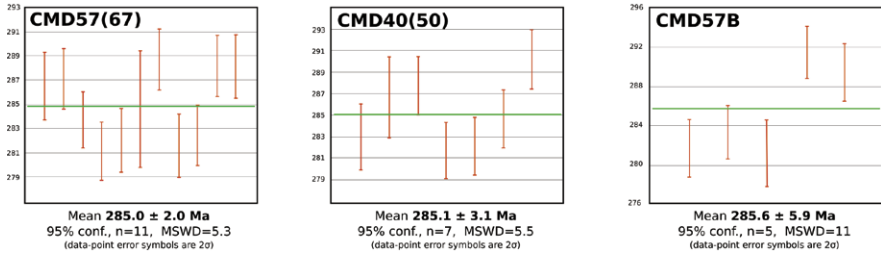


The zircon crystals were dated by LA-ICP-MS U–Pb analysis (Tab 4); the $^{206}\text{Pb}/^{238}\text{U}$ ages and related 2σ errors are shown in weighted average diagrams, while the ratios between $^{207}\text{Pb}/^{235}\text{U}$ and $^{206}\text{Pb}/^{238}\text{U}$ are plotted in the Concordia diagrams. A weighted mean $^{206}\text{Pb}/^{238}\text{U}$ age has been determined for each sample, considered only the sub-concordant spot analyses (Fig 57).

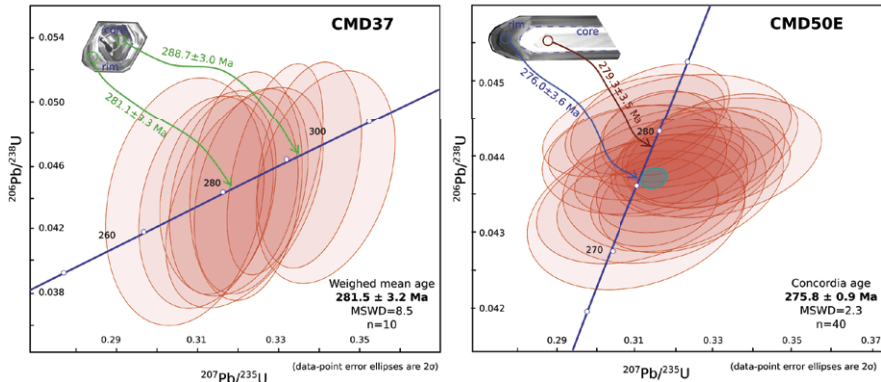
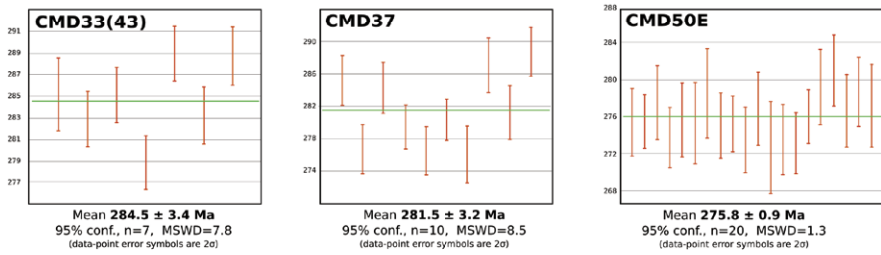
The analyses related to the metagranitoids performed on both centres and rims yield apparent spot ages that vary from 272 to 305 Ma, with most of the data forming a cluster at ca 288 Ma. Most of the spot analyses are discordant and only twenty-one analyses passed the <10% discordancy test. The five samples analysed for metagranitoids yielded weighted average $^{206}\text{Pb}/^{238}\text{U}$ ages between 281.5 ± 3.2 Ma ($n=10$, MSWD = 8.5, CMD37) and 285.6 ± 5.9 Ma ($n=5$, MSWD = 11, CMD57B). Although the MSWD values are $\gg 1$, the weighted average ages are almost the same for the three samples belonging to the CPU (285 ± 3 Ma). Zircon spot ages for the epidote-bearing metagabbros (CMD50E) give a Concordia age of 275.8 ± 0.9 Ma, calculated on 20 data-points with a good

Figure 57. Weighted average diagrams of the samples CMD57(67), CMD40(50), CMD57, CMD33(43), CMD37 and CMD50E and Concordia diagrams of the samples CMD37 and CMD50E.

Castiglione-Popolasca Unit



Venaco-Ghisoni Unit



MSWD value of 1.3. On the whole, comparing the magmatic ages of the two rock types sampled in the Ghisoni area (i.e. CMD37, CMD33(43) and CMD50E) we note that the average age estimated for the metagranitoids (283.0 ± 3.1 Ma) is slightly older than that of the epidote-bearing metagabbros (275.8 ± 0.9 Ma). Considering the respective errors the scatter is very small; however, similar ages for the cores of the epidote-bearing metagabbros and the rims of the metagranitoids have been observed.

6.2.2 The magmatic ages of metagranitoids and metagabbros: petrological implications on the batholith's intrusion

The geochronological data available for the Corsica Island regard the post-Zircon crystals were found in the metagranitoids of CPU and GHU and in the epidote-bearing metagabbros of GHU. The regular oscillatory zoning that characterized those of the metagranitoids suggest a magmatic origin; moreover, the elongated shapes occurring in the crystals belonging to both rock types are commonly ascribed to rapid growth from a supersaturated melt (Elburg 1996). Even if all the samples come from deformed and metamorphosed rocks, no metamorphic rims around the zircon crystal have been found. Therefore, the ages

Table 4. Results of the U-Pb dating of zircon

Sample	Locality	Age (Ma)	MSWD	n. analysis considered	Total n. of analysis
CMD 57(67)	Steles (CPU)	285.1 ± 3.1	5.5	7	10
CMD 40(50)	Cistern a (CPU)	285.0 ± 2.0	5.3	11	20
CMD 57B	Vallett o (CPU)	285.6 ± 5.9	11	5	10
CMD 33(43)	Ajeluz icco (GHU)	284.5 ± 3.4	7.8	7	20
CMD37	Sampo lo (GHU)	281.5 ± 3.2	8.5	10	20
CMD50E	Sampo lo (GHU)	275.8 ± 0.9	1.3	20	40

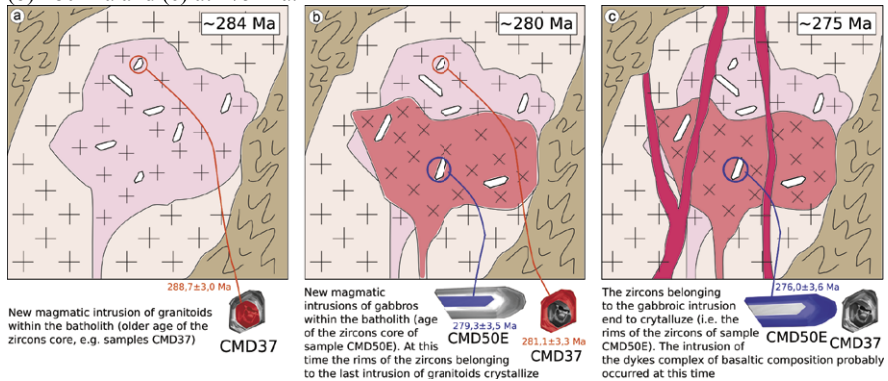
calculated for the metagranitoids (286-281 Ma) and the epidote-bearing metagabbros (~275 Ma) provide crystallization age.

Through these data, some considerations about the timing of the intrusion could be done. All the three samples of metagranitoids belonging to the CPU have a statistically equivalent age of 285 Ma. Even if the errors associated to each age vary (the case of the sample CMD57B exceed 5 Ma), the average age of the CPU metagranitoids is better constrained than those of GHU that, despite smaller 2σ errors, is calculated from samples having 284 and 281 Ma. Some small but appreciable differences have been found between cores and rims of all the zircons analyzed. However, the ages calculated for the metagranitoids are in agreement with those of the peralkaline to slightly peraluminous A-type granites (290-280 Ma, Paquette et al. 2003; Cocherie et al. 2005) that characterized the last

magmatic event related to the Permo-Carboniferous Corsica batholith.

The epidote-bearing metagabbros outcropping in the Ghisoni area had never been properly described and dated before. Other mafic rocks associated to the Permo-Carboniferous batholith occur in several other places of the island (i.e. the mafic-ultramafic and dioritic complex of Cocherie et al. 2005). Rossi et al. (1992) dated at 278 Ma these mafic rocks, linked by fractional crystallization processes with assimilation of metasediments (Cocherie et al. 1994).

Figure 58. Schematic interpretation of the Ghisoni Permian intrusions at (a) 284 Ma, (b) 280 Ma and (c) at 275 Ma.



The stratified complexes of troctolite, olivine gabbro, gabbro-norite and diorite of Tenda, Pila-Canale and Levie localities, dated by Ohnstedter and Rossi (1985) at 290-280 Ma, are interpreted as the remnants of magmatic chambers (Rossi et al. 1992). They state that the geometry of mafic products and granites was controlled by the rheological state of the magma, as suggested by their relationships of synchronism or posteriority. 281 ± 3 Ma is instead the age proposed for the undeformed gabbro-granite complex of Porto (Renna et al. 2007). Evidence of the mafic rocks intrusion within the not completely solidified granites, evolved by fractional crystallization, occur in this site. As a rule, most of the ages obtained in the mafic rocks are younger than those of granites and andesitic products (Cocherie et al. 2005).

The Concordia age calculated for the epidote-bearing metagabbros (275 ± 0.9 Ma) fits with the age estimated in the other localities. It is noticed that this age is considerably younger than those of the metagranitoids belonging to the same tectonic unit (i.e. CMD37, 281.5 ± 3.2 Ma) and sampled close to the contact with the epidote-bearing metagabbros. More in detail, it is observed that the age related to the rims of the metagranitoids (e.g. 281 ± 3.3 Ma) are similar to those determined for the cores of the epidote-bearing metagabbros (e.g. 279 ± 3.5 Ma, Fig 32). Even if field evidence indicating the emplacement of the metagranitoids before those of the epidote-bearing metagabbros are missing, meso-scale observations (§ Cap 4.4) highlight that mixing between the two magmatic pulses didn't occur. The contact, well exposed along the Ghisoni-Sampolo road (D344),

consists in an alternation of epidote-bearing metagabbros and metagranitoids within a 20 m thick band, that suggests rapid emplacement of the magmatic body. In conclusion, with the U-Pb zircon dating we constrained the magmatic age of some products of the Corsica batholith outcropping along its eastern rim. This batholith is the large magmatic intrusion that composes 2/3 of the island and represent the anorogenic stage before the onset of the Alpine cycle (Bonin et al., 1987). The emplacement of the calc-alkaline suite studied, including mafic and silicic products, probably took place at middle-low crustal level and occurred through several, discrete and short-lived episodes (<5 Ma), over a ~60 Ma timespan (Paquette et al. 2003). Our data confirm that the last magmatic event includes calc-alkaline sialic and mafic rocks, whose emplacements occurred between 286 and 275 Ma (Fig 58). The association of mafic products (volumetrically limited but sistematically present) to the main sialic body may be referred to the emplacement of mantle-derived magmas in the Early Permian (Casini et al. 2015). Owing the lack of additional geochemical analysis, a crustal contamination for the epidote-bearing metagabbros, as established by Tribuzio et al. (2009) for the Bocca di Tenda olivine-gabbronorites, could be only supposed. Only in the Eocene, after the emplacement of the Mesozoic-Tertiary sedimentary covers, the European margin was partially involved in the Alpine orogeny, leading the formation of tectonic units and the deformation of the rocks inside them (i.e. the metagranitoids and the epidote-bearing metagabbros studied).

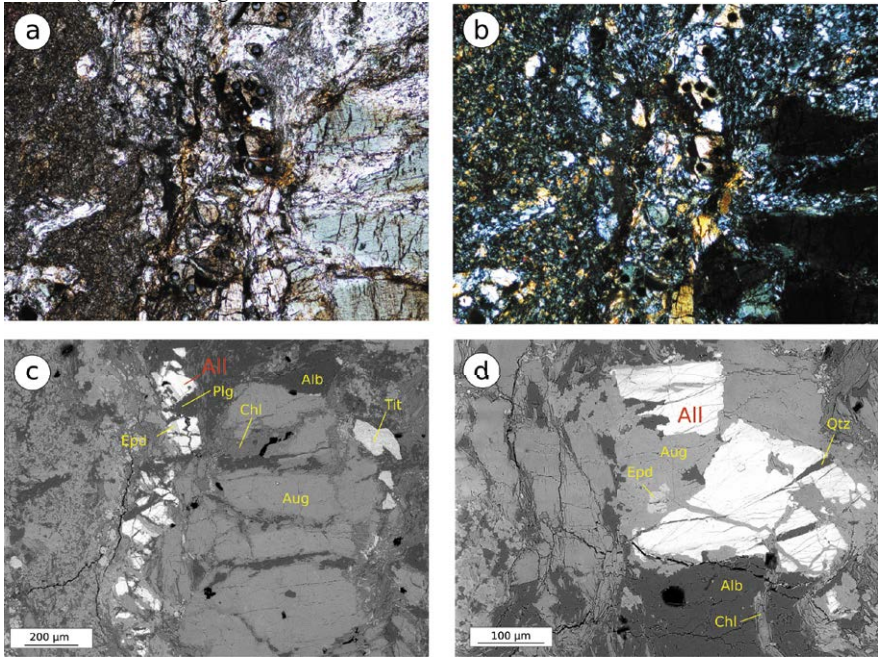
6.3 U-Pb geochronology on allanites

6.3.1 Allanite texture

Allanites were found in the sample CMD122A coming from Venaco (Lat:42°13'42.03"N; Long:9°10'31.25"E). In this sample the primary contact between the metagranitoids and the mafic dykes is observed (Fig 29b). The allanite crystals are found in both the mafic dykes and the hosting metagranitoids, even if they seem more abundant along the contact between them. In thin section the crystals usually appear within brownish area within the mylonitic foliation, mainly made by Chl, Alb, Qtz and Epd (Fig 59a,b). BSE observations do not reveal any zonation within the allanite crystals; they are fractured and partially substituted by Epd (Fig 59c,d). Their size is surprisingly big (up to 150 μm), much greater than those of the other minerals set within the shear zone. This textural evidence, together with its "altered" aspect, suggests that allanite is not in equilibria with the mylonitic assemblage that reach the greenschists facies during the Alpine age.

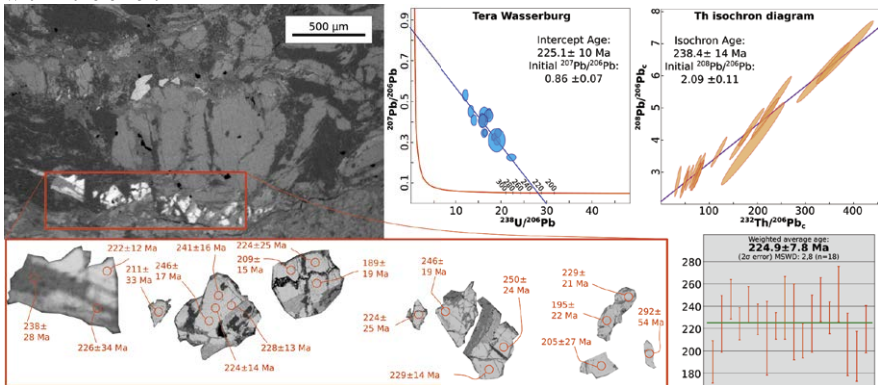
Allanite crystals were dated by LA-ICP-MS U-Pb *in situ* analysis; the $^{206}\text{Pb}/^{238}\text{U}$ ages and related 2σ errors are shown in weighted average diagrams,

Figure 59. Microphotographs of the sample CMD122A at (a) parallel and (b) crossed nicols. (c-d) SEM images of the sample CMD122A.



while the ratios between $^{238}\text{U}/^{206}\text{Pb}$ and $^{207}\text{Pb}/^{206}\text{Pb}$ are plotted in the Tera Wasserburg and the ratio between $^{232}\text{Th}/^{206}\text{Pb}$ and $^{208}\text{Pb}/^{206}\text{Pb}$ are plotted in the Th isochron diagram (Fig 60). The ^{238}U age of the sample has been determined through the intercept of the Tera Wasserburg diagram, considered only the sub-concordant spot analyses.

Figure 60. Analysis points on allanite (in situ), Tera-Wasserburg (inverse Concordia) plot and Th-isochron diagram of the sample CMD122A. LA-ICP-MS data show agreement within the error.

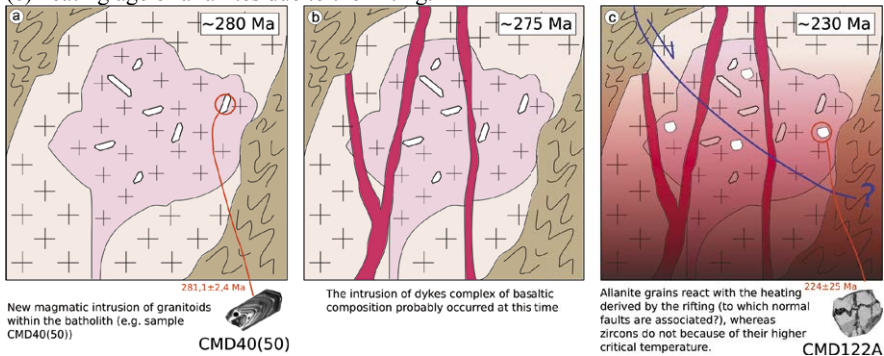


The 19 spot analyses performed on both centres and rims yield apparent spot ages that vary from 190 to 290 Ma, with most of the data forming a cluster at ca 227 Ma. The samples yield weighted average ^{238}U ages of 224.9 ± 7.8 Ma ($n=18$, $\text{MSWD} = 2.8$). The metagranitoids of the same outcrop has been sampled in order to estimate the magmatic age through zircons (i.e. CMD33(43)). The magmatic age calculated with the U-Pb method, calculated on an average of 20 spots (284.5 ± 3.4 Ma), is considerably older than the U age resulting from allanites (§ Cap 5.1.2).

6.3.2 Zircons vs. allanite ages: pre-Alpine rifting

Allanite is a common LREE-rich accessory phase in metamorphic rocks (Gieré and Sorensen 2004). They are a useful petrogenetic indicators because they occur in a variety of metamorphic environment, from the greenschist facies (Smith and Barreiro 1990; Tomkins and Pattinson 2007) to the blueschist-eclogite facies conditions (Janots et al. 2006). In this thesis a cross-study of U-Pb ages performed on the metagranitoids of Venaco is proposed. In the previous sections (§ Cap 3.2.2 and 3.2.3) two different ages were obtained: Early Permian (284.5 ± 3.4 Ma) calculated on zircons, and Late Triassic (224.9 ± 7.8 Ma) calculated on allanites. Considering that the annealing temperature of allanite ($\sim 600^\circ\text{C}$, Heaman and Parrish 1991; Bonazzi and Menchetti 1994) is lower than those of zircon ($\sim 900^\circ\text{C}$, Cherniak 2010), the age obtained by zircons is assumed as the magmatic age. This assumption is supported by the other Early Permian magmatic ages obtained for this work and listed in literature (Paquette et al. 2003; Cocherie et al. 2005; Renna et al. 2007). To explain the Late Triassic age estimated through the allanites, further consideration must be done.

Figure 61. Schematic interpretation of the CPU on the base of zircons and allanites ages. (a) magmatic age of the metagranitoids, (b) emplacement of the dykes complex and (c) heating age of allanites due to the rifting.



Annealing can occur in allanite (Karioris et al. 1981) and structurally damage or metamict grains are quite common, but the data interpretation requires caution because radiation-damaged grains may have healed after a period of open system

behavior (Engi 2017). In some case has been observed that non-metamict allanites occasionally appear younger than zircons (e.g. Gieré and Sorensen 2004; Catlos et al. 2000). This effect is probably due to the mobility of U and Th (Barth et al. 1994), Pb-loss (Barth et al. 1994) and to the hydrothermal fluids, to the attack of which allanite is more sensitive than zircon (Smye et al. 2014). Although there are no clear evidence of the U and Th mobility, because of the lack of accessory phases enriched in these elements associated to allanite, the lead loss, that largely affects the age uncertainties and may occur at $T > 750^{\circ}\text{C}$ (Kamber et al. 1998), cannot be excluded in our case. Moreover, small differences between zircon and allanites ages (of the magnitude of ~ 4 Ma) belonging to the same sample and due to the different closure temperatures of the two mineral phases have been described in the Alps (e.g. Oberli et al. 2004). However, in our case the ages differ of ~ 50 Ma, and therefore it would be forced to explain this age gap in this way.

From the optical micro-observations it has been observed that the allanite crystals do not belong to the metamorphic paragenesis of the shear zones in which they occur, that is in equilibrium in the greenschist facies. This is anomalous, because studies (Janots et al. 2008) show that allanite is expected to be stable at P-T conditions of 0.5 GPa and 400°C , and in several places of the Alpine belt synkinematic allanite occur in greenschist facies mylonites (e.g. those of the Mont Blanc Massif described by Cenko-Tok et al. 2014).

Allanites of the sample CMD122A occur in big crystals and are partially substituted by Epid; the fractures and the subhedral shapes that characterize them suggest that they are relics of the protoliths or of an intermediate paragenesis related to a geodynamic event younger than the emplacement of the batholith (~ 300 Ma) and older than the Alpine metamorphism (Corsica continental crust ~ 45 Ma, Brunet et al. 2000). At the Alpine belt scale, a diffuse igneous activity and high-temperature metamorphism corresponding to a Permo-Triassic high geothermic regime have been described by many authors (Lardeaux and Spalla 1991; Quick et al. 1992; Gardien et al. 1994; Vavra et al. 1996; Colombo and Tunesi 1999; Tribuzio et al. 1999; Schaltegger and Brack 2007; Peressini et al. 2007; Roda and Zucali 2008; Manzotti et al. 2012). This anomalous geothermic regime requires a heating mechanism, like the mantle upwelling under the continental crust (Hermann and Müntener 1996; Lardeaux and Spalla 1991; Marotta and Spalla 2007; Trommsdorff et al. 1993). As a consequence, the continental rifting followed by the Jurassic oceanization occurs (Lardeaux and Spalla 1991; Diella et al. 1992; Rebay and Spalla 2001; Müntener and Hermann 2001; Schuster and Stüwe 2008). Several stratigraphic and tectonic studies devoted to the Permo-Triassic rift-related inheritance (Manatschal and Müntener 2009; Beltrando et al. 2010; Mohn et al. 2011; Vitale Brovarone et al. 2014) have been coupled with metamorphic and petrochronological data, collected in all the sector of the Alpine belt: in the Western Alps (Lardeaux and Spalla 1991; Gardien et al. 1994; Manzotti et al. 2012), in the Eastern Alps (Miller and Thöni 2009), in the Malenco Valley (Hermann and Rubatto 2003) and Ivrea Zone (Vavra et al. 1996). In Corsica, Martin et al. (2011) described relics of Permian

metamorphism in the Alpine Corsica.

On the whole, the age associated to the Permian metamorphism ranges between 295 and 220 Ma (Borsi et al. 1980; Brodie et al. 1989; Sanders et al. 1996; Vavra et al. 1996; 1999; Schuster and Frank 1999; Thöni and Miller, 2000; Schuster et al. 2001; Habler and Thoeni 2001; Gaidies et al. 2006; Peressini et al. 2007; Pinarelli and Boriani 2007; Tropper et al. 2007). In this framework, our Late Triassic age could be interpreted as related to the geothermic pulses during extension-related decompression or due to a late regional geothermic event, as proposed for other sectors of the Alpine belt (Fig 61, Lu et al. 1997; Vavra et al. 1999; Manzotti et al. 2012).

It must take into account the role of fluids. Although we lack specific data necessary to model their circulation in the rock volume, their presence is to be expected in the extensional systems (Bertotti et al. 1993; Biino and Meisel 1996; Pinarelli and Boriani 2007; Marotta et al. 2009). Their effect probably produced the mobilization of some elements in the metagranitoids interested by the rifting, but a detailed study on other isotopes is needed to deepen this issue.

As regards the lack of the Alpine metamorphic imprint in the allanite studied, two different explanations could be done: the first is that the temperature reached by the continental crust during the continental subduction/exhumation never exceed the annealing temperature of this mineral (Bonazzi and Menchetti 1994) and it is confirmed by the data we obtain on the metapelites of the same tectonic unit (T peak of GHU: 270°C). The second explanation comes from the mechanical behavior and the chemical features that characterize allanite during the mylonitic foliation. In the Monte Mucrone, Cenko-Tok et al. (2011) observed that allanites involved in an eclogite facies shear zone preserve the Permian age, and explain that as an extreme effect of the strain partitioning on the neighboring minerals (i.e. Epid).

Chapter 7

Geodynamic implications

The geodynamic scenario proposed for the Alpine belt (e.g., Handy et al. 2010 and references therein) at the end of the oceanic subduction requires the involvement of the thinned European margin into tectonic processes related to continental collision (e.g., Schmid et al. 1996; Stampfli et al. 1998; Handy et al. 2010). During the collision, the thinned continental crust of the European plate underwent to progressive underthrusting, deformation and subsequent exhumation into the orogenic wedge, as evidenced by the metamorphic continental units from Western Alps (e.g. Oberhänsli et al. 2004). In this scenario, the collected data about the lithostratigraphic, structural and metamorphic setting of the Lower Units allow a detailed reconstruction of the tectonic history related to a continental fragment during the convergence between Europe and Africa plates. The lithostratigraphic setting of the Lower Units clearly indicates their origin from the continental margin of the Europe plate. This continental margin, constituted by the Panafrican-Variscan basement intruded by post-collisional granitoids (Early Permian, § Cap 6.2), experienced a sinking from Triassic to Early Jurassic. Evidence of the rifting phase are the U-Pb ages of allanites that indicate the increases of the temperatures in the Middle Triassic (§ Cap 6.4). The progressive deepening, associated to extension, causes the development of rift-related structures, like normal faulting that controlled the sedimentation in the whole European margin (e.g., Durand-Delga 1984). No information about the Cretaceous history has been preserved. However, the most important feature of this succession is the unconformity that occurs at the base of the Middle to Late Eocene Metabreccia and Metasandstone Fms. In this time

Maria Di Rosa, University of Pisa, Italy, maria.dirosa.scaglia@gmail.com, 0000-0002-1154-7429
FUP Best Practice in Scholarly Publishing (DOI 10.36253/fup_best_practice)

Maria Di Rosa, *Tectono-metamorphic evolution of the continental units along the edge between Alpine and Hercynian Corsica. Constraints for the exhumation models in the continental collision setting*, © 2021 Author(s), content CC BY 4.0 International, metadata CC0 1.0 Universal, published by Firenze University Press (www.fupress.com), ISSN 2705-0297 (online), ISBN 978-88-5518-420-5 (PDF), DOI 10.36253/978-88-5518-420-5

span, the continental crust was already involved in the continental subduction processes whose inception is regarded as Paleocene in age (Maggi et al. 2012 and references therein). After the pioneering intuition of Nardi (1968) and Boccaletti et al. (1971), in the 1980s the tectonic structures of the Alpine Corsica were interpreted as produced within an E-dipping “Alpine” subduction zone and Corsica itself considered as the southern prosecution of the Western Alps, basing on the lithostratigraphic and tectono-metamorphic evidences (Mattauer et al. 1981; Cohen et al. 1981; Durand-Delga 1984; Harris 1985; Warburton 1986; Caron 1994; Dallon and Puccinelli 1995). In the following paragraphs some of these issues will be reported and new argumentations based on the data collected in this thesis are proposed.

7.1 Middle to late Eocene history of the European margin: insights from the stratigraphy

The detailed field analysis allowed to reconstruct accurate stratigraphic logs for the different units of the Cima Pedani, Corte, Venaco and Noceta-Ghisoni areas. The lack of ophiolitic clasts belonging to the Schistes Lustrés Complex or to the Upper Units suggests that the source of these deposits was solely the European margin. This implies that at this stage of the convergence between Europe and Adria plates (i.e. in the Middle to Late Eocene) the forming accretionary wedge was completely submerged. Differently from other authors (e.g. Amaudric du Chaffaut et al. 1983; Durand-Delga 1984; Rossi et al. 1994), we proposed a unique stratigraphic reconstruction that refer to a single representative log through the different tectonic units and the different areas. As proposed by Durand-Delga (1984), we recognized rocks belonging to two main cycles, the Variscan and the Alpine cycles, divided by a regional angular unconformity.

The Variscan sequence is mainly made up of Devonian to Early Carboniferous low- to medium grade metamorphic rocks, i.e. the Roches Brunes Fm.. This metamorphic complex is unconformably covered and intruded by the Paleozoic part of the “Alpine cycle succession”, i.e. the Permo-Carboniferous monzogranites and the Permian volcanics and volcanoclastic sediments (i.e. Volcanic and Volcanoclastic Fm. of Noceta-Ghisoni, Metavolcanic and Metavolcanoclastic Fm. of the Lower Units). Unconformably above the Paleozoic Variscan cycle, the Alpine cycle is characterized by two stratigraphic sequences, separated by a younger angular unconformity. This unconformity, located at the base of Middle to Late Eocene metabreccias and metasediments, crosscut not only the Jurassic-Triassic carbonates of the first sequence, but also the Variscan sequence, as observed in Corte and in Venaco areas (§ Cap 4.2, 4.3). In summary, the angular unconformity inside the Alpine cycle represents a regional surface formed before the sedimentation of the Eocene foredeep sequence. The meaning of this surface must be searched in the mechanisms that

affected the continental lithosphere (i.e. the future Lower Units) during its approach to the Late Eocene subduction zone. In particular, the Middle to Late Eocene erosion of the continental lithosphere could be produced or enhanced by a local uplift (i.e. forebulge) located in the subduction-related peripheral bulge (Beaumont 1981; Jordan 1981; DeCelles and Giles 1996). The forebulge is a topographic high caused by flexural uplift when the lower plate is arched to compensate the forces present at the compressive front (Byrne et al. 1988; Dubois et al. 1988; Burov and Diament 1995; Burov 2011). This phenomenon occurs when the lower plate (i.e. European plate) reacts to the imminent subduction with the uplift and the erosion of the forebulge (e.g. Cloetingh et al. 1982). In response to the consequent tilting, the base of the foredeep basin filled at this time is marked by an angular unconformity (§ Cap 5.1). Some authors claim that a Late Cretaceous to Middle Eocene age for the subduction of the European continental margin is altogether supported by regional data (Molli et al. 2006; Molli 2008) such as the presence of detritic glaucophane in Maastrichtian sediments of NW Sardinia (Dieni and Massari 1982) and because in SE Corsica Late Eocene sediments lacking HP/LT assemblages rest unconformably on basement of HCY and Schistes Lustrés Complex (Egal 1992; Caron 1994). Moreover, Amaudric du Chaffaut and Saliot (1979) reported the presence of HP/LT Phg in the Tertiary breccias at the top of the HCY, in the area south of Botro. The detailed structural mapping carried out for this thesis highlighted the area they considered HCY is actually the southern continuation of CPU (§ Cap 4.2 and 5.2.2); thus, the pre-Eocene deformation of the European margin cannot be supported by this data (e.g. Malavieille et al. 1998). Moreover, the lack metamorphism in the Late Eocene sediments that unconformably top the HCY has been observed also in the areas of Corte (§ Cap 4.2, Di Rosa et al. 2017b), Venaco (§ Cap. 4.3) and Ghisoni (§ Cap. 4.4). Considering the Eocene regional unconformity affecting the European margin (i.e. the HCY and the Lower Units) caused by the flexural uplift of the downgoing plate, already proposed by Durand-Delga (1984) and supported in this thesis, the lack metamorphism in these sediments cannot be regarded as a proof of the pre-Eocene deformation, because not all the forebulge were subducted. Regarding the occurrence of the blue amphibole reported in the NW Sardinia an ophiolitic origin could be postulated; however, in absence of other constraints, a proto-Alpine belt cannot be excluded. In any case, in all the formations of the Lower Units studied originally attributed to the Cretaceous (e.g. Amaudric du Chaffaut 1975; Rossi et al. 1994) evidence of a Middle to Late Eocene age have been verified (Ferrandini et al. 2010; Di Rosa et al. 2017a). Therefore, according with Di Rosa et al. (2017a) and on the base of new stratigraphic data collected for this thesis, we support the Lutetian age for the angular unconformity and the Middle to Late Eocene age for the deposition of the cover above the unconformity and of the subsequent onset of the deformation of the Lower Units.

The evolution of the forebulge from its erosion to its deformation and overthrusting was described for the first time by Allen et al. (1991) in the Glarus—Graubuden area (eastern Switzerland). They observed that the basal

unconformity separates the overlying Eocene Nummulitic Limestones from the underlying lithologies with an increasing stratigraphic gap toward the foreland. Subsequently, Sinclair (1997), extending his studies at the Alpine belt-scale and comparing his observation with those made for foreland basin worldwide, defined the so-called “underfilled trinity”, a stratigraphic sequence composed by three lithostratigraphic units: the lower unit, that underlain the unconformity, that comprises shallow marine limestones and sandstone, the middle unit composed by mudstones and the upper unit made of sandstones and siltstone suggesting a deep-water turbidite systems. In the subsequent years, several authors devotes their work to the study of the flexural bulge, finding numerous examples in the French and Swiss Alps (e.g. Burkhard and Sommaruga 1998; Ford et al. 1999; Michard and Martinotti 2002) and worldwide (e.g. Jarrard 1986; Ussami et al. 1999; Yu and Chou, 2001; Irfan et al. 2005; Chang et al. 2012; 2015) or providing numerical models aimed to explain the mechanics that govern them (i.e. Allen et al. 2001).

Basing on the Hecynian Corsica and the Lower Units stratigraphies reconstructed for this thesis, we note that the type-sequence proposed by Sinclair (1997) is only partially found: the Nummulitic Limestones occur only at the top of CDU (i.e. Nummulite-bearing Metalimestone Fm.) in the Corte area; the middle unit, made of mudstones, completely lack while the upper units is well developed in both the HCY and the Lower Units. Regional and local causes, like the rigidity of the underlying plate and the margin structure itself, may explain the almost totally lack of the lower and middle units (Dorobek 1995). In addition, abundant breccias (carbonatic and polygenic) are found everywhere in Corsica above the Eocenic unconformity (excepts the Monte Fuata, where the Nummulitic-bearing Metalimestone Fm. occurs). The lack of the mudstone could thus be explained with the subsidence in the foreland driven by the activity of normal faults. The voids between the blocks start to be filled by deposits (e.g. breccias and sandstones) coming from the erosion of the forebulge itself, and only where the low-sea conditions are present, the lithification of Eocenic limestones occurs. Although in the study-area these normal faults have not been preserved (reactivated by thrusting?), they are described in other places in the Alps (e.g. Michard and Martinotti, 2002) and are however provided both by Sinclair (1997) and Allen et al. (2001). On the whole, being the forebulge formed in consequence of the continental margin subduction, it constitutes the first event that testifies the involvement of the European plate in the Alpine Orogeny, and it constitutes a crucial constrain for the timing of the subduction, that it is thus postdated to the Middle to Late Eocene (Di Rosa et al. 2017a; 2017b).

7.2 Tectono-metamorphic history of the Lower Units, the Alpine shear zones of the Hercynian Corsica and of the associated tectonic slices belonging to the Schistes Lustrés Complex

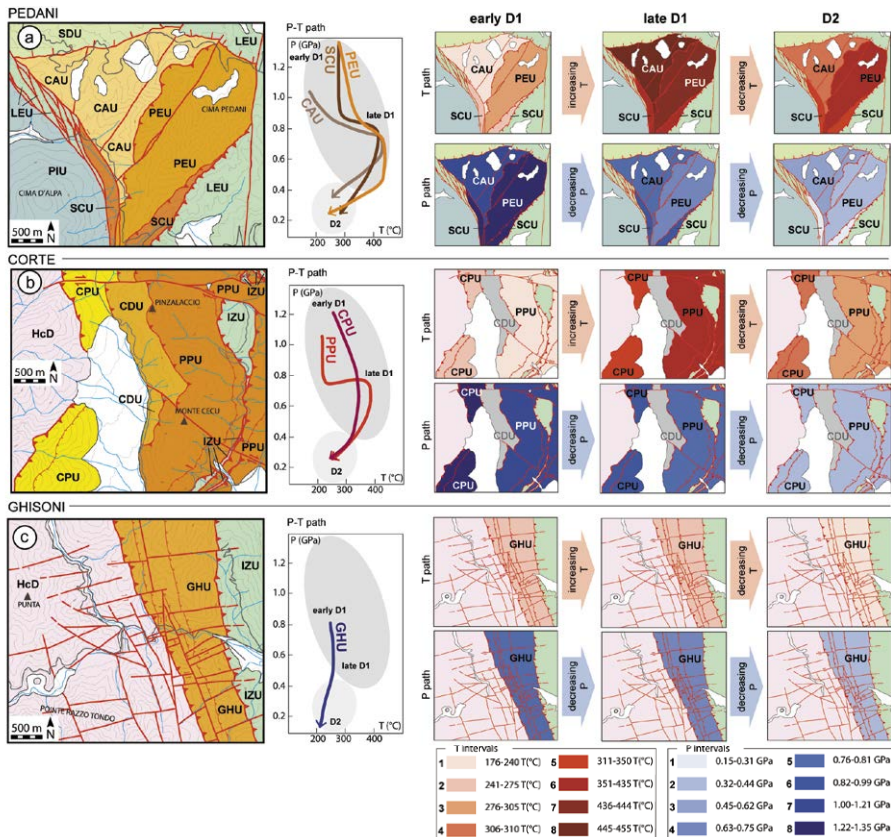
7.2.1 Exhumation during compression: the D1 and D2 phases of the Lower Units

The metamorphic study of the Lower Units highlighted the lack of preservation of the prograde path related to their underthrusting and their transfer at the base of the Alpine Corsica wedge. The metamorphic recrystallization registered by Chl and Phg during the D1 and D2 phases is related to the retrograde path and to the exhumation of the Lower Units, along the subduction channel and inside the wedge, up to shallower levels (e.g. Lanari et al. 2012; Di Rosa et al. 2018a; 2018b) (Figs 62-65). According to Di Rosa et al. (2017a), the metamorphism indicates that the retrograde history preserved in the continental units of Alpine Corsica is characterized by three steps in a trend of decreasing pressure between the P- and T-peak (i.e. the D1 phase), down to LP-LT conditions (i.e. the D2 phase). This evolution records the progressive exhumation of the continental units in the orogenic wedge, from the deepest structural levels reached during subduction and incorporation to the wedge, up to the surface. Associating the metamorphic estimates to the microstructural data has been observed that the exhumation processes of the Lower Units in Cima Pedani, Corte and Noceta-Ghisoni areas (Fig 62) already started during the D1 phase, once the units reached the maximum depth (Di Rosa et al. 2018a; 2018b).

All analysed units are characterized by this three steps evolution, but the reconstructed P-T paths present differences between units, both in the P- and T-values and in the trajectories, suggesting that each unit followed an independent way of exhumation until the end of the D2 phase (Fig. 62). Despite the different P-T absolute values, it has been observed that during their exhumation the Lower Units followed two different types of path (Figs 62-63): the isothermic path (e.g. GHU and CPU) or the warmed path (e.g. SCU, PPU, CAU and PEU). The isothermic path (e.g. CPU in Corte area and GHU in Venaco-Ghisoni area, Figs 62-63) characterizes the units which are located in the lowest position of the pile, directly superimposed to the HCY (Fig 64). CPU and GHU share similar, almost isothermic paths during the development of the D1 and D2 phases (Fig 64). The small difference in pressure values between the P-peak and the T-peak observed in GHU (~40°C, Fig 64c) suggests that during the D1 the geothermic conditions remained unvaried; CPU shows bigger differences in temperature values between P-peak and T-peak (~100°C, Fig 64a), but the regular trends of the increasing and decreasing temperatures are comparable with those of GHU. The reasons why these units registered this kind of path could be (i) the proximity to the lower plate (i.e. HCY, Fig 64) that acts as a geothermic barrier with respect to the hotter lithospheric mantle in which the continental slab is immersing and (ii) a short staying of these units at great depth followed by a fast exhumation for CPU from 40 to 18 km and for GHU from 27 to 4,3 km.

The warmed path (e.g. CAU, PEU and SCU of Cima Pedani area and PPU of Corte area, Fig. 62-63) is associated to the units that occupy the uppermost positions in the tectonic stack of the Lower Units and are overthrust by the

Figure 62. Tectonic sketch of (a) Cima Pedani, (b) Corte and (c) Ghisoni areas. The P-T paths related to the Lower Units outcropping in each area are also shown, as well as the pressure and temperature conditions estimated for each unit in three different stages of their tectono-metamorphic history (early D1, late D1 and D2). These maps have been produced choosing P and T ranges that put in evidence the differences between the tectonic units. While the P conditions decrease in each units from the early D1 to the D2 phases, the T conditions follow two kinds of path (isothermic and warmed paths) that are shown in the T path maps of the late D1 phase (after Di Rosa et al. 2018b).



Schistes Lustrés Complex (i.e. SCU with LEU in Cima Pedani area in Fig 64b and PPU with IZU in Corte area in Fig 64a) and the other units sandwiched between them and those showing the isothermic path (i.e. CAU and PEU in Fig 64b). Despite the different P-T absolute values registered during the D1 phase, the warmed units preserve comparable P-T paths, characterized by a progressive warming from the P-peak to the T-peak (Figs 62-64). The differences in $T > 160^{\circ}\text{C}$ up to 280°C observed (Fig 64a,b) could be explained with their parking

between ~45 and 15 km, during which they experienced progressive heating due to the geothermic re-equilibration of the surrounded environment (Fig 66). Similar to SCU and PPU, CAU and PEU exceeded 430°C at the end of the D1 phase, but the transition from the D1 to the D2 phases is in these units characterized by an almost isobaric cooling (e.g. Figs 63, 64b). Such behaviour has been described in other orogens as related with the thrusting of initially warmer material over colder material (Chamberlain and Karabinos 1987; Wakabayashi 2004). While field observations establish that PEU is overthrust above CAU, what is located at base of CAU is unknown. The first possibility is that CAU overthrust directly onto the HCY: in this case the observed temperature gap would be justified by the fact that, during the D2 phase, CAU gets in touch with a portion of the European margin that never underwent subduction (Lin 2000). Alternatively, we could postulate an overthrusting of CAU over other, unexposed cooler Lower Units. If so, we could argue, similarly to the scenario depicted for CPU in the Corte area, that this hypothetical unit experienced a much faster exhumation than CAU, because of its position in the units pile (i.e. closer to the HCY).

As regards the Chl-Phg couples forming the LP/LT step (i.e. the D2 phase), only weak differences in the P and T values are performed by the samples studied. This suggests a general trend of decreasing T and P during the D2 phase, due to the displacement of the Lower Units to superficial levels (CAU at 11 km, PEU at 8 km, SCU at 9 km, CPU and PPU at 8 km and GHU at 4 km). Being the late D1 and the D2 phases developed during exhumation, a partial obliteration of the pre-existing fabric cannot be excluded. However, in this thesis, the map- to microscale structures constraint the D1 and D2 phase in which the metamorphic minerals are grown (Di Rosa et al. 2017a; 2018a; 2018b). This approach allowed to reconstruct the tectono-metamorphic history of the subducted continental crust (Fig 65), previously interpreted as the result of the accretion processes of continental slices at the orogenic wedge (e.g. Egal 1992).

In the Western Alps, the top-to N-NW direction of nappe emplacement and shearing accommodated the earliest and rapid exhumation of HP-UHP continental units. This tectonic phase (i.e. the D1) is interpreted everywhere as a thrusting phase (Agard et al. 2002; Markley et al. 1998; Bousquet et al. 2002; Reddy et al. 2003; Bucher et al. 2003; Ganne et al. 2007; Le Bayon and Ballèvre 2006), while the top-to-E-SE shearing (i.e. D2) of the Piedmont zone accommodates a significant part of the exhumation in an extensional setting (Agard et al. 2002; Reddy et al. 1999; Rolland et al. 2000; Ganne et al. 2006; 2007). Comparing with the Alpine Corsica, the D1 phase of the Western Alps correspond to the D1+D2 phases, i.e. the exhumation in a compressional setting. To the D2 phase of the Western Alps, taken under an extensional regime, can be associated the top-to-E structures of the D3 phase recognized in the Lower Units (§ Cap 7.2.4).

Figure 63. Summary of the pressure-temperature-deformation (P-T-d) paths of the Lower Units in the three selected areas (Cima Pedani, Corte and Ghisoni). P-T-d paths of CAU, PEU and SCU are after Di Rosa et al. (2018a), those of CPU, CDU and PPU are after Di Rosa et al. (2017a) and GHU after Di Rosa et al. (2018b).

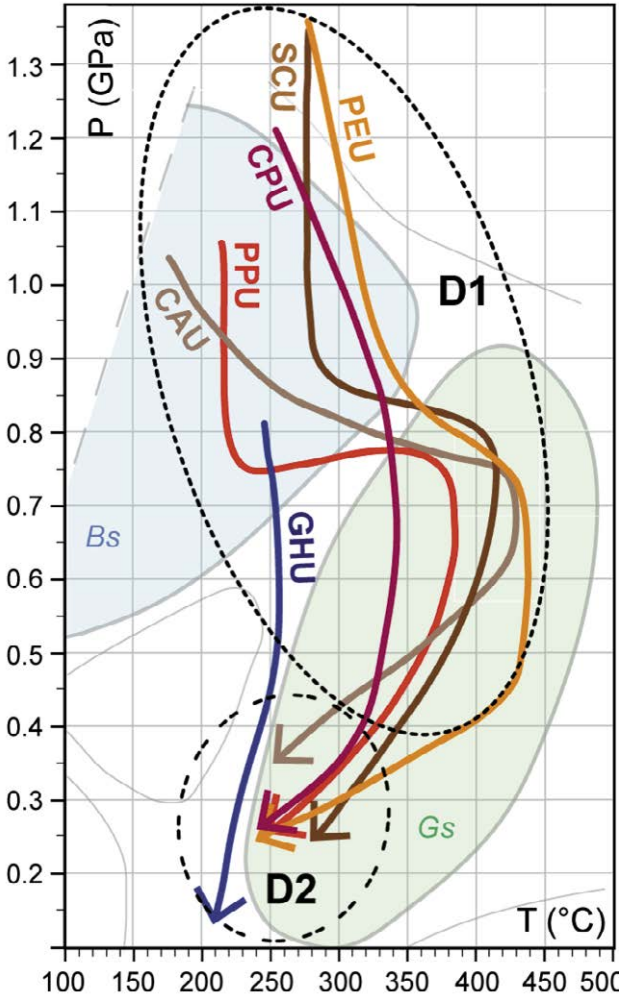


Figure 64. Cross sections of the Lower Units stacking above the Hercynian Corsica (HCY) and the under the Schistes Lustrés Complex (LEU, IZU) and the Upper Units (SDU – Serra Debbione Unit): (a) Corte, (b) Pedani and (c) Ghisoni. The related diagrams illustrate the distance from the HCY (in the case of Pedani the distance is measured from the normal fault that rims the tectonic window toward NE) vs. pressure and temperature variations measured in the samples. These diagrams show the spatial variations of the P and T values related to the three generations of Chl-Phg: the pressure diagrams show that, despite differences in absolute values of P, each sample registered a decreasing trend from early D1 (1°Chl-Phg) to D2 (3°Chl-Phg). In the temperature diagrams the difference between isothermic and warmed paths are shown.

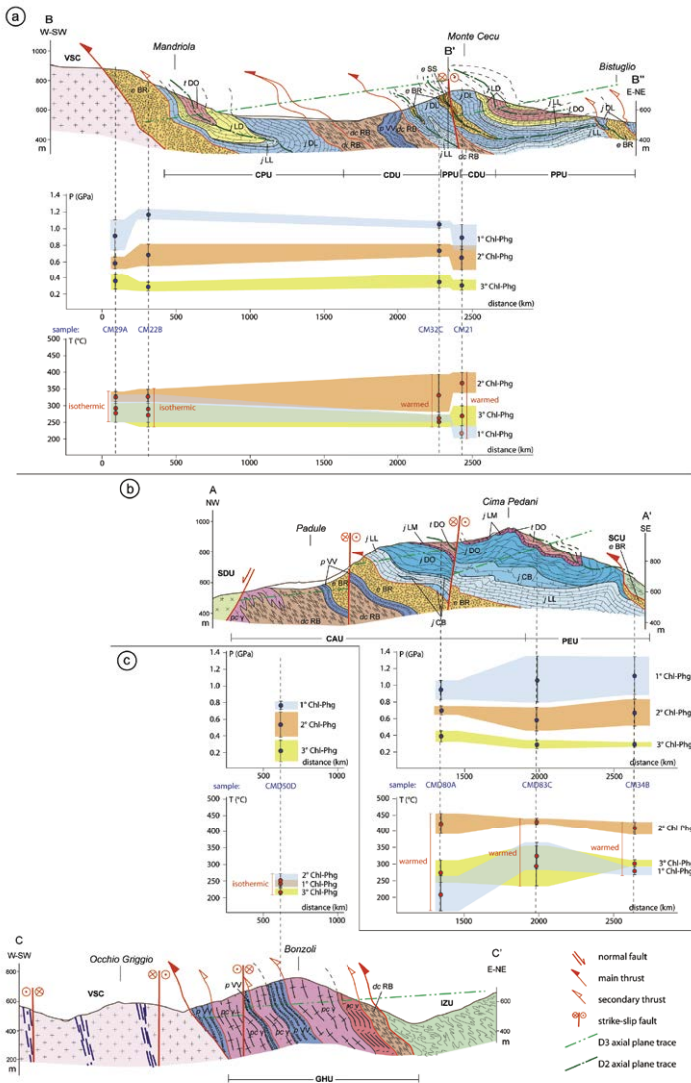
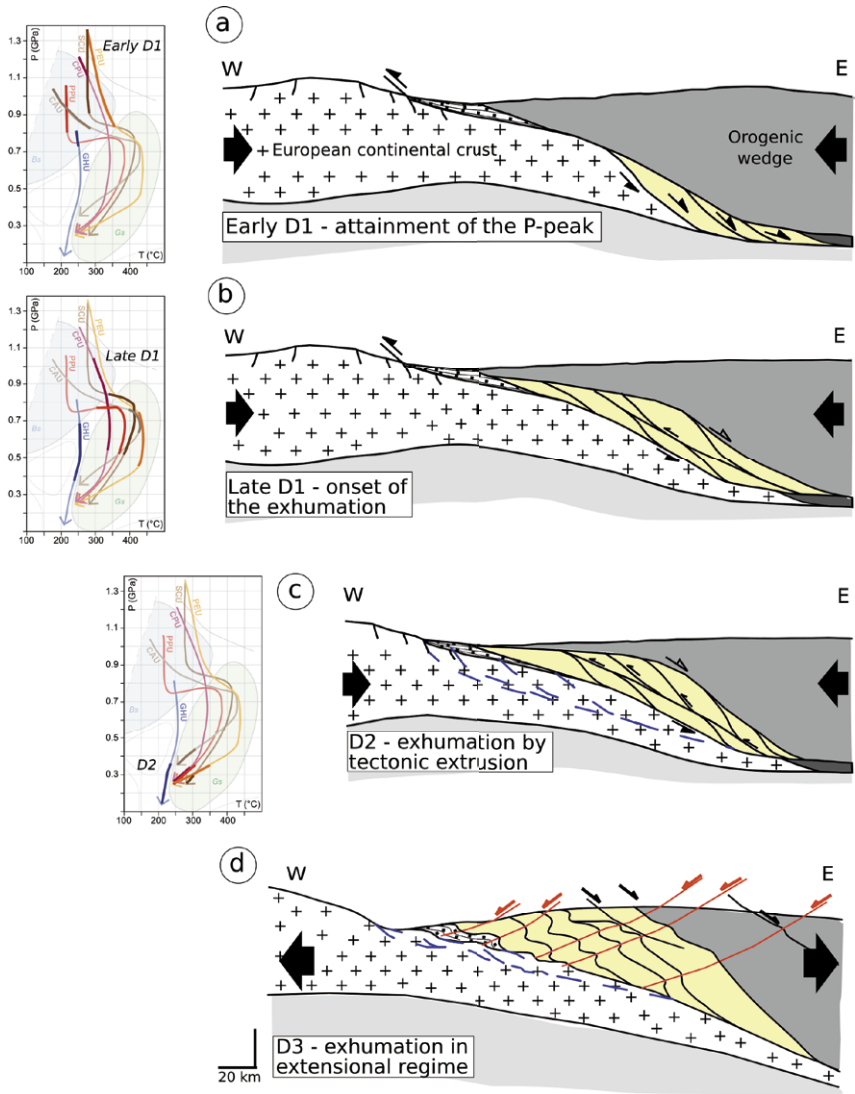


Figure 65. Summary sketch illustrating the tectono-metamorphic evolution of the Lower Units studied (in yellow) in this thesis in the Late Eocene-Oligocene time span. (a) reaching of the maximum depth (~45 km) during the early D1 phase; (b) onset of the exhumation in the late D1 phase; (c) continuation of the exhumation during the D2 phase up to ~10 km of depth and development of ductile shear zones in the HCY (blue dashed lines) and (d) coupling of the Lower Units with the Schistes Lustrés Complex and with rock volumes of the HCY and development of the open asymmetric folds with sub-horizontal axial plane foliation (red lines) verging toward E (modified after Di Rosa et al. 2017a). The metamorphic data related to the stages a-c are also reported (modified after Di Rosa et al. 2018b).



7.2.2 Syn-convergence deformation of the Hercynian Corsica

As regards the Alpine deformation registered by the HCY, three areas were analyzed in this thesis (i.e. Asco-Castirla, Razzo Bianco and Noceta-Ghisoni). They are accomanated by the presence of top-to-W shear zones that crosscut the Permo-Carboniferous granitoids with a strike direction similar to those of the main tectonic contact between the Lower Units and the HCY (i.e. ~N-S). The tectono-metamorphic study of these shear zones highlighted that three ductile phases are present: relics of the first phase have been recognized only in the thin section of the metapelitic lithotypes. The second phase is characterized by a subvertical mylonitic foliation, that is N-S oriented and shows a top-to-W sense of shear, while the younger phase produces open asymmetric folds with associated a N-S striking subhorizontal foliation that gently dips towards W. Being this latter phase corresponding to the D3 recognized in the Lower Units and related slices of Schistes Lustrés Complex, it is likely that the subvertical mylonitic foliation recognized in the Asco, Venaco and Ghisoni shear zones have been developed contemporary to the D2 phase of the Lower Units.

In the Asco-Castirla and Noceta-Ghisoni areas the ductile deformation is localized in few meters thick bands that cut the undeformed HCY. Razzo Bianco can be instead though as rock volume which was transferred to different crustal levels in an uniform manner. The polyphased deformation history is in full associated to the retrograde path followed by this portion of continental crust from mid-crustal position to the surface. In the sample of metasandstone related to Razzo Bianco (CMD98), the differences in composition between the cores and the rims of the S1 Chl (Chl1 and Chl2, respectively) and S1 Phg (Phg1 and Phg2, respectively) allowed to define two P-T equilibrium related to the D1 phase (Fig66). Assuming an average geothermic gradient reasonable for the continental crust of 27 MPa/km (Best 2003) it is estimated that this sector of the European margin reached the maximum depth of about 42 km (cores of Chl1-Phg1 couples), after which it started to move up to the surface. At the end of the D1 phase, Razzo Bianco was probably placed at about 40 km of depth, as testified by the P-T equilibrium condition of the rims of the S1 Chl (Chl2) and Phg (Phg2, Fig 66). From the P-T conditions related to the Chl-Phg couples selected on the S2 foliation (Chl3 and Phg3), it is clear that the development of D2 phase occurred at depths ranging between 28 and 9 km.

In summary, the spatial distribution of Asco-Castirla, Razzo Bianco and Noceta-Ghisoni shear zones and of the temperatures associated to the microstructures depict a narrow zone within the undeformed HCY where different rates of strain developed brittle to ductile fabrics (Figs 65, 67). The tectono-metamorphic study of Asco, Razzo Bianco and Ghisoni carried out in this thesis provides the tectono-metamorphic evidence that the foreland, represented by the European continental margin, was partially involved in the Alpine processes of subduction and exhumation (Fig 67), and therefore the boundary between the Alpine and HCY does not represent the limit of the Alpine metamorphism in the Corsica island.

Figure 66. P-T path estimated for Razzo Bianco (sample CMD98), calculated with the Chl-Phg-Qtz-wt multiequilibrium approach. The Chl-Phg couples have been sampled in three different microareas (two on the S1 foliation and one on the S2 foliation). Relics of the S1 foliation as well as the S2-S3 interference pattern are shown in the microphotograph.

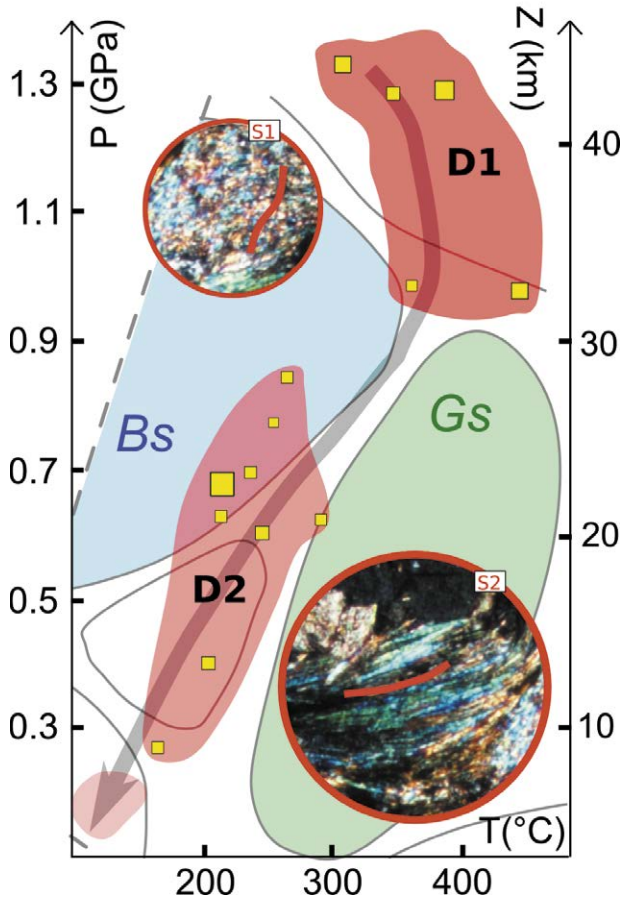
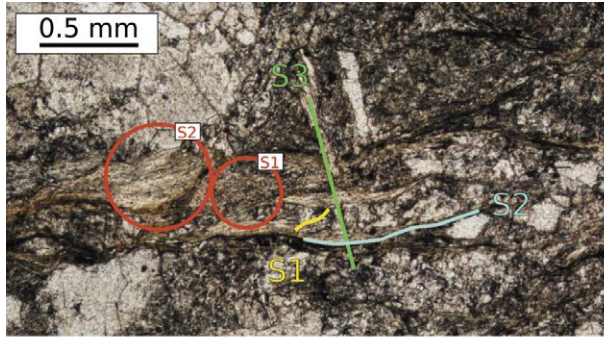
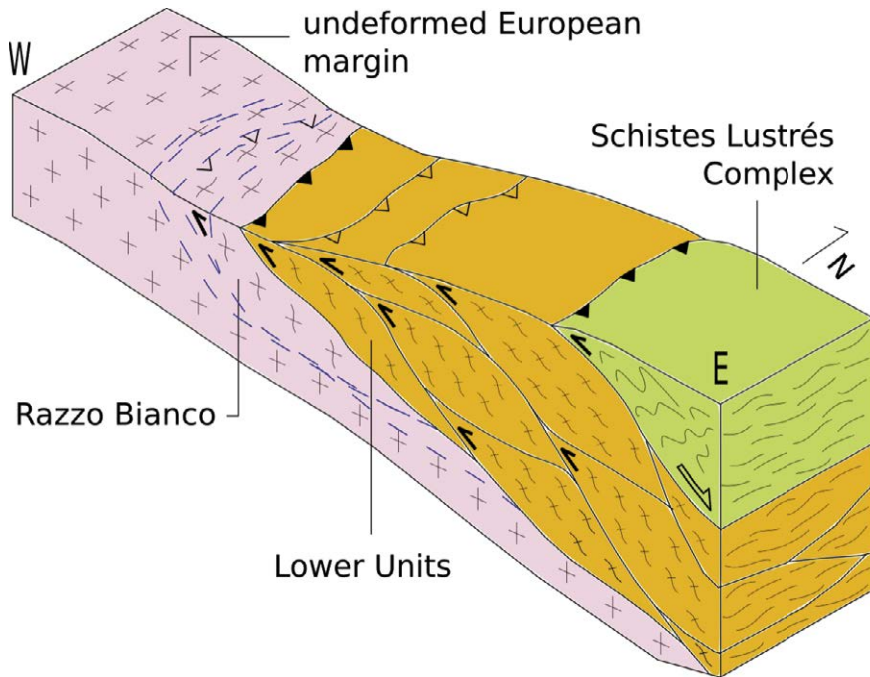


Figure 67. Schematic 3D sketch of the D2 setting in the Central Corsica. The Alpine shear zones within the HCY (e.g. Asco, Razzo Bianco and Ghisoni) are indicated with blue dashed lines (modified after Rossetti et al. 2015).



7.2.3 The post-D2 coupling with the Schistes Lustrés Complex

In Cima Pedani, Corte and Noceta-Ghisoni areas, the Lower Units are coupled with the Schistes Lustrés Complex. Although their structural positions and their volumes are different compared to those of the Lower Units in the three areas, in both cases has been observed that the coupling between the continental and oceanic units predates the last ductile event, corresponding to the D3 in the Lower Units.

In the Cima Pedani area, the P-T-peaks conditions estimated for the LEU by Levi et al. (2007) highlighted that the maximum depth reached by LEU is between ca. 31 and 23 km; this implies that the Lower Units were buried at greater depth than LEU. Reliable geochronological data for the Schistes Lustrés Complex of LEU indicate 37.5 Ma as the age of the peak metamorphism (Vitale Brovarone and Hewartz 2013). These data suggest that, meanwhile the Tertiary clastic deposits found at the top of the successions in the continental units (i.e. the Carbonate Metabreccia the Metabreccia and the Metasandstone Fms.) were sedimented, the oceanic crust was already deformed and located within the orogenic wedge. Therefore, LEU was accreted at the base of the orogenic wedge

before and at shallower depth than CAU, PEU and SCU.

In the Corte area, two slices of IZU were studied (i.e. IZU Botro and IZU Buttinacce) in order to characterize the metamorphism (Fig 68). These two tectonic slices overthrust CPU and, even if they are not laterally continuous, they are characterized by the same deformation history (§ Cap 5.5.2). The results indicate that the D1 phase is a relic of the prograde path of these slices of Schistes Lustrés Complex during the oceanic subduction, whereas the D2 phase is related to the maximum depths reached by these units and their subsequent exhumation. Assuming an average crustal geobaric gradient of 30 MPa/km (Best 2003), these slices of IZU registered the D1 phase at ~20-25 km of depth; subsequently, during the early D2, they first reached the maximum depth of ~28-30 km, and then were exhumed up to ~15-20 km, as suggested by the P-T equilibrium condition of the late S2 (Fig 68). Comparing the P-T values obtained on IZU Botro and IZU Buttinacce with those of CPU (sample CM22B) and PPU (sample CM21) the difference between oceanic and continental units in the retrograde paths is observed (Fig 68). P- and T-peaks of the Schistes Lustrés Complex are those typical of the oceanic subduction and are always lower than those of the Lower Units that are instead typical of the continental collision setting (e.g. Berger and Bousquet 2008). While IZU Botro and IZU Buttinacce follow an almost isothermic trend during their exhumation (i.e. between S2 and late S2), the geothermic conditions of the continental units registered a heating event in the late D1 phase, that changes again towards lower temperatures during the D2 phase.

Another important observation is that the last metamorphic event registered by all the units (i.e. late D2 for IZU Botro and IZU Buttinacce and D2 for CPU and PPU) occurs within a relatively small pressure range (~0.25-0.45 GPa, Fig.7.7). Although the D1 and the D2 phases affected the Schistes Lustrés Complex and the Lower Units in different times, similar P-T conditions related to the late D2 of IZU Botro and IZU Buttinacce and of the D2 of CPU and PPU, roughly indicate the depth at which the coupling between oceanic and continental units must occur in the pre-D3 phase (~10 km, Fig 69). As shown, the relationships between LEU and IZU and the studied continental units of Cima Pedani, Corte and Ghisoni areas are sealed by the last ductile event (i.e. the D3 phase) that folds the tectonic contact between them. In the southeastern boundary of the Pedani tectonic window, LEU overthrust SCU through a SE-dipping and top-to-NW shear zone (Fig 69b), while in the Corte area all the slices of IZU are sandwiched between the Lower Units or between the Lower Units and the HCY through E-dipping and top-to-W shear zone (Fig 69c). Data related to the metamorphism of IZU that in the Ghisoni area are missing; however, field evidence highlights a similar deformation history that suggest the coupling between the Schistes Lustrés Complex and GHU in the pre-D3 phase (Fig 69d). The top-to-W shear zones to which a subvertical mylonitic foliation is associated are therefore related to the late-D2 thrusting phase, during which the coupling of the continental and the oceanic units produced the present

Figure 68. Tectonic sketch and related cross sections of the Corte area and P-T paths of the tectonic units studied in this area that are thrust above the HCY: CPU and PPU (Lower Units, modified after Di Rosa et al. 2017b) and IZU-Botro and IZU-Buttinacce (Schistes Lustrés Complex). The sample location is shown in the map and in the cross sections. From these sketches the structural relationships between the Lower Units and the IZU-bearing units are also highlighted. The P-T plot puts in evidence the differences in the metamorphism between the paths related to oceanic and continental units. These latter in turn show isothermic (CPU) and warmed (PPU) paths.

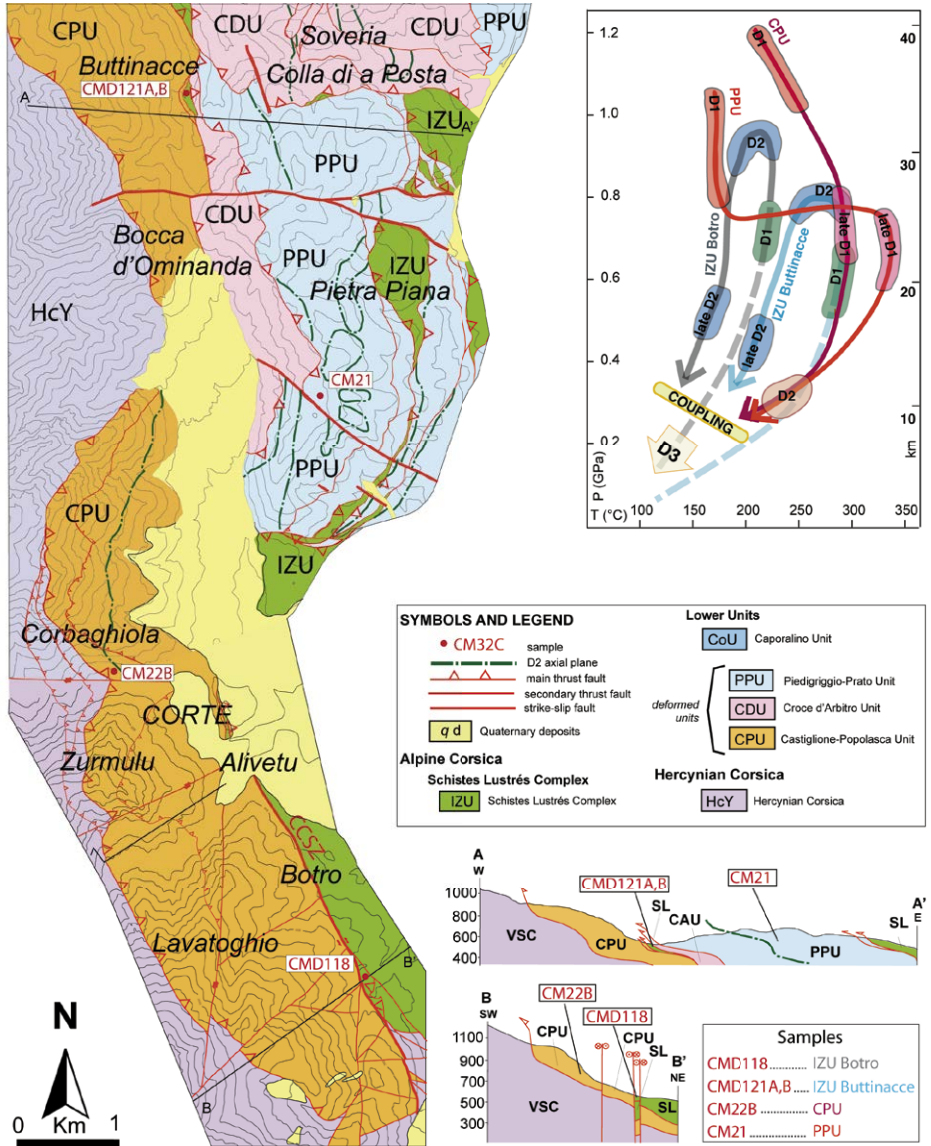
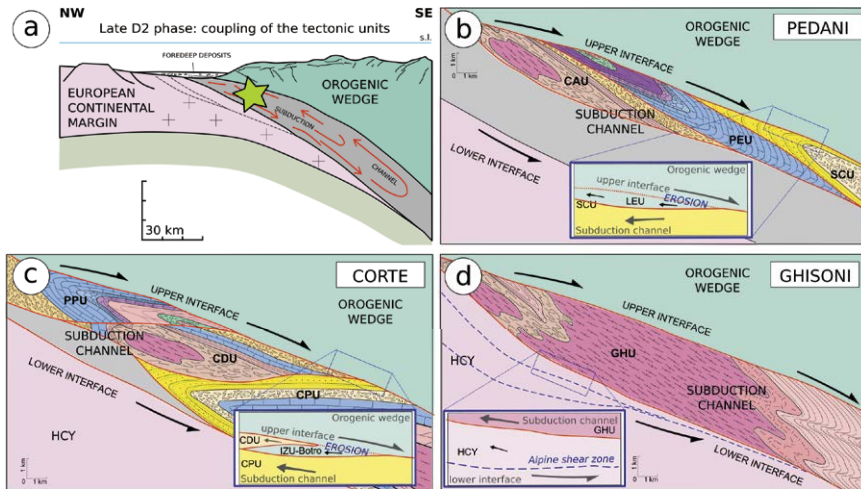


Figure 69. (a) Generic model of the subduction channel in a collisional setting. Green star indicates the position of the Lower Units studied in this work during the late D2 phase, to which are referred the (b), (c) and (d) schemes. (b) Sketch of the Lower Units in Cima Pedani area; zoom indicates the model proposed for the coupling between the Schistes Lustrés Complex (LEU) and the Lower Units (modified after Di Rosa et al. 2018a). (c) Sketch of the Lower Units in Corte area; zoom indicates the model proposed for the coupling between the Schistes Lustrés Complex (IZU) and the Lower Units. (d) Sketch of the Lower Units in Ghisoni area; zoom indicates the Alpine shear zones formed during the D2 phase within the HCY.



stack of tectonic units. However, the shear zone juxtaposes a less metamorphic unit, (LEU and IZU) over more metamorphic units (i.e. the continental units of Cima Pedani and Corte) as confirmed the metamorphic conditions registered (Fig 68). Based on these observations, we hypothesize that the Lower Units, during their exhumation, eroded the bottom of the tectonic wedge made of the Schistes Lustrés Complex, made of tectonic slices that stationed at ~15-20 km of depth during all continental subduction/exhumation (Fig 69b,d). Therefore, the shear zones that mark the tectonic contact between the continental and oceanic units possibly originated as a (ductile?) structure with an original “normal” sense of shear, that allowed the coupling of LEU and IZU over the continental units and that was later obliterated by brittle deformation after the D2 exhumation phase (Fig 69).

The mechanical coupling of rocks having different rheology is an issue recently addressed by many authors, in relations to the study of mature subduction and continental collision settings (e.g. Lapen et al. 2007; Agard et al. 2018 and reference therein). Cases in which this phenomenon is associated to the exhumation of HP-LT rocks has been described in the Western Alps (Zermatt-Saas/Monte Rosa and Gran Paradiso transect, Lapen et al. 2007), in Western Anatolia (Plunder et al. 2015) and in Oman (Agard et al. 2016). The causes of the coupling are partially understood (e.g. the heat flow and the differences in the

exhumation rate and in the viscosity, Agard et al. 2016; Liao et al. 2018); however, many aspects need to be clarified, for example (i) if the coupling is a continuous process during the exhumation of the HP-LT units, (ii) if it occurs along the entire subduction channel/orogenic wedge interface and (iii) if the basal erosion of the orogenic wedge reactivates pre-existing structures inherited from the underplating stage. To solve these issues requires additional field and metamorphic data to those presented in this thesis; however, the studied area is suitable for this type of investigation.

7.2.4 The D3 phase: extrusion vs. backthrusting

The D3 phase do not produce any metamorphic recrystallization in the Lower Units, in Razzo Bianco and the Schistes Lustrés Complex. However, field evidence of the folded tectonic contacts between them implies that their coupling must occur before the D3 phase. Whereas the S3 foliation is sub-horizontal or gently dipping in all the studied areas, the attitude of the A3 axes is not homogeneous. The A3 axes, always gently dipping, are NNE-SSW trending in Corte and Ghisoni areas whereas in Pedani area show a clear ENE-WSW trend. On the whole, the A3 axes as well as the S3 foliation show a moderate dispersion around a sub-horizontal, N-S trending axis. This dispersion can be probably considered as induced by the Miocene, open folds with sub-vertical axial plane that deform all the pile of tectonics units of Alpine Corsica. However, this weak deformation cannot explain the shifting of the A3 axes trend that changes going south to north from NNE-SSW to ENE-WSW. This change can be instead attributed to a pre-existing rotation around vertical axes, induced by the strike-slip tectonics connected with the development of the CCSZ whose activity is estimated as pre-Miocene in age (Lacombe and Jolivet 2005). Thus, the ENE-WSW trend of the A3 axes detected in Pedani area can be regarded as the result of re-orientation produced by strike-slip fault, located westward of this area.

The D3 phase structures with a top-to-the-E shear sense have been described for the metamorphic oceanic and continental units in the areas of Balagne (Malasoma and Marroni 2007), Cima Pedani (Di Rosa et al. 2018a; 2018b) Corte (Bezert and Caby 1988; Malasoma et al. 2006; Di Rosa et al. 2017b; 2018b), Tenda (Molli et al. 2006; Maggi et al. 2014), Ghisoni (Garfagnoli et al. 2009; Di Rosa et al. 2018b) and in the Ligurian ophiolite units (Marroni et al. 2004; Meneghini et al. 2009). In the Alpine Corsica, these structures are interpreted by Brunet et al. (2000) as referred to an Early to Late Oligocene age, whereas Rossetti et al. (2015) have proposed a Late Oligocene-Early Miocene age. These age data match the map-scale observation that D3 structures are clearly sealed by the Burdigalian deposits of the Francardo Basin north of Corte (Malasoma et al. 2006).

The top-to-E shear sense have been described since long time in the internal part of the Alps, and various models have been proposed to explain these structures: backthrusting or *retrocharriage* (Caby et al. 1978; Tricart 1984; Steck 1984; Sartori 1987; Freeman et al. 1997; Gabalda et al. 2008), back-folding

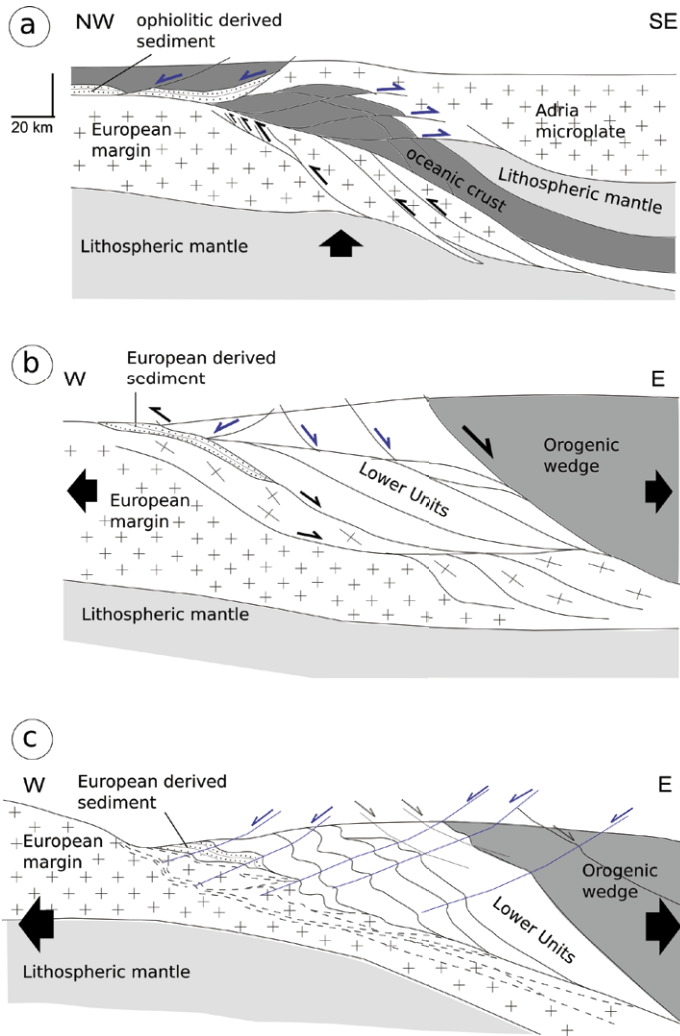
(Bucher et al. 2003), detachment related to extension (Ganne et al. 2007; Gerber 2008). In the case of the Briançonnais units, the top-to-E shear zones root to the W on the Penninic frontal thrust, and thus are interpreted as backthrusting coeval with the activation of major thrusting towards the external part of the belt that mark the end of continental subduction and the start of the continental collision in the Western Alps (Bucher et al. 2003; Tricart and Sue 2006; Ganne et al. 2006; Strzeczynski et al. 2012). However, in other sectors of the Western Alps (Dora Maira, Sesia) has been observed that evidence for true backthrusting associated to the E-directed shearing are missing and the duplication of layering not necessarily imply crustal shortening (Philipot 1990; Wheeler and Butler 1993). Similarly, also in the Alpine Corsica the hinterland-directed

top-to-E shear zones have been described in the rest of the Alpine Corsica and date from the Oligocene (Brunet et al. 2000) or the Late Oligocene-Early Micoene (e.g. Malasoma et al. 2006) In line with these authors, the D3 phase is here interpreted as produced during extensional tectonics (Jolivet et al. 1990; 1991; Fournier et al. 1991; Daniel et al. 1996; Di Rosa et al 2018b). Regardless of its geodynamic interpretation, the D3 phase was strictly connected with the emplacement of the Lower Units at very shallow structural levels (<200°C) before the deposition of the Miocene deposits. In this frame, the D3 phase can be regarded as developed during the transition between the extension driven by the overthickening of the orogenic wedge and that connected with the anticlockwise rotation of the Corsica and the related opening of the Liguro-Provençal basin between the Corsica and the Europe (Brunet et al. 2000; Fournier et al. 1991; Gueydan et al. 2017; Zarki-Jakni et al. 2004).

7.3 The post-D3 phase: further exhumation during transtension?

A set of brittle structures acquired at shallow structural level after the D3 phase have been recognized in the whole study area. The NNW-SSE main fault system with related N-S synthetic and E-W antithetic secondary systems, all characterized by proto- to ultracataclastic fabrics, constitute the anastomosed network of the Central Corsica Shear Zone (Maluski et al. 1973). The main system, consisting in a sinistral strike-slip faults, crosscuts the Corsica Island from Ile Rousse to Solenzara passing from Corte and Vezzani (Waters 1990), but several secondary branches develop eastward (i.e. those of Cima Pedani) and westward (i.e. those of Ghisoni). Although the CCSZ roughly cover the boundary between the HCY and the Alpine Corsica, the cataclastic shear zones are located in both the domains, juxtaposing rocks belonging to different tectonic groups with granitoids of the HCY and fragmenting the structures formed during the D1-D3 phases. The subvertical fault planes of the main system observed often rework previous structures (i.e. the top-to-W shear zones of the D2 phase), thus the dip of ~20° toward both ENE and WSW sometimes observed is probably due to the tilting of the S2 foliation occurred during the D3 folding. In other places of the Alpine Corsica, the normal sense of shear superimposed on

Figure 70. Schematic interpretation of the last stage of exhumation in the Alpine Corsica: (a) Warburton 1986; (b) Fournier et al. 1991 and (c) in this thesis (modified after Di Rosa et al. 2017a).



the ductile deformation like the East Tenda Shear Zone, separating the Tenda Massif from the Schistes Lustrés Complex (Fournier et al. 1991; Daniel et al. 1996; Jolivet et al. 1998; Molli et al. 2006; Maggi et al. 2014; Beaudoin et al. 2017; Gueydan et al., 2017) is found, but no evidence of a strike-slip component has no longer recognized. In the whole study area, slickenlines indicate a strike-slip kinematics coherent with the sense of shears suggested by the displacement of the S2 foliation. However, in Asco Valley and in the Ghisoni-Noceta area an

older generation of slickenlines, coherent with a normal sense of shear has been observed. The faults network of Ghisoni-Noceta area, where at least two main faults systems (NNE-SSW sinistral main system and ENE-WSW dextral antithetic system) with related slickenlines have been recognized, suggests a local extensional setting related to the main strike-slip kinematics. This mechanism has been described by Kim et al. (2004), who asserted that blocks rotate as slip builds up along the boundary faults. Faults within the step are antithetic to the main fault system, and extension fractures occur around the rotated blocks. Such small-scale block rotation is typically associated with triangular openings at the intersections between faults (Kim et al. 2000), that in this case correspond to the two branches of the CCSZ that are developed south of Venaco.

The activity of the CCSZ is constrained in the Late Eocene – Early Oligocene (Lacombe and Jolivet 2005). In this time lapse the geodynamic setting of the Western Mediterranean change dramatically because of the switching of the tectonic regime from compressional to extensional (Fig 71). The role of the CCSZ is thus crucial to understand the relative motion of the plates in this changing setting: syn-rift deposits in the Liguro-Provencal Basin indicated that this back-arc basin started to open in the Oligocene - Miocene time by the rotation of the Corsica-Sardinia block (Auzende et al. 1973; Dewey et al. 1973) as a consequence of the indentation of the European plate by the Adria microplate (Tapponier et al. 1986; Waters 1990), causing the Apennine subduction (Réhault et al. 1984; Gueguen et al. 1998). The activity of sinistral strike-slip faults along the western side of Adria is required to accommodate the plates displacement: the CCSZ can therefore be compared to the Oligocenic – Miocenic sinistral Villalvernia-Varzi line (Elter and Pertusati 1973, Laubscher 1991; Laubscher 1991, Schmid et al. 2017) and the dextral Sestri-Voltaggio line (Cortesogno and Haccard 1984) interpreted as antithetic (Capponi et al. 2009; Federico et al. 2009; Marroni et al. 2010). In the Early Miocene time the Alpine Corsica underwent a generalized extension (Cavazza et al. 2001; Danisik et al. 2007; Zarki-Jakni et al. 2004) leading development of Saint Florent Basin and Aleria Plain (Fig.7.10). The age of these two basins is the same of Francardo Basin (i.e. Early Miocene), but differently to this latter, their develop were controlled by normal faults with NE-SE and N-S trends (Gueydan et al. 2017). Although the relationships between CCSZ activity and the Burdigalian basin of Francardo are still unclear, the activity of the CCSZ prolonged until the Late Oligocene, as proposed for the East Tenda Shear Zone (Brunet et al. 2000; Fellin et al. 2006; Danisik et al. 2007) cannot be excluded.

7.4 From data to model: extrusion tectonics

7.4.1 The perturbation of the geothermal field as consequence of the involvement of cold lithosphere into the subduction zone

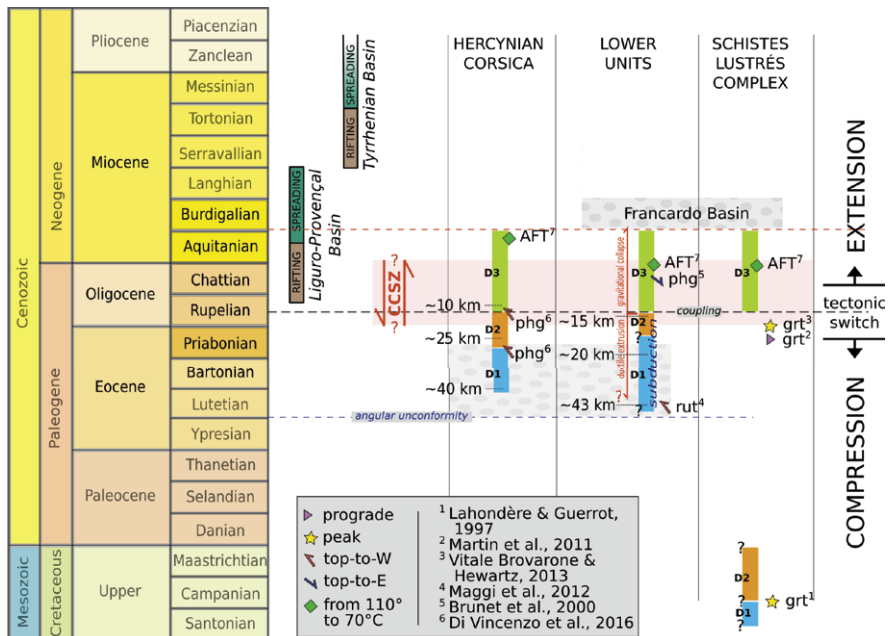
The thermobarometric data obtained on the metamorphism of continental and oceanic units of Cima Pedani (CAU, PEU, SCU and LEU), Corte (CPU, PPU and IZU) and Ghisoni (GHU) areas confirm the general model in which HP/LT conditions are associated with the subduction processes, whereas the LP/HT conditions are related to collision-related processes (e.g. Berger and Bousquet 2008). Starting from the data presented in this thesis, additional considerations about the effect on the geothermic structure acquired during the continental subduction and exhumation could be done. The approach is the same employed in several sectors of the Alps (Bousquet et al. 1997; Jamieson et al. 1998; Roselle et al. 2002; Goffè et al. 2003), and consists in estimating the depths at which the Lower Units are located using the P values associated to the different phases of their exhumation. Since the geobaric gradient for a “normal” crust is 27 MPa/km (Best 2003) and considering that the lithostatic pressure exerted on the Lower Units is given by the accretionary wedge in which metamorphosed oceanic and continental crusts are mixed, an average crustal geobaric gradient of 30 MPa/km has been employed for the calculations made in this study.

The P-peak event, even if corresponds to P-T different values different for each unit, is associated to a geothermic gradient ranging from 5 to 11°C/km, that are typical values for subduction zone (e.g. Ganne et al. 2007; Kearey 2009) and in agreement with those calculated for other units of the Alpine Corsica (Malasoma and Marroni 2007; Vitale Brovarone et al. 2012). Such differences are due to the different path followed by each unit and suggest that they were buried in a similar subduction setting, in which the geothermic conditions are similar and thus likely in a short time lapse. With the onset of the decompression, the rising of the temperatures during the D1 phase testifies that the geothermic re-equilibration within the tectonic wedge was in progress simultaneously with the exhumation of the Lower Units (Fig 72, England and Richardson, 1977; Spear et al. 1984; Grasemann et al. 1998). Evidence of the warming event is the ascent of the tectonic units from variable depths (i.e. at the beginning of the early D1 phase; CAU: 23 km, PEU: 18 km, SCU: 23 km, CPU: 27 km, PPU: 25 km and GHU: 22 km) to shallower (i.e. at the end of the late D1 phase; CAU: 19 km, PEU: 15 km, SCU: 17 km, CPU: 18 km, PPU: 20 km and GHU: 13 km) contemporary with the increase of the geothermic gradient up to 23°C/km (Fig 72b).

During the D2 a trend of decreasing temperatures and pressure has been registered by all the units, which reached the depth of ~7 km at the end of this phase, while the geothermic gradient associated to the D2 increases for each unit (CAU: 15°C/km, PEU: 20°C/km, SCU: 37°C/km, CPU: 27°C/km, PPU: 32°C/km and GHU: 48°C/km), assuming values typical of post-collisional setting (Fig 72c, Schlunegger and Willett 1999; Rubatto and Hermann 2001).

Owing the lack of P-T data related to the D3 phase, it is not possible to constrain the latest part of the P-T paths; however, given the similar P-T conditions reached by the units during the D2 and that the D3 phase involves the pile of units already stacked, the Lower Units were surely exhumed together from ~7 km to the surface (Fig 72d).

Figure 71. Review of the age constraints related to the Alpine metamorphism in the Hercynian Corsica, the Lower Units and the Schistes Lustrés Complex. The geochronological data published (legend in the grey box) are completed with stratigraphic observations (angular unconformity, deposition of Francardo Basin), with the information related to the post-D3 deformation (Central Corsica Shear Zone) and geodynamic observations (tectonic switch from compression to extension) made in this thesis.



To complete the framework, some considerations in terms of geothermic gradients must do for the slices of Schistes Lustrés Complex sandwiched between the Lower Units (§ Cap 4.4, 5.3.2). The P-peak conditions related to the D2 phase, reached during the intra-oceanic subduction stage, fix the maximum burial depth at 33 km for IZU-Botro unit and at 28 km for IZU-Buttinacce Unit; the associated geothermic gradient (6-11°C/km) is typical of subduction zone, as predicted also for the Lower Units. However, differently from the latter, these gradients do not change during the exhumation: during the late D2, IZU-Botro unit goes up to 16 km while IZU-Buttinacce to 13 km under geothermic gradients of 9 and 12°C/km respectively. Cold P-T paths are typical of subduction setting, unlike those related to collisional setting that experienced a

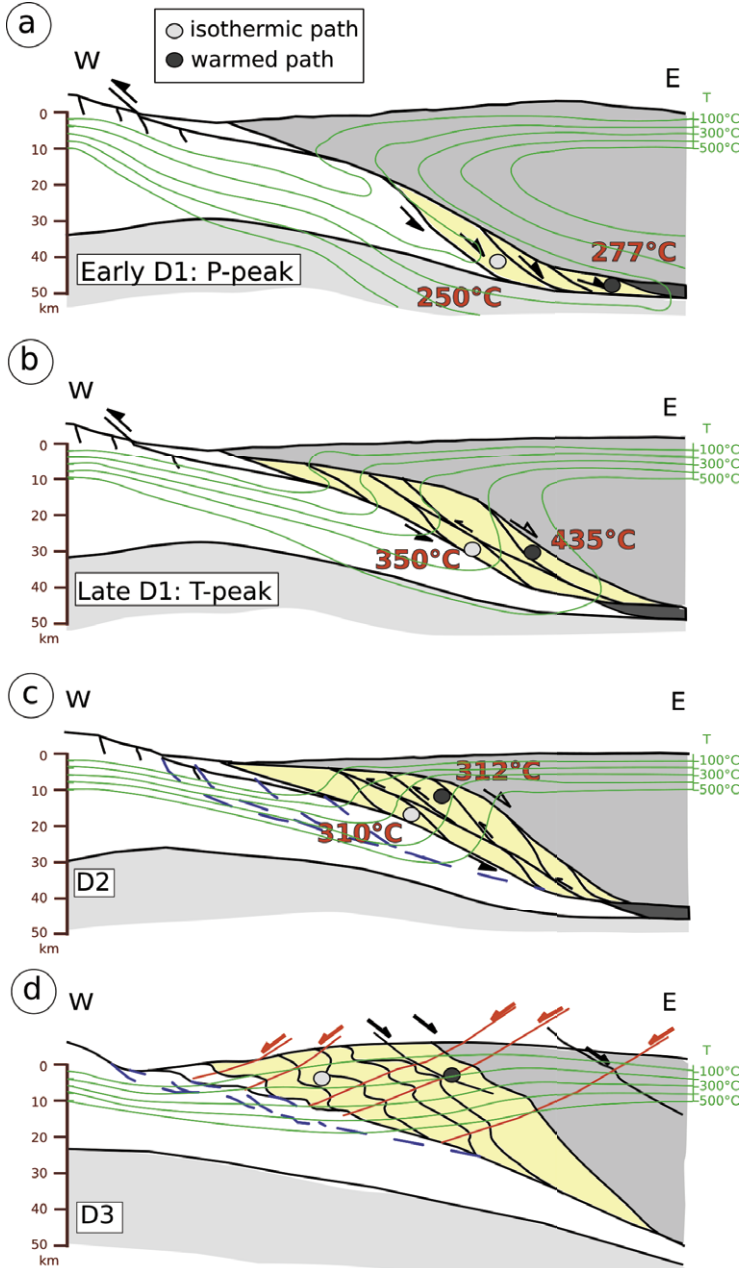
warming phase during the exhumation (e.g. Berger and Bousquet 2008). Therefore, the data here presented confirm that the exhumation of the Schistes Lustrés Complex occurred in the oceanic subduction setting that predates the subduction of the European-derived units.

7.4.2 From subduction to the wedge: toward a new geothermic equilibrium

It would be interesting to quantify the contribution on the geothermic condition of the Lower Units given by the geothermic field, which attempts to re-configure passing from the subduction to the continental collision setting. Geochronological data related to the metamorphism of the Lower Units are missing and is not possible to constrain the timing of the D1 and the D2 of the studied units so far. This prevents to calculate the exhumation rate related to the Lower Units, and thus to verify if cooling is only due to exhumation. However, Berger et al. (2011) attested that wedging and underthrusting of continental lower plate material produces heat input into the lower crustal levels, and this process is responsible for predominantly conductive heat transport in the overlying units. This phenomenon is the main responsible of the final Barrovian metamorphic field gradient (Winter 2001), described by several authors in the many collisional setting (e.g. Miyashiro 1973; England and Thompson 1984; Guillot et al. 2003). The geothermic gradients estimated in this thesis for the D2 phase of the Lower Units (37°C/km for SCU, 28°C/km for CPU, 32°C/km for PPU and 48°C/km for GHU) are close to those that consider the classical Barrovian metamorphism (30°C/km). Are an exception CAU and PEU (18°C/km and 22°C/km respectively). As already mentioned in the previous chapters, we do not know what they are resting on; in addition, the extension of these units, together with SCU, is reduced compared to the other Lower Units studied. Therefore, while the geothermic condition of SCU could be explained by its proximity with the LEU, the geothermic regime of CAU and PEU could be conditioned by those of the underlying rock volume (i.e. other slices of European-derived units or the lower plate itself).

In the Alps (e.g. Berger et al. 2011) and in other collisional belts (Abalos et al. 2003; O'Brien 2000) HP relics testify, as in our case, a subduction setting which predates the continent collision. The maximum T reached (as in our case at pressures < P max) is due to two main causes: the heat redistribution during the exhumation of HP units and their emplacement at middle crustal levels (i.e. the wedging). The exhumation of HP tectonic fragments along the subduction channel, that causes the fast reorganization of the geothermic structure typical of subduction setting (Roselle et al. 2002; Goffè et al. 2003), does not transport heat enough to produce the Barrovian overprint (Engi et al. 2001). Therefore, the additional heat needed must necessarily come from the thickening of the wedge itself. Berger et al. (2011) asserts that the effect of the progressive underthrusting and accretion has three main effects: the addition of radiogenic material to the

Figure 72. Cartoon illustrating the geodynamic evolution of the Lower Units proposed in this thesis. (a) early D1 phase, (b) late D1 phase, (c) D2 phase and (d) D3 phase. Light grey indicates the path followed by the isothermic units (e.g. CPU ad GHU), while dark grey those of the warmed units (e.g. CAU, PEU, SCU and PPU).



system (England and Thompson 1984; Chamberlain and Sonder 1990; Huerta et al. 1998; Goffé et al. 2003; Bousquet et al. 2008, Gerya et al. 2008; Wiederkehr et al. 2008; 2009), the heat advection from the nappe stack toward external positions (previously cooled) and the increasing heat transported from the lower crustal wedge to the central part. This late process leads to the thickening of the wedge, replacing warmer upper crust material with other coming from the colder lower plate. All of these processes are thus required for Barrovian conditions, as confirmed by numerical models (Berger et al. 2008). In this framework, the thermobarometry allows to verify the contribution of the viscous heating to the geothermic conditions during the collision (Ernst 1990). For example, Burg and Gerya (2005) demonstrated that in the Lepontine dome the energy locally dissipated during deformation produced an additional 100-200°C temperature increase.

The Barrovian-type geothermic overprinted above polyphase exhumation described in the central Alps (e.g. Wiederkehr et al. 2009) shows similar features with the P-T paths reconstructed for the Cima Pedani Units (CAU, PEU and SCU) and PPU of Corte area. Despite differences in the absolute P and T values related to the P- and T-peaks, the increasing temperatures trend between these two events is in agreement with those of Val Luzzzone (NW rim of the Lepontine dome, Central Alps, Wiederkehr et al. 2009). Accordingly, we attribute the trend of increasing temperatures observed between the P- and T-peaks of CAU, PEU, SCU and PPU to the accretion of European continental crust. In this view, the isothermic exhumation of CPU and GHU seems to be anomalous. However, their geothermic gradients follow the overmentioned path and the lack of a shaped path due to a sharp increase of temperature is attributable to their “peripheral” position in the wedge, strongly influenced by the cold condition of the lower plate over which they are located.

7.4.3 Extrusion vs. erosion

The continental subduction, occurring between oceanic subduction to continental collision, produces HP and UHP rocks (Chopin 1987), those exhumation occurs during the oceanic/continental subduction or continental collision (Ernst 2001; Agard et al. 2008). The reported dataset on the tectono-metamorphic path of the continental units from Cima Pedani, Corte, Venaco and Ghisoni provide useful constraints to propose a model for their exhumation. This model must explain an exhumation of coherent but highly deformed fragments of continental crust from 35-45 km up to about 10 km of depth, where these units have been coupled with a less metamorphosed oceanic unit (i.e. the Schistes Lustrés Complex and the Upper Units) before their exposition to the surface.

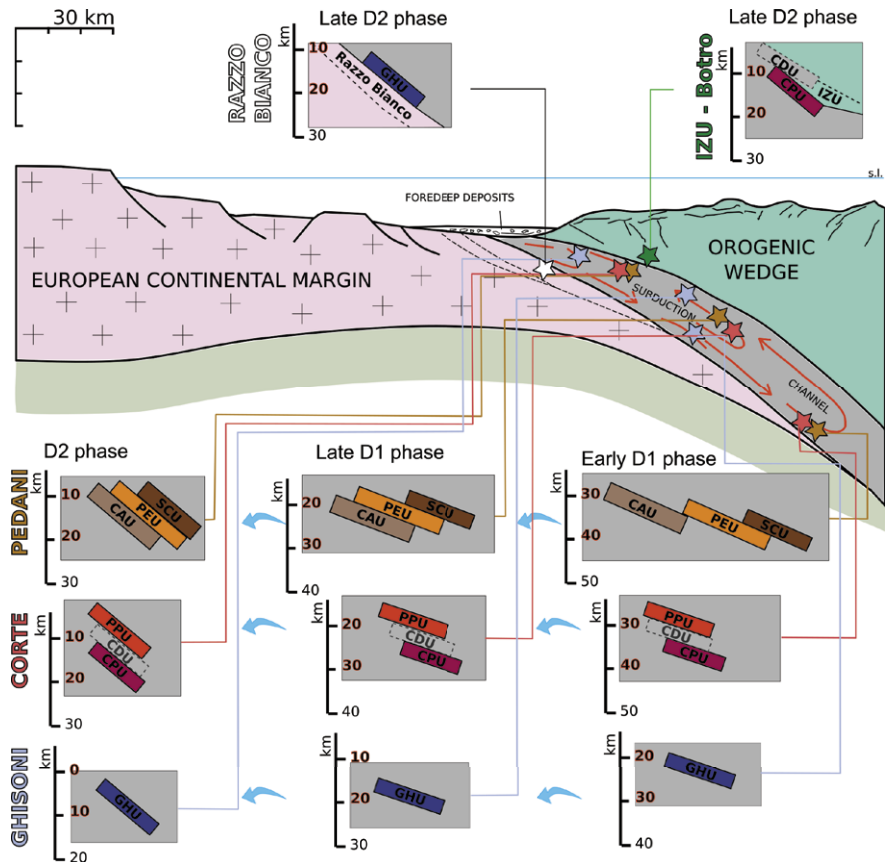
Several mechanisms have already been proposed in literature to explain the exhumation of HP continental and oceanic units (for a review see Platt 1993; Guillot et al. 2009; Erdman and Lee 2014). These mechanisms include: wedge

extrusion of crustal material detached from the down-going plate (Ernst 1975; Chemenda et al. 1995); ductile extrusion by return flow along the down-going slab–mantle interface (Cloos 1982; Grujic et al. 1996; Burov et al. 2001; 2014; Gerya et al. 2002), extensional–erosional collapse (Platt 1993), the nappe intrusion mechanism (Malavieille et al. 1998) and diapiric ascent of continental material (e.g. Hall and Kincaid 2001; Gerya et al. 2006). Models based on lithospheric-scale extension in a thrust wedge setting (Platt 1986; England and Houseman 1989) first applied in Corsica (Jolivet et al. 1990; 1991; Fournier et al. 1991; Daniel et al. 1996) have been discarded over time because (i) the lack of widespread extensional structures related to the first stages of exhumation (i.e. D1-D2) and (ii) the HP/LT peak are associated temperatures typical of subduction setting (Caron et al. 1981; Lahondère 1991; Tribuzio and Giacomini 2002; Molli and Tribuzio 2004). These features imply a syn-contractual westward thrusting as possible mechanism. Therefore, Chemenda et al. (1995) have proposed that upward tectonic extrusion occurs when a fragment of upper continental crust is detached from the subducted lithosphere and, given its lower bulk density, is buoyantly transported back to the surface, while the rest of the lithosphere continues to be subducted (Platt 1987; Wijbrans et al. 1993). This model, already applied to the Tenda Massif by Molli et al. (2006) and Molli (2008), provides that the fragment moves upward between a basal thrust and a coeval upper normal-sense detachment operating in compressional tectonic setting. In contrast, Malavieille et al. (1998) have suggested that the occurrence of HP metamorphic rocks bounded by foreland-directed shear zones can be explained by an extraction of a discrete volume of rocks by two faults merged together at the trailing edge of the extracted body. Both these models imply that the previously subducted crustal fragment is exhumed as a large and rigid body.

However, several field evidences including this present one indicate that the exhumed crustal material is dismembered in several, small tectonic units that are strongly deformed in a ductile way. Thus, models depicting exhumation of metamorphic rocks at depth not deeper than 70 km occur by a ductile extrusion in the subduction interface zone referred to as subduction channel (Grujic et al. 1996; Burov et al. 2001; 2014; Beaumont et al. 2001; 2006; Godin et al. 2006) seem to be more applicable to what we observed in Alpine Corsica. The ductile extrusion occurs in these models in a confined, up to several km thick subduction channel (Cloos and Shreve 1988), through a protracted upward flow of a weak, viscous crustal rocks between relatively rigid walls. As the crustal rocks are extruded in a ductile way (Grujic et al. 1996), deformation is heterogenous but pervasively distributed within with localized sheared bands bounding volumes of less deformed rocks. Studied examples (Godin et al. 2006) indicate that the deformations are characterized by a top-to-the foreland sense of shear for most of the subduction channel, with top-to-the-hinterland shearing only appearing in its top-most part. This model implies that at the end of the exhumation the metamorphic crustal fragments are bounded by less metamorphic rocks, leading to an inverted metamorphic sequence at the orogen scale. The deformation within the exhumed crust may be dominated by a perfect simple shear, or more

likely by a general shear combining components of simple shear and pure shear (Grujic et al. 1996; Escher and Beaumont 1997; Law et al. 2004; Jessup et al. 2006).

Figure 73. Generic model for the subduction channel and kinematic models proposed for the Lower Units, the Schieses Lustrés Complex and Razzo Bianco studied in this thesis. The stars in the subduction channel represents the positions of the Lower Units in specific stage of the deformation history, grouped by localities. The depths have been calculated on the base of the pressure conditions. Modified after Di Rosa et al. 2018a.



During exhumation, the crustal rocks move from mid-crustal ductile to upper crustal brittle levels acquiring the appearance of several phases of deformation recorded as foliation overprinting, refolded folds, fold and fabric transposition (e.g. Airaghi et al. 2017; Balen et al. 2017; Loury et al. 2018). Similarly, the overall features of the D1 and D2 phases recognized in the continental units of the studied areas suggest a polyphased exhumation evolution involving extrusion by an upward return flow in the subduction interface zone (Burov et al. 2001;

2014; Beaumont et al. 2001; 2006; Godin et al. 2006). The data on the metamorphism indicate that both S1 and S2 foliations represent two steps of the same, continuous exhumation process, similarly to what suggested for the Ligurian Alps (e.g. Federico et al. 2005). This evolution was accompanied by continuous decrease of pressure associated with a temperature increase during the late stage of the D2 phase (Fig 73). The sense of shear associated to the D2 phase is generally top-to- NW, i.e. top-to-the foreland considering the E-dipping subduction plane reconstructed for the Alpine evolution of this sector of Corsica. In addition, the stacking of the continental units occurred before the D3 phase, i.e. during the exhumation in compressional regime (Fig 73). All these features suggest that the D1 and D2 phases were probably acquired during the ascent path by ductile exhumation in the subduction channel in a syn-contractual westward thrusting, according with Chemenda et al. (1995) and Molli and Tribuzio (2004).

In the ductile extrusion model, the ductile exhumation of continental metamorphic units was thus driven by simultaneous activation of a thrusting system at their base and an extensional fault system at their top (Godin et al. 2006 and references therein). In this view, a basal thrust and an upper normal-sense detachment is needed to explain the exhumation of the Lower Units. The thrusting system observed between the HCY and the CPU is well exposed in the Corte area (e.g. Golo, Tavignano and Restonica Valleys, Di Rosa et al. 2017b); In the Venaco and Noceta-Ghisoni area this contact is badly preserved because it was subsequently reworked by the CCSZ. In Cima Pedani the basal thrust of the channel cannot be observed because the basal contact of the lowermost unit (i.e. CAU) is not exposed. On the contrary, in Cima Pedani the normal fault that top the Lower Units can be placed at the base of the oceanic units of the Schistes Lustrés Complex (i.e. LEU) and would be represented by the hypothesized shear zone with normal sense responsible for the coupling between the LEU and the Cima Pedani continental units and that is now overprinted by the brittle structure bounding the tectonic window to the south-east (Di Rosa et al. 2018a). In the others studied area the normal fault at the top of the Lower Units could only be hypotized, because not clear evidence of structures like that have been found.

The syn-subduction rise of the crustal material implies the rapid exhumation of HP/LT rocks. To constrain in time the exhumation of the Lower Units, $^{40}\text{Ar}/^{39}\text{Ar}$ dating and apatite- and zircon-fission tracks derived from the HCY and Alpine Corsica available in literature help in the reconstruction of our model (Fig 71). Data related to the deformation history of the Lower Units are not available so far, but Di Vincenzo et al. (2016), studying three samples belonging to the Alpine shear zones located in the HCY immediately west of Corte, detected two populations of muscovites recrystallized at >45 Ma and at 37-32 Ma, with a syn-exhumation geothermic re-equilibration at <33-32 Ma. Comparing the description of the microstructure they do with our samples, it is believable that the older generation of muscovite corresponds to our S1 Phg, whereas the younger to our S2 Phg. These age are in agreement with those estimated by Molli and Tribuzio (2004) for the Tenda Massif: they distinguished an HP/LT stage (i.e. our D1) at <47 Ma (Brunet et al. 2000) and two stages of greenschist

facias condition corresponding to the older top-to-W stage (47-37 Ma, Brunet et al. 2000) and to the younger top-to-E normal faulting (35-25 Ma, Brunet et al. 2000). Rossetti et al. (2015) obtained younger ages for the top-to-W (32-29 Ma) and the top-to-E (27-20 Ma) stages (Fig 71). However, two of the three samples they used are characterized by extremely high values of MSDW (>600); the only acceptable sample (MSDW=19) has 31.8 Ma, that is coherent with those estimated by Brunet et al. (2000). Therefore, exhumation during compression ends around 32 Ma, that corresponds to the opening of the Ligure-Provencal Basin (Chamot-Rooke et al. 1999). The extension associated to the opening of this back-arc basin, indeed, implies the switching of the tectonic regime, which until then had been compressive (e.g. Sage et al. 2011). Accordingly, the exhumation during extension related to the top-to-E stage of the Tenda Massif and the D3 described in the Lower Units occurs after 32 Ma (Brunet et al. 2000; Molli and Tribuzio 2004; Rossetti et al. 2015; Di Vincenzo et al. 2016), i.e. during the rifting of the Ligure-Provencal Basin (Fig 71).

The last stage of the Lower Units ductile exhumation (i.e. the D3 phase), caused by gravitational collapse (§ Cap 7.1.4), is constrained by the apatite fission tracks. Danisik et al. (2007) estimated for the whole island (i.e. HCY, Lower Units, Schistes Lustrés Complex and Upper Units) the time in which the rock volume reached the temperature of 110-70°C and obtained in the area studied in this thesis ages always younger than 25 Ma. Danisik (2005) recognized in the central Corsica a trend of younging from W to E in the area between Asco (~25 Ma) and Cima Pedani (~15 Ma), and in the HCY an opposite trend of younging from E to W between Calacuccia (~24 Ma) and Galeria (~16 Ma). Danisik (2005) attested that during this last stage of exhumation the cooling and denudation are produced by a combination of tectonic denudation and surface erosion caused by the orogenic collapse, which drives the Lower Units exhumation during the post-32 Ma, i.e. after the switching from compression to extension. Although the quantification of the tectonic denudation and surface erosion is difficult to quantify, mostly because it implies the knowledge of the exhumation rate and of the geothermic gradient's variation of different sectors of the belt, the contribution of both mechanisms cannot be excluded. In this setting, the rifting in the Ligure-Provencal Basin may produced the contemporary younging from E to W in the HCY by rift-related erosion and from W to E in the Lower Units by a dominant tectonic denudation (Danisik et al. 2007).

Chapter 8

Conclusions

The study of the area between Asco and Fium'Orbo valleys allowed to improve the knowledge about the Alpine Corsica stack and its relationships with the adjacent Hercynian Corsica. The data obtained provided new information about the stratigraphy, the tectono-metamorphic history and the geochronology of the Lower Units, i.e. the set of continental units located at the base of the Alpine Corsica stack, that represent the portion of the European margin involved in the subduction/exhumation processes in the Late Eocene – Early Miocene time span. The Lower Units are composed by pre-Carboniferous complex of metamorphic rocks intruded by Permo-Carboniferous granitoids (~281 Ma, § Cap 6.2) with minor mafic products (~276 Ma, § Cap 6.3). From the Permian to the Middle to Late Eocene two successions of covers occur: the older is characterized by a Permian volcanoclastic succession, separated from the basement by an unconformity and topped by a Mesozoic succession of limestones and dolostones. The order with which the lithotypes occur indicate a progressive deepening of the carbonate platform, typical of a continental margin involved in the rifting processes. Supporting this stratigraphic evidence, the geochronological data attested the occurrence of a heating event in the Triassic (~225 Ma, § Cap 6.3) compatible with the thinning of the continental crust. The younger succession of cover consists of Nummulitic limestones, breccias, sandstones and siltstones of the Middle to Late Eocene; they lie in angular unconformity above both the Paleozoic basement and the Mesozoic covers (§ Cap 5.1). The origin of the unconformity is attributed, in this study as well as in Di Rosa et al. (2017a), to the bulging of the lower plate (i.e. Europe) approaching the subduction zone in the Middle to Late Eocene (§ Cap 7.1). From the

Maria Di Rosa, University of Pisa, Italy, maria.dirosa.scaglia@gmail.com, 0000-0002-1154-7429
FUP Best Practice in Scholarly Publishing (DOI 10.36253/fup_best_practice)

Maria Di Rosa, *Tectono-metamorphic evolution of the continental units along the edge between Alpine and Hercynian Corsica. Constraints for the exhumation models in the continental collision setting*, © 2021 Author(s), content CC BY 4.0 International, metadata CC0 1.0 Universal, published by Firenze University Press (www.fupress.com), ISSN 2705-0297 (online), ISBN 978-88-5518-420-5 (PDF), DOI 10.36253/978-88-5518-420-5

subduction onwards, the Lower Units experienced an intense polyphase deformation history and registered different P-T conditions due to the depth at which they were coherently buried.

As already described in Di Rosa et al. for Corte (2017a; 2017b) and Pedani and Ghisoni (2018b) areas, three ductile deformation phases (D1-D2-D3) have been recognized in all the lithotypes belonging to the Lower Units of the area studied in this thesis; the metamorphism associated during the first two phases highlighted that:

- Every single unit belonging to the Lower Units has an independent path of subduction/exhumation, as testified by the difference in the P- and T-peaks registered during the D1 and D2 phase (§ Cap 5.3);
- Although differences in absolute values, the Lower Units studied are all characterized by three distinct P-T conditions of equilibrium. The first two P-T conditions are calculated using the compositions of chlorite-phengite couples contained in the S1 foliation, and are related to the P-peak reached in the blueschist facies, and T-peaks, reached in the greenschist facies. The third P-T equilibrium is instead related to the D2 phase and it is reached at low-greenschist facies conditions (§ Cap 5.3 and 7.2.1 and in Di Rosa et al. 2017a; 2018a; 2018b);
- The decreasing pressure trend from the P-peak to the T-peak observed in all the units indicates that the exhumation of the Lower Units already started during the D1 phase (§ Cap 5.3 and 7.2.1 and in Di Rosa et al. 2017a). This implies a tectonic extrusion mechanism for the exhumation of the Lower Units from ~45 km (early D1) to ~10 km (D2 phase) in a still convergent setting (Chemenda et al. 1995; Di Rosa et al. 2017a; 2018a);
- During their retrograde path, two different trends are followed by the Lower Units: the “isothermic” path, in which the T range in the D1-D2 phase does not exceed of 150°C (Di Rosa et al. 2018b), and the “warmed” path, characterized by a heating related to the T-peak (i.e. Barrovian-type geothermic overprint of Wiederkehr et al. 2009). It has been observed that there is a relationship between the two different trends and the position of the unit in question respect to the Hercynian Corsica and the Schistes Lustrés Complex (§ Cap 7.2.1): the isothermic path is followed by the units which directly overthrust the Hercynian Corsica (i.e. CPU, GHU), while moving away from the foreland prevails the warmed path (i.e. CAU, PEU, SCU and PPU, Di Rosa et al. 2018b);
- From the geodynamic point of view, the recognition of the two trends (isothermic and warmed) implies that the CPU and GHU were rapidly exhumed and didn't have time to re-equilibrate themselves to the geothermic conditions that characterized the continental collision (e.g. Berger et al. 2011), as the other Lower Units studied did (§ Cap 7.4.2).

The study of the metamorphism of two tectonic slices belonging to the Schistes Lustrés Complex outcropping in the Corte area between the CPU and CDU (§ Cap 5.5.2) confirmed that that they were involved in the Alpine Orogeny before the Lower Units, as testified by the cold path typical of the

oceanic subduction (e.g. Berger and Bousquet 2008) and didn't experience depth higher than ~30 km (§ Cap 7.2.3). This implies that, after an early exhumation from the deepest positions, they stationed at the base of the orogenic wedge at depth of ca. ~13 km, where they were coupled, at the end of the continental subduction, with the arising Lower Units. Therefore, the basal erosion of the orogenic wedge is evoked in this thesis as mechanism responsible of the coupling of the Lower Units with the Schistes Lustrés Complex during the late D2 phase.

Also related to the D2 phase are several top-to-W shear zones identified in the Lower Units (Di Rosa et al. 2017b). These ductile shear zones, characterized by proto-mylonitic to mylonitic fabrics, have been found also in the Hercynian Corsica at the rim with the Alpine Corsica (§ Cap 5.4), that separate volumes of undeformed rocks (e.g. Asco and Ghisoni, § Cap 5.4.1 and 5.4.3) or slices of deformed and metamorphosed rocks (e.g. Razzo Bianco, § Cap 5.4.2) from the foreland. This is a new important constraint for the Alpine Orogeny in Corsica, because these shear zones have been locally observed (Amaudric du Chaffaut 1980; Amaudric du Chaffaut et al. 1985) and dated (Di Vincenzo et al. 2016) but their belt scale interpretation is provided for the first time in this thesis.

The D3 phase represents the last phase of ductile exhumation recognized in the Lower Units. Only the recrystallization of calcite is associate to this late phase, therefore the characterization of the associated metamorphism was not possible. However, the map- and meso-scale study of the D3 allowed to constrain the final stage of exhumation of the Lower Units. The subhorizontal S3 foliation related to this phase is coherent with the vertical maximum shortening, as widely observed in the Alps (Ratschbacher et al. 1989; Wheeler and Butler 1994), and implies a change in the strain regime from compression (D1-D2 phases) to extension (D3 phase). The ductile extension tectonics represents the last stage of exhumation in a continental collision setting induced by the orogenic collapse (Fournier et al. 1991). In addition, it has been observed that the D3 phase folds together the Lower Units with the Schistes Lustrés Complex (§ Cap 5.5), as well as the ductile shear zones found in the Hercynian Corsica, predating both the coupling within the Alpine stack and the shearing of the foreland.

The switching from compression to extension is strictly linked with the Oligocene rifting of the Liguro-Provençal Basin, that lead the anticlockwise rotation of the Corsica-Sardinia block; to accommodate this rotation, a sinistral strike-slip fault system (i.e. CCSZ) was activated in the central Corsica (§ Cap 5.6). Although the strike-slip kinematic is clearly registered, downdip slickenlines indicating a normal sense of shear were locally observed (e.g. Asco and Ghisoni areas) along the faults that reworked the D2 top-to-W shear zones (§ Cap 7.3). Even if this observation needs to be improved by additional data, a post-D3 transtensional kinematics cannot be excluded.

Chapter 9

Supplementary materials

The peak metamorphism of the samples studied is represented by the mineral assemblage Chl+Phg+Alb+Qtz. Vidal and Parra (2000) demonstrated that in low- to medium-grade garnet-free metapelites, the Chl-Phg local equilibria can be used to constrain the P–T evolution of exhumed high-pressure rocks. The concept of local equilibrium is consistent with the observed chemical variability among different grains of the same phase coexisting in the same thin section. This reflects the lack of equilibrium at distances above a few millimetres, and the coexistence of several mineral generations that did not reequilibrate during the metamorphic P-T evolution. Therefore, the estimation of metamorphic conditions is based on the composition of Chl and Phg coexisting in thermodynamic equilibrium (Vidal and Parra 2000; Vidal et al. 2001; 2006; Parra et al. 2002a; Dubacq et al. 2010). This method consists in estimating the T-P conditions from the composition of these phases, that are geothermometer (e.g. Cathelineau 1988; Hillier and Velde 1991; Lanari et al. 2014a) and geobarometer (e.g. Massonne and Schreyer 1987), respectively. The pairs selected for the P-T estimates occur within the microstructures of the D1 and D2 phases.

After a preliminary study under the optical microscope, the best micro-areas were analyzed with a microprobe. The EPMA data have been acquired using the JEOL-JXA 8230 electron microprobe of the IsTerre of Grenoble, equipped with five wavelength-dispersive spectrometers and calibrated with the following standards: wollastonite (Ca, Si), orthoclase (K), albite (Al), periclase (Mg), rhodonite (Mn), TiO₂ (Ti), Al₂O₃ (Al), Fe₂O₃ (Fe) and Cr₂O₃ (Cr). The

operating conditions were 15 keV accelerating voltage, 12 nA sample current and 200 to 300 ms per grid point counting time. The analytical spot size was set at 1 μm , as recommended by Lanari et al. (2014c) to detect any zonation of the Phg. According with Vidal and Parra (2000), only the data respecting the two following chemical criteria were considered for the study:

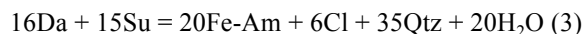
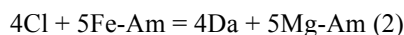
1. Chlorite analyses having more than 0.5% ($\text{Na}_2\text{O}+\text{K}_2\text{O}+\text{CaO}$) and phengite analyses having more than 0.5% ($\text{MnO}+\text{TiO}_2+\text{Cl}$) were rejected;

2. Only the compositions that could be expressed as a linear combination of the following end-members were retained: (Fe, Mg)-Am, Cl, Da and Su for Chl and (Fe, Mg)-Ce, Mu and Py for Phg (for mineral abbreviation § Cap 5.2).

The thermodynamic calculations were made using the solid solution models of Vidal et al. (2006) for chlorite and Dubacq et al. (2010) for phengite. The elemental maps were calibrated using point analyses (De Andrade et al., 2006) using the XMapTools software (Lanari et al. 2014c). The ChlMicaEqui software (Lanari 2012, Lanari et al. 2012) was used to estimate the P-T equilibria conditions for each Chl-Phg couple of the studied samples (e.g. Lanari et al. 2012; Scheffer et al. 2016). The software employs the solid solution models of Vidal et al., (2006) for Chl (14-oxygens based) and Dubacq et al. (2010) for Phg (11-oxygens based), and the standard state properties of Vidal et al. (2006) for Chl and Parra et al. (2002a) for Phg. For the calculation, the water activity was set up to 1 and the convergence between equilibria was achieved for a minimal XFe^{3+} .

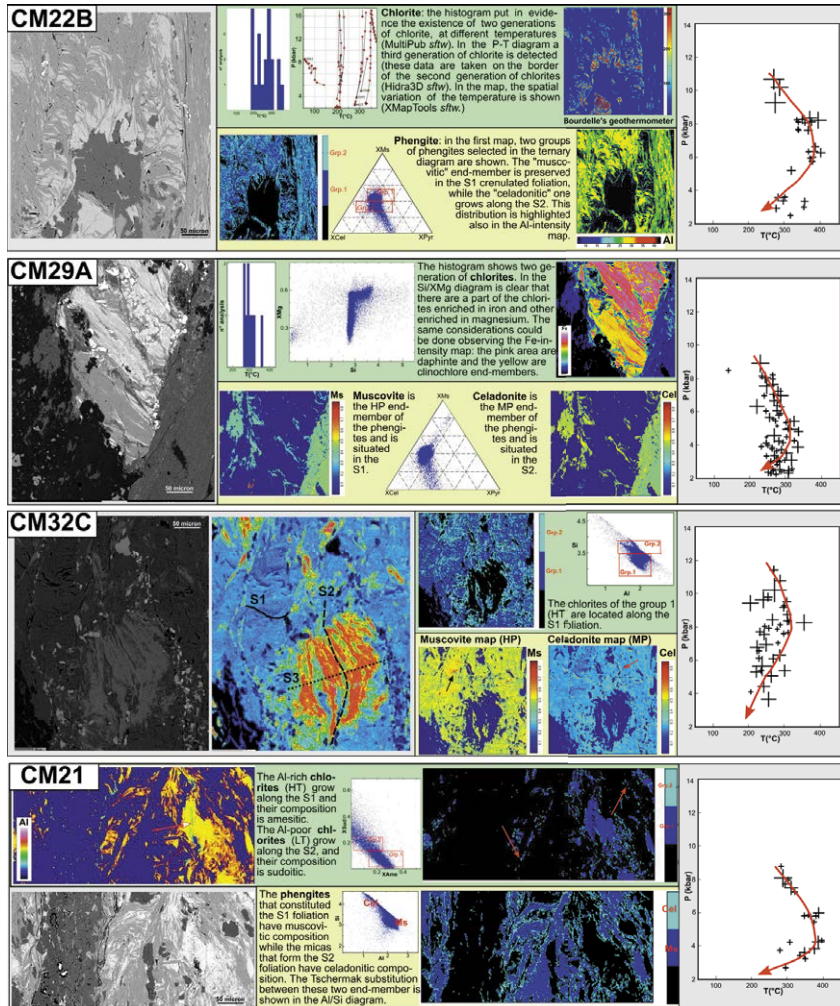
9.1.1 Chlorite

The structural formula of Chl was calculated on 14 anhydrous oxygens. By varying T values, the di/trioctahedral and Tschermak substitutions on Chl cause the switch from Su to Da and Cl (increasing Fe+Mg content) or Am (decreasing Si content, Leoni et al. 1998; Vidal et al. 2001). Vidal et al. (2006) attested that the increase/decrease of Al^{IV} in tetrahedral sites and the decrease of the vacancies in Chl structure increasing T can be modelled by the substitutions between five end-members: Cl, Fe- and Mg-Am, Da and Mg-Su. Using these end-members, four reactions (two independents) can be written for the Chl-Qtz-wt assemblage:



The temperature locations of the equilibria (1) to (4) depend on the activity of the Cl, Da, Su and Am end-members as well as the activity of water. At fixed water activity and pressure, an increase in Su component (increase in vacancies)

Figure 74. Examples of chlorites and phengites and related P-T paths (CPU and PPU, Corte area).



and Cl + Da components (increase in Si) leads to a shift in the equilibria towards lower temperatures, consistent with the numerous empirical thermometers based on the amount of Al^{IV} in Chl (e.g. Cathelineau and Nieva 1985; Hillier and Velde 1991). Vidal et al. (2005; 2006) suggested that a simultaneous estimation of Fe^{3+} in chlorite and equilibrium temperature for the Chl-Qtz-H₂O assemblage can be made using criterion based on the convergence of equilibria (1) to (4) at given pressure, which is achieved for a minimal $XFe^{3+} = (Fe^{3+}/Fe_{tot})$ of chlorite. Following this approach, XFe^{3+} is increased and the structural formula of chlorite is recalculated until convergence of (1) to (4) is achieved at maximum temperature of chlorite crystallization.

9.1.2 Phengite

The thermobarometric data obtained on the metamorphism of continental and The structural formula of Phg was calculated on 11 anhydrous oxygens. The composition of the Phg varies on the base of the proportion of the Ce, Mu and Py end-members. The P-T dependencies of Phg leads to the formation of Si-rich and (K+Na)-poor Phg containing significant proportion of Py (i.e. illite) at LP/LT conditions, and (K+Na)-rich Phg of composition intermediate between Ce and Mu at HT (Vidal and Parra 2000). The proportion of Ce content of Phg increases with P (Velde 1965; Massonne and Schreyer 1987; Massonne and Szpurka 1997) and forms the basis of a popular geobarometer in which Si isopleths have been calculated for phengite coexisting with K-feldspar, phlogopite, quartz and water in the $K_2O-MgO-Al_2O_3-SiO_2-H_2O$ end-members system (Massonne and Szpurka 1997).

Chl-Phg-Qtz-wt multiequilibrium approach

The Chl-Phg-Qtz-wt multiequilibrium calculation is a semi-empirical approach based on the thermodynamic database proposed by Breman (1988) and implemented by Vidal and Parra (2000), Vidal et al. (2001; 2006), Parra et al. (2002a) and Dubacq et al. (2010). This method consists in the determination of the points in the P/T diagram where all the independent reactions are intersected; such condition is satisfied whenever the Chl-Phg pairs are in equilibrium within the microstructure. For each sample, several Chl-Phg pairs have been selected within the S1 and S2 foliations, in order to test the P-T conditions related to the D1 and D2 phases. In the system $K_2O-Al_2O_3-MgO-SiO_2-H_2O$, the assemblage Chl+Phg+Qtz+ H_2O has two degrees of freedom. The number of independent equilibria (IR) that can be calculated from this assemblage depends on the number of end-members (EM) used to describe the composition of Chl and Phg:

$$IR=(EM+2) -C$$

Where “+2” correspond to the presence of water and quartz. The P-T conditions have been calculated using 64 equilibria involving the five Chl (Cl, Fe- and Mg-Am, Da and Mg-Su) and four dioctahedral Phg (Mg- and Fe-Ce, Mu and Py) end-members (Vidal et al. 2006 and references therein).

To test the accuracy of the Chl-Phg-Qtz-wt multiequilibrium approach, other thermodynamic methods were applied on the Phg (Massonne and Schreyer, 1987) and the Chl (Cathelineau 1988; Hillier and Velde 1991; Lanari et al. 2014a). The results obtained using the three methods are listed in Tab 6.

Equilibrium was considered to be achieved if the intersections between all equilibria present a scatter lower than 25°C and 0.08 GPa; these values have

been calculated with the Monte Carlo technique, as recommended by Vidal and Parra (2000).

Figure 75. Results obtained with ChlMicaEqui (Lanari 2012) for the samples CM21 and CM32C (PPU). (From Di Rosa et al. 2017a).

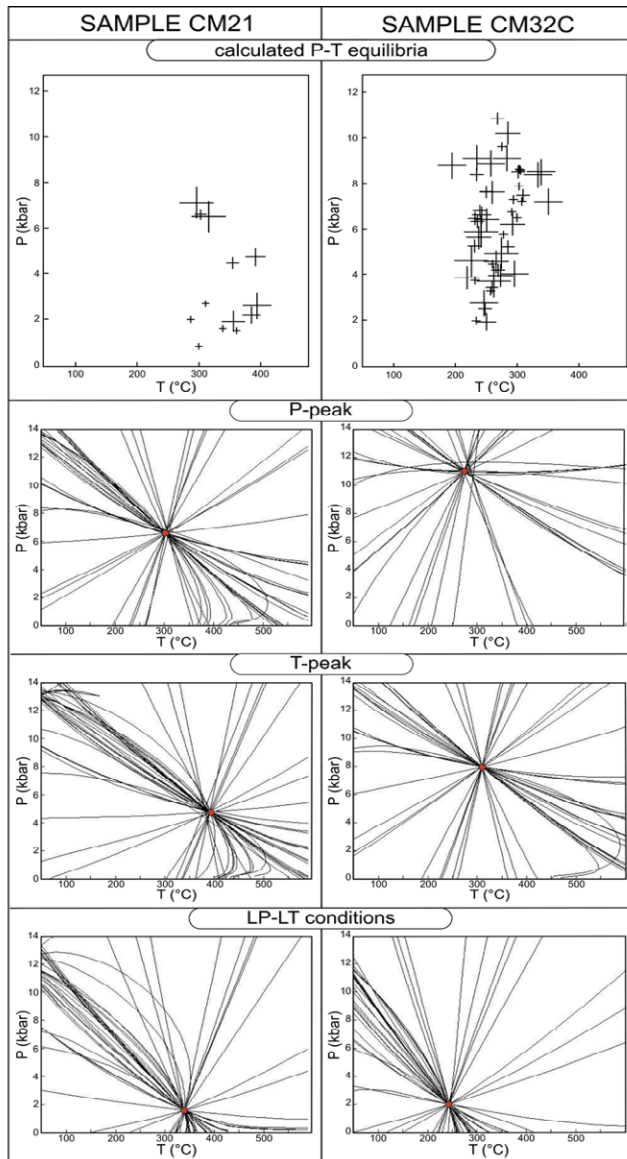


Table 5. Representative electron microprobe analysis of the Chl-Phg pairs of the metapelites of the Lower Units (from Di Rosa et al. 2018b).

Analyse	CAU (CMD80A)						PEU (CMD83A)						SCU (CM34B)					
	S1 (P-peak)		S1 (T-peak)		S2		S1 (P-peak)		S1 (T-peak)		S2		S1 (P-peak)		S1 (T-peak)		S2	
	C	P	C	P	C	P	C	P	C	P	C	P	C	P	C	P	C	P
	hl	h	hl	h	hl	h	hl	h	hl	h	hl	h	hl	h	hl	h	hl	h
	7	g	1	g	1	g	1	g	1	g	1	g	1	g	1	g	1	g
	0	7	6	4	9	2	2	5	8	1	0	2	1	0	1	8	5	7
Wt%																		
Si	2	5	2	5	2	5	2	4	2	4	2	5	2	5	2	5	2	5
O ₂	5.9	1.5	7.2	2.7	7.6	2.3	3.6	0.5	3.7	0.5	4.2	0.4	4.5	1.9	6.4	0.9	7.3	1.2
Ti	0.4	0.7	0.6	0.8	0.8	0.8	0.5	0.6	0.4	0.3	0.9	0.4	0.4	0.2	0.3	0.3	0.3	0.7
O ₂	0.0	0.0	0.0	0.0	0.0	0.0	0.1	0.1	0.1	0.2	0.4	0.0	0.0	0.0	0.0	0.0	0.0	0.0
Al ₂	1.1	5.1	6.1	6.1	6.7	4.6	7.8	3.4	7.8	3.4	6.3	4.6	6.3	4.6	6.3	4.6	6.4	4.6
O ₃	8.7	6.1	7.3	5.7	7.4	4.9	9.2	5.6	9.2	5.6	6.3	7.4	6.4	6.4	6.4	6.4	6.4	6.4
Fe	2.2	4.2	2.4	4.2	2.4	4.1	3.9	3.8	3.3	8.2	3.6	2.4	2.7	4.2	2.5	7.2	2.4	4.2
O	1.7	0.2	2.2	2.3	6.3	7.4	3.7	4.3	9.0	7.1	5.8	5.8	5.1	3.0	0.0	0.8	0.6	8.8
Mn	0.4	0.0	0.4	0.0	0.3	0.7	0.0	0.2	0.0	0.4	0.0	0.2	0.0	0.5	0.0	0.3	0.0	0.4
O	2.2	4.2	2.4	4.7	3.9	9.9	9.9	9.5	6.8	8.5	5.6	5.6	6.6	6.8	8.4	8.4	8.4	8.4
Mg	1.5	3.4	1.8	3.8	1.8	4.1	0.8	2.5	1.9	7.2	2.1	3.1	3.2	3.1	3.8	2.4	3.7	3.1
O	9.1	9.8	5.2	8.5	9.4	2.5	4.5	1.1	1.1	7.9	7.9	9.2	2.2	2.7	2.7	4.1	7.1	1.1
Ca	0.1	0.2	0.1	0.1	0.0	0.0	0.0	0.2	0.1	2.1	0.1	0.1	0.1	0.1	0.1	0.1	0.1	0.0
O	5.7	1.8	3.8	3.8	8.0	6.8	6.5	6.0	3.1	3.1	3.3	3.3	3.3	3.3	3.3	3.3	3.3	3.3
Na	0.0	0.0	0.0	0.0	0.0	0.0	0.0	0.0	0.0	0.0	0.0	0.0	0.0	0.0	0.0	0.0	0.0	0.0
O	4.4	4.4	5.3	5.3	5.2	5.6	6.6	6.2	5.2	5.2	2.5	2.2	2.2	2.2	2.2	2.2	2.2	2.2
K ₂	0.0	0.0	0.8	0.5	0.4	0.0	0.3	0.3	0.1	0.8	0.8	0.8	0.8	0.8	0.8	0.8	0.8	0.8
O	5.8	8.8	3.6	6.4	4.9	9.0	0.1	1.5	0.8	8.8	8.8	8.8	9.1	8.9	8.6	8.6	7.7	8.7
tot.	8.3	9.6	8.9	8.9	8.9	8.9	7.9	7.9	8.9	8.9	8.9	8.9	8.9	8.9	8.9	8.9	8.9	8.9
	1.4	1.9	8.4	8.4	1.3	1.3	0.1	0.1	9.4	9.4	1.0	1.0	4.9	4.9	5.2	5.2	2.2	2.2
	5.6	5.4	7.7	7.1	9.0	9.0	6.3	6.3	6.8	6.8	2.5	2.5	5.0	5.0	1.9	1.9	9.9	9.9
Cations																		
Si	2.8	3.4	2.8	3.5	2.9	3.4	2.6	2.9	2.8	3.5	2.8	3.5	2.8	3.5	2.8	3.5	2.8	3.5
Ti	4.4	2.8	1.1	1.1	3.3	0.4	0.8	0.0	0.0	0.0	0.0	0.0	0.2	0.2	2.8	2.8	4.4	4.4
Al	2.4	2.1	2.0	2.0	2.9	1.6	2.8	3.1	2.8	2.8	1.2	1.2	4.8	2.9	2.9	2.9	1.9	1.9
Fe ₂₊	1.9	0.2	1.9	0.3	2.9	2.9	5.3	3.5	3.5	1.3	0.3	0.7	2.6	2.6	2.6	2.6	2.5	2.5
	9.2	7.4	4.9	4.9	4.9	4.8	5.9	5.9	1.5	8.8	0.0	0.0	5.0	5.0	0.9	0.9	2.2	2.2

Mn	0.0	0.0	0.0	0.0	0.0	0.0	0.0	0.0	0.0	0.0	0.0	0.0	0.0	0.0	0.0	0.0	0.0	0.0
	0	-	0	-	0	-	0	0	0	-	0	0	0	-	0	-	0	-
	4		4		3		8	1	3		5	1	3		5		4	
Mg	2.5	0.3	2.9	0.3	2.8	0.4	1.7	0.2	0.9	0.2	1.2	0.2	0.3	0.1	2.3	0.3	0.0	0.3
	9	5	4	8	4	2	2	9	7	0	5	5	4	7	1	9	6	8
Ca	0.0	-	0.0	-	0.0	0.0	0.0	-	0.0	-	0.0	0.0	-	0.0	-	0.0	-	-
	0		0		0		0		0		0		0		0		0	
	3		2		2		1		1		4		1		2		1	
Na	-	-	0.0	0.0	0.0	0.0	-	0.0	0.0	0.0	0.0	0.0	-	-	-	-	-	-
			1	1	1	1		2	1	1	1	6						
K	0.0	0.8	0.7	0.2	0.8	0.2	0.8	0.9	0.7	0.6	0.6	0.7	0.6	0.7	0.7	0.7	0.7	0.7
	1	8	1	2	1	2	1	8	5	3	7	6	9	6	2	7	2	
su	1	1	1	1	1	1	1	1	1	1	1	1	1	1	1	1	1	1
m	4	1	4	1	4	1	4	1	4	1	4	1	4	1	4	1	4	1
ox																		

Sampl e	CPU (CM22B)						PPU (CM21)						GHU (CMD50D)					
	S1 (P- peak)		S1 (T- peak)		S2		S1 (P- peak)		S1 (T- peak)		S2		S1 (P- peak)		S1 (T- peak)		S2	
Domai n	Chl	Phg	Chl	Phg	Chl	Phg	Chl	Phg	Chl	Phg	Chl	Phg	Chl	Phg	Chl	Phg	Chl	Phg
Analys e	757	269	856	55	26	136	31	18	18	13	12	5	2414	1112	48	124	43	322
Wt%																		
SiO ₂	25.7	50.8	27.2	52.9	28.1	45.3	28.2	48.4	25.5	50.2	30.6	55.2	28.65	49.57	28.1	50.5	28.2	50.0
	7	1	2	2	4	6	7	0	8	2	7	7	9	8	1	8		
TiO ₂	0.03	0.27	0.03	0.18	0.03	0.23	0.02	0.11	0.03	0.12	0.03	0.21	0.22	0.04	0.03	0.06	0.04	0.04
Al ₂ O ₃	19.6	20.8	22.3	28.7	19.5	22.0	22.6	30.5	20.9	29.7	23.6	28.3	22.94	28.25	22.1	29.1	19.0	29.0
	8	6	5	7	1	6	1	6	8	7	7	6	5	8	8	3		
FeO	24.4	4.30	23.5	3.48	24.8	4.19	22.5	3.31	26.9	3.06	19.8	3.48	22.10	4.26	21.7	4.00	22.5	3.61
	7		8		5		4		1		7				0		1	
MnO	0.42	0.02	0.36	0.03	0.36	0.04	0.04	2.29	0.03	2.27	0.03	0.03	0.58	0.04	0.63	0.05	0.60	0.03
MgO	14.9	3.17	13.2	3.65	15.1	2.69	13.9	0.03	13.3	0.03	13.1	3.62	18.03	3.19	17.7	2.83	18.9	2.67
	4		1		5		9		6		9				6		2	
CaO	0.01	0.04	0.01	0.01	0.01	0.03	0.04	0.01	0.04	0.01	0.03	0.02	0.04	0.05	0.05	0.07	0.09	0.05
Na ₂ O	0.02	0.17	0.02	0.03	0.02	0.07	0.05	0.14	0.05	0.15	0.05	0.04	0.01	0.11	0.03	0.11	0.02	0.12
K ₂ O	0.05	7.13	0.02	8.21	0.02	7.90	0.68	8.98	0.06	9.01	1.12	8.29	0.01	9.85	0.01	9.87	0.02	10.2
																		8
tot.	85.5	86.7	86.8	97.2	88.0	82.5	88.2	93.8	87.0	94.6	88.6	99.3	92.58	95.36	90.5	96.7	89.4	95.9
	7	7		8	9	7	4	3	4	4	6	2			5	5	9	1
Cations																		
Si	2.97	3.86	3.04	3.62	3.13	3.69	3.10	3.48	2.91	3.56	3.29	3.69	3.02	3.54	3.04	3.54	3.1	3.55
Ti	-	0.02	-	0.01	-	0.02	-	0.01	-	0.01	-	0.01	0.02	-	-	-	-	-
Al	2.29	1.59	2.50	1.97	2.17	1.79	2.48	2.20	2.39	2.11	2.54	1.89	2.41	2.01	2.39	2.04	2.10	2.06
Fe ²⁺	2.83	0.33	2.64	0.24	2.76	0.34	2.47	0.24	3.06	0.22	2.13	0.23	2.33	0.3	2.34	0.28	2.48	0.26
Mn	0.05	-	0.04	-	0.04	-	-	0.16	-	0.16	-	-	0.06	-	0.07	-	0.07	-
Mg	1.72	0.24	1.48	0.25	1.68	0.22	1.54	-	1.52	-	1.41	0.24	1.90	0.23	1.92	0.20	2.08	0.19
Ca	-	-	-	-	-	-	0.01	0.01	0.01	0.01	0.01	-	-	-	0.01	-	0.01	-
Na	-	0.01	-	-	-	-	0.07	0.65	0.01	0.64	0.12	0.55	-	0.01	-	0.01	-	-
K	0.01	0.54	-	0.56	-	0.64	3.10	3.48	2.91	3.56	3.29	3.69	-	0.7	-	0.69	-	0.73
sum ox	14	11	14	11	14	11	14	11	14	11	14	11	14	11	14	11	14	11

- : below deection limit

Table 6. P-T conditions of the studied samples obtained with the chlorite-phengite-quartz-water multiequilibrium approach (Vidal and Parra 2000), and classical thermobarometry. (From Di Rosa et al. 2018b).

	S1~ P-peak (Vidal and Parra 2000)	S1~T -peak (Vidal and Parra 2000)	P max (GPa) (Massonne and Schreyer 1987)	T max (°C)	S2 (Vidal and Parra 2000)
SCU	1.34-0.9 GPa, 277-280°C	0.83-0.51 GPa, 435-388°C	0.81	401 (Lanari et al., 2014)	0.31-0.26 GPa, 312- 278°C
PEU	1.35-0.8 GPa, 280-360°C	0.75-0.45 GPa, 440-435°C	1.25	452 (Cathelineau, 1988)	0.35-0.23 GPa, 351- 237°C
CAU	1.04-0.82 GPa, 176- 262°C	0.76-0.63 GPa, 393-455°C	1.08	470 (Hillier and Velde, 1991)	0.45-0.33 GPa, 310- 247°C
PPU	1.04-0.75 GPa, 200- 240°C	0.80-0.51 GPa, 340-400°C	1.19	344 (Lanari et al., 2014)	0.38-0.23 GPa, 300- 240°C
CPU	1.22-1.10 GPa, 250- 330°C	0.82-0.56 GPa, 320-350°C	1.26	350 (Lanari et al., 2014)	0.36-0.25 GPa, 310- 230°C
GHU	0.81-0.72 GPa, 245- 250°C	0.68-0.39 GPa, 263-243°C	0.92	272 (Lanari et al., 2014)	0.37-0.13 GPa, 228- 209°C

Table 7. Representative electron microprobe analysis of the Chl-Phg pairs of the metapelites of Razzo Bianco.

Sample Domain Mineral	CMD98			
	S1		S2	
	<i>chl4</i>	<i>Phg3</i>	<i>Chl1</i>	<i>Phg1</i>
Wt%				
SiO ₂	26.96	49.80	31.12	49.62
TiO ₂	0.04	0.11	0.05	0.12
Al ₂ O ₃	20.07	27.79	22.80	28.94
FeO	23.86	2.23	22.77	2.62
MnO	0.02	0.02	0.03	0.01
MgO	18.05	3.09	25.86	3.79
CaO	0.10	0.09	0.24	0.08
Na ₂ O	0.03	0.12	0.04	0.01
K ₂ O	0.95	10.29	2.10	7.82
Total	90.08	93.54	95.01	93.01
Cations				
Si	2.75	3.378	2.96	3.38
Ti	-	0.01	-	0.01
Al	2.42	2.22	2.56	2.96
Fe ²⁺	2.04	0.13	1.81	0.15
Mn	-	-	-	-
Mg	2.75	0.31	2.25	0.38
Ca	0.01	0.01	0.02	0.01
Na	0.01	0.01	0.01	-
K	0.124	0.89	0.13	0.67
Sum OX	14	11	14	11

- : below detection limits.

Table 8. Representative electron microprobe analysis of the Chl-Phg pairs of the metapelites of the Schistes Lustrés Complex in the Corte area.

Sample Domain in Analyse	Schistes Lustrés Complex - Botro (CMD118)						Schistes Lustrés Complex - Buttinacce (CMD121B)					
	S1		S2		Late S2		S1		S2		Late S2	
	Chl 27	Phg 20	Chl 65	Phg 10	Chl 64	Phg 23	Chl 38	Phg 2	Chl 8	Phg 6	Chl 12	Phg 1
Wt%												
SiO ₂	27.9 5	50.0 7	28.0 5	44.0 2	28.6 5	46.8 7	25.9 1	48. 29	26. 20	48. 08	26.4 1	48. 09
TiO ₂	0.02	0.09	0.02	0.08	0.02	0.09	0.02	0.1 4	0.0 1	0.1 4	0.02	0.1 6
Al ₂ O ₃	18.8 0	29.9 2	23.9 5	26.7 0	22.8 7	27.7 5	19.5 7	31. 32	19. 38	28. 65	19.4 5	29. 89
FeO	25.9 9	2.10	25.9 1	6.64	25.2 2	5.60	25.2 8	2.4 0	25. 71	2.9 6	25.6 4	2.9 5
MnO	0.15	0.02	0.09	0.02	0.09	0.01	0.70	0.0 4	0.7 2	0.0 6	0.70	0.0 4
MgO	16.1 3	2.91	11.1 1	4.43	11.4 9	4.00	15.0 5	2.7 1	13. 71	2.9 7	13.8 3	2.9 2
CaO	0.03	0.02	0.03	0.02	0.03	0.02	0.07	0.0 5	0.0 9	0.0 5	0.09	0.0 7
Na ₂ O	0.03	0.09	0.03	0.09	0.04	0.11	0.04	0.1 3	0.0 8	0.1 2	0.07	0.1 4
K ₂ O	0.06	10.3 1	0.22	7.90	0.21	8.24	0.33	9.6 6	0.2 7	9.7 3	0.27	9.5 9
tot.	89.1 6	95.5 4	89.4 1	89.3 4	88.6 2	92.6 9	86.9 9	94. 74	86. 17	92. 76	86.4 8	93. 85
Cations												
Si	2.90	3.32	2.87	3.18	2.94	3.24	2.77	3.2 3	2.8 3	3.3 0	2.84	3.2 7
Ti	-	-	-	-	-	0.01	-	0.0 1	-	0.0 1	-	0.0 1
Al	2.30	2.34	2.89	2.27	2.77	2.26	2.47	2.4 7	2.4 7	2.3 2	2.46	2.3 9
Fe ²⁺	2.25	0.12	2.22	0.40	2.17	0.32	2.26	0.1 3	2.3 2	0.1 7	2.31	0.1 7
Mn	0.01	-	0.01	-	0.01	-	0.06	-	0.0 7	-	0.06	-
Mg	2.49	0.29	1.69	0.48	1.76	0.41	2.40	0.2 7	2.2 1	0.3 0	2.22	0.3 0
Ca	-	-	-	-	-	-	0.01	-	0.0 1	-	0.01	0.0 1
Na	0.01	0.01	0.01	0.01	0.01	0.02	0.01	0.0 2	0.0 2	0.0 2	0.02	0.0 2
K	0.01	0.87	0.03	0.67	0.03	0.73	0.05	0.8 2	0.0 4	0.8 5	0.04	0.8 3
sum ox	14	11	14	11	14	11	14	11	14	11	14	11

- : below detection limits.

9.2 P estimates based on sodic amphibole

The geobarometer of Brown (1977) is based on the Na content in the M4 site of amphibole, that it is strongly dependent by the P conditions (Brown 1977; Spear 1993; Otsuki and Banno 1990). The reaction:



correlates Na-amphiboles of the blueschist facies with Ca- amphiboles of the greenschist facies (Brown 1977) and establishes that the transition between these two metamorphic facies is marked by an increase in Ca (i.e. actinolite) and Al^{4+} and a decrease in Na content (i.e. glaucophane or Mg-riebeckite). Otherwise, increasing T the activation of Edenite and Tschermakite substitutions leads the increasing of Al^{IV} in actinolites. Thus, the compositions of the amphiboles studied (Tabs 9-11, calculated following the recommendations of Leake et al. 1997) have been plotted in an $\text{Al}^{\text{IV}}/\text{Na}$ content in M4 site diagram, where the most studied orogenic belts are also plotted (§ Cap 5.3.2, Fig 43).

Table 9. EPMA analyses of representative hornblende from sample CMD69

	A20	A35	A36	A51	A72	A118
Wt%						
SiO ₂	49.766	48.199	47.919	47.469	44.311	45.350
TiO ₂	0.089	0.519	1.770	0.243	0.391	0.532
Al ₂ O ₃	4.672	8.448	7.416	5.534	12.103	10.558
FeO	19.098	19.453	19.756	18.888	20.596	19.391
MnO	0.108	0.250	0.315	0.357	0.243	0.222
MgO	5.042	8.814	8.539	9.538	7.422	8.746
CaO	5.909	11.139	10.243	12.395	11.548	11.669
Na ₂ O	1.257	1.034	1.366	1.225	1.082	1.118
K ₂ O	1.194	0.495	0.441	0.322	0.773	0.629
Cr ₂ O ₃	0.002	0.000	0.014	0.001	0.016	0.003
Total	87.137	98.352	97.781	95.963	98.483	98.217
Cations						
<i>sum T</i>						
Si	8.435	7.075	7.096	7.169	6.533	6.666
Al ⁴⁺	0.000	0.925	0.904	0.831	1.467	1.334
<i>sum C</i>						
Al ⁶⁺	1.508	0.412	0.350	0.265	0.183	0.182
Fe ³⁺	0.000	0.499	0.472	0.668	0.879	0.843
Ti	0.011	0.057	0.197	0.028	0.043	0.059
Cr	0.000	0.000	0.001	0.000	0.002	0.000
Mg	1.274	1.929	1.885	2.148	1.631	1.917
Fe ²⁺	3.737	2.053	2.128	1.684	2.143	1.891
Mn	0.008	0.015	0.020	0.022	0.015	0.014
<i>sum B</i>						
Mg	0.000	0.000	0.000	0.000	0.000	0.000
Mn	0.008	0.017	0.020	0.023	0.015	0.014
Fe ²⁺	0.368	0.000	0.000	0.033	0.000	0.000
Ca	1.073	1.752	1.625	2.006	1.824	1.838
Na	0.205	0.146	0.195	0.177	0.153	0.158
<i>sum A</i>						

Na	0.208	0.148	0.197	0.182	0.256	0.161
K	0.130	0.047	0.043	0.031	0.073	0.060
Tot.	15.133	14.910	14.980	15.268	14.636	14.785

Table 10. EPMA analyses of representative Na-amphibole from sample CMD69.

	A10	A28	A52	A55	A66	A67
Wt%						
SiO ₂	53.391	53.488	51.997	53.936	53.663	53.578
TiO ₂	0.040	0.052	0.092	0.031	0.013	0.041
Al ₂ O ₃	2.533	2.437	3.779	2.308	2.115	2.410
FeO	27.397	27.092	28.198	27.797	27.181	27.579
MnO	0.247	0.211	0.499	0.253	0.147	0.156
MgO	5.381	5.499	4.347	5.576	5.770	5.217
CaO	1.398	1.484	2.656	1.408	1.295	0.775
Na ₂ O	6.745	6.651	6.032	6.550	6.517	6.987
K ₂ O	0.141	0.116	0.363	0.101	0.099	0.101
Cr ₂ O ₃	0.029	0.013	0.022	0.004	0.005	0.011
Total	97.299	97.045	97.963	96.805	96.853	94.076
Cations						
<i>sum T</i>						
Si	7.931	7.966	7.719	7.962	8.007	7.996
Al ⁴⁺	0.069	0.034	0.281	0.038	0.000	0.004
<i>sum C</i>						
Al ⁶⁺	0.760	0.787	0.657	0.770	0.801	0.815
Fe ³⁺	1.252	1.166	1.392	1.216	1.144	1.190
Ti	0.004	0.006	0.010	0.003	0.001	0.005
Cr	0.003	0.002	0.003	0.000	0.001	0.001
Mg	1.192	1.221	0.961	1.227	1.283	1.161
Fe ²⁺	1.696	1.734	1.852	1.724	1.719	1.755
Mn	0.015	0.013	0.031	0.016	0.009	0.010
<i>sum B</i>						
Mg	0.000	0.000	0.000	0.000	0.000	0.000
Mn	0.016	0.013	0.032	0.016	0.009	0.010
Fe ²⁺	0.455	0.474	0.259	0.492	0.528	0.497
Ca	0.222	0.237	0.422	0.222	0.210	0.124
Na	0.959	0.948	0.860	0.927	0.931	0.997
<i>sum A</i>						
Na	0.984	0.973	0.876	0.948	0.954	1.025
K	0.014	0.011	0.034	0.010	0.010	0.010
Tot.	15.572	15.584	15.387	15.571	15.598	15.598

	A85	A86	A87	A88	A89	A90
Wt%						
SiO ₂	50.924	53.763	53.008	53.050	52.940	52.127
TiO ₂	0.012	0.040	0.030	0.000	0.014	0.053
Al ₂ O ₃	3.642	2.141	2.521	2.622	1.963	3.590
FeO	28.221	28.395	28.843	28.847	29.825	27.991
MnO	0.174	0.105	0.177	0.246	0.124	0.217
MgO	4.074	5.222	4.480	4.346	4.467	4.348
CaO	1.167	1.261	0.820	0.452	1.024	1.018
Na ₂ O	5.635	7.305	7.295	7.335	7.038	6.576
K ₂ O	0.219	0.144	0.090	0.068	0.	0.495
Cr ₂ O ₃	0.008	0.011	0.000	0.008	0.002	0.000
Total	98.387	97.263	96.975	97.478	96.680	96.680
Cations						
<i>sum T</i>						
Si	7.860	7.920	7.913	7.938	7.917	7.809
Al ⁴⁺	0.140	0.080	0.087	0.062	0.083	0.191

TECTONO-METAMORPHIC HISTORY OF CONTINENTAL UNITS IN ALPINE CORSICA

	<i>sum C</i>					
Al ⁶⁺	0.800	0.713	0.741	0.776	0.697	0.732
Fe ³⁺	1.124	1.355	1.374	1.349	1.421	1.446
Ti	0.001	0.004	0.003	0.000	0.002	0.006
Cr	0.001	0.001	0.000	0.001	0.000	0.000
Mg	0.937	1.147	0.997	0.969	0.996	0.971
Fe ²⁺	2.043	1.640	1.763	1.799	1.784	1.738
Mn	0.011	0.006	0.011	0.015	0.008	0.014
	<i>sum B</i>					
Mg	0.000	0.000	0.000	0.000	0.000	0.000
Mn	0.011	0.007	0.011	0.016	0.008	0.014
Fe ²⁺	0.355	0.503	0.463	0.462	0.526	0.324
Ca	0.193	0.199	0.131	0.073	0.164	0.163
Na	0.840	1.025	1.039	1.048	1.005	0.944
	<i>sum A</i>					
Na	0.847	1.062	1.072	1.080	1.036	0.966
K	0.022	0.014	0.009	0.007	0.008	0.074
Tot.	15.306	15.676	15.616	15.595	15.653	15.341

	A91	A92	A96	A97	A98	A101	A111	A112
Wt%								
SiO ₂	52.340	53.502	54.034	54.554	52.748	54.110	53.487	
TiO ₂	0.030	0.013	0.038	0.047	0.033	0.045	0.054	
Al ₂ O ₃	1.896	2.277	3.209	2.984	2.814	3.053	2.176	
FeO	27.899	28.428	27.060	26.570	28.332	27.009	28.493	
MnO	0.116	0.248	0.251	0.121	0.137	0.298	0.167	
MgO	5.616	4.846	5.129	5.067	5.223	4.934	4.986	
CaO	1.670	0.742	0.956	1.676	1.207	1.108	0.994	
Na ₂ O	6.396	7.321	7.249	5.736	6.702	6.836	6.910	
K ₂ O	0.322	0.132	0.138	0.164	0.406	0.118	0.123	
Cr ₂ O ₃	0.001	0.006	0.000	0.000	0.000	0.011	0.007	
Total	96.195	97.514	98.064	96.919	97.602	97.523	97.396	
Cations								
	<i>sum T</i>							
Si	7.888	7.956	7.942	8.174	7.807	8.023	7.968	
Al ⁴⁺	0.112	0.044	0.058	0.000	0.193	0.000	0.032	
	<i>sum C</i>							
Al ⁶⁺	0.664	0.762	0.826	1.045	0.660	0.896	0.767	
Fe ³⁺	1.411	1.316	1.194	0.515	1.549	0.919	1.262	
Ti	0.003	0.001	0.004	0.005	0.004	0.005	0.006	
Cr	0.002	0.001	0.000	0.000	0.000	0.001	0.001	
Mg	1.260	1.074	1.124	1.132	1.152	1.091	1.107	
Fe ²⁺	1.585	1.722	1.735	2.325	1.546	2.005	1.777	
Mn	0.007	0.015	0.015	0.008	0.008	0.018	0.010	
	<i>sum B</i>							
Mg	0.000	0.000	0.000	0.000	0.000	0.000	0.000	
Mn	0.007	0.016	0.016	0.08	0.009	0.019	0.011	
Fe ²⁺	0.516	0.497	0.397	0.489	0.413	0.425	0.511	
Ca	0.269	0.118	0.151	0.269	0.191	0.176	0.159	
Na	0.922	1.038	1.018	0.825	0.951	1.040	0.984	
	<i>sum A</i>							
Na	0.945	1.073	1.048	0.841	0.972	0.996	1.012	
K	0.015	0.013	0.013	0.016	0.039	0.011	0.011	
Tot.	15.607	15.647	15.503	15.478	15.493	15.603	15.618	

Table 11. EPMA analyses of representative Ca-amphibole from sample CMD69.

	A4	A7	A19	A21	A23	A29	A30	A31
Wt%								
SiO ₂	52.223	48.199	48.680	49.489	50.601	52.406	44.880	41.032
TiO ₂	0.053	7.762	0.038	0.299	0.305	0.091	0.450	0.279
Al ₂ O ₃	6.749	2.016	4.417	5.210	5.154	3.526	9.340	5.932
FeO	23.662	20.344	21.817	25.673	25.806	24.726	21.550	19.679
MnO	0.196	0.124	0.130	0.409	0.427	0.194	0.284	0.561
MgO	5.163	5.353	8.347	5.576	5.311	7.294	7.198	5.747
CaO	3.318	8.126	4.538	5.578	4.407	4.267	9.978	14.253
Na ₂ O	5.567	4.379	4.100	4.404	5.047	4.812	1.832	2.986
K ₂ O	1.042	0.148	1.274	0.355	0.311	0.323	0.637	0.340
Cr ₂ O ₃	0.000	0.003	0.002	0.014	0.009	0.010	0.017	0.005
Total	97.972	96.450	93.342	97.006	97.378	97.650	96.164	90.813
Cations								
	<i>sum T</i>							
Si	7.652	7.356	7.431	7.426	7.533	7.697	6.785	6.554
Al ⁴⁺	0.348	0.069	0.569	0.574	0.467	0.303	1.215	1.446
	<i>sum C</i>							
Al ^{B+}	0.838	0.146	0.435	0.493	0.591	0.610	0.218	0.000
Fe ³⁺	0.954	0.282	1.523	1.204	1.203	1.248	0.999	2.280
Ti	0.006	0.891	0.004	0.033	0.034	0.010	0.051	0.033
Cr	0.000	0.000	0.000	0.002	0.001	0.001	0.002	0.001
Mg	1.128	1.218	1.900	1.247	1.179	1.597	1.622	1.368
Fe ²⁺	1.930	2.585	1.040	1.901	1.884	1.481	1.991	0.890
Mn	0.012	0.008	0.008	0.026	0.027	0.012	0.180	0.037
	<i>sum B</i>							
Mg	0.000	0.000	0.000	0.000	0.000	0.000	0.000	0.000
Mn	0.012	0.008	0.008	0.026	0.027	0.012	0.018	0.038
Fe ²⁺	0.015	0.000	0.223	0.117	0.126	0.308	0.000	0.000
Ca	0.521	1.329	0.742	0.897	0.703	0.672	1.616	2.439
Na	0.782	0.644	0.601	0.635	0.722	0.682	0.266	0.456
	<i>sum A</i>							
Na	0.800	0.652	0.612	0.647	0.735	0.689	0.271	0.469
K	0.098	0.014	0.125	0.034	0.030	0.030	0.062	0.035
Tot.	15.096	15.506	15.222	15.262	15.261	15.352	14.870	15.221

	A34	A41	A42	A44	A49	A50	A56	A57
Wt%								
SiO ₂	50.813	50.483	59.725	50.458	52.274	47.885	54.634	53.327
TiO ₂	0.248	0.199	0.118	0.144	0.049	0.556	0.050	0.033
Al ₂ O ₃	4.877	4.802	3.196	4.424	3.003	7.567	2.673	2.411
FeO	26.792	26.092	18.178	24.262	24.536	21.097	24.133	24.217
MnO	0.478	0.386	0.197	0.350	0.207	0.284	0.233	0.236
MgO	4.996	5.462	5.892	7.206	7.170	8.096	7.570	7.761
CaO	4.183	4.449	4.335	6.754	3.333	9.642	3.963	4.528
Na ₂ O	4.916	4.820	3.092	3.688	5.443	2.404	4.874	4.894
K ₂ O	0.266	0.257	0.238	0.256	0.249	0.509	0.197	0.189
Cr ₂ O ₃	0.005	0.010	0.009	0.008	0.000	0.011	0.004	0.029
Total	97.574	97.319	94.980	97.550	96.263	98.061	98.331	97.626
Cations								
	<i>sum T</i>							
Si	7.568	7.573	8.00	7.491	7.765	7.066	7.972	7.837
Al ⁴⁺	0.432	0.427	0.000	0.509	0.235	0.933	0.028	0.163
	<i>sum C</i>							
Al ^{B+}	0.603	0.602	1.937	0.485	0.636	0.327	0.810	0.655
Fe ³⁺	1.230	1.201	0.000	1.088	1.344	0.854	0.815	1.105
Ti	0.028	0.022	0.013	0.016	0.005	0.063	0.006	0.004
Cr	0.001	0.001	0.001	0.001	0.000	0.001	0.000	0.003
Mg	1.109	1.213	1.330	1.595	1.588	1.781	1.227	1.700

Fe ²⁺	1.951	1.880	3.483	1.719	1.352	1.844	1.699	1.458
Mn	0.230	0.025	0.013	0.022	0.013	0.018	0.014	0.015
<i>sum B</i>								
Mg	0.000	0.000	0.000	0.000	0.000	0.000	0.000	0.000
Mn	0.030	0.025	0.013	0.022	0.013	0.018	0.014	0.015
Fe ²⁺	0.156	0.169	0.419	0.205	0.352	0.000	0.430	0.413
Ca	0.667	0.710	0.703	1.074	0.530	1.524	0.619	0.713
Na	0.705	0.691	0.456	0.527	0,778	0.340	0.685	0.692
<i>sum A</i>								
Na	0.714	0.701	0.452	0.535	0.789	0.348	0.694	0.702
K	0.025	0.025	0.023	0.024	0.024	0.048	0.018	0.018
Tot.	15.250	15.264	15.241	15.313	15.424	15.072	15.453	15.493

	A69	A71	A77	A78	A79	A80	A105	A117
Wt%								
SiO ₂	50.756	51.701	36.278	38.935	47.191	51.542	57.247	52.464
TiO ₂	0.121	0.036	0.049	0.015	0.331	0.105	0.030	0.165
Al ₂ O ₃	5.844	2.500	4.300	2.103	8.521	4.045	1.851	2.970
FeO	26.325	21.884	16.932	20.589	24.634	25.826	19.280	25.372
MnO	0.423	0.133	0.267	0.509	0.359	0.279	0.140	0.167
MgO	4.737	9.847	2.837	2.750	5.267	5.719	9.158	7.380
CaO	3.812	7.501	16.432	16.432	7.023	3.769	7.510	3.753
Na ₂ O	5.318	2.427	4.113	4.709	3.842	5.201	2.323	5.414
K ₂ O	0.395	0.316	0.565	0.045	0.589	0.277	0.145	0.201
Cr ₂ O ₃	0.000	0.013	0.009	0.000	0.000	0.006	0.000	0.000
Total	97.731	96.356	81.781	85.820	97.756	96.768	97.685	97.887
Cations								
<i>sum T</i>								
Si	7.525	7.683	6.296	6.569	7.965	7.692	8.419	7.682
Al ⁴⁺	0.475	0.317	1.704	1.431	0.965	0.308	0.000	0.318
<i>sum C</i>								
Al ⁶⁺	0.641	0.512	0.000	0.000	0.384	0.655	1.189	0.546
Fe ³⁺	1.240	0.951	4.067	3.727	1.180	1.222	0.000	1.435
Ti	0.014	0.004	0.006	0.002	0.037	0.012	0.003	0.018
Cr	0.000	0.001	0.001	0.000	0.000	0.001	0.000	0.000
Mg	1.047	2.183	0.734	0.692	1.170	1.272	2.008	1.611
Fe ²⁺	1.944	1.368	0.000	0.000	2.068	1.754	2.358	1.315
Mn	0.026	0.008	0.020	0.036	0.022	0.018	0.009	0.010
<i>sum B</i>								
Mg	0.000	0.000	0.000	0.000	0.000	0.000	0.000	0.000
Mn	0.027	0.008	0.020	0.036	0.023	0.018	0.009	0.010
Fe ²⁺	0.080	0.401	0.000	0.000	0.000	0.247	0.514	0.356
Ca	0.606	1.194	3.055	2.924	1.122	0.603	1.183	0.589
Na	0.759	0.350	0.688	0.764	0.548	0.747	0.331	0.763
<i>sum A</i>								
Na	0.771	0.350	0.696	0.777	0.563	0.758	0.331	0.774
K	0.038	0.030	0.063	0.005	0.057	0.027	0.014	0.019
Tot.	15.191	15.359	15.083	15.526	14.997	15.333	15.449	15.447

9.3 Calcite twins

Mechanical twinning is the dominant crystal-plastic deformation mechanism in rocks deformed under the low-grade metamorphic conditions, and it is used to estimate the T under which calcite has been deformed (e.g. Ferrill et al. 2004). Morphology and thickness of calcite twins are T dependent; on the base of the thickness they could be divided in thin (<1 µm) and thick (>5 µm) twins

(Groshong 1972; 1974; Conel 1962; Ferrill et al. 2004). Basing on the morphology, calcite twins could be classified in type 1 to 4 increasing T (Burkhard 1993):

- Type 1: thin twins;
- Type 2: tabular thick twins;
- Type 3: curved, tapered and lensoid thick twins;
- Type 4: Thick patchy twins modified by dynamic recrystallization.

Following Ferrill et al. (2004), two parameters must be measured on calcite crystals of each sample: the mean twin width and the twin intensity. The mean twin width is determined calculating the average twin width for each twin set, and thus averaging the twin-set averages. The twin intensity (twin planes/mm) for each twin set is calculated dividing the number of twins in a set by the width of the host grain measure perpendicular to the twins. The mean twin intensity is obtained averaging the twin intensities of the sets measured.

From these parameters it is possible to calculate an average shear strain for each sample using the equation proposed by Groshong (1972) and modified by Ferrill et al. (2004):

$$\gamma = T t 2 \tan\left(\frac{\alpha}{2}\right)$$

Where γ is the shear strain, T the twin intensity, t the twin width and α the angle of rotation of the grain edge from the untwinned to the twinned position, that is equal to $38^{\circ}17'$.

9.4 LA-ICP-MS dating

9.4.1 U-Pb zircon dating on separates

Zircons were extracted from five samples of metagranitoids and one sample of epidote-bearing metagabbros (§ Cap 6.2, Tab 12) at the University of Geneva (Switzerland) by standard crushing, gravimetric- and magnetic-separation techniques. Approximately 260 zircon crystals were selected from each hand sample. These crystals were hand-picked under a binocular microscope and mounted in epoxy resin. The mounts were polished to expose the crystal interior domains and imaged by cathodoluminescence using a JEOL JSM-7001F Schottky scanning electron microscope at the University of Geneva.

In-situ zircon U-Pb isotope analysis were performed at the Institute of Earth Sciences of the University of Lausanne (Switzerland) using a Thermo ELEMENT XR sector field ICP-MS coupled with a Resonetics Resolution M-50 193 nm Excimer laser ablation system. Data were acquired in time-resolved, peak-jumping, pulse-counting mode utilizing a routine where 30 seconds of background measurement were followed by 30 seconds of sample ablation. Laser induced fractionation of Pb and U was minimized during analysis by employing

a soft ablation regime using a repetition rate of 5 Hz and an energy density of ~ 3 J/cm² per pulse. Laser spot sizes were 30 μ m. The measurement protocol and the parameters of mass spectrometer optimization follow Ulianov et al. (2012). Laser-induced elemental fractionation and instrumental mass discrimination were corrected by normalization to the reference zircon GJ-1. To test the accuracy and external reproducibility of the obtained age data, the Plešovice reference zircon (Sláma et al. 2008) was measured after every ~ 8 unknowns (Tab. S5). The Plešovice secondary standard gave a weighted mean age of 337.5 \pm 0.6 Ma (2SD, n = 21; MSWD = 0.66). The calculated age is consistent, within uncertainty, with the ID-TIMS value reported by Sláma et al. (2008). All raw data from Lausanne was processed using the LAMTRACE software package (Jackson 2008) and no common Pb correction was applied due to the presence of trace ²⁰⁴Hg in the Ar gas. Common Pb was dealt with by monitoring ²⁰¹Hg, ²⁰⁴(Hg+Pb) as well as (²⁰⁴Pb+²⁰⁴Hg)/²⁰⁶Pb ratios. The homogeneity of the ablated material was confirmed by monitoring the ²⁰⁶Pb/²³⁸U and ²⁰⁷Pb/²³⁵U vs. time spectra, and fluctuations in these ratios were interpreted to represent mixing between different age domains within the crystals. Spectra with mixed domains were subsequently discarded. Only the analysis that have a concordance value between 90 and 110% were considered to calculate the average age of the sample.

Table 12. Results of zircon LA-ICP-MS U-Pb age determination of the samples CMD50E, CMD40(59), CMD37, CMD33(43), CMD57B and CMD57(67). The results related to the secondary standard “Plešovice” are also reported. “ ρ ” indicates the ratio

$(^{206}\text{Pb}/^{238}\text{U}_{(2\text{S.D.})}/^{206}\text{Pb}/^{238}\text{U}) / (^{207}\text{Pb}/^{235}\text{U}_{(2\text{S.D.})}/^{207}\text{Pb}/^{235}\text{U})$. “Conc.” Indicates the ratio $(\text{Age } ^{206}\text{Pb}/^{238}\text{U}) / (\text{Age } ^{207}\text{Pb}/^{206}\text{Pb}) * 100$.

	Isotopic ratios				ρ	Age (Ma)		Apparent ages (Ma)				Conc. (%)
	²⁰⁶ Pb/ ²³⁸ U	2S.D.	²⁰⁷ Pb/ ²³⁵ U	2S.		²⁰⁶ Pb/ ²³⁸ U	S.	²⁰⁷ Pb/ ²³⁵ U	S.	²⁰⁷ Pb/ ²⁰⁶ Pb	S.	
<i>CMD50E</i>												
jn11a0	0,0439	0,0006	0,316	0,02	0,2	276,9	4,3	278,8	16	356	13	77,8
5		94		1	4						6	
jn11a0	0,0436	0,0005	0,314	0,02	0,2	275,4	3,6	277,3	15,	260	12	105,
6		84		1	0				9		4	9
jn11a0	0,0437	0,0004	0,3133	0,01	0,2	275,4	2,9	276,7	9,9	310	82	88,8
7		72		3	6							
jn11a1	0,0434	0,0005	0,3147	0,01	0,2	273,7	3,2	277,8	12,	308	96	88,9
0		12		6	3				4			
jn11a1	0,0437	0,0006	0,3214	0,02	0,2	275,6	4	283	17,	344	12	80,1
1		47		3	1				4		6	
jn11a1	0,0436	0,0007	0,3167	0,02	0,2	275,3	4,4	279,3	16,	374	13	73,6
2		15		1	5				3		0	
jn11a1	0,0442	0,0007	0,319	0,02	0,2	278,5	4,8	281,2	20,	282	17	98,8
3		78		7	1				9		0	
jn11b0	0,0438	0,0006	0,307	0,01	0,2	276,1	3,9	271,9	11,	230	10	120,

5		22		5	9				5		0	0
jn11b0	0,0436	0,0005	0,3207	0,01	0,2	275	3,5	282,5	12	338	94	81,4
6		67		6	7							
jn11b0	0,0436	0,0004	0,3151	0,01	0,2	275,2	3	278,1	11,	300	98	91,7
7		88		5	3				9			
jn11b0	0,0433	0,0005	0,3109	0,01	0,2	273,5	3,5	274,9	13,	278	11	98,4
8		63		7	3				5		4	
jn11b0	0,0439	0,0006	0,31	0,02	0,2	276,8	3,9	274,2	15,	274	12	101,
9		32		0	3				3		6	0
jn11b1	0,0432	0,0008	0,3105	0,02	0,2	272,6	5	274,6	18,	324	14	84,1
0		12		4	4				5		8	
jn11b1	0,0433	0,0006	0,3102	0,02	0,2	273,5	3,8	274,3	16,	276	11	99,1
1		15		1	1				1		6	
jn11b1	0,0433	0,0005	0,323	0,01	0,2	273,1	3,3	284,2	12,	310	11	88,1
2		37		6	5				5		2	
jn11b1	0,0436	0,0006	0,3086	0,02	0,2	275,1	4	273,1	17,	214	13	128,
3		45		3	0				5		6	6
jn11b1	0,0425	0,0006	0,2973	0,01	0,2	268,3	3,7	264,3	13,	214	12	125,
4		04		8	4				7		4	4
jn11g0	0,045	0,0005	0,3334	0,01	0,2	283,6	3,5	292,2	12,	310	10	91,5
8		58		6	5				5		2	
jn11g0	0,0386	0,0014	0,2772	0,04	0,2	244,3	9,2	248,4	31,	334	32	73,1
9		82		0	7				9		0	
jn11gl	0,0437	0,0005	0,3077	0,01	0,2	276	3,6	272,4	12,	222	11	124,
0		77		6	5				7		2	3
jn11gl	0,0443	0,0005	0,3084	0,01	0,2	279,3	3,5	272,9	14,	216	10	129,
1		58		9	1				5		6	3
jn11gl	0,0436	0,0009	0,3083	0,03	0,1	275,4	5,8	272,9	29,	246	22	112,
2		33		8	7				5		4	0
jn11gl	0,0437	0,0004	0,3057	0,01	0,2	276	2,9	270,8	9,1	266	78	103,
3		81		2	9						8	
jn11gl	0,0443	0,0006	0,3219	0,02	0,2	279,2	4	283,4	17,	358	13	78,0
4		56		2	1				1		4	
jn11u0	0,0445	0,0006	0,3157	0,01	0,2	280,9	3,8	278,6	12,	262	10	107,
5		05		6	7				5		6	2
jn11u0	0,0448	0,0008	0,3063	0,02	0,2	282,3	5,6	271,3	22,	220	17	128,
6		96		9	1				2		6	3
jn11u0	0,0438	0,0006	0,3235	0,02	0,2	276,6	3,9	284,6	16,	348	12	79,5
7		39		1	2				3		4	
jn11u1	0,0442	0,0005	0,3129	0,01	0,2	278,6	3,7	276,4	13,	278	11	100,
1		92		8	4				8		8	2
jn11u1	0,0427	0,0005	0,3177	0,02	0,2	269,8	3,7	280,2	15,	346	12	78,0
2		98		0	2				4		2	
jn11u1	0,0439	0,0007	0,3166	0,02	0,2	277,2	4,4	279,3	18,	280	13	99,0
4		11		4	1				6		8	

CMD40(50)

jn11c0	0,0432	0,0005	0,3189	0,01	0,2	272,9	3,5	281	13,	350	11	78,0
7		62		7	4				2		0	
jn11c1	0,0455	0,0004	0,3433	0,00	0,3	287,1	2,5	299,7	6	388	48	74,0
0				8	8							
jn11c1	0,045	0,0003	0,3213	0,00	0,3	283,7	2,3	282,9	6	286	50	99,2
1		69		8	4							
jn11c1	0,0465	0,0004	0,3361	0,00	0,3	292,9	2,5	294,2	6,1	294	50	99,6
2		09		8	7							
jn11c1	0,0446	0,0003	0,324	0,00	0,3	281,1	2,4	285	5,6	326	46	86,2
3		84		7	8							

TECTONO-METAMORPHIC HISTORY OF CONTINENTAL UNITS IN ALPINE CORSICA

jn11d0 5	0,0447 29	0,0004	0,3346	0,00 8	0,3 9	282	2,6	293,1	6,3	378	50	74,6
jn11d0 7	0,0458 03	0,0004	0,3338	0,00 7	0,4 2	288,7	2,5	292,5	5,4	332	44	87,0
jn11d1 0	0,0457 11	0,0004	0,3326	0,00 9	0,3 3	288,2	2,5	291,6	6,9	340	52	84,8
jn11d1 2	0,0465 56	0,0004	0,3485	0,01 1	0,3 1	292,7	2,8	303,6	8,2	380	66	77,0
jn11d1 3	0,0457 2	0,0004	0,3308	0,00 7	0,4 1	288,1	2,6	290,2	5,7	314	50	91,8
jn11d1 4	0,3251 56	0,0030	7,1225	0,24 6	0,2 7	1814,4	14, 9	2126,9	30, 8	2468	18	73,5

CMD37

jn11h0 5	0,0427 58	0,0006	0,3005	0,01 7	0,2 7	269,4	4,1	266,8	13, 5	280	13	96,2 0
jn11h0 6	0,0461 79	0,0004	0,3244	0,01 2	0,2 8	290,5	3	285,3	9,1	274	74	106, 0
jn11h0 7	0,0461 52	0,0004	0,3261	0,01 0	0,3 2	290,3	2,8	286,6	7,7	266	62	109, 1
jn11h0 8	0,0452 97	0,0004	0,341	0,01 4	0,2 6	285,2	3	298	10, 9	398	76	71,7
jn11h0 9	0,0468 34	0,0005	0,3424	0,01 4	0,2 9	294,7	3,3	299	10, 2	362	82	81,4
jn11h1 0	0,0439 0	0,0005	0,3226	0,01 5	0,2 4	276,8	3,1	283,9	11, 7	334	94	82,9
jn11h1 1	0,0451 32	0,0005	0,3299	0,01 3	0,3 1	284,3	3,3	289,5	9,7	326	80	87,2
jn11h1 2	0,042 63	0,0005	0,3006	0,01 5	0,2 6	265,3	3,5	266,9	11, 9	290	10	91,5 8
jn11h1 3	0,0443 7	0,0004	0,3169	0,01 3	0,2 6	279,4	2,9	279,5	9,9	300	84	93,1
jn11h1 4	0,0467 86	0,0004	0,3328	0,01 1	0,3 1	294	3	291,7	8,4	254	64	115, 7
jn11i0 5	0,0438 91	0,0004	0,3122	0,01 4	0,2 5	276,5	3	275,9	10, 7	274	94	100, 9
jn11i0 6	0,0445 01	0,0004	0,3247	0,01 1	0,2 8	280,4	2,5	285,5	8	320	66	87,6
jn11i0 8	0,0459 33	0,0006	0,3259	0,01 6	0,2 9	289,6	3,9	286,4	12	250	10	115, 6 8
jn11i0 9	0,0437 68	0,0005	0,3066	0,01 6	0,2 5	276	3,5	271,5	12, 4	254	10	108, 2 7
jn11i1 0	0,0455 28	0,0005	0,333	0,01 3	0,2 9	287	3,3	291,9	10, 2	336	80	85,4
jn11i1 1	0,0442 69	0,0004	0,3129	0,01 1	0,3 2	278,8	2,9	276,4	8,1	238	72	117, 1
jn11i1 2	0,0446 44	0,0005	0,3202	0,01 5	0,2 7	281,1	3,3	282	11, 3	274	96	102, 6
jn11i1 3	0,0458 95	0,0004	0,3344	0,01 5	0,2 4	288,7	3	292,9	11, 4	310	86	93,1

CMD33(43)

jn11i0 5	0,0458 03	0,0004	0,3302	0,00 8	0,3 8	288,9	2,5	289,7	5,8	284	46	101, 7
jn11i0	0,0421	0,0006	0,3063	0,01	0,3	266	4	271,3	9,9	320	84	83,1

8		4		3	7							
jnl1l1	0,0449	0,0004	0,3258	0,00	0,4	282,9	2,5	286,4	5	316	44	89,5
1		04		7	5							
jnl1l1	0,0458	0,0004	0,3279	0,00	0,3	288,7	2,7	287,9	6,3	262	52	110,2
3		4		8	8							
jnl1lm	0,0442	0,0003	0,3251	0,00	0,4	278,9	2,4	285,8	5,4	344	42	81,1
07		89		7	1							
jnl1lm	0,0449	0,0004	0,3235	0,00	0,3	283,2	2,6	284,6	5,8	300	44	94,4
10		13		8	9							
jnl1lm	0,0452	0,0004	0,3206	0,00	0,3	285,1	2,5	282,3	5,9	266	48	107,2
14		07		8	8							

CMD57B

jnl1r0	0,0447	0,0004	0,3233	0,00	0,3	281,7	2,8	284,4	6,7	322	56	87,5
6		56		9	8							
jnl1r0	0,0446	0,0005	0,3318	0,01	0,3	281	3,3	290,9	10,	320	86	87,8
9		44		3	0				1			
jnl1r1	0,0462	0,0004	0,3375	0,00	0,3	291,4	2,7	295,3	7	336	54	86,7
1		34		9	5							
jnl1r1	0,0459	0,0004	0,3335	0,01	0,3	289,5	2,9	292,2	8,4	346	66	83,7
3		68		1	1							

CMD57B

jnl1s0	jnl1s06	0,0006	0,3419	0,01	0,2	286,7	3,8	298,6	12,	356	10	80,5
6		19		7	7				8		2	
jnl1s1	jnl1s10	0,0004	0,3269	0,00	0,3	282,1	2,7	287,2	6,3	310	54	91,0
0		38		8	9							
jnl1s1	jnl1s11	0,0004	0,3316	0,00	0,4	284,7	2,7	290,8	6,2	354	48	80,4
1		42		8	0							
jnl1s1	jnl1s12	0,0004	0,3367	0,00	0,4	290,3	2,7	294,7	6,1	340	50	85,4
2		43		8	0							

Plešovice

ples-	0.0535	0.0004	0.4025	0.00	0.3	335.9	2.6	343.5	5.8	392	40	85.7
a15		17		8	9							
ples-	0.054	0.0004	0.3954	0.00	0.3	338.8	2.6	338.3	5.8	330	40	102.7
b15		21		8	9							
ples-	0.0538	0.0004	0.3957	0.00	0.3	337.8	2.8	338.5	6.5	334	46	101.1
b16		63		9	8							
ples-	0.054	0.0004	0.4008	0.00	0.4	339	2.7	342.2	5.4	356	38	95.2
c15		32		7	3							
ples-	0.0536	0.0004	0.4008	0.01	0.3	336.9	2.6	342.2	7.1	372	50	90.6
d15		29		0	3							
ples-	0.0536	0.0004	0.4031	0.00	0.3	336.3	2.7	343.9	6.8	378	44	89.0
e16		50		9	6							
ples-	0.0538	0.0004	0.3915	0.00	0.4	337.9	2.9	335.4	6.5	322	46	104.9
f16		84		9	0							
ples-	0.054	0.0004	0.3924	0.00	0.3	339.1	2.8	336.1	6.9	318	50	106.6
h15		54		9	5							
ples-	0.0537	0.0004	0.4098	0.01	0.3	337.1	2.8	348.8	6.9	402	44	83.9
i15		62		0	7							
ples-	0.0537	0.0004	0.3991	0.01	0.3	337.4	2.9	341	7.6	348	50	97.0
i16		73		1	3							
ples-	0.0536	0.0004	0.3847	0.00	0.4	336.9	2.8	330.5	5.4	312	40	108.

m15		61		7	5							0
ples-	0.0539	0.0004	0.4001	0.00	0.4	338.7	2.8	341.7	6.1	356	42	95.1
m16		64		8	1							
ples-	0.0537	0.0004	0.4011	0.00	0.4	337.3	2.9	342.5	5.9	382	38	88.3
n16		72		8	3							
ples-	0.0538	0.0004	0.3964	0.00	0.4	337.6	2.8	339	5.8	348	44	97.0
o16		5		8	2							
ples-	0.0539	0.0004	0.3952	0.00	0.4	338.2	2.7	338.2	5.7	344	38	98.3
p15		41		8	1							
ples-	0.054	0.0004	0.4062	0.00	0.4	339.1	2.9	346.2	6.2	354	38	95.8
r15		75		9	2							
ples-	0.0535	0.0004	0.3993	0.00	0.3	336.1	2.7	341.1	6.1	378	40	88.9
t15		38		8	9							
ples-	0.054	0.0004	0.3937	0.01	0.3	338.9	2.9	337.1	7	338	50	100.
t16		86		0	7							3
ples-	0.0537	0.0004	0.3946	0.00	0.4	336.9	2.7	337.7	5.7	350	42	96.3
u16		51		8	2							
ples-	0.0535	0.0004	0.3905	0.00	0.4	336	3	334.7	6.1	338	42	99.4
v15		81		8	2							
ples-	0.0535	0.0004	0.404	0.00	0.4	335.8	3	344.5	6.4	386	40	87.0
z16		92		9	2							

9.4.2 U-Pb allanite in-situ dating

One sample of metagranitoids and two of metabreccias have been selected for in situ U-Pb dating of allanite. This is a LREE mineral that usually host high radionuclide concentration, notably Th and U, forming the basis of their utility as geochronometers. This cyclosilicate, for a long time classified as epidote, has peculiar features that allowed to describe it as a distinct mineral species (Ercit 2002; Armbruster et al. 2006). For instance, differently to epidote, in allanite the LREE And Fe^{2+} are structural essential constituent. Allanite crystals frequently show chemical zoning, due to the solid solution with epidotes.

U-Th-Pb Laser ablation inductively-coupled-plasma mass spectrometry (LA-ICP-MS) dating was performed on allanites in situ (on polished thin section). The instrument of the University of Berne (Switzerland) is a GeolLasPro (Compex 102; Lambda Physics) laser system combined with an Elan DRC-e (Perkin Elmer) ISP-QMS. The methodology is based on (e.g. Darling et al. 2012):

- The line-raster ablation, in order to minimize time-dependent elemental fractionation;
- The external normalization to the zircon standard Plešovice (Sláma et al. 2008);
- The use of measured ^{204}Pb to correct for inherited common-Pb.

Following Gregory et al. (2012), to overcome the issue related to the determination of initial lead two approaches are used for both Th-Pb and U-Pb system:

- The single-spot correction (Cumming and Richards 1975; Stacey and Kramers 1975), based on the assumption that a model Pb

composition does not change during allanite growth, and whose isotopic ratio is predicted by a global lead evolution model;

- The isochron method (Engi 2017), based on the assumption that a single stage of growth is characterized by common age but variable chemistry. Therefore, the determination of initial lead is made with the composition from internal heterogeneity within an allanite crystal.

The data showing variably non-radiogenic Pb, plotted in a Tera-Wasserburg diagram, are used to obtain the age.

Table 13. Results of allanite LA-ICP-MS U-Pb isotopic ratio of the sample CMD122A. The results related to the secondary standard "Plešovice" are also reported.

	Isotopic ratios (\varnothing 24 μ m)											
	^{208}Pb b/ ^{232}Tl h	2 S.D	$^{238}\text{U}/$ ^{206}Pb	2 S.D	^{206}Pb / ^{208}Pb	2 S.D	^{207}Pb b/ ^{206}Pb b	2 S.D	^{208}Pb b/ ^{232}Tl h _{rad}	2 S.D	^{238}U rad/ ^{206}Pb b	2 S.D
d0 7	0,02 35	7,73 E- 04	17,3 466	0,62 06	0,52 67	0,01 84	0,44 02	0,02 38	0,01 1	0,00 16	0,02 99	0,00 3
d0 8	0,04 15	0,00 19	15,8 232	0,83 88	0,75 09	0,04 16	0,40 7	0,03 5	0,01 27	0,00 44	0,03 54	0,00 41
d0 9	0,02 2	6,42 E- 04	16,3 478	0,61 82	0,52 42	0,01 93	0,34 45	0,02 13	0,01 32	0,00 12	0,03 9	0,00 29
d1 0	0,02 15	6,24 E- 04	18,6 058	0,63 68	0,62 28	0,02 18	0,32 69	0,01 79	0,01 19	0,00 13	0,03 54	0,00 23
d1 1	0,03 1	8,09 E- 04	16,5 794	0,60 29	0,74 62	0,02 81	0,34 76	0,01 74	0,01 28	0,00 21	0,03 82	0,00 27
d1 2	0,02 34	6,43 E- 04	19,0 518	0,67 59	0,72 2	0,02 58	0,30 42	0,01 64	0,01 23	0,00 14	0,03 61	0,00 22
d1 3	0,04 73	0,00 14	12,2 289	0,54 51	0,58 97	0,02 43	0,53 03	0,02 97	0,01 26	0,00 43	0,03 33	0,00 53
d1 4	0,01 8	6,36 E- 04	22,3 179	0,96 6	0,74 74	0,03 17	0,22 58	0,01 57	0,01 19	9,64 E- 04	0,03 51	0,00 19
d1 5	0,01 76	6,73 E- 04	13,4 708	0,62 14	0,30 12	0,01 4	0,44 91	0,03 01	0,01 21	8,68 E- 04	0,03 77	0,00 45
d1 6	0,02 05	0,00 12	19,0 41	1,94 78	0,79 26	0,08 3	0,30 94	0,05 77	0,00 96	0,00 3	0,03 57	0,00 55
e0 7	0,03 92	0,00 14	19,2 208	0,67 57	0,94 54	0,03 99	0,34 63	0,02 31	0,01 08	0,00 39	0,03 3	0,00 25
e0 8	0,05 38	0,00 28	15,9 978	1,09 03	0,88 01	0,04 72	0,40 07	0,03 11	0,01 08	0,00 64	0,03 55	0,00 41
e0 9	0,13 33	0,00 62	17,6 264	0,74 52	1,35 15	0,06 76	0,30 52	0,02 58	0,01 46	0,02 06	0,03 89	0,00 32
e1 01	0,03 85	0,00 1	18,3 748	0,61 47	0,94 07	0,03 24	0,32 07	0,01 69	0,01 32	0,00 32	0,03 63	0,00 23

TECTONO-METAMORPHIC HISTORY OF CONTINENTAL UNITS IN ALPINE CORSICA

e1	0,05	0,00	14,0	0,64	0,80	0,03	0,40	0,02	0,01	0,00	0,03	0,00
1	35	21	566	2	9	89	88	66	33	54	97	4
e1	0,07	0,00	16,2	1,15	0,78	0,04	0,43	0,03	0,01	0,00	0,03	0,00
2	67	32	683	08	38	11	41	75	71	91	24	45
Standard: Plešovice												
Pd	0,01	0,00	18,5	0,33	27,2	2,92	0,05	0,00	0,01	0,00	0,05	9,67
03	64	13	205	17	054	63	28	26	64	25	4	E-04
Pd	0,01	0,00	18,7	0,46	37,4	5,28	0,05	0,00	0,01	0,00	0,05	0,00
04	7	14	002	68	89	8	38	32	7	29	35	13
Pd	0,01	0,00	18,8	0,41	42,5	4,31	0,05	0,00	0,01	0,00	0,05	0,00
05	56	15	392	63	229	54	05	32	56	31	31	12
Pd	0,01	0,00	18,8	0,39	39,9	11,0	0,04	0,00	0,01	0,00	0,05	0,00
06	66	15	35	41	313	141	99	37	66	3	31	11
Pd	0,01	0,00	18,4	0,40	42,7	5,04	0,05	0,00	0,01	0,00	0,05	0,00
20	69	15	482	98	063	7	66	36	69	3	42	12
Pd	0,01	0,00	18,5	0,44	37,9	4,45	0,05	0,00	0,01	0,00	0,05	0,00
21	7	15	684	86	22	7	15	31	7	3	39	13
Pd	0,01	0,00	18,5	0,42	34,5	3,66	0,05	0,00	0,01	0,00	0,05	0,00
22	7	13	758	25	834	81	15	29	7	26	38	12
Pd	0,01	0,00	18,6	0,44	34,7	3,14	0,05	0,00	0,01	0,00	0,05	0,00
23	68	13	497	36	089	14	02	35	68	26	36	13
Pe	0,01	0,00	18,7	0,44	34,5	3,66	0,05	0,00	0,01	0,00	0,05	0,00
03	7	13	998	8	834	81	15	29	7	26	32	13
Pe	0,01	0,00	18,8	0,46	34,7	3,14	0,05	0,00	0,01	0,00	0,05	0,00
04	67	13	746	85	089	14	02	35	67	26	3	13
Pe	0,01	0,00	18,5	0,44	37,9	4,45	0,05	0,00	0,01	0,00	0,05	0,00
05	7	15	684	86	22	7	15	31	7	3	39	13
Pe	0,01	0,00	18,6	0,43	42,7	5,04	0,05	0,00	0,01	0,00	0,05	0,00
06	68	15	706	54	063	7	66	36	68	29	36	12
Pe	0,01	0,00	18,7	0,47	37,9	4,45	0,05	0,00	0,01	0,00	0,05	0,00
07	69	15	923	32	22	7	15	31	69	3	32	13
Pe	0,01	0,00	18,5	0,47	38,7	8,40	0,05	0,00	0,01	0,00	0,05	0,00
19	72	14	282	37	087	75	21	3	72	28	4	14
Pe	0,01	0,00	18,1	0,49	43,7	7,46	0,05	0,00	0,01	0,00	0,05	0,00
20	66	15	299	13	578	88	2	32	66	3	52	15
Pe	0,01	0,00	18,6	0,37	38,9	3,14	0,05	0,00	0,01	0,00	0,05	0,00
21	64	12	803	16	875	23	3	24	64	25	35	11
Pe	0,00	4,96	32,8	1,78	0,16	0,00	0,67	0,04	0,00	6,09	0,00	0,00
22	21	E-05	076	4	79	79	28	31	15	E-05	64	17
Pe	0,00	4,34	33,4	2,02	0,11	0,00	0,68	0,05	0,00	4,93	0,00	0,00
23	19	E-05	399	6	32	63	26	11	15	E-05	59	2
Pd	0,00	4,39	33,7	1,73	0,11	0,00	0,66	0,05	0,00	5,05	0,00	0,00
18	19	E-05	562	32	56	55	32	3	15	E-05	65	2
Pd	0,00	4,09	30,0	1,54	0,13	0,00	0,66	0,04	0,00	4,95	0,00	0,00
19	2	E-05	614	69	25	6	1	65	16	E-05	74	2
Pd	0,00	4,57	29,7	1,57	0,15	0,00	0,71	0,05	0,00	6,05	0,00	0,00
20	21	E-05	33	72	97	72	17		15	E-05	54	21
Pd	0,00	5,99	33,1	2,46	0,15	0,00	0,63	0,04	0,00	6,68	0,00	0,00
21	21	E-05	778	73	9	88	74	25	16	E-05	76	17

Table 14. Results of allanite LA-ICP-MS U-Pb isotopic ratio of the sample.

	Ages (Ma)			
	²³² Th-age	2 S.D	²³⁸ U-age	2 S.D
d07	219,8184	31,2125	189,8958	19,0067
d08	252,7935	88,4347	224,271	25,6
d09	263,7078	23,883	246,6682	17,8553
d10	238,019	25,0973	224,359	14,3288
d11	254,4637	42,65	241,7831	16,4672
d12	244,8574	28,5104	228,4123	13,5334
d13	251,3487	86,7645	211,4108	33,0603
d14	237,4631	19,2513	222,5109	12,0669
d15	242,449	17,3349	238,594	28,0835
d16	191,0316	59,8175	226,0878	34,1269
e07	213,2779	77,4105	209,3826	15,6259
e08	213,2801	127,5224	224,6311	25,812
e09	270,2406	411,4266	246,2448	19,8097
e101	260,5601	63,1606	229,8485	14,1605
e11	263,636	108,357	250,9948	24,8487
e12	334,1563	181,4924	205,8177	27,9101
Standard:				
Plešovice				
Pd03	329,0931	25,0392	338,9965	5,8388
Pd04	341,2246	28,5759	335,8238	8,1578
Pd05	313,5772	30,2288	333,4088	7,1911
Pd06	333,7193	29,4384	333,4805	6,8552
Pd20	338,0752	28,9109	340,2919	7,3623
Pd21	340,4908	29,9337	338,1449	7,9424
Pd22	341,6923	25,9525	338,015	7,3961
Pd23	336,1384	26,2763	336,7084	7,7609
Pe03	340,2075	25,6499	334,0901	7,7556
Pe04	334,6775	26,0577	332,7982	8,0316
Pe05	340,4908	29,6408	338,1449	8,0197
Pe06	336,606	29,1071	336,3412	7,6851
Pe07	339,0111	29,6666	334,2184	8,1594
Pe19	343,8364	27,6027	338,8605	8,5479
Pe20	332,7013	30,1532	346,1089	9,1013
Pe21	329,5801	24,405	336,1724	6,4506
Pe22	31,1779	1,2282	40,8059	10,8924
Pe23	30,7873	0,9949	37,6704	12,6938
Pd18	31,3265	1,0185	41,9699	12,9352
Pd19	31,4199	0,9988	47,7152	12,7062
Pd20	30,4525	1,2215	34,4012	13,689
Pd21	32,7017	1,3489	49,027	11,0544

References

- Abalos, B., Puellas, P., Gil Iburguchi, J. 2003. "Structural assemblage of high-pressure mantle and crustal rocks in a subduction channel (Cabo Ortegal, NW Spain)." *Tectonics* 22(2): TC1006.
- Abbate, E., Bortolotti, V., Principi, G. 1980. "Appennine ophiolites: a peculiar oceanic crust." *Ophioliti* Special Issue 5(1): 59-96.
- Agard, P., Monié, P., Jolivet, L., Goffé, B. 2002. "In situ laser probe $^{40}\text{Ar}/^{39}\text{Ar}$ dating of the Schistes Lustrés complex: implications for the exhumation of the Western Alps." *Journal of Metamorphic Geology* 20: 599-618.
- Agard, P., Yamato, P., Jolivet, L., Burov, E. 2009. "Exhumation of oceanic blueschists and eclogites in the subduction channel: timing and mechanisms." *Earth Science Review* 92: 53-79.
- Agard, P., Omrani, J., Jolivet, L., Whitechurch, H., Vrielynck, B., Spakman, W., Monié, P., Meyer, B., Wortel, R. 2011. "Zagros orogeny: a subduction dominated processes." *Geological Magazine* 148(5-6): 692-725.
- Agard, P., Yamato, P., Soret, M., Prigent, C., Guillot, S., Plunder, A., Dubacq, B., Chauvet, A., Monié, P. 2016. "Plate interference rheological switches during subduction infancy: Control on slab penetration and metamorphic sole formation." *Earth and Planetary Science Letters* 451: 208-220.

- Agard, P., Plunder, A., Angiboust, S., Bonnet, G., Ruh, J. 2018. "The subduction plate interference: rock record and mechanical coupling (from long to short timescales)." *Lithos* 320-321: 537-566.
- Aicard et al., 1962. "Le gite plombo-zincifere de la Finosa près Ghisoni." *Bulletin BRGM* 3.
- Airaghi, L., de Sigoyer, J., Lanari, P., Guillot, S., Vidal, O., Monié, P., Sautter, B., Tan, X. 2017. "Total exhumation across the Beichuan fault in the Longmen Shan (eastern Tibetan plateau, China): Constraints from petrology and thermobarometry." *Journal of Asian Earth Science* 140: 108-121.
- Alessandri, J.A., Magné, J., Pilot, M.D., Samuel, E. 1977. "Le Miocène de la région de Corte-Francardo." *Bulletin de la Société Scientifique de Histoire Naturelle de la Corse* 622 : 51-54.
- Allen, P.A., Homewood, P., Williams, G.D. 1986. "Foreland basin: an introduction." *Foreland basin Special Publication* 8 : 3-12.
- Allen, P.A., Crampton, S.L., Sinclair, H.D. 1991. "The inception and early evolution of the North Alpine foreland basin, Switzerland." *Basin Research*. 3: 143-163.
- Allen, P.A., Burgess, P.M., Galewsky, J., Sinclair, H.D. 2001. "Flexural-eustatic numerical model for drowning of the Eocene perialpine carbonate ramp and implications for Alpine geodynamics." *GSA Bulletin* 113(8): 1052-1066.
- Alvarez, W. 1972."Rotation of the Corsica-Sardinia microplate." *Nature Physical Science* 235 (58): 103-105.
- Amaudric du Chaffaut, S. 1975. "L'unité de Corte: un témoin de "Piémontais externe" en Corse?" *Bulletin de la Société Géologique de France* 7 : 739-745.
- Amaudric du Chaffaut, S. 1980. "Les unités alpines a la marge orientale du massif cristallin corse." Ph.D. thesis. Université de Paris.
- Amaudric du Chaffaut, S., Saliot, P. 1979. "La region de Corte: secteur-clé pour la comprehension du métamorphisme alpine en Corse." *Bulletin de la Société Géologique de France* 21: 149-154.
- Amaudric du Chaffaut, S., Caron J.M., Delcey R., Lemoine M. 1972. "Données nouvelles sur la stratigraphie des schistes lustrés de Corse: La série de l'Inzecca. Comparaison avec les Alpes Occidentales et l'Apennin ligure." *Comptes Rendus de Académie de Sciences Paris* 275 : 2611-2614.
- Amaudric du Chaffaut, S., Kienast J.R., Saliot P. 1976. "Répartition de quelques minéraux de métamorphisme alpin en Corse." *Bulletin de la Société Géologique de France* 18(5) : 1179-1182.
- Amaudric du Chaffaut, S., Villey M. 1979. "Une coupe des Alpes de l'Argentiera-Mercantour a la zone de Sestri-Voltaggio." *Bulletin de la Société Géologique de France* 12(4) : 349-378.
- Amaudric du Chaffaut, S., Caron J.M., Jauzein A., Bonin B., Rossi P., Conchon C., Perthuisot J.P. 1983. "Carte Geologique de la France (1/50000), feuille Venaco (111a)" *BRGM*, Orléans.
- Amaudric du Chaffaut, S., Bonin, B., Caron, J.M., Conchon, O., Rossi, P., Bimbier, A., Damiani, L., Dominici, R., Heetveld, H., Rouire, J. 1985. "Carte Géologique de la France (1/50000), feuille Venaco (1114)" *BRGM*, Orléans.

- Argand, E. 1924. "Des Alpes et de l'Afrique." *Bulletin de la Société vaudoise des Sciences Naturelles* 55, 233-236.
- Armbruster, T., Bonazzi, P., Akasaka, M., Bermanec, V., Chopin, C., Gieré, R., Heuss-Assbichler, S., Liebscher, A., Menchetti, S., Yuanming, P.A., Pasero, M. 2006. "Recommended nomenclature of epidote group minerals." *European Journal of Mineralogy* 18: 551-567.
- Auzende, J.M., Bonnin, J., Olivet, J.L. 1973. "The origin of the Western Mediterranean basin." *Geological Society of London* 19: 607-620.
- Bache, F., Olivet, J.L., Gorini, C., Aslanian, D., Labails, C., Rabineau, M. 2010. "Evolution of rifted continental margins: the case of Gulf of Lions (Western Mediterranean Basin)." *Earth and Planetary Science Letters* 292: 345-356.
- Balen, D., Massonne, H.J., Lihter, I. 2017. "Alpine metamorphism of low-grade schists from the Slavonian Mountains (Croatia): new P-T and geochronological constraints." *International Geology Review* doi: 10.1080/00206814.2017.1328710.
- Barruol, G., Granet, M. 2002. "A Tertiary asthenospheric flow beneath the southern French Massif Central indicated by upper mantle seismic anisotropy and related to the west Mediterranean extension." *Earth and Planetary Science Letters* 202: 31-47.
- Barth, S., Oberli, F., Meier, M. 1994. "Th-Pb versus U-Pb isotope systematics in allanite from co-genetic rhyolites and granodiorite: implications for geochronology." *Earth and Planetary Science Letters* 124: 149-159.
- Beaudoin, A., Augier, R., Jolivet, L., Jourdon, A., Raimbourg, H., Scaillet, S., Cardello, G.L. 2017. "Deformation behavior of continental crust during subduction and exhumation: strain distribution over the Tenda Massif (Alpine Corsica, France)." *Tectonophysics* 705: 12-32.
- Beaumont, C. 1981. "Foreland basins." *Geophys. Journal of Royal Astronomical Society* 65: 291-329.
- Beaumont, C., Jamiessont, R.A., Niguyen, M.H., Lee, B. 2001. "Himalayan tectonics explained by extrusion of a low-viscosity crustal channel coupled to focused surface denudation." *Nature* 414 : 738-742.
- Beaumont, C., Nguyen, M.H., Jamieson, R.A., Ellis, S. 2006. "Crustal flow models in large hot orogens." " In: Law, R.D., Searle, M.P., and Godin, L. (eds.) Channel Flow, Ductile Extrusion and Exhumation in Continental Collision Zones. *Geological Society of London Special Publication* 268:91-145.
- Bellon, H., Coulon, C., Edel, J.B. 1977. "Le déplacement de la Sardaigne. Synthèse des données géochronologiques, magmatiques et paléomagnétiques." *Bulletin de la Société Géologique de France* 7: 825-831.
- Beltrando, M., Compagnoni, R., Lombardo, B. 2010. "(Ultra-) high-pressure metamorphism and orogenesis: an Alpine perspective." *Gondwana Research* 18: 147-166.
- Berger, A., Bousquet, R. 2008. "Subduction-related metamorphism in the Alps: review of isotopic ages based on petrology and their geodynamic consequences." In: Sigismund, S., Fugenschuh, B., Froitzheim, N. (eds.) Tectonic Aspects of the Alpine-Dinaride-Carpathian system 298 *Geological Society of London Special Publication* 117-144.

- Berger, A., Burri, T., Alt-Epping, P., Engi, M. 2008. "Tectonically controlled fluid flow and water assisted melting in the middle crust: an example from Central Alps." *Lithos* 102: 598-615.
- Berger, A., Schmid, S.M., Engi, M., Bousquet, R., Wiederkehr, M. 2011. "Mechanism of mass and heat transport during Barrovian metamorphism: a discussion based on field evidence from the Central Alps (Switzerland/Northern Italy)." *Tectonics* 30: TC1007.
- Bertotti, G., Picotti, V., Bernoulli, D., Castellarin, A. 1993. "From rifting to drifting: tectonic evolution of the South-Alpine upper crust from the Triassic to the Early Cretaceous." *Sedimentary Geology* 86: 53-76.
- Best, M.G. 2003. *Igneous and metamorphic petrology*. Brigham Young University: Blackwell Publishing.
- Bezert P., Caby R. 1988. "Sur l'âge post-bartonien des événements tectonométamorphiques alpins en bordure orientale de la Corse cristalline (Nord de Corte)." *Bulletin de la Société Géologique de France* 4(6): 965-971.
- Biino, G., Meisel, T. 1996. "Ar-Ar, Re-Os, Rb-Sr, Sm-Nd and U-Pb isotopic, trace element and petrologic study of alkaline mineralized ultramafic pipes in the Ivrea-Verbano Zone, Italy." *Schweizerische Mineralogische und Petrographische Mitteilungen* 76: 98-99.
- Bill, M., Bussy, E., Cosca, M.A., Masson, H., Hunziker, J.C. 1997. "High-precision U-Pb and ^{40}Ar - ^{39}Ar dating of an Alpine ophiolite (Géts nappe, French Alps)." *Eclogae Geologicae Helvetiae* 90: 43-54.
- Boccaletti M., Elter P., Guazzone G. 1971. "Plate tectonic models for the development of the western Alps and northern Apennines." *Nature* 234: 108-111.
- Bonazzi, P., Menchetti, S. 1994. "Structural variations induced by heat treatment in allanite and REE-bearing piemontite." *American Mineralogist* 79: 1176-1184.
- Bonin, B., Platevoet, B., Viallette, Y. 1987. "The geodynamic significance of alkaline magmatism in the Western Mediterranean compared with West Africa." In: Bowden, P., Kinnaird, J.A. (eds.) African Geology reviews. *Geological Journal* (Thematic issue) 22: 361-387.
- Borsi, S., Del Moro, A., Sassi, F.P., Visonà, D., Zirpoli, G. 1980. "On the existence of Hercynian aphtes and pegmatites in the Lower Aurina Valley (Ahrntal, Austrides, Eastern Alps)." *Neus Jahrbuch fur Mineralogische*: 501-514.
- Boullin, J.P., Durand-Delga, M., Olivier, P. 1986. "Betic-Rifain and Tyrrhenian Arcs: distinctive features, genesis and development stages." In: Wezel, F.C. (eds.) The Origins of Arcs. *Elsevier* 281-304.
- Bousquet, R., Goffé, B., Henry, P., Le Pichon, X., Chopin, C. 1997. "Kinematic, thermal and petrological model of the Central Alps: Lepontine metamorphism in the upper crust and eclogitisation of the lower crust." *Tectonophysics* 273: 105-127.
- Bousquet, R., Goffé, B., Vidal, O., Oberhaensli, R., Patriat, M. 2002. "The tectono-metamorphic history of the Valaisan Domain from the Western to the Central Alps: new constraints on the evolution of the Alps." *GSA Bulletin* 114: 207-225.

- Bousquet, R., Goffé, B., Wiederkehr, M., Koller, F., Schmid, S.M. Schuster, R., Engi, M., Martinotti, G. 2008. "Metamorphism of metasediments at the scale of an orogen: a key to the Tertiary geodynamic evolution of the Alps." In: Siegesmund, S., Fugenschuh, B., Froitzheim, N. (eds.) *Tectonic aspects of the Alpine-Dinaride-Carpathian: Geological Society of London Special Publication 298*: 393-411.
- Breman, R.G. 1988. "Internally-consistent thermodynamic data for stoichiometric minerals in the system $\text{Na}_2\text{O-K}_2\text{O-CaO-MgO-FeO-Fe}_2\text{O}_3\text{-Al}_2\text{O}_3\text{-SiO}_2\text{-TiO}_2\text{-H}_2\text{O-CO}_2$." *Journal of Petrology* 29: 445-522.
- Brodie, K.H., Rex, D., Rutter, E.H. 1989. "On the age of deep crustal extensional faulting in the Ivrea Zone, Northern Italy. Alpine Tectonics." In: Park, R.G. (eds.) *Geological Society of London Special Publication 45*: 461-471.
- Brown, E.H. 1977. "The crosstie content of Ca-amphibole as a guide to pressure of metamorphism." *Journal of Petrology* 18: 53-72.
- Brunet, C., Monié, P., Jolivet, L., Cadet J.P. 2000. "Migration of compression and extension in the Tyrrhenian Sea, insights from $^{40}\text{Ar}/^{39}\text{Ar}$ ages on micas along a transect from Corsica to Tuscany." *Tectonophysics* 321: 127-155.
- Bucher, S., Schmid, S.M., Bousquet, R., Fugenschuh, B. 2003. "Late-stage deformation in a collisional orogeny (Western Alps): nappe refolding, back-thrusting or normal faulting?" *Terra Nova* 15(2): 109-117.
- Burg, J.P., Gerya, T.V. 2005. "The role of viscous heating in Barrovian metamorphism of collisional orogens: thermomechanical models and application to the Lepontine Dome in Central Alps." *Journal of Metamorphic Geology* 23: 75-95.
- Burkhard, M. 1993. "Calcite twins, their geometry, appearance and significance as stress-strain markers and indicators of tectonic regime: a review." *Journal of Structural Geology* 15: 351-368.
- Burkhard M., Sommaruga A. 1998. "Evolution of the western Swiss Molasse basin: structural relations with the Alps and the Jura belt." In Mascle A., Puidefàbregas C., Luterbacher H.P., Fernández M. (eds.) *Cenozoic foreland basins of the western Europe, Geological Society of London Special Publication 134*: 279-298.
- Burov, E. 2011. "Rheology and strength of the lithosphere." *Marine and Petroleum Geology* 28(8):1402-1443.
- Burov, E., Diament, M. 1995. "Effective elastic thickness of the continental lithosphere, what does it really mean?" *Journal of Geophysical Research* 100: 39-3927.
- Burov, E., Jolivet, L., Le Pourhiet, L., Poliakov, A. 2001. "A thermomechanical model of exhumation of high pressure (HP) and ultra-high pressure (UHP) metamorphic rocks in Alpine-type collision belts." *Tectonophysics* 342(1): 113-136.
- Burov, E., Francois, T., Yamato, P., Wolf, S. 2014. "Mechanisms of continental subduction and exhumation of HP and UHP rocks." *Gondwana Research* 25 : 464-493.
- Burrus, J. 1984. "Contribution to a geodynamic synthesis of the Provencal basin (northwestern Mediterranean)." *Marine Geology* 55: 247-269.

- Byrne, D.E., Davis, D.M., Sykes, L.R. 1988. "Minimum and maximum size of thrust earthquakes and the mechanics of the shallow region of subduction zones." *Tectonics* 7: 833-857.
- Cabanis, B., Cochemé, J.J., Vellutini, P.J., Joron, J.L., Treuil, M. 1990. « Post-collisional Permian volcanism in northwestern Corsica: an assessment based on mineralogy and trace-element geochemistry." *Journal of Volcanology and Geothermal Research* 44: 51-67.
- Caby R., Jacob C. 2000. "La transition croute/manteau dans la nappe de Santa Lucia di Mercurio (Corse alpine): les raciness d'un rift permien." *Géologie de France* 1: 21-24.
- Caby, R., Kienast, J.R., Saliot, P. 1978. "Structure, métamorphisme et modèle d'évolution tectoniques des Alpes Occidentales." *Revue de Géographie Physique et Géologie Dynamique* 20: 307-322.
- Capponi, G., Crispini, L., Federico, L., Piazza, M., Fabbri, B. 2009. "Late Alpine tectonics in the Ligurian Alps: constraints from the Tertiary Piedmont Basin conglomerates." *Geological Journal* 44(2): 211-224.
- Carmignani, L., Conti, P., Cornamusini, G., Meccheri, M. 2004. "The internal Northern Apennines, the Northern Tyrrhenian Sea and the Sardinia-Corsica Block." *Italian Journal of Geological Society* special volume.
- Caron, J.M. 1977. "Lithostratigraphie et tectonique des Schistes Lustrés dan les Alpes méridionales et en Corse orientale." Msc thesis. Université de Strasbourg.
- Caron, J.M. 1994. "Metamorphism and deformation in Alpine Corsica." *Schweizerische Mineralogische und Petrographische Mitteilungen* 74(1): 105-114.
- Caron, J.M., Delcey, R., 1979. "Lithostratigraphie des Schistes Lustrés corses : diversité des séries post-ophiolitiques. " *Comptes Rendus de Académie de Sciences Paris* 288: 1525-1528.
- Caron, J.M., Delcey, R., Scius, H., Eissen, J.P., De Fraipont, P., Mawhin, B., Reuber, I. 1979. "Répartition cartographique des principaux types de séries dans les Schistes lustrés de Corse." *Comptes Rendus de Académie de Sciences Paris* 288(D): 1363-1366.
- Caron, J.M., Kienast, J.R. Triboulet, C. 1981. "High-pressure/low-temperature metamorphism and polyphase Alpine deformation at Sant'Andrea di Cotone (Eastern Corsica, France)." *Tectonophysics* 78: 419-451.
- Casini, L., Cuccuru, S., Puccini, A., Oggiano, G., Rossi, P. 2015. "Evolution of the Corsica-Sardinia batholith and the late orogenic shearing of the Variscides." *Tectonophysics* 646: 65-78.
- Cathelineau, M. 1988." Cation site occupancy in chlorites and illites as a function of temperature." *Clay Minerals* 23: 471-485.
- Cathelineau, M., Nieva, D. 1985. "A chlorite solid solution geothermometer. The Los Azufres (Mexico) geothermal system." *Contributions to Mineralogy and Petrology* 91: 235-224.
- Catlos, E.J., Sorensen, S.S., Harrison, T.M. 2000. "Th-Pb ion microprobe dating for allanite." *American Mineralogist* 85: 633-648.
- Cavazza, W., Zattin, M., Ventura, B., Zuffa, G.G. 2001. "Apatite fission track analysis of Neogene exhumation in northern Corsica (France)." *Terra Nova*

13: 51-57.

- Cavazza, W., DeCelles, P.G., Fellin, M.G., Paganelli, L. 2007. "The Miocene Saint-Florent Basin in northern Corsica stratigraphy, sedimentology and tectonic implications." *Basin Research* 19: 507-527.
- Cenki-Tok, B., Oliot, E., Rubatto, D., Berger, A., Engi, M., Janots, E., Thomsen, T.B., Manzotti, P., Regis, D., Spandler, C., Robyr, M., Goncalves, P. 2011. "Preservation of Permian allanite within an Alpine eclogite facies shear zone at Mt. Mucrone, Italy: Mechanical and chemical behavior of allanite during mylonitization." *Lithos* 125: 40-50.
- Cenki-Tok, B., Darling, J.R., Rolland, Y., Dhuime, B., Storey, D. 2014. "Direct dating of mid-crustal shear zones with synkinematic allanite: new in situ U-Th-Pb geochronological approaches applied to the Mont Blanc massif." *Terra Nova* 26: 29-37.
- Ceriani, S., Fugenschuh, B., Schmid, S.M. 2001. "Multi-stage thrusting at the "Penninic Front" in the Western Alps between Mont Blanc and Pelvoux massifs." *International Journal of Earth Sciences* 90: 685-702.
- Chamberlain, C.P., Karabinos, P. 1987. "Influence of deformation on pressure-temperature paths of metamorphism." *Geology* 15: 42-44.
- Chamberlain, C.P., Sonder, L.J. 1990. "Heat-producing elements and the thermal and baric patterns of metamorphic belts." *Science* 250: 763-769.
- Chamot-Rooke, N., Gaulier, J.M., Jestin, F. 1999. "Constraints on Moho depth and crustal thickness in the Liguro-Provencal basin from a 3D gravity inversion: geodynamic implications." In: Durand, B., Jolivet, L., Horvath, F., Séranne, M., (eds.) *The Mediterranean basin: Tertiary extension within the Alpine Orogen. Geological Society of London Special Publication* 156: 37-61.
- Chang, J.H., Yu, H-S., Hsu, H.H., Liu, C.S. 2012. "Forebulge migration in late Cenozoic Western Taiwan Foreland basin." *Tectonophysics* 578: 117-125.
- Chang, J.H., Hsu, H.H., Su, C.C., Liu, C.S., Hung, H.T., Chiu, S.D. 2015. "Tectono-sedimentary control on modern sand deposition on the forebulge of the Western Taiwan Foreland basin." *Marine Petroleum and Geology* 66: 970-977.
- Chappell, B.W., White, A.J. 1974. "Two contrasting granite types: 25 years later." *Australian Journal of Earth Sciences* 48: 489-499.
- Chemenda, A.I., Mattauer, M., Malavieille, J., Bokun, A.N. 1995. "A mechanism for syn-collisional deep rock exhumation and associated normal faulting: Results from physical modeling." *Earth and Planetary Science Letters* 132: 225-232.
- Chemenda, A.I., Mattauer, M., Bokun, A.N. 1996. "Continental subduction and a mechanism for exhumation of high-pressure metamorphic rocks: new modeling and field data from Oman." *Earth and Planetary Science Letters* 143: 173-182.
- Cherniak, D.J. 2010. "Diffusion in accessory minerals: zircons, titanite, apatite, monazite and xenotime." *Reviews in Mineralogy and Geochemistry* 72: 827-869.
- Chopin, C. 1984. "Coesite and pure pyrope in high-grade blueschists of the Western Alps: a first record and some consequences." *Contributions to Mineralogy and Petrology* 86: 107-118.

- Chopin, C. 1987. "Very high pressure metamorphism in the Western Alps: implications for subduction of continental crust." *Philosophical Transaction of the Royal Society of London* 321: 183-197.
- Chopin, C., Beyssac, O., Bernard, S., Malavieille, J., 2008. "Aragonite-grossular intergrowths in eclogite-facies marble, Alpine Corsica." *European Journal of Mineralogy* 20: 857-865.
- Cloetingh, S.A.P.L., Wortel, M.J.R., Vlaar, N.J. 1982. "Evolution of passive continental margins and initiation of subduction zones." *Nature* 297: 139-142.
- Cloos, M. 1982. "Flow melanges: Numerical modeling and geological constraints on their origin in the Franciscan subduction complex." *GSA Bulletin* 93: 330-345.
- Cloos, M., Shreve, R. 1988. "Subduction-channel model of prism accretion, mélange formation, sediment subduction, and erosion at convergent plate margins: 2. Implications and discussion." *Pageoph* 128 (3/4): 501-545.
- Cocherie, A., Rossi, P., Fuillac, A.M., Vidal, O. 1994. "Crust and mantle contribution to granite genesis - an example from the Variscan batholith of Corsica, France, studied by trace elements and Nd-Sr-O isotope systematic." *Chemical Geology* 115: 173-211.
- Cocherie, A., Rossi, P., Fanning, C.M., Guerrot, C. 2005. "Comparative use of TIMS and SHRIMP for U-Pb zircon dating of A-type granites and mafic tholeiitic layered complexes and dykes from the Corsican batholith (France)." *Lithos* 82: 185-219.
- Cohen, C.R., Schweickert, R.A., Odom, A.L. 1981. "Age of emplaced of the Schistes Lustrés nappe, Alpine Corsica." *Tectonophysics* 73: 267-283.
- Colombo, A., Tunesi, A. 1999. "Pre-Alpine metamorphism in the southern Alps." *Schweizerische Mineralogische und Petrographische Mitteilungen* 78: 163-168.
- Compagnoni, R., Rolfo, F. 2003. "UHPM units in the Western Alps." EMU notes in *Mineralogy* 5(2): 13-49.
- Conel, J.E. 1962. "Studies of the development of fabrics in some naturally deformed limestones." Ph.D thesis. University of California.
- Cortesogno, L., Haccard, D. 1984. "Note illustrative alla carta geologica della zona Sestri-Voltaggio." *Memorie della Società Geologica d'Italia* 28: 115-150.
- Cumming, G., Richards, J. 1975. "Ore lead isotope ratios in a continuously changing Earth." *Earth and Planetary Science Letters* 28: 155-171.
- D'Agostino, N., Avallone, A., Cheloni, D., D'Anastasio, E., Mantenuto, S., Selvaggi, G. 2008. "Active tectonics of the Adriatic region from GPS and earthquake slip vectors." *Journal of Geophysical Research* 113: B12413.
- Dal Piaz, G.V., Zirpoli, G. 1979. "Occurrence of eclogites relics in the ophiolite nappe from Marine d'Albo, Northern Corsica." *Neues Jahrbuch für Mineralogie* 3: 118-122.
- Dallan, L., Nardi, R. 1984. "Ipotesi dell'evoluzione dei domini "liguri" della Corsica nel quadro della paleogeografia e della paleotettonica delle unità alpine." *Bollettino della Società Geologica Italiana* 103: 515-527.
- Dallan, L., Puccinelli, A., 1995. "Geologia della regione tra Bastia e St-Florent (Corsica Settentrionale)." *Bollettino della Società Geologica Italiana* 114: 23-66.

- Daniel, J.M., Jolivet, L., Goffé, B., Poinssot, C. 1996. "Crustal-scale strain partitioning: footwall deformation below the Alpine Oligo-Miocene detachment of Corsica." *Journal of Structural Geology* 18(1): 41–59.
- Danisik, M. 2005. "Cooling history and relief evolution of Corsica (France) as constrained by fission track and (U-Th)/He thermochronology." Ph.D. thesis. Universitat Tubingen.
- Danisik, M., Kuhlemann, J., Dunkl, I., Székely, B., Frisch, W. 2007. "Burial and exhumation of Corsica (France) in the light of fission track data." *Tectonics* 26: TC1001.
- Danisik, M., Kuhlemann, J., Dunkl, I., Evans, N.J., Szekely, B., Frisch, W. 2012. "Survival of ancient landforms in a collisional setting as revealed by combined fission track and (U-Th)/He thermochronometry : a case study from Corsica (France)." *The Journal of Geology* 120 : 155-173.
- Darling, J., Storey, C., Engi, M. 2012. "Allanite U-Th-Pb geochronology by laser ablation ICP-MS." *Chemical Geology* 292-293: 103-115.
- De Andrade, V., Vidal, O., Lewin, E., O'Brien, P., Agard, P. 2006. "Quantification of electron microprobe compositional maps of rock thin sections: an optimized method and examples." *Journal of Metamorphic Geology* 24: 655-668.
- De Giorgi, A. 2016. "Storia tettono-metamorfica di un settore di crosta continentale durante la collisione continentale: l'esempio delle Scaglie di Corte, Corsica Alpina." Msc thesis. Università di Pisa.
- De Jong, K.A., Manzoni, M., Zijdeveld, J.D.A. 1969. "Paleomagnetism of the Alghero Trachyandesites." *Nature* 224: 67-69.
- Decandia F.A., Elter P. 1969. "Riflessioni sul problema delle ofioliti nell'Appennino Settentrionale (nota preliminare)." *Atti della Società Toscana di Scienze Naturali* 76: 1-9.
- DeCelles, P.G., Giles, K.A. 1996. "Foreland basin systems." *Basin Research* 8(2): 105-123.
- Deino A., Gattacceca J., Rizzo R., Montanari A. 2001. "⁴⁰Ar/³⁹Ar dating and paleomagnetismo of the Miocene volcanic succession of Monte Furrù (western Sardinia): implications for the rotation history of the Corsica-Sardinia microplate." *Geophysical Research Letters* 28: 3373-3376.
- Delcey M.R. 1974. "Données sur deux nouvelles séries lithostratigraphiques de la zone des Schistes Lustrés de la Corse nord-orientale." *Comptes Rendus de Académie de Sciences Paris* 279: 1693-1696.
- Denizot, G. 1952. "La structure géologique de la Corse." *Revue Scientifique* 90(2), 3316: 104-119.
- Deseta, N., Andersen, T.B., Ashwal, L.D. 2014. "A weakening mechanism for intermediate-depth seismicity? Detailed petrographic and microtextural observations from blueschist facies pseudotachylites, Cape Corse, Corsica." *Tectonophysics* 610: 138-149.
- Dewey, J.F. 1988. "Extensional collapse of orogens." *Tectonics* 7(6): 1123-1139.
- Dewey, J.F., Pitman, W.C., Ryan, W.B.F., Bonin, J. 1973. "Plate tectonics and evolution of the Alpine system." *GSA Bulletin* 84: 3137-3180.
- Dewey, J.F., Ryan, P.D., Andersen, T.B. 1993. "Orogenic uplift and collapse, crustal thickness, fabrics and metamorphic phase changes: the role of

- eclogites.” In Prichard, H.M., Alabaster, T., Harris, N.B.W., and Neary, C.R. (eds.) *Magmatic Processes and Plate Tectonics. Geological Society of London Special Publication 76*: 324-343.
- Di Rosa, M., De Giorgi, A., Marroni, M., Vidal, O. 2017a. “Syn-convergence exhumation of continental crust: evidence from structural and metamorphic analysis of the Monte Cecu area, Alpine Corsica (Northern Corsica, France).” *Geological Journal* 52 : 919-937.
- Di Rosa, M., De Giorgi, A., Marroni, M., Pandolfi, L. 2017b. “Geology of the area between Golo and Tavignano Valleys (Central Corsica): a snapshot of the continental metamorphic units of Alpine Corsica.” *Journal of Maps* 13: 644-653.
- Di Rosa, M., Meneghini, F., Marroni, M., Hobbs, N., Vidal, O. “The exhumation of continental crust in collisional belts: insights from the deep structure of Alpine Cordica in the Cima Pedani area. *The Journal of Geology* (2018a), 127(3): 263-288.
- Di Rosa, M., Frassi, C., Meneghini, F., Marroni, M., Pandolfi, L., De Giorgi, A. 2018b. “Tectono-metamorphic evolution in the European continental margin involved in the Alpine subduction: new insights from the Alpine Corsica, France.” *Comptes Rendus de Académie de Sciences Paris* 351 (5): 384-394.
- Di Vincenzo, G., Grande, A., Prosser, G., Cavazza, W., DeCelles, P.G. 2016. ” $^{40}\text{Ar}/^{39}\text{Ar}$ laser dating of ductile shear zones from central Corsica (France): Evidence of Alpine (middle to late Eocene) syn-burial shearing in Variscan granitoids.” *Lithos* 262: 369-383.
- Diella, V., Spalla, M.I., Tunesi, A. 1992. “Contrasting thermomechanical evolutions in the Southalpine metamorphic basement of the Orobic Alps (Central Alps, Italy).” *Journal of Metamorphic Geology* 10(2): 1-52.
- Dieni, I., Massari, F. 1982. “Présence de glaucophane détritiques dans le Maastrichtien inférieur de Sardaigne orientale. Implications géodynamiques.” *Comptes Rendus de Académie de Sciences Paris* 295: 679-682.
- Dieni, I., Massari, F., Stunari, C. 1966. “Segnalazione di Ammoniti nel Giurese della Sardegna orientale.” *Atti dell’Accademia Nazionale dei Lincei* 8(40): 99-107.
- Dogliani, C. 1991. “A proposal of kinematic modelling for W-dipping subductions – Possible applications to the Tyrrhenian-Apennines system.” *Terra Nova* 3: 423-434,
- Dogliani, C., Gueguen, E., Sàbat, F., Fernandez, M. 1997. “The Western Mediterranean extensional basins and the Alpine orogen.” *Terra Nova* 9: 109-112.
- Dogliani, C., Mongelli, F., Piali, G. 1998. “Boudinage of the Alpine belt in the Apenninic back-arc.” *Memorie della Società Geologica Italiana* 52, 457–468.
- Dogliani, C., Gueguen, E., Harabaglia, P., Mongelli, F. 1999. “On the origin of wes-directed subduction zone and applications to the western Mediterranean.” In: the Mediterranean Basin: Tertiary Extension within the Alpine Orogen. Edited by B. Durand et al. *Geological Society of London Special Publication* 156, 541-570.
- Dorobek, S.L. 1995. “Synorogenic carbonate platforms and reefs in foreland basins: controls on stratigraphic evolution and platform/reef morphology.” In:

- Dorobek, S.L. and Ross, G.M. (eds.) Stratigraphic evolution of foreland basins: *SEPM* (Society for sedimentary geology). Special Publications 52: 127-147.
- Dubacq, B., Vidal, O., De Andrade, V. 2010. "Dehydration of dioctahedral aluminous phyllosilicates: thermodynamic modelling and implications for thermobarometric estimates." *Contributions to Mineralogy and Petrology* 159 : 159–174.
- Dubois, J., Delpus, C., Diament, M., Danie, J., Colot, J.-Y. 1988. "Subduction of the Bouganville seamount (Vanuatu): mechanical and geodynamic implications." *Tectonophysics* 149: 111-119.
- Dunnet, D. 1969. "A technique of finite strain analysis using particles." *Tectonophysics* 7: 117-136.
- Durand-Delga, M. 1974. "La Corse." *Géologie de la France* 2: 465-478.
- Durand-Delga, M. 1978. "Corse." *Guide de Géologie Régionaux*.
- Durand-Delga M. 1984. "Principaux traits de la Corse Alpine et correlations avec les Alpes Ligures." *Memorie della Società Geologica Italiana* 28: 285-329.
- Durand-Delga, M. Peybernès, B., Rossi, P. 1997. "Arguments en faveur de la position, au Jurassique, des ophiolites de Balagne (Haute-Corse, France) au voisinage de la marge continentale européenne." *Comptes Rendus de Académie de Sciences Paris* 325: 973-981.
- Edel, J.B., Lortscher A. 1977. "Paleomagnetisme du volcanisme tertiaire de la Sardaigne. Nouveaux résultats et synthèse." *Bulletin de la Société Géologique de France* 19: 815- 824.
- Egal E., Caron, J.M. 1988. "Tectonique polyphasée dans l'Eocène autochtone à la bordure ouest de la Nappe de Balagne (Corse)." *Bulletin de la Société Géologique de France* 8: 315–321.
- Egal, E. 1992. "Structures and tectonic evolution of the external zone of Alpine Corsica." *Journal of Structural Geology* 14: 1215-1228.
- Elburg, M.A. 1996. "U-Pb ages and morphologies of zircon in microgranitoid enclaves and peraluminous host granite: evidence for magma mingling." *Contributions to Mineralogy and Petrology* 123, 177-189.
- Elter, P., Pertusati, P.C. 1973. "Considerazioni sul limite Alpi-Appennino e sulle relazioni con l'arco della Alpi Occidentali." *Memorie della Società Geologica Italiana* 12: 359-375.
- Engi, M. 2017. "Petrochronology based on REE-Minerals: Monazite, Allanite, Xenotime, Apatite." *Reviews in Mineralogy and Geochemistry* 83: 365-418.
- Engi, M., Berger, A., Roselle, G. 2001. "The role of the tectonic accretion channel in collisional orogeny." *Geology* 29: 1143-1146.
- England, P.C., Houseman, G.A. 1989. "Extension during continental convergence, with application to the Tibetan plateau." *Journal of Geophysical Research* 51: 17561-17579.
- England, P.C., Richardson, S.W. 1977. "The influence of erosion upon the mineral facies of rocks from different metamorphic environments." *Geological Society of London Special Publication* 134: 201-213.
- England, P.C., Thompson, A.B. 1984. "Pressure-temperature-time paths of regional metamorphism. 1. Heat transfer during the evolution of region of thickened continental crust." *Journal of Petrology* 25: 894-928.

- Ercit, T.S. 2002. "The mess that is allanite." *Canadian Mineralogist* 40: 1411-1419.
- Erdman, M.E., Lee, C.-T.A. 2014. "Oceanic-and continental-type metamorphic terranes: Occurrence and exhumation mechanisms." *Earth Science Review* 139: 33-46.
- Ernst, W.G. 1975. "Systematics of large-scale tectonics and age progressions in Alpine and circum-Pacific blueschist belts." *Tectonophysics* 26: 229-246.
- Ernst, W.G. 1990. "Thermobaric and fluid-expulsion history of subduction zones." *Journal of Geophysical Research* 95: 9047-9053.
- Ernst, W.G. 2001. "Subduction, ultrahigh-pressure metamorphism, and regurgitation of buoyant crustal slices – implications for arcs and continental growth." *Physics of the Earth and Planetary Interiors* 1: 253-275.
- Ernst, W.G. 2005. "Alpine and Pacific styles of Phanerozoic mountain building: subduction-zone petrogenesis of continental crust." *Terra Nova* 17(2): 165-188.
- Escher, A., Beaumont, C. 1997. "Formation, burial and exhumation of basement nappes at crustal scale: a geometric model based on the western Swiss- Italian Alps." *Journal of Structural Geology* 19: 995-974.
- Faccenna, C., Mattei, M., Funicicello, R., Jolivet, L. 1997. "Styles of back-arc extension in the Central Mediterranean." *Terra Nova* 9: 126-130.
- Faccenna, C., Becker, T.W., Lucente, F.P., Jolivet, L., Rossetti, F. 2001. "History of subduction and back-arc extension in Central Mediterranean." *Geophysical Journal International* 145: 809-820.
- Faccenna, C., Priomallo, C., Crespo-Blanc, L., Jolivet, L., Rossetti, F. 2004. "Lateral slab deformation and the origin of Western Mediterranean arcs." *Tectonics* 23: TC1012.
- Faure, M., Malavieille, J. 1981. "Étude structurale d'un cisaillement ductile: le charriage ophiolitique corse dans la région de Bastia." *Bulletin de la Société Géologique de France* 23(4): 335-343.
- Favre, P., Stampfli, G.M. 1992. "From rifting to passive margin: the example of the Red Sea, Central Atlantic and Alpine Tethys." *Tectonophysics* 215: 69-97.
- Federico, L., Capponi, G., Crispini, L., Scambelluri, M., Villa, I.M. 2005. "³⁹Ar/⁴⁰Ar dating of high-pressure rocks from the Ligurian Alps: Evidence for a continuous subduction–exhumation cycle." *Earth and Planetary Science Letters* 240(3): 668-680.
- Federico, L., Spagnolo, C., Crispini, L., Capponi, G. 2009. "Fault-slip analysis in the metaophiolites of the Voltri Massif: constraints for the tectonic evolution at the Alps/Apennine boundary." *Geological Journal* 44(2): 225-240.
- Fellin, M.G., Picotti, V., Zattin, M. 2005. "Neogene to Quaternary rifting and inversion in Corsica: Retreat and collision in the western Mediterranean." *Tectonics* 24: TC1011, doi:10.1029/2003TC001613.
- Fellin, M.G., Vance, J.A., Garver, J.I., Zattin, M. 2006. "The thermal evolution of Corsica as recorded by zircon fission tracks." *Tectonophysics* 421: 299-317.
- Ferrandini, M., Ferrandini, J., Loye-Pilot, M.D., Butterlin, J., Cravatte, J., Janin, M.C. 1998. "Le Miocène du bassin de Saint-Florent (Corse): modalités de la transgression du Burdigalien supérieur et mise en évidence du Serravallien." *Geobios* 31(1): 125-137.

- Ferrandini, J., Gattacceca, J., Ferrandini, M., Deino, A., Janin, M.C., 2003. "Chronostratigraphie et paléomagnétisme des dépôts oligo-miocènes de Corse: implications géodynamiques pour l'ouverture du bassin liguro-provençal." *Bulletin de la Société Géologique de France* 174 (4) : 357–371.
- Ferrandini, J., Ferrandini, M., Rossi, P., Savary-Sismondini, B. 2010. "Définition et datation de la formation de Venaco (Corse): dépôt d'origine gravitaire d'âge Priabonien." *Comptes Rendus de Geoscience* 342: 921-929.
- Ferrill, D.A., Morris, A.P., Evans, M.A., Burkhard, M., Groshong, R.H., Onasch, C.M. 2004. "Calcite twin morphology: A low-temperature deformation geothermometer." *Journal of Structural Geology* 26: 1521–1529.
- Ford, M., Lickorish, W.H., Kuszniir, N.J. 1999. "Tertiary foreland sedimentation in the Southern Subalpine Chains, SE France: a geodynamic appraisal." *Basin Research* 11: 315–336.
- Fournier, M., Jolivet, L., Goffé, B., Dubois, R. 1991. "The Alpine Corsica metamorphic core complex." *Tectonics* 10: 1173–1186.
- Freeman, S.R., Inger, S., Butler, R.W., Cliff, R.A., 1997. "Dating deformation using Rb–Sr in white mica: Greenschist facies deformation ages from the Entrelor shear zone, Italian Alps." *Tectonics* 16(1): 57-76.
- Froitzheim, N., 1992. "Formation of recumbent folds during synorogenic crustal extension (Austroalpine nappes, Switzerland)." *Geology* 20: 923-926.
- Froitzheim, N., Manatchal, G. 1996. "Kinematics of Jurassic rifting, mantle exhumation, passive margin formation in the Austroalpine and Penninic nappes (Eastern Switzerland)." *Geological Society Annual Bulletin* 108: 1120-1333.
- Gabalda, S., Jolivet, L., Agard, P., Chopin, C. 2008. "Thermal structure of a fossil subduction wedge in the Western Alps." *Terra Nova*: 28-34.
- Gaidies, F., Abart, R., De Capitani, C., Schuster, J.A., Connolly, E., Reusser, E. 2006. "Characterization of polymetamorphism in the Austroalpine basement east of Tauern Window using garnet isopleth geothermobarometry." *Journal of Metamorphic Geology* 24: 451-475.
- Ganne, J., Marquer, D., Rosenbaum, G., Bertrand, J.M., Fudral, S. 2006. "Partitioning of deformation within a subduction channel during exhumation of high-pressure rocks: a case study from the Western Alps." *Journal of Structural Geology* 28: 1193-1207.
- Ganne, J., Bertrand, J.M., Fudral, S., Marquer, D., Vidal, O. 2007. "Structural and metamorphic evolution of the Ambin massif (western Alps): toward a new alternative exhumation model for the Briançonnais domain." *Bulletin de la Société Géologique de France* 178: 437–458.
- Gardien, V., Reusser, E., Marquer, D. 1994. "Pre-Alpine metamorphic evolution of the gneisses from the Volpeline series (Western Alps, Italy)." *Schweizerische Mineralogische und Petrographische Mitteilungen* 74: 489-502.
- Gardner, R.L., Piazzolo, S., Daczko, N.R. 2015. "Pinch and swell structures: evidence for strain localisation by brittle-viscous behaviour in the middle crust." *Solid Earth* 6: 1045-1061.
- Garfagnoli, F., Menna, F., Pandeli, E., Principi, G. 2009. "Alpine metamorphic and tectonic evolution of the Inzecca-Ghisoni area (southern Alpine Corsica,

- France)." *Geological Journal* 44: *Geological Journal* 191–210.
- Gelmini, R., Mantovani, M.P. 1982. "La successione triassica di Col de Serna (Corsica Settentrionale)." *Rivista Italiana di Paleontologia* 88(1): 11-20.
- Gerber, W. 2008. "Evolution tectono-metamorphique du Brianconnais interne (Alpes occidentales, massifs de la Vanoise et d'Ambin): compotement du socle et de sa couverture dans un context de subduction continentale profonde." Ph.D. thesis. Université Paris.
- Gerya T.V., Perchuk L.L., Maresch, W.V., Willner A.P., Van Reenen, D.D., Smit, C.A. 2002. "Thermal regime and gravitational instability of multi-layered continental crust: implications for the buoyant exhumation of high-grade metamorphic rocks." *European Journal of Mineralogy* 14: 687-699.
- Gerya, T., Stockhert, B. 2006. "Two-dimensional numerical modeling of tectonic and metamorphic histories at active continental margins." *International Journal of Earth Sciences* 95: 250–274.
- Gerya T.V., Perchuk, L.L., Burg J.P. 2008. "Transient hot channels: perpetrating and regurgitating ultrahigh-pressure, high temperature crust-mantle associations in collision belts." *Lithos* 103: 236-256.
- Giacomini, F., Dallai, L., Carminati, E., Tiepolo, M., Ghezzi, C. 2008. "Exhumation of a Variscan orogenic complex: insights into the composite granulitic-amphibolitic metamorphic basement of south-east Corsica (France)." *Journal of Metamorphic Geology* 26: 403-436.
- Gibbons, W., Horak, J., 1984. "Alpine metamorphism of Hercynian hornblende granodiorite beneath the blueschist facies Schistes Lustrés nappe of NE Corsica." *Journal of Metamorphic Geology* 2: 95-113.
- Gibbons, W., Waters, C., Warburton, J. 1986. "The blueschist facies Schistes Lustrés of Alpine Corsica: a review." *GSA Bulletin Memoires* 164: 301-331.
- Gieré, R., Sorensen, S.S. 2004. "Allanite and other REE-rich Epidote-group minerals." *Reviews in Mineralogy and Geochemistry* 56: 431-493.
- Godin, L., Grujic, D., Law, R.D., Searle, M.P. 2006. "Channel Flow, Ductile Extrusion and Exhumation in Continental Collision Zones." *Geological Society of London Special Publication* 268: 1-23.
- Goffé, B., Bousquet, R., Henry, P., Le Pichon, X. 2003. "Effect of the chemical composition of the crust on the metamorphic evolution of orogenic wedges." *Journal of Metamorphic Geology* 21: 123-141.
- Gorini, C., Mauffret, A., Guennoc, P., Le Marrec, A. 1994. "Structure of the Gulf of Lions (northwestern Mediterranean Sea): a review." In: Mascle, A. (eds.) Hydrocarbon and Petroleum Geology of France." *Association of Petroleum Geology* 4: 223-243.
- Gradstein, F.M., Ogg, J.G., Schmitz, M.D. 2012. "The Geologic Time Scale 2012." Boston, USA, *Elsevier*. doi: 10.1016/B978-0-444-59425-9.00004-4.
- Grasemann, B., Ratschbacher, L., Hacker, B. R. 1998. "Exhumation of Ultrahigh-pressure Rocks: thermal boundary conditions and cooling history. In: Hacker, B.R., Liou, J.G. (eds.) When Continents collide: Geodynamic and Geochemistry of ultrahigh pressure rocks." *Kluwer*: 117-139.
- Gregory, C.J., Rubatto, D., Hermann, J., Berger, A., Engi, M. 2012. "Allanite behavior during incipient melting in the southern Central Alps." *Geochimica and Cosmochimica Acta* 84: 433-458.

- Groshong, R.H. 1972. "Strain calculated from twinning in calcite." *GSA Bulletin* 82: 2025-2038.
- Groshong, R.H. 1974. "Experimental test of least-squares strain gage calculation using twinned calcite." *GSA Bulletin* 86: 1363-1376.
- Grujic, D., Manckletow, N.S. 1996. "Structure of the northern Maggia and Lebendun Nappes, Central Alps, Switzerland." *Eclogae Geologicae Helveticae*. 89(1): 461-504.
- Gueguen, E., Doglioni, C., Fernandez, M., 1998. "On the post-25 Ma geodynamic evolution of the western Mediterranean." *Tectonophysics* 298: 259-269.
- Guerrera, F., Martin-Algarra, A., Perrone, V. 1993. "Late Oligocene-Miocene syn-/late-orogenic successions in Western and Central Mediterranean Chains from Betic Cordillera to the Southern Apennines." *Terra Nova* 6: 525-544.
- Gueydan, F., Leroy, Y.M., Jolivet, L., Agard, P. 2003. "Analyses of continental midcrustal strain localization induced by microfaulting and reaction softening." *Journal of Geophysical Research* 108: 2064-2081.
- Gueydan, F., Brun, J-P, Phillippon, M., Noury, M. 2017. "Sequential extension as a record of Corsica Rotation during Apennines slab roll-back." *Tectonophysics* doi:10.1016/j.tecto.2016.12.028.
- Guieu, G., Loyer-Pilot, M.D., Lahondère, D., Ferrandini, J. 1994. "Carte géol. France (1/50000), feuille Bastia (1111)." BRGM, Orléans.
- Guillot, S., Hattori, K.H., de Sigoyer, J., Nagler, T., Auzende, A.-L. 2001. "Evidence of hydration of the mantle wedge and its role in the exhumation of eclogites." *Earth and Planetary Science Letters* 193: 115-127
- Guillot, S., Garzanti, E., Baratoux, D., Marquer, D., Mahéo, G., de Sigoyer, J. 2003. "Reconstructing the total shortening history of the NW Himalaya." *Geochemistry Geophysics Geosystems* 4(1): 1-22.
- Guillot S., Hattori K., Agard P., Schwartz S., Vidal O. 2009. "Exhumation Processes in Oceanic and Continental Subduction Contexts: A Review." In: Lallemand S. and Funicello F. (eds.), *Subduction Zone Geodynamics*, Springer-Verlag Berlin: 175-205.
- Habler, G., Thöni, M. 2001. "Preservation of Permo-Triassic low-pressure assemblages in the Cretaceous high pressure metamorphic Saualpe crystalline basement (Eastern Alps, Australia)." *Journal of Metamorphic Geology* 19: 679-697.
- Hall, P.S., Kincaid, C. 2001. "Diapiric flow at subduction zones: A recipe for rapid transport." *Science* 292: 2472-2475. doi:10.1126/SCIENCE.1060488.
- Handy, M.R., Schmid, S.M., Bousquet, R., Kissling, E., Bernoulli, D. 2010. "Reconciling plate-tectonic reconstructions of Alpine Tethys with the geological-geophysical record of spreading and subduction in the Alps." *Earth Science Review* 102: 121-158.
- Harris, L., 1985. "Progressive and polyphase deformation of the Schistes Lustrés in Cap Corse, Alpine Corsica." *Journal of Structural Geology* 7(6): 637-650
- Heaman, L.M., Parrish, R.R. 1991. "*U-Pb geochronology of accessory minerals*." Mineralogical Association: Canada.
- Hermann, J., Müntener, O. 1996. "Extension-related structures in the Malenco-Margna system: implications for the Paleogeography and consequences for

- rifting and Alpine tectonics.” *Schweizerische Mineralogische und Petrographische Mitteilungen* 76: 501-519.
- Hillier, S., Velde, B. 1991. “Octahedral occupancy and the chemical composition of diagenetic (low-temperature) chlorites.” *Clay Minerals* 26: 146–168.
- Hirt, G., Tullis, J. 1994. “The brittle-plastic transition in experimentally deformed quartz aggregates.” *Journal of Geophysical Research* 99: 11731-11747.
- Hobbs, N. 2014. “Structural and tectonic study of Pedani and the surrounding area (Alpine Corsica).” Msc. Thesis. Università di Pisa.
- Holland, T., Blundy, J. 1994. “Non-ideal interactions in calcic amphiboles and their bearing on amphibole-plagioclase thermometry.” *Contributions to Mineralogy and Petrology* 116: 433-447.
- Huerta, A.D., Royden, L.H., Hodges, K.V. 1998. “The thermal structure of collisional orogens as a response to accretion, erosion and radiogenic heating.” *Journal of Geophysical Research* 103:15.287-15.302.
- Irfan, M., Shahid, M., Haroon, M., Abbas Zaidi, N. 2005. “Sargodha High: flexure forebulge of the Himalayan foreland basin.” *Geological Bulletin of the University of Peshawar* 38: 149-156.
- Jackson, S. 2008. “LAMTRACE data reduction software for LA-ICP-MS. In: Sylvester P. (Eds.), Laser ablation-ICP-mass spectrometry in the Earth sciences: Current practices and outstanding issues.” *Mineralogical Association of Canada Short Course Series* 40: 305–307.
- Jakni, B., Poupeau, G., Sosson, M., Rossi, P., Ferrandini, J., Guennoc, P. 2000. “Dénudations cénozoïques en Corse: une analyse thermochronologique par traces de fission sur apatites.” *Comptes Rendus de Académie de Sciences Paris* 331: 775-782.
- Jamieson, R.A., Beaumont, C., Fulsack, P. 1998. “Barrovian regional metamorphism: where’s the heat? In: Treloar, P.J., O’Brian, P.J. (eds.) What drives metamorphism and metamorphic reactions?” *Geological Society Special Publications* 138: 23-46.
- Janots, E., Negro, F., Brunet, F., Goffé, B., Engi, M., Bouybaouene, M.L. 2006. “Evolution of the REE mineralogy in HP-LT metapelites of the Sebide complex, Rif, Morocco: monazite stability and geochronology.” *Lithos* 87: 214-234.
- Janots, E., Engi, M., Berger, A., Allaz, J., Schwartz, J.O., Spandler, C. 2008. “Prograde metamorphic sequence of REE minerals in pelitic rocks of Central Alps: implications for allanite-monazite-xenotime phase relations from 250 to 610°C.” *Journal of Metamorphic Geology* 26: 509-526.
- Jarrard, R. 1986. “Relation among subduction parameters.” *Revision in Geophysics* 24(2): 217-284.
- Jessup, M.J., Law, R.D., Searle M.P., Hubbard, M.S. 2006. “Structural evolution and vorticity of flow during extrusion and exhumation of the Greater Himalayan Slab, Mount Everest massif, Tibet/Nepal: implications for orogeny-scale flow partitioning.” In: Law, R.D., Searle, M.P., Godin, L., (eds.) Channel Flow, ductile Extrusion and exhumation in Continental collision zones. *Geological Society of London Special Publication* 268: 379-413.

- Jolivet, J. 1993. "Extension of thickened continental crust, from brittle to ductile deformation: examples from Alpine Corsica and Aegean Sea." *Annali di Geofisica* 36 (2): 139-153.
- Jolivet L., Dubois R., Fournier M., Goffé B., Michard A., Jordan C. 1990. "Ductile extension in Alpine Corsica." *Geology* 18: 1007–1010.
- Jolivet, L., Daniel, J.M., Fournier, M. 1991. "Geometry and Kinematics of ductile extension in Alpine Corsica." *Earth and Planetary Science Letters* 104: 278-291.
- Jolivet, L., Faccenna, C., Goffé, B., Mattei, M., Rossetti, F., Brunet, C., Storti, F., Funicciello, R., Cadet, J.-P., D'Agostino, N., Parra, T. 1998. "Midcrustal shear zones in post-orogenic extension: Example from the Tyrrhenian Sea." *Journal of Geophysical Research* 103: 12-123.
- Jolivet, L., Faccenna, C., Goffé, B., Burov, E., Agard, P. 2003. "Subduction tectonics and exhumation of high-pressure metamorphic rocks in the Mediterranean orogens." *American Journal of Sciences* 303 : 353-409.
- Jolivet, L., Gorini, C., Smit, J., Leroy, S. 2015. "Continental breakup and dynamics of rifting in back-arc basins: The Gulf of Lion margin." *Tectonics* 34: 662-679.
- Jordan, T.E. 1981. "Thrust loads and foreland basin evolution. Cretaceous, Western United States." *American Association of Petroleum Geology Bulletin* 65: 2506-2520.
- Jourdan, C. 1988. "Balagne orientale et massif du Tenda (Corse septentrionale): etude structural, interpretation des accidents et des deformation reconstructions géodynamiques." Ph.D. thesis. Université de Paris.
- Kamber, F., Frei, R., Gibb, A. 1998. "Pitfalls and new approaches in granulite chronometry: an example from the Limpopo belt, Zimbabwe." *Precambrian Research* 91: 269-285.
- Karioris, F.G., Gowda, K., Cartz, L. 1981. "Heavy ion bombardment on monoclinic ThSiO₂, ThO₂ and monazite." *Radiation Effects Letters* 58:1-3.
- Kastens et al., 1987. "Proc. ODP Init. Repts., 107." College station, Tex (Ocean Drilling Program).
- Kearey, P., Klepeis, K.A., Vine, F.J. 2009. *Global tectonics*. Wiley-Blackwell.
- Kim, Y.S., Andrews, J.R., Sanderson, D.J. 2000. "Damage zones around strike-slip fault systems and strike-slip fault evolution, Carkington Haven, southwest England." *Geoscience Journal* 4: 53-72.
- Kim, Y.S., Peacock, D.C.P., Sanderson, D.J. 2004. "Fault damage zones." *Journal of Structural Geology* 26: 503-517.
- Krenn, E., Finger, F. 2007. "Formation of monazite and rhabdophane at the expense of allanite during Alpine low temperature retrogression of metapelitic basement rocks from Crete, Greece: microprobe data and geochronological implication." *Lithos* 95: 130-147.
- Lacombe, O., Jolivet, L. 2005. "Structural and kinematic relationships between Corsica and the Pyrenees-Provence domain at the time of the Pyrenean orogeny." *Tectonics* 24: TC1003, doi: 10.1029/2004TC001673
- Lagabriele, Y., Lemoine, M. 1997. "Alpine, Corsican and Appennine ophiolites: the slowspreading ridge model." *Comptes Rendus de Académie de Sciences Paris* 325 : 909 - 920.

- Lagabrielle, Y., Polino, R. 1988. "Un schéma structural du domaine des Schistes Lustrés ophiolitifères au nord-ouest du massif du mont Viso (Alpes sudoccidentales) et ses implications." *Comptes Rendus de Académie de Sciences Paris* 323 : 957-964.
- Lahondère, D. 1983. "Carte géol. France (1/50000)." *BRGM*, Orléans.
- Lahondère, D. 1988. "Le métamorphisme éclogitique dans les orthogneiss et les metabasites ophiolitiques de la région de Farinole (Corse)." *Bulletin de la Société Géologique de France* 8 : 579-585.
- Lahondère D. 1991. "Les schistes bleus et les éclogites à lawsonite des unités continentales et océaniques de la Corse alpine: Nouvelles données pétrologiques et structurales." Ph.D. thesis. Université Montpellier.
- Lahondère, D. 1996. "Les schistes bleus et les éclogites à lawsonite des unités continentales et océaniques de la Corse alpine: Nouvelles données pétrologiques et structurales (Corse)." *Documents du BRGM*, 240.
- Lahondère, D., Caby, R. 1989. "Les méta-conglomérates polygéniques des schistes lustrés de la vallée du Golo (Corse alpine): signification paléogéochronologique et conséquence tectoniques." *Comptes Rendus de Académie de Sciences Paris* 309 : 727-732.
- Lahondère, D., Guerrot, C. 1997. "Datation Sm-Nd du métamorphisme éclogitique en Corse alpine: un argument pour l'existence au Crétacé supérieur d'une zone de subduction active localisée sous le bloc corso-sarde." *Géologie de France* 3 :3-11.
- Lahondère, J.C., Lahondère, D. 1988. "Organisation structurale des schistes Lustrés du Cap Corse (Haute Corse)." *Comptes Rendus de Académie de Sciences Paris* 307 : 1081-1086.
- Lahondère D., Rossi P., Lahondère J.C. 1999. "Structuration alpine d'une marge continentale externe: le massif du Tenda (Haute-Corse). Implication géodynamiques au niveau de la transversale Corse-Appennins." *Géologie de France* 4: 27-44.
- Lanari, P. 2012. "Micro-cartographie P-T-' dans les roches métamorphiques. Applications aux Alpes et à l'Himalaya." Ph.D. thesis. Université de Grenoble.
- Lanari, P., Guillot, S., Schwartz, S., Vidal, O., Tricart, P., Riel, N., Beyssac, O. 2012. "Diachronous evolution of the alpine continental subduction wedge: evidence from P-T estimates in Briançonnais zone houillère (France-Western Alps)." *Journal of Geodynamics* 56-57: 39-54.
- Lanari, P., Wagner, T., Vidal, O. 2014a. "A thermodynamic model for di-trioctahedral chlorite from experimental and natural data in the system MgO-FeO-Al₂O₃-SiO₂-H₂O: applications to P-T sections and geothermometry." *Contributions to Mineralogy and Petrology* 167. doi:10.1007/s00410-014-0968-8.
- Lanari, P., Rolland, Y., Schwartz, S., Vidal, O., Guillot, S., Tricart, P., Domont, T. 2014b. "P-T-t estimation of deformation in low-grade quartz-feldspar-bearing rocks using thermodynamic modelling and ⁴⁰Ar/³⁹Ar dating techniques: example of the Plan-de-Phasy shear zone unit (Briançonnais Zone, Western Alps)." *Terra Nova* 26: 130-138.

- Lanari, P., Vidal, O., De Andrade, V., Dubacq, B., Lewin, E., Grosch, E., Schwartz, S. 2014c. "XMAPTOOLS: a MATLAB c -based program for electron microprobe X-ray image processing and geothermobarometry." *Computers and Geoscience* 62 : 227-240.
- Lapen, T.J., Johnson, C.M., Baumgartner, L.P., Dal Piaz, G.V., Skora, S., Beard, B. 2007. "Coupling of oceanic and continental crust during Eocene eclogite-facies metamorphism : evidence from Monte Rosa nappe, Western Alps." *Contributions to Mineralogy and Petrology* 153 : 139-157.
- Laporte, D., Fernandez, A., Orsini, J.B. 1991. "Le complexe d'île Rousse, Balagne, Corse du Nord-Ouest: pétrologie et cadre de mise en place des granitoïdes magnésio-potassiques." *Géologie de France* 4: 15-30.
- Lardeaux, J.M., Spalla, M.I. 1991. "From granulites to eclogites in the Sesia zone (Italian Western Alps): a record of the opening and closure of the Piedmont ocean." *Journal of Metamorphic Geology* 9: 15-30.
- Laubscher, H.P. 1991. "The arcs of western Alps today." *Eclogae Geologicae Helvetiae* 84: 613-651.
- Law, R.D., Searle, M.P., Simpson, R.L. 2004. "Strain, deformation temperatures and vorticity of flow at the top of Greater Himalayan Slab, Everest Massif, Tibet." *Journal of Society of London* 161: 305-320.
- Le Bayon, B., Ballèvre, M. 2006. "Deformation history of a subducted continental crust (Gran Paradiso, Western Alps): continuing crustal shortening during exhumation." *Journal of Structural Geology* 28: 793-815.
- Leake, B.E., Wooley, A.R., Arps, C.E.S., Birch, W.D., Gilbert, M.C., Grice, J.D., Hawthorne, F.C., Kato, A., Kisch, H.I., Krivovichev, V.G., Linthout, K., Laird, J., Mandarino, J.A., Maresch, W.V., Nickel, E.H., Rock, N.M.S., Schumacher, J.C., Smith, D.C., Stephenson, N.C.N., Ungaretti, L., Whittaker, E., Youzhi, G. 1997. "Nomenclature of Amphiboles. Report of the subcommittee on amphiboles of the International Mineralogical Association Commission on New Minerals and Mineral Names." *Mineralogical Magazine* 61: 259-321.
- Leoni, L., Sartori, F., Tamponi, M. 1998. "Compositional variation in K-white micas and chlorites coexisting in Al-saturated metapelites under late diagenetic to low-grade metamorphic conditions (internal Liguride Units, Northern Apennines, Italy)." *European Journal of Mineralogy* 10:1321-1339.
- Levi, N., Malasoma, A., Marroni, M., Pandolfi, L., Paperini, M. 2007. "Tectono-metamorphic history of the ophiolitic Lento unit (northern Corsica): evidences for the complexity of accretion-exhumation processes in a fossil subduction system." *Geodinamica Acta* 20(1): 99-118.
- Liao, J., Malusà, M.G., Zhao, L., Baldwin, S.L., Fitzgerald, P.G., Gerya, T. 2018. "Divergent plate motion derives rapid exhumation of (ultra)high pressure rocks." *Earth and Planetary Science Letters* 491: 67-80.
- Libourel, G. 1985. "Le complexe de Santa Lucia di Mercurio (Corse): in équivalente possible des complexes de la zone d'Ivrée." *Comptes Rendus de Académie de Sciences Paris* 307: 1067-1073.
- Libourel, G. 1988. "Le complexe de Santa Lucia di Mercurio (Corse)." Ph.D. thesis. Université de Toulouse.
- Lin, C.-H. 2000. "Thermal modeling of continental subduction and exhumation

- constrained by heat flow and seismicity in Taiwan.” *Tectonophysics* 324: 198-201.
- Llyod, G.E., Freeman, B. 1994. “Dynamic recrystallization of quartz and quartzites.” *Journal of Structural Geology* 16: 867-881.
- Loury, C., Rolland, Y., Guillot, S., Lanari, P., Ganino, C., Melis, R., Jourdan, A., Petit, C., Beysac, O., Galet, S., Monié, P. 2018. “Tectonometamorphic evolution of the Atbashi high-P units (Kyrgys CAO, Tien Shan): Implications for the closure of the Turkestan Ocean and continental subduction-exhumation of the South Kazakh continental margin.” *Journal of Metamorphic Geology* 1-27. Doi: 10.1111/jmg.12423.
- Lu, M.H., Hofmann, A.W., Mazzucchelli, M., Rivalenti, G. 1997. “The mafic-ultramafic complex near Finero (Ivrea-Verbano Zone). 2. Geochronology and isotope geochemistry.” *Chemical Geology* 140(3-4): 223-235.
- Lucente, F., Margheriti, L., Piromallo, C., Barruol, G. 2006. “Seismic anisotropy reveals the long route of the slab through the western-central Mediterranean mantle.” *Earth and Planetary Science Letters* 241: 517-529.
- Maggi M., Rossetti, F., Corfu, F., Theye, T., Andersen, T.B., Faccenna, C. 2012. “Clinopyroxene-rutile phyllonites from East Tenda Shear Zone (Alpine Corsica, France): pressure-temperature-time constraints to the Alpine reworking of Variscan Corsica.” *Geological Society of London* 169: 723-732.
- Maggi, M., Rossetti, F., Ranalli, G., Theye, T. 2014. “Feedback between fluid infiltration and rheology along a regional ductile-to-brittle shear zone the East Tenda Shear Zone (Alpine Corsica).” *Tectonics* 33: 253-280.
- Mailhé, D. 1982. “Application des méthodes de datation $^{40}\text{Ar}/^{39}\text{Ar}$ et traces de fission à l’étude du déroulement de l’orogénèse en Corse.” Ph.D. thesis. Université de Montpellier.
- Malasoma, A. 2006. “Tectono-metamorphic evolution of the external continental units of “Alpine Corsica” (Northern Corsica, France).” Ph.D. thesis. Università di Pisa.
- Malasoma, A., Marroni, M., Musumeci, G., Pandolfi, L. 2006. “High pressure mineral assemblage in granitic rocks from continental units, Alpine Corsica, France.” *Geological Journal* 41: 49-59.
- Malasoma, A., Marroni, M. 2007. “HP/LT metamorphism in the Volparone Breccia (Northern Corsica, France): evidence for involvement of the Europe/Corsica continental margin in the Alpine subduction zone.” *Journal of Metamorphic Geology* 25: 529-545.
- Malavieille, J. 1983. “Etude tectonique de la nappe de socle Centuri (zone de Schistes Lustrés de la Corse); Conséquence pour la géométrie de la chaîne alpine.” *Bulletin de la Société Géologique de France* 25: 195-204.
- Malavieille, J., Chemenda, A., Larroque, C. 1998. “Evolutionary model for the Alpine Corsica: mechanism for ophiolite emplacement and exhumation of high-pressure rocks.” *Terra Nova* 10: 317-322.
- Malinverno, A., Ryan, W.B.F. 1986. “Extension in the Tyrrhenian Sea and shortening in the Apennines as a result of arc migration driven by the sinking of the lithosphere.” *Tectonics* 5: 227-245.
- Maluski, H., Mattauer, M., Matte, P.H. 1973. “Sur la présence de décrochement alpins en Corse.” *Comptes Rendus de l’Académie de Sciences Paris* 276 : 709-712.

- Maluski, H. 1977. "Application de la méthode $^{40}\text{Ar}/^{39}\text{Ar}$ aux minéraux des roches cristallines perturbées par des événements thermiques et tectoniques en Corse." Ph.D. thesis. Université de Montpellier.
- Manatschal, G. 1995. "Jurassic rifting and formation of a passive continental margin (Platta and Err nappes, Eastern Switzerland): geometry, kinematics and geochemistry of fault rocks and comparison with Galicia margin." Ph.D. thesis. Zurich Universitat.
- Manatschal, G., Müntener, O. 2009. "A type-sequence across an ancient magma-poor ocean-continent transition: the example of the western Alpine Tethys ophiolites." *Tectonophysics* 473 (1-2): 4-19.
- Manzotti, P., Rubatto, D., Darling, J., Zucali, M., Cenko-Tok, B., Engi, M. 2012. "From Permo-Triassic lithospheric thinning to Jurassic rifting at the Adriatic margin: Petrological and geochronological record in Valourneche (Western Italian Alps)." *Lithos* 146-147: 276-292.
- Markley, M.J., Teyssier, C., Cosca, M.A. Caby, R., Hunziker, J.C., Sartori, M. 1998. "Alpine deformation $^{40}\text{Ar}/^{39}\text{Ar}$ geochronology of synkinematic white mica in the Siviez-Mischabel Nappe, western Pennine Alps, Switzerland." *Tectonics* 17: 407-425.
- Marotta, A.M., Spalla, M.I. 2007. "Permian-Triassic high thermal regime in the Alps: results of the Late Variscan collapse or continental rifting? Validation by numerical modeling." *Tectonics* 26(4).
- Marotta, A.M., Spalla, M.I., Gosso, G. 2009. "Upper to lower crustal evolution during lithospheric extension: numerical modelling and natural footprints from the European Alps." In: Ring, U., Wernicke, B. (eds.) *Extending a Continent: architecture, Rheology and heat budget. Geological Society of London Special Publication* 321: 33-72.
- Marroni, M., Pandolfi, L. 2003. "Deformation history of the ophiolite sequence from the Balagne Nappe, northern Corsica: insights in the tectonic evolution of the Alpine Corsica." *Geological Journal* 38: 67-83
- Marroni, M., Pandolfi, L. 2007. "The architecture of an incipient oceanic basin: a tentative reconstruction of the Jurassic Liguria-Piemonte basin along the Northern Apennine-Alpine Corsica transect." *International Journal of Earth Sciences*: 1059-1078.
- Marroni, M., Monechi, S., Perilli, N., Principi, G., Treves, B. 1992. "Cretaceous flysch deposits of the Northern Apennines, Italy: age of inception of orogenesis-controlled sedimentation." *Cretaceous Research* 13: 487-504.
- Marroni, M., Molli, G., Montanini, A., Tribuzio R. 1998. "The association of continental crust rocks with ophiolites in the Northern Apennines (Italy): implications for the continent-ocean transition in the Western Tethys." *Tectonophysics* 292: 43 - 66.
- Marroni, M., Molli, G., Ottria, G., Pandolfi, L. 2001. "Tectono-sedimentary evolution of the External Liguride units (Northern Apennines, Italy). Insights in the pre-collisional history of a fossil ocean-continent transition zone." *Geodinamica Acta* 14: 307 - 320.
- Marroni, M., Pandolfi, L., Meneghini, F. 2004. "From accretion to exhumation in a fossil accretionary wedge: a case history from Gottero Unit (Northern Apennines, Italy)." *Geodinamica Acta* 17: 41-53.

- Marroni, M., Meneghini, F., Pandolfi, L. 2010. "Anatomy of the Ligure-Piemontese subduction system: evidence from Late Cretaceous-Middle Eocene convergent margin deposits from Northern Apennines (Italy)." *International Geology Review* 10-12: 1160-1192.
- Martin, A.J., Rubatto, D., Vitale Brovarone, A., Hermann, J. 2011. "Late Eocene lawsonite-eclogite facies metasomatism of a granulite sliver associated to ophiolites in Alpine Corsica." *Lithos* 125: 620-640.
- Massonne, H.J., Schreyer, W. 1987. "Phengite geobarometry based on the limiting assemblage with K-feldspar, phlogopite, and quartz." *Contributions to Mineralogy and Petrology* 96: 212-224.
- Massonne, H.J., Szpurka, Z. 1997. "Thermodynamic properties of white micas on the basis of high-pressure experiments in the systems K_2O - MgO - Al_2O_3 - SiO_2 - H_2O and K_2O - FeO - Al_2O_3 - SiO_2 - H_2O ." *Lithos* 41: 229-250.
- Massonne, H.J., Cruciani, G., Franceschelli, M., Musumeci, G. 2017. "Anticlockwise pressure-temperature paths record Variscan upper-plate exhumation: example from micaschists of the Porto Vecchio region, Corsica." *Journal of Metamorphic Geology*: 1-23.
- Mattauer, M., Proust, F. 1975. "La Corse alpine: un modèle de genèse du métamorphisme haute pression par subduction de croûte continentale sous du matériel océanique." *Comptes Rendus de Académie de Sciences Paris* 282: 1249-1252.
- Mattauer, M., Proust, F. 1976. "La Corse alpine: un modèle de genèse du métamorphisme haute pression par subduction de croûte continentale sous du matériel océanique." *Comptes Rendus de Académie de Sciences Paris* 282: 1249-1251.
- Mattauer, M., Proust, F., Etchecopar, A. 1977. "Linéation "a" et mécanisme de cisellement simple liés au chevauchement de la nappe de schistes lustrés en Corse." *Bulletin de la Société Géologique de France* 14: 841-945.
- Mattauer, M., Faure, M., Malavieille, J. 1981. "Transverse lineation and large-scale structures related to Alpine obduction in Corsica." *Journal of Structural Geology* 3(4): 401-409.
- Mauffret, A., Contrucci, I., Brunet, C. 1999. "Structural evolution of the northern Tyrrhenian Sea from new seismic data." *Marine and Petroleum Geology* 16: 381-407.
- Maury, E. 1910. "Feuille de Corte." *Bulletin du Service de Carte géologique de France* 21: 128.
- Meneghini, F., Marroni, M., Moore, J.C., Pandolfi, L., Rowe, C.D. 2009. "The record of underthrusting and underplating in the geologic record: Structural diversity between the Franciscan Complex (California), the Kodiak Complex (Alaska) and the Internal Ligurian Units (Italy)." *Geological Journal* 44(2): 126-152.
- Ménot, R.P., Orsini, J.B. 1990. "Evolution du socle anté-stéphanien de Corse: événements magmatiques et métamorphiques." *Schweizerische Mineralogische und Petrographische Mitteilungen* 70 : 35-53.
- Ménot, R.P. 1990. "Evolution du socle anté-Stéphanien de Corse." *Schweizerische Mineralogische und Petrographische Mitteilungen* 70: 35-54.

- Meresse, F., Lagabrielle, Y., Malavieille, J., Ildefonse, B. 2012. "A fossil ocean-continent transition of the Mesozoic Tethys preserved in the Schistes Lustrés nappe of northern Corsica." *Tectonophysics* 579: 4-16.
- Michard, A., Martinotti, G. 2002. "The Eocene unconformity of the Briançonnais domain in the French-Italian Alps, revisited (Marguareis massif, Cuneo); a hint for a Late Cretaceous-Middle Eocene frontal bulge setting." *Geodinamica Acta* 15: 289-301.
- Michard, A., Chalouan, A., Feinberg, H., Goffé, B., Montigny, R. 2002. "How does the Alpine belt end between Spain and Morocco?" *Bulletin de la Société Géologique de France* 173 : 3-15.
- Miller, C., Thöni, M. 2009. "The "Permian event" in the Eastern European Alps: Sm-Nd and P-T data recorded by multi-stage garnet from the Plankogel unit." *Chemical Geology* 260: 20-36.
- Miyashiro, A. 1973. "Paired and unpaired metamorphic belts." *Tectonophysics* 17: 241-254.
- Moeller, S., Grevemeyer, I., Ranero, C.R., Berndt, C., Kleschen, D., Sallares, V., Zitellini, N., de Franco, R. 2013. "Early-stage rifting of the northern Tyrrhenian Sea Basin: results from a combined wide-angle and multichannel seismic study." *Geochemistry, Geophysics and Geostatistics* 14: 3032-3052.
- Moeller, S., Grevemeyer, I., Ranero, C.R., Berndt, C., Kleschen, D., Sallares, V., Zitellini, N., de Franco, R. 2014. "Crustal thinning in the northern Tyrrhenian rift: insights from multichannel and wide-angle seismic data across the basin." *Journal of Geophysical Research* 119: 1655-1677.
- Mohn, G., Manatschal, G., Muntener, O., Beltrando, M., Masini, E. 2009. "Unravelling the interaction between tectonic and sedimentary process during lithospheric thinning in the Alpine Tethys margins." *International Journal of Earth Sciences* 99: S75-S101.
- Mohn, G., Manatschal, G., Masini, E., Muntener, O. 2011. "Rift-related inheritance in orogens: a case study from the Austroalpine nappes in Central Alps (SE-Switzerland and N-Italy)." *International Journal of Earth Sciences* 100: 937-961.
- Molli, G. 2008. "Northern Apennine-Corsica orogenic system: an updated overview." In: Siegesmund S., Fugenschuh B., Froitzheim N. (eds.) *Tectonic Aspects of the Alpine-Dinaride-Carpathian System*, *Geological Society of London Special Publication* 298: 413-442.
- Molli, G., Malavieille J. 2011. "Orogenic processes and the Corsica/Apennines geodynamic evolution: insights from Taiwan." *International Journal of Earth Sciences* 100: 1207-1224.
- Molli, G., Tribuzio, R. 2004. "Shear zones and metamorphic signature of subducted continental crust as tracers of the evolution of the Corsica/Northern Apennine orogenic system." In: Alsop, G.I., Holdsworth, R.E., McCaffrey, K.J.W., Handy, M. (eds.) *Flow processes in faults and shear zones* *Geological Society of London Special Publication* 224: 321-335.
- Molli, G., Tribuzio, R., Marquer, D. 2006. "Deformation and metamorphism at the eastern border of Tenda Massif (NE Corsica): a record of subduction and exhumation of continental crust." *Journal of Structural Geology* 28: 1748-1766.

- Molli, G., Menegon, L., Malasoma, A. 2017. "Switching deformation mode and mechanisms during subduction of continental crust: a case study from Alpine Corsica." *Solid Earth Discussion* Doi:10.5194/se-2017-11.
- Montigny, R., Edell, J.B. 1981. "Oligo-Miocene rotation of Sardinia: K-Ar ages and paleomagnetic data of Tertiary volcanics." *Earth and Planetary Science Letters* 54: 261-271.
- Müntener, O., Hermann, J. 2001. "The role of lower crust and continental upper mantle during formation of non-volcanic passive margin: evidence from the Alps." *Geological Society of London Special Publication* 267-288.
- Nardi, R. 1968. "Le unità alloctone della Corsica e loro correlazione con le unità delle Alpi Occidentali e Appennini." *Memorie della Società Geologica Italiana* 7: 323-344.
- Nardi, R., Puccinelli, A., Verani, M. 1978. "Carta geologica della Balagne "sedimentaria" (Corsica) alla scala 1:25000 e note illustrative." *Bollettino della Società Geologica Italiana* 97: 3-22.
- Netelbeek, T.A.F. 1951. "Géologie et pétrologie de la région entre Vezzani et Lugo di Nazza." Ph.D. thesis. University of Amsterdam.
- O'Brien, P.J. 2000. "The fundamental Variscan problem: High temperature metamorphism at different depths and high-pressure metamorphism at different temperatures." In: Franke, W. et al. (eds.) *Orogenic processes: quantification and modelling in the Variscan Belt. Geological Society of London Special Publication* 179: 369-386.
- Oberhänsli, R., Bousquet, R., Engi, M., Goffé, B., Gosso, G., Handy, M.R., Höck, V., Koller, F., Lardeaux, J.M., Polino, R., Rossi, Ph., Schuster, R., Schwartz, S., Spalla, I., 2004. "Metamorphic structure of the Alps." *Commission for the Geological Map of the World, Paris, scale 1:1.000.000.*
- Oberli, F., Meier, M., Berger, A., Rosemberg, C.L., Gieré, R. 2004. "U-Th-Pb and ²³⁰Th-²³⁸U disequilibrium isotope systematics: precise accessory mineral chronology and melt evolution tracing in the Alpine Bergell intrusion." *Geochimica and Cosmochimica Acta* 68: 2543-2560.
- Ohnenstetter, M., Rossi P. 1985. "Découverte d'une paléochambre magmatique exceptionnelle dans le massif du Tenda, Corse hercynienne." *Comptes Rendus de Académie de Sciences Paris* 300: 853-858.
- Otsuki, M. and Banno, S. 1990. "Prograde and retrograde metamorphism of hematite-bearing basic schists in the Sambagawa belt in central Shikoku." *Journal of Metamorphic Geology* 8: 425-439.
- Padoa, E. 1999. "Les ophiolites du massif d'Inzecca (Corse alpine): lithostratigraphie, structure géologique et évolution géodynamique." *Géologie de France* 3: 37- 48.
- Padoa, E., Saccani, E., Durand-Delga, M. 2001. "Structural and geochemical data on the Rio Magno Unit: evidences for a new "Apenninic" ophiolitic unit in Alpine Corsica and its geodynamic implications." *Terra Nova* 13: 135-142.
- Pandolfi, L., Marroni, M., Malasoma, A. 2016. "Stratigraphic and structural features of the Bas-Ostriconi Unit (Corsica): paleogeographic implications." *Comptes Rendus de Geoscience* 348: 630-640.
- Paperini, M. 2004. "Rilevamento geologico e analisi strutturale delle unità tettoniche alpine nella bassa valle del Golo (Corsica Settentrionale)." Msc.

- Thesis. Università di Pisa.
- Paquette, J.L., Ménot, R.P., Pin, C., Orsini, J.B. 2003. "Episodic and short-lived granitic pulses in a post-collisional setting: evidence from precise U-Pb zircon dating through a crustal cross-section in Corsica." *Chemical Geology* 198: 1-20.
- Parra, T., Vidal, O., Agard, P. 2002a. "A thermodynamic model for Fe-Mg dioctahedral K white micas using data from phase-equilibrium experiments and natural pelitic assemblages." *Contributions to Mineralogy and Petrology* 143: 706-732
- Parra, T., Vidal, O., Jolivet, L. 2002b. "Relation between the intensity of deformation and retrogression in blueschists metapelites of Tinos Island (Greece) evidenced by chlorite-mica local equilibria." *Lithos* 63: 41-66.
- Passchier, C.W. 1982. "Mylonitic deformation in the Saint-Barthélemy Massif, French Prenees, with emphasis on the genetic relationship between ultramylonite and pseudotachylite." *GUA Paper Geology Sere 1* 16, 1-173.
- Passchier, C.W., Trouw, R.A.J. 2005. *Microtectonics*. Berlin, New York, Springer.
- Peguinot, G., Lardeaux, J.M., Caron, J.M. 1984. "Recrystallization d'éclogites de basse temperature dans le metabasalte corse." *Comptes Rendus de Académie de Sciences Paris (2)* 299: 871-874.
- Pèguinot, G., Potdevin, J.L. 1984. "Métamorphisme et tectonique dans les Schistes Lustrés à l'Est de Corte (Corse)." Ph.D. thesis. Université de Lyon.
- Peressini, G., Quick, J.E., Sinigoi, S., Hofmann, A.W., Fanning, M. 2007. "Duration of a large mafic intrusion and heat transfer in the lower crust: a SHRIMP U-Pb zircon study in the Ivrea-Verbano Zone (Western Alps, Italy)." *Jornal of Petrology* 48(6): 1185-1218.
- Philippot, P. 1990. "Opposite vergence of nappes and crustal extension in the French-Italian Western Alps." *Tectonics* 9(5): 1143-1164.
- Pinarelli, I., Boriani, A. 2007. "Tracing metamorphism, magmatism and tectonics in the southern Alps (Italy): constraints from Rb-Sr and Pb-Pb geochronology, and isotope geochemistry." *Periodico di Mineralogia* 76: 5-24.
- Platt, J.P. 1986. "Dynamics of orogenic wedges and the uplift of high-pressure metamorphic rocks." *GSA Bulletin* 97: 1037-1053.
- Platt, J.P. 1987. "The uplift of high pressure/low temperature metamorphic rocks." *Philosophical Transaction of the Royal Society of London (A)* 321: 87 - 103.
- Platt, J.P. 1993. "Exhumation of high-pressure rocks: a review of concepts and processes." *Terra Nova* 5: 119-133.
- Plunder, A., Agard, P., Chopin, C., Pourteau, A., Okay, A.I. 2015. "Accretion, undeplating and exhumation along subduction interface: from subduction initiation to continental subduction (Tavsanlı zone, W Turkey)." *Lithos* 226: 233-254.
- Principi, G., Treves, B. 1984. "Il sistema corso-appenninico come prisma d'accreszione. Riflessi sul problema generale del limite Alpi-Appennini." *Memorie della Società Geologica Italiana* 28: 49-576.

- Puccinelli, A., Perilli, N., Cascella, A. 2012. "Stratigraphy of the Caporalino-Sant'Angelo Unit: a face jurassic-Eocene succession of the Alpine Corsica." *Rivista Italiana di Paleontologia Stratigrafica* 118(3): 471-491.
- Quick, J., Sinigoi, S., Negrini, L., Demarchi, G., Mayer, A. 1992. "Synmagmatic deformation in the underplated igneous complex of the Ivrea-Verbano Zone, northern Italy". *US Geological survey*; Geologic investigations series Map 1-2776.
- Ramsay, J.G. 1967. *Folding and fracturing of rocks*. New York: McGraw-Hill.
- Ramsay, J.G., Huber, M.I. 1987. "The Techniques of Modern Structural Geology, Volume 2: Folds and Fractures." London, Orlando, San Diego, New York, Austin, Boston, Sydney, Tokyo, Toronto: Academic Press 11.
- Ratschbacher L., Frisch W., Neubauer F., Schmid S.M., Neugebauer R. 1989. "Extension in compressional orogenic belts: The Eastern Alps." *Geology* 17: 404-407.
- Ravna, E.J.K., Andersen, T.B., Jolivet, L., De Capitani, C. 2010. "Cold subduction and the formation of lawsonite-eclogite from prograde evolution of eclogitized pillow lava from Corsica." *Journal of Metamorphic Geology* 28: 381-395.
- Rebay, G., Spalla, M.I. 2001. "Emplacement at granulite facies conditions of the Sesia-Lanzo metagabbros: an early record of Permian rifting?" *Lithos* 58, 85-104.
- Reddy, S.M., Wheeler, J., Cliff, R.A. 1999. "The geometry and timing of orogenic extension: an example from the Western Italian Alps." *Journal of Metamorphic Geology* 17: 573-589.
- Reddy, S.M., Wheeler, J., Butler, R.H.W., Cliff, R.A., Freeman, S., Inger, S., Pickles, C., Kelley, S.P. 2003. "Kinematic reworking and exhumation within the convergent Alpine Orogen." *Tectonophysics* 365: 77-102.
- Rehault, J.P., Boillot, G., Mauffred, A. 1984. "The western Mediterranean Basin Geological Evolution." *Marine Geology* 55, 447-477.
- Renna, M.R., Tribuzio, R., Tiepolo, M. 2007. "Origin and timing of the post-Variscan gabbro-granite complex of Porto (Western Corsica)." *Contributions to Mineralogy and Petrology* 157: 813-835.
- Rey, P., Vanderhaeghe, O., Teyssier, C. 2001. "Gravitational collapse of the continental crust: definition, regimes and modes." *Tectonophysics*. 342: 435-449.
- Ricour, J. 1949. "Présence du calcaire à Gryphées du Monte di Tuda près de Saint-Florent." *Comptes Rendus de Académie de Sciences Paris*. 9: 171-172.
- Rieuf, M. 1980. Etude stratigraphique et structurale des unités au Nord-Est de Corte (Corse). Ph.D. thesis. Université de Toulouse.
- Roda, M., Zucali, M. 2008. "Meso and microstructural evolution of the Mont Marion metaintrusive complex (Dent Blanche nappe, Austroalpine domain, Valpelline, Western Italian Alps)." *Italian Journal of Geoscience* 127: 105-123.
- Rodriguez, G. 1981. "Etude géologique sw l'unité de la Cima Pedani (Corse)." Ph.D. thesis. Université de Toulouse.
- Rolland, Y., Lardeaux, J.M., Guillot, S., Nicollet, C. 2000. "Extension syn-convergence poinconnement vertical et unites métamorphiques contrastés en bordure Ouest du Grand Paradis (Alpes Franco-Italiennes)." *Geodinamica Acta* 13: 133-148.

- Roselle, G.T., Thuring, M., Engi, M. 2002. "MELONPIT: A finite element code for simulating tectonic mass movement and heat flow within subduction zones." *American Journal of Sciences* 302: 381-409.
- Rosenbaum, G., Lister, G. S. Duboz, C. 2002. "Relative motion of Africa, Iberia and Europe during Alpine orogeny." *Tectonophysics*. 359: 117 - 129.
- Rossetti, F., Glodny, J., Theye, T., Maggi, M. 2015. "Pressure temperature deformation- time of the ductile Alpine shearing in Corsica from orogenic construction to collapse." *Lithos* 218-219: 99-116.
- Rossi, P., Cocherie, A., Lahondère, D. 1992. "Relations entre les complexes mafiques-ultramafiques et le volcanisme andésitique stéphanoo-Permien de Corse Occidentale, témoins de phénomènes d'amincissement crustal néo-varisiques." *Comptes Rendus de Académie de Sciences Paris* 315: 1779-1788.
- Rossi, P., Durand-Delga, M., Caron, J.M., Guieu, G., Conchon, O., Libourel, G., Loye-Pilot, M. 1994. "Carte Géologique de la France (1/50,000), feuille Corte (1110)." *BRGM*, Orléans.
- Rossi, P., Durand-Delga, M., Lahondère, J.C., Baud, J.P., Egal, E., Lahondère, D., Laporte, D., Lluch, D., Loyle, M.D., Ohnenstetter, M., Palagi, P. 2001. "Carte Géologique de France (1/50000), feuille Santo Pietro di Tenda (1106)" *BRGM*, Orléans.
- Rossi, P., Cocherie, A., Lahondère, D., Fanning, C.M., 2002. "La marge européenne de la Téthys jurassique en Corse: datation de trondhjémites de Balagne et indices de croûte continentale sous le domaine Balano-Ligure. " *Comptes Rendus Geosciences* 334 : 313-322.
- Rossi, P. Cocherie, A., Fanning, C.M., Deloule, E. 2006. "Variscan to Eo-Alpine events recorded in European lower crust zircons sampled from the French Massif Central and Corsica, France. " *Lithos* 87: 235-260.
- Rossi, P., Oggiano, G. Cocherie, A. 2009. "A restored section of the "southern Variscan realm" the Corsica-Sardinia microcontinent. " *Comptes Rendus Geosciences* 341 : 224-238.
- Rossi, P., Cocherie, A., Fanning, M. 2015. "Evidence in Variscan Corsica of a brief and voluminous Late Carboniferous to Early Permian volcanic-plutonic event contemporaneous with a high-temperature/Low-pressure metamorphic peak in the lower crust. *Bulletin de la Société Géologique de France* 186(2-3): 171-192.
- Rubatto, D., Hermann, J. 2001. "Exhumation as fast as subduction? " *Geology* 29: 3-6.
- Rubatto, D., Hermann, J. 2007. "Zircon behaviour in deeply subducted rocks." *Elements* 3, 31-35.
- Saccani, E.; Padoa, E.; and Tassinari, R. 2000. "Preliminary data on the Pineto gabbroic massif and Nebbio basalts: progress toward the geochemical characterization of alpine Corsica ophiolites. " *Ophioliti* 25: 75-86.
- Sage, F., Beslier, M.O., Thinon, I., Larroque, C., Dessa, J-X., Migeon, S., Angelier, J., Guennoc, P., Schreiber, D., Michaud, F., Stephan, J.F., Sonnette, L. 2011. "Structure and evolution of a passive margin in a compressive environment: Example of the south-western Alps-Ligurian basin junction during the Cenozoic." *Marine and Petroleum Geology* 28: 1263-1282.

- Sagri, M., Aiello, E., Certini, L., 1982. "Le unità torbiditiche cretacee della Corsica." *Rendiconti della Società Geologica Italiana* 5: 87-91.
- Sanders, C.A., Bertotti, G., Tommasini, S., Davies, G.R., Wijbrans, R. 1996. "Triassic pegmatites in the Mesozoic middle crust of the Southern Alps (Italy): fluid implications, radiometric dating and tectonic implications." *Eclogae Geologicae Helveticae* 89: 505-525.
- Sanfilippo, A., Tribuzio, R. 2012. "Building of deepest crust at a fossil slow-spreading centre (Pineto gabbroic sequence, Alpine Jurassic ophiolites)." *Contributions to Mineralogy and Petrology* doi:10.1007/s00410-012-0831-8.
- Sartori, M. 1987. "Structure de la zone du Combin entre les Diablons et Zermatt." *Eclogae Geologicae Helveticae* 80:789-814.
- Sartori, R. 1990. "The main results of ODP leg 107 in the frame of Neogene to recent geology of peritethyan areas." In: Kastens, K.A. (eds.) *Proc. ODP, Scientific Results* 107.
- Savostin, L.A., Sibuet, J.C., Zonenshain, L.P., Le Pichon, X., Roulet, M.J. 1986. "Kinematic evolution of the Thetis belt from the Atlantic Ocean to the Pamirs since the Triassic." *Tectonophysics* 123: 1-35.
- Schaltegger, U., Brack, P. 2007. "Crustal scale magmatism systems during intracontinental strike-slip tectonics: U, Pb and Hf isotopic constraints for Permian magmatic rocks of the Southern Alps." *International Journal of Earth Sciences* 96: 1131-1151.
- Scheffer, C., Vanderhaeghe, O., Lanari, P., Tarantola, A., Ponthus, L., Photiades, A., France, L. 2016. "Syn- to post-orogenic exhumation of metamorphic nappes: structure and thermobarometry of the western Attic-Cycladic metamorphic complex (Lavrion, Greece)." *Journal of Geodynamics* 96: 174-193.
- Schlunegger, F., Willett, S. 1999. "Spatial and temporal variation in exhumation of the central Swiss Alps and implications for exhumation mechanism." In: Ring, U., et al. (eds.) *Exhumation processes: normal faulting, ductile flow and erosion. Geological Society of London Special Publication* 154: 157-179.
- Schmalholz, S.M., Medvedev, S., Lechmann, S.M., Podladchikov, Y. 2014. Relationship between tectonic overpressure, deviatoric stress, driving force, isostasy and gravitational potential energy. *Geophysical Journal* 197: 680-696.
- Schmid, S., Kissling, E. 2000. "The arc of the western Alps in the light of geophysical data on deep crustal structure." *Tectonics* 19: 62-85.
- Schmid, S.M., Pfiffner, O.A., Froitzheim, N., Schönborn, G., Kissling, E. 1996. "Geophysical-geological transect and tectonic evolution of the Swiss-Italian Alps." *Tectonics* 15(5): 1036-1064.
- Schmid, S.M., Kissling, E., Diehl, T., Douwe, J.J., van Hinsenberg, J.J., Molli, G. 2017. "Ivrea mantle wedge, arc of the Western Alps and kinematic evolution of the Alps-Appennines orogenic system." *Swiss Journal of Geoscience* 110: 581-612.
- Schuster, R., Frank, W. 1999. "Metamorphic evolution of the Austroalpine units east of the Tauern Window: indications for Jurassic strike slip tectonics." *Mitteilungen der Geologischen Gesellschaft* 42: 37-58.

- Schuster, R., Stüwe, K. 2008. "Permian metamorphic event in the Alps." *Geology* 36(8): 603-606.
- Schuster, R., Schabert, S., Abart, R., Frank, W. 2001. "Permo-Triassic extension and related HT/HP metamorphism in the Austroalpine-Southalpine realm." *Mitteilungen der Geologischen Gesellschaft* 45: 111-141.
- Sérrane, M. 1999. "The Gulf of Lion continental margin (NW Mediterranean) revisited by IBS: an overview." In: Durand, B., Jolivet, L., Horvath, F., Sérrane, M. (eds.) *Mediterranean Basins. Geological Society of London* 156: 15-36.
- Shelley, D. 1993. *Igneous and metamorphic rocks under the Microscope*. Chapman and Hall: London.
- Sibson, R.H. 1977. "Fault rocks and fault mechanisms." *Journal of the Geological Society of London* 133: 191-213.
- Sinclair, H.D. 1997. "Tectonostratigraphic model for underfilled peripheral foreland basins: an Alpine perspective." *GSA Bulletin* 109: 324-346.
- Sláma, J., Košler, J., Condon, D.J., Crowley, J.L., Gerdes, A., Hanchar, J.M., Horstwood, M.S.A., Morris, G.A., Basdala, L., Norberg, N., Schaltegger, U., Schoene, B., Tubrett, M.N., Whitehouse, M.J. 2008. "Plešovice zircon – A new natural reference material for U-Pb and Hf isotopic microanalysis." *Chemical Geology* 249: 1-35.
- Smith, H.A., Barreiro, B. 1990. "Monazite U-Pb dating of staurolite grade metamorphism in pelitic schists." *Contributions to Mineralogy and Petrology* 105: 602-615.
- Smye, A.J., Robertz, M.N.W., Condon, D.J., Horstwood, M.S.A., Parrish, R.R. 2014. "Characterising the U-Th-Pb systematics of allanite by ID and LA-ICP-MS: implications for geochronology." *Geochimica and Cosmochimica Acta* 135: 1-28.
- Spear, F.S., Selverstone, J., Hickmott, D., Crowley, P., Hodges, K.V. 1984. "P-T path from garnet zoning: a new technique for deciphering tectonic processes in crystalline terranes." *Geology* 12: 87-90.
- Spear, F.S. 1993. "The metamorphism of mafic rocks. In: Metamorphic phase Equilibria and Pressure-Temperature-Time paths." *Mineralogical Society of America*.
- Speranza, F. 1999. "Paleomagnetism and the Corsica-Sardinia rotation: a short review." *Bollettino della Società Geologica Italiana* 118: 537-543.
- Speranza, F., Villa, I.M., Sagnotti, L., Florindo, F., Cosentino, D., Cipollari, P., Mattei, M. 2002. "Age of the Corsica-Sardinia rotation and Liguro-Provençal Basin spreading: new paleomagnetic and Ar/Ar evidence." *Tectonophysics* 347: 231-251.
- Spry, A. 1969. *Metamorphic textures*. Oxford: Pergamon Press.
- Stacey, J.S., Kramers, J.D. 1975. "Approximation of terrestrial lead isotope evolution by a 2-stage model." *Earth and Planetary Science Letters* 26: 207-221.
- Stampfli, G.M., Mosar, J., Marquer, D., Marchant, R., Baudin, T., Borel, G. 1998. "Subduction and obduction processes in the Swiss Alps." *Tectonophysics* 296: 159-204.

- Stampfli, G.M., Borel, G.D. 2004. "The TRANSMED transect in space and time: constraints on the Paleotectonic evolution of the Mediterranean Domain." In: Cavazza W., Roure F., Spakman W., Stampfli G.M., Ziegler P.A. (eds.) *The TRANSMED atlas - The Mediterranean region from crust to mantle*. Berlin Heidelberg, *Springer*, 53-80.
- Staub, R. 1924. *Der Bau der Alpen*. Beitr. Geology. Karte. *Schweiz*: 46.
- Steck, A. 1984. "Structures de deformations tertiaires dans les Alpes centrales (transversal Aar-Simplon-Ossola)." *Eclogae Geologicae Helveticae* 77: 55-100.
- Steck, A., Epard, J.-L., Vannay, J.-C., Hunziker, J., Girard, M., Morard, A., Robyr, M. 1998. "Geological transect across the Tso Moriri and Spiti areas: The nappe structures of the Tethys Himalaya." *Eclogae Geologicae Helveticae* 91: 103-121.
- Stipp, M., Stünitz, H., Heilbronner, R., Schmid, S.M. 2002a. "The Eastern Tonale fault zone: a 'natural laboratory' for crystal plastic deformation of quartz over a temperature range of 250-700°C." *Journal of Structural Geology* 24: 1861-1884.
- Stipp, M., Stünitz, H., Heilbronner, R., Schmid, S.M. 2002b. "Dynamic recrystallization of quartz: correlation between natural and experimental conditions." In: De Meer, S., Drury M.R., De Bresser J.H.P. and Pennock G.M. (eds.) *Deformation Mechanisms, Rheology and Tectonics: Current Status and Future Perspectives*. *Geological Society of London* 200: 171-190.
- Strzeczynski, P., Guillot, S., Leloup, P.H., Arnaud, N., Vidal, O., Ledru, P., Corrioux, G., Darmendrail, X. 2012. "Tectono-metamorphic evolution of Briançonnais zone (Modane-Aussois and Southern Vanoise units, Lyon Turin transect, Western Alps)." *Journal of Geodynamics* 56-57: 55-75.
- Tapponier, P., Peltzer, G., Armijo, R. 1986. "On the mechanics of the collision between India and Asia." In: Coward, M.P., Ries, A.C. (eds.) *Collision tectonics*, *Geological Society of London Special Publication* 19: 115-157.
- Termier, P., Maury, E. 1928. "Nouvelles observations géologiques dans la Corse orientale." *Comptes Rendus de Académie de Sciences Paris* 186: 1077, 1168, 1247, 1324.
- Thompson, A.B., Schulmann, K., Jezek, J. 1997. "Thermal evolution and exhumation in obliquely convergent (transpressive) orogens." *Tectonophysics* 280: 171-184.
- Thöni, M., Miller, C. 2000. "Permo-Triassic pegmatites in the eo-Alpine eclogite-facies Koralpe complex, Austria: age and magma source constraints from mineral chemical, Sb-Rb and Sm-Nd isotope data." *Schweizerische Mineralogische und Petrographische Mitteilungen* 80(2): 169.
- Tomkins, H.S., Pattinson, D.R.M. 2007. "Accessory phase petrogenesis in relation to major phase assemblages in pelites from Nelson contact aureole, Southern British Columbia." *Journal of Metamorphic Geology* 25: 401-421.
- Tommasini, S., Poli, G., Halliday, A.N. 1995. "The role of sediment subduction and crustal growth in the Hercynian plutonism: isotopic and trace element evidence from the Sardinia-Corsica batholith." *Journal of Petrology* 36: 1305-1332.

- Tribuzio, R., Giacomini, F., 2002. "Blueschist facies metamorphism of peralkaline rhyolites from Tenda crystalline massif (northern Corsica): evidence for involvement in the Alpine subduction event?" *Journal of Metamorphic Geology* 20: 513-526.
- Tribuzio, R., Thirlwall, M.F., Messiga, B. 1999. "Petrology, mineral and isotope geochemistry of the Sondalo gabbroic complex (Central Alps, Northern Italy): implications for the origin of post-Variscan magmatism." *Contributions to Mineralogy and Petrology* 136: 48-62.
- Tribuzio, R., Renna, M.R., Braga, R., Dallai, L. 2009. "Petrogenesis of Early Permian olivine-bearing cumulate and associated basalt dykes from Bocca di Tenda (Northern Corsica): implications for post-collisional Variscan evolution." *Chemical Geology* 259: 190-203.
- Tricart, P. 1984. "From passive margin to continental collision – a tectonic scenario for the Western Alps." *American Journal of Sciences* 284: 97-120.
- Tricart, P., Sue, C. 2006. "Faulted backfold versus reactivated backthrust: the role of inherited structures during late extension in the frontal Piedmont nappes east of Pelvoux (Western Alps)." *International Journal of Earth Sciences* 95: 827-840.
- Trincardi, F., Zitellini, N. 1987. "The rifting of the Tyrreian Basin." *Geo-Marine Letters* 7: 1-6.
- Trommsdorff, V., Piccardo, G.B., Montrasio, A. 1993. "From magmatism through metamorphism to sea floor emplacement of subcontinental Adria lithosphere during pre-Alpine rifting (Malenco, Italy)." *Schweizerische Mineralogische und Petrographische Mitteilungen* 73: 191-203.
- Tropper, P., Harlov, D., Krenn, E., Finger, F., Thede, D., Bernhard, F. 2007. "Zr-bearing minerals as indicators for the polymetamorphic evolution of the eastern, lower Austroalpine nappes (Stubenberg granite contact aureole, Styria, Eastern Alps, Austria)." *Lithos* 95: 72-86.
- Ulianov, A., Müntener, O., Schaltegger, U., Bussy, F. 2012. "The data treatment dependent variability of U-Pb zircon ages obtained using mono-collector, sector field, laser ablation, ICPMS." *Journal of Analytical Atomic Spectrometry* 27(4): 663-676.
- Ussami, N., Shiraiwa, S., Landim Dominguez, J.M. 1999. "Basement reactivation in a sub-Andean foreland flexural bulge: the Pantanal wetland, SW Brazil." *Tectonics* 18(1): 25-39.
- van Der Voo, R. 1993. *Paleomagnetism of the Atlantic, Tethys, and Iapetus Oceans*. Cambridge University Press, Cambridge.
- Vavra, G., Gebauer, D., Schmid R., Compton, W. 1996. "Multiple zircon growth and recrystallization during polyphase Late Carboniferous to Triassic metamorphism in granulites of Ivrea zone (southern Alps): an ion microprobe (SCHRIMP) study." *Contributions to Mineralogy and Petrology* 122: 337-358.
- Vavra, G., Schmid, R., Gebauer, D. 1999. "Internal morphology, habit and U-Th-Pb microanalysis of amphibolite-to-granulite facies zircon: geochronology of the Ivrea Zone (Southern Alps)." *Contributions to Mineralogy and Petrology* 134(4): 380-404.

- Velde, B. 1965. "Phengitic micas: synthesis, stability and natural occurrence." *American Journal of Sciences* 263: 886-913.
- Vidal, O., Parra, T. 2000. "Exhumation paths of high-pressure metapelites obtained from local equilibria for chlorite–phengite assemblage." *Geological Journal* 35: 139–161.
- Vidal, O., Dubracq, B. 2009. "Thermodynamic modelling of clay dehydration, stability and compositional evolution with temperature, pressure and H₂O activity." *Geochimica and Cosmochimica Acta* 73: 6544-6564.
- Vidal, O., Parra, T., Trotet, F. 2001. "A thermodynamic model for Fe-Mg aluminous chlorite using data from phase equilibrium experiments and natural pelitic assemblages in the 100– 600 °C, 1–25 kbar P–T range." *American Journal of Sciences* 301: 557–592.
- Vidal, O., Parra, T., Vieillard, P. 2005. "Thermodynamic properties of the Tschermark solid solution in Fe-chlorite: Application to natural examples and possible role of oxidation." *American Mineralogist* 90: 347-358.
- Vidal, O., De Andrade, V., Lewin, E., Munoz, M., Parra, T., Pascarelli, S. 2006. "P–T-deformation-Fe²⁺/Fe³⁺ mapping at the thin section scale and comparison with XANES mapping: application to a garnet-bearing metapelite from the Sambagawa metamorphic belt (Japan)." *Journal of Metamorphic Geology* 24: 669-683.
- Vidal, O., Lanari, P., Munoz, M., Bourdelle, F., De Andrade, V. 2016. "Deciphering temperature, pressure and oxygen-activity conditions of chlorite formation." *Clay Minerals* 51: 615-633.
- Vigliotti, L., Kent, D.V. 1990. "Paleomagnetic results of Tertiary sediments from Corsica: Evidence of Post-Eocene rotation." *Physics of the Earth and Planetary Interiors* 62: 97-108.
- Vigliotti, L., Langenheim, V.E. 1995. "When did Sardinia stop rotating? New paleomagnetic results." *Terra Nova* 7: 424-435.
- Vitale Brovarone, A., Herwartz, D. 2013. "Timing of HP metamorphism in the Schistes Lustrés of Alpine Corsica: new Lu-Hf garnet and lawsonite ages." *Lithos* 172-173: 175–191.
- Vitale Brovarone, A., Beyssac, O., Malavieille, J., Molli, G., Beltrando, M., Compagnoni, R. 2012. "Stacking and metamorphism of continuous segments of subducted lithosphere in a high-pressure wedge: The example of Alpine Corsica (France)." *Earth Science Reviews*. 116: 35-56.
- Vitale Brovarone, A., Picatto, M., Beyssac, O., Lagabrielle, Y., Castelli, D. 2014. "The blueschist-eclogite transition in the Alpine chain: P-T paths and the role of slow-spreading extensional structures in the evolution of HP-LT mountain belts." *Tectonophysics* 615: 96–121.
- Wakabayashi J. 2004. "Tectonic mechanisms associated with P-T paths of regional metamorphism: alternatives to single-cycle thrusting and heating." *Tectonophysics* 392: 193-218.
- Warburton, J., 1986. "The ophiolite-bearing Schistes Lustrés nappe in Alpine Corsica: a model for the emplacement of ophiolites that have suffered HP/LT metamorphism." *GSA Bulletin Memoirs* 164: 313-331.
- Waters, C.N. 1990. "The Cenozoic tectonic evolution of Alpine Corsica." *Geological Society of London* 147: 811-824.

- Westphal, M., Orsini, J., Vellutini, J. 1976. "Le microcontinent corsarde, sa position initialw: données paléomagnétiques et raccord géologiques." *Tectonophysics* 30: 141-157.
- Wheeler, J., Butler, R.W.H. 1993. "Evidence for extension in the western Alpine orogen: the contact between the oceanic Piemonte and overlying continental Sesia units." *Earth and Planetary Science Letters* 117: 457-474.
- Wheeler, J., Butler, R.W.H. 1994. "Criteria for identifying structures related to true crustal extension in orogens." *Journal of Structural Geology* 16: 1023-1027.
- Wiederkehr, M., Bousquet, R., Schmid, S.M. Berger, A. 2008. "From subduction to collision: thermal overprint of HP/LT meta-sediments in the north-eastern Lepontine Dome (Swiss Alps) and consequences regarding the tectono-metamorphic evolution of the Alpine orogenic wedge." In: Froithzeim, N., Schmid, S.M. (eds.) *Orogenic processes in the Alpine collision zone: Swiss Journal of Geoscience* 101: S127-S155 (Supplement 1).
- Wiederkehr, M., Sudo, Bousquet, R., Schmid, S.M. Berger, A. 2009. "Alpine orogenic evolution from subduction to collisional thermal overprint: the 40Ar-39Ar age constraints from the Valaisan Ocean, Central Alps." *Tectonics* 28: 1-28.
- Wijbrans, J.R., van Wees, J.D., Stephenson, R.A. Cloetingh, S.A.P.L. 1993. "Pressure-temperature-time evolution of the high-pressure metamorphic complex of Sifnos, Greece." *Geology* 21: 443-446.
- Wing, B.A., Ferry, J.M., Harrison, T.M. 2003. "Prograde destruction and formation of monazite and allanite during contact and regional metamorphism of pelites. Petrology and geochronology." *Contributions to Mineralogy and Petrology* 145: 228-250.
- Winter, J.D. 2001. *An introduction to igneous and metamorphic petrology*. Prentice Hall: Upper Seddle River..
- Worley, B.; Powell, R.; and Wilson, C. 1997. "Crenulation cleavage formation: Evolving diffusion, deformation and equilibration mechanisms with increasing metamorphic grade." *Journal of Structural Geology* 19:" 1121-1135.
- Yu, H.S., Chou, Y.W. 2001. "Characteristics and development of the flexural forebulge and basal unconformity of WesternTaiwan Foreland Basin." *Tectonophysics* 333: 277-291.
- Zarki-Jakni B., Van Der Beek P., Poupeau G., Sosson M., Labrin E., Rossi P., Ferrandini J. 2004. "Cenozoic denudation of Corsica in response to Ligurian and Tyrrhenian extension: results from apatite fission track thermochronology." *Tectonics* 23: TC1003, DOI: 10.1029/ 2003TC001535.
- Zibra I., Kruhl, J.H., Braga, R. 2010. "Late Paleozoic deformation in post-Variscan lower crust: shear zone widening due to strain localization during retrograde shearing." *International Journal of Earth Sciences* 99: 973-991.
- Zibra, I. 2006. "Late-Hercynian granitoid plutons emplaced along a deep crstal shear zone. A case study from the Santa Lucia Nappe (Alpine Corsica, France)." Ph.D. thesis. Università di Pisa.

PREMIO TESI DI DOTTORATO

TITOLI PUBBLICATI

ANNO 2007

Bracardi M., *La Materia e lo Spirito. Mario Ridolfi nel paesaggio umbro*

Coppi E., *Purines as Transmitter Molecules. Electrophysiological Studies on Purinergic Signalling in Different Cell Systems*

Mannini M., *Molecular Magnetic Materials on Solid Surfaces*

Natali I., *The Ur-Portrait. Stephen Hero ed il processo di creazione artistica in A Portrait of the Artist as a Young Man*

Petretto L., *Imprenditore ed Università nello start-up di impresa. Ruoli e relazioni critiche*

ANNO 2008

Bemporad F., *Folding and Aggregation Studies in the Acylphosphatase-Like Family*

Buono A., *Esercito, istituzioni, territorio. Alloggiamenti militari e «case Herme» nello Stato di Milano (secoli XVI e XVII)*

Castenasi S., *La finanza di progetto tra interesse pubblico e interessi privati*

Colica G., *Use of Microorganisms in the Removal of Pollutants from the Wastewater*

Gabbiani C., *Proteins as Possible Targets for Antitumor Metal Complexes: Biophysical Studies of their Interactions*

ANNO 2009

Decorosi F., *Studio di ceppi batterici per il biorisanamento di suoli contaminati da Cr(VI)*

Di Carlo P., *I Kalasha del Hindu Kush: ricerche linguistiche e antropologiche*

Di Patti F., *Finite-Size Effects in Stochastic Models of Population Dynamics: Applications to Biomedicine and Biology*

Inzitari M., *Determinants of Mobility Disability in Older Adults: Evidence from Population-Based Epidemiologic Studies*

Macri F., *Verso un nuovo diritto penale sessuale. Diritto vivente, diritto comparato e prospettive di riforma della disciplina dei reati sessuali in Italia*

Pace R., *Identità e diritti delle donne. Per una cittadinanza di genere nella formazione*

Vignolini S., *Sub-Wavelength Probing and Modification of Complex Photonic Structures*

ANNO 2010

Fedi M., *«Tuo lumine». L'accademia dei Risvegliati e lo spettacolo a Pistoia tra Sei e Settecento*

Fondi M., *Bioinformatics of genome evolution: from ancestral to modern metabolism. Phylogenomics and comparative genomics to understand microbial evolution*

Marino E., *An Integrated Nonlinear Wind-Waves Model for Offshore Wind Turbines*

Orsi V., *Crisi e Rigenerazione nella valle dell'Alto Khabur (Siria). La produzione ceramica nel passaggio dal Bronzo Antico al Bronzo Medio*

Polito C., *Molecular imaging in Parkinson's disease*

Romano R., *Smart Skin Envelope. Integrazione architettonica di tecnologie dinamiche e innovative per il risparmio energetico*

ANNO 2011

Acciaoli S., *Il trompe-l'œil letterario, ovvero il sorriso ironico nell'opera di Wilhelm Hauff*

Bernacchioni C., *Sfingolipidi bioattivi e loro ruolo nell'azione biologica di fattori di crescita e citochine*

Fabrizi N., *Bragg spectroscopy of quantum gases: Exploring physics in one dimension*

Gordillo Hervás R., *La construcción religiosa de la Hélade imperial: El Panhelenion*

Mugelli C., *Indipendenza e professionalità del giudice in Cina*
Pollastri S., *Il ruolo di TAF12B e UVR3 nel ciclo circadiano dei vegetali*
Salizzoni E., *Paesaggi Protetti. Laboratori di sperimentazione per il paesaggio costiero euro-mediterraneo*

ANNO 2012

Evangelisti E., *Structural and functional aspects of membranes: the involvement of lipid rafts in Alzheimer's disease pathogenesis. The interplay between protein oligomers and plasma membrane physicochemical features in determining cytotoxicity*
Bondi D., *Filosofia e storiografia nel dibattito anglo-americano sulla svolta linguistica*
Petrucci F., *Petri Candidi Decembrii Epistolarum iuvenilium libri octo. A cura di Federico Petrucci*
Alberti M., *La 'scoperta' dei disoccupati. Alle origini dell'indagine statistica sulla disoccupazione nell'Italia liberale (1893-1915)*
Galdani R., *Using the Patch-Clamp technique to shed light on ion channels structure, function and pharmacology*
Adessi A., *Hydrogen production using Purple Non-Sulfur Bacteria (PNSB) cultivated under natural or artificial light conditions with synthetic or fermentation derived substrates*
Ramalli A., *Development of novel ultrasound techniques for imaging and elastography. From simulation to real-time implementation*

ANNO 2013

Lunghi C., *Early cross-modal interactions and adult human visual cortical plasticity revealed by binocular rivalry*
Brancaleoni I., *Architettura e illuminismo: filosofia e progetti di città nel tardo Settecento francese*
Cucinotta E., *Produzione poetica e storia nella prassi e nella teoria greca di età classica*
Pellegrini L., *Circostanze del reato: trasformazioni in atto e prospettive di riforma*
Locatelli M., *Mid infrared digital holography and terahertz imaging*
Muniz Miranda F., *Modelling of spectroscopic and structural properties using molecular dynamics*
Bacci M., *Dinamica molecolare e modelli al continuo per il trasporto di molecole proteiche - Coarse-grained molecular dynamics and continuum models for the transport of protein molecules*
Martelli R., *Characteristics of raw and cooked filets in species of actual and potential interest for Italian aquaculture: rainbow trout (*Oncorhynchus mykiss*) and meagre (*Argyrosomus regius*)*

ANNO 2014

Lana D., *A study on cholinergic signal transduction pathways involved in short term and long term memory formation in the rat hippocampus. Molecular and cellular alterations underlying memory impairments in animal models of neurodegeneration*
Lopez Garcia A., *Los Auditoria de Roma y el Athenaeum de Adriano*
Pastorelli G., *L'immagine del cane in Franz Kafka*
Bussoletti A., *L'età berlusconiana. Il centro-destra dai poli alla Casa della Libertà 1994-2001*
Malavolti L., *Single molecule magnets sublimated on conducting and magnetic substrates*
Belingardi C., *Comunanze urbane. Autogestione e cura dei luoghi*
Guzzo E., *Il tempio nel tempio. Il tombeau di Rousseau al Panthéon di Parigi*

ANNO 2015

Lombardi N., *MEREFaPS: uno Studio di Farmacovigilanza Attiva e Farmacoepidemiologia in Pronto Soccorso*
Baratta L., *«A Marvellous and Strange Event». Racconti di nascite mostruose nell'Inghilterra della prima età moderna*

Richichi I.A., *La teocrazia: crisi e trasformazione di un modello politico nell'Europa del XVIII secolo*
Palandri L., *I giudici e l'arte. Stati Uniti ed Europa a confronto*
Caselli N., *Imaging and engineering optical localized modes at the nano scale*
Calabrese G., *Study and design of topologies and components for high power density dc-dc converters*
Porzilli S., *Rilevare l'architettura in legno. Protocolli metodologici per la documentazione delle architetture tradizionali lignee: i casi studio dei villaggi careliani in Russia*

ANNO 2016

Martinelli S., *Study of intracellular signaling pathways in Chronic Myeloproliferative Neoplasms*
Abbado E., *“La celeste guida”. L'oratorio musicale a Firenze: 1632-1799*
Focarile P., *I Mannelli di Firenze. Storia mecenatismo e identità di una famiglia fra cultura mercantile e cultura cortigiana*
Nucciotti A., *La dimensione normativa dell'imprenditorialità accademica. Tre casi di studio sugli investigatori principali, i loro gruppi di ricerca e i fattori di innesco dell'imprenditorialità accademica*
Peruzzi P., *La inutilizzabilità della prestazione*
Lottini E., *Magnetic Nanostructures: a promising approach towards RE-free permanent magnets*
Uricchio T., *Image Understanding by Socializing the Semantic Gap*

ANNO 2017

Valenti R., *Cerebral Small Vessel Disease and Cerebral Amyloid Angiopathy: neuroimaging markers, cognitive features and rehabilitative issues*
Starnini M., *L'uomo tutto intero. Biografia di Carlo Livi, psichiatra dell'Ottocento*
Verardi D., *La scienza e i segreti della natura a Napoli nel Rinascimento: la magia naturale di Giovan Battista Della Porta*
Minicucci G., *Il dolo nella bancarotta. Alla ricerca della tipicità soggettiva della fattispecie patrimoniale*
Pattelli L., *Imaging light transport at the femtosecond scale: a walk on the wild side of diffusion*
Egea Molines M.T., *Etnobotánica en el Alto Valle del Reno (Toscana y Emilia-Romaña, Italia). Etnobotanica nell'Alta Valle del Reno (Toscana ed Emilia-Romagna, Italia)*
Romano I.M., *Pressione turistica sul Centro Storico di Firenze - sito UNESCO. Un modello per la valutazione dell'impatto percettivo*

ANNO 2018

Costa A., *Histaminergic neurotransmission as a gateway for the effects of the fat sensing molecule Oleoylethanolamide. Focus on cognition and stress-reactivity*
Solera D., *«Sotto l'ombra della patente del Santo Ufficio». I familiares dell'Inquisizione romana tra XVI e XVII secolo*
Landi G., *Secession and Referendum. A new Dimension of International Law on Territorial Changes?*
Sacchetti A., *La costituente libertaria di Camillo Berneri. Un disegno politico tra federalismo e anarchismo*
Livi L.F., *New quantum simulations with ultracold Ytterbium gases*
Bellini E., *Ambienti sensoriali “terapeutici” che rendono Abili. Un progetto integrato di vita per persone con Disturbi dello Spettro Autistico*
Piscitelli L.R., *Serviceability and post-failure behaviour of laminated glass structural elements*

ANNO 2019

Molinaro A., *New insights into creatine transporter deficiency. Identification of neuropathological and metabolic targets for treatment*

Romano M., *Soldati e neuropsichiatria nell'Italia della Grande Guerra. Controllo militare e pratiche assistenziali a confronto (1915-1918)*

Venturi M.T., «Io vivo fra le cose e invento, come posso, il modo di nominarle». Pier Paolo Pasolini e la lingua della modernità

Rossi F., *Apparenza del diritto e rapporti di fatto nell'esperienza giuridica di Roma antica*

Turrini L., *Development of optical methods for real-time whole-brain functional imaging of zebrafish neuronal activity*

Moschetti V., *Camere Azzurre. Costruzione di un'antologia mediterranea. Da Palladio a Peter Märkli*

Talluri L., *Micro turbo expander design for small scale ORC. Tesla turbine*

ANNO 2020

De Vita D., *Functional validation of genetic variants identified by next generation sequencing in malformations of cortical development*

Al Owaidi R., *La letteratura cavalleresca e il mondo arabo: il caso di Andrea da Barberino. Regesto e studio critico*

Galante A., *Legalità e mutamenti giurisprudenziali nel diritto penale. Fondamento e limiti del divieto di retroattività dei mutamenti giurisprudenziali sfavorevoli*

Colzi L., *Isotopic fractionation study towards massive star-forming regions across the Galaxy*

Di Rosa M., *Tectono-metamorphic evolution of the continental units along the edge between Alpine and Hercynian Corsica. Constraints for the exhumation models in the continental collision setting*

Miccinesi L., *Advanced Ground-Based Real and Synthetic Aperture Radar*

Ricci C., *Santa Maria degli Angeli: un monastero camaldolese "dimenticato" nel centro di Firenze. Analisi del percorso storico-architettonico in età moderna e contemporanea*

Premio Tesi Dottorato

Firenze University Press - Università degli Studi di Firenze

2020

Tectono-metamorphic evolution of the continental units along the edge between Alpine and Hercynian Corsica

In this work the central area of Corsica island was studied in order to reconstruct the tectono-metamorphic history of the continental and oceanic high pressure units that occupy the structurally deeper levels of the tectonic stacking of Alpine Corsica and their stratigraphic and structural relationship with the European margin (Hercynian Corsica). The study includes the geological mapping, the meso-scale and microscale structural analysis, the acquisition of chemical analyzes and micromaps with the microprobe, thermobarometric estimation through specific methodologies for metapelites, U-Th-Pb dating of zircons and allanites. The results obtained allows to reconstruct the geodynamic model of this sector of the Alpine belt from the Permian to the Burdigalian.

MARIA DI ROSA graduated in Pisa in Geological Sciences and Technologies (2015) in structural geology. She specializes in thermobarometry in Grenoble and at the École Normale Supérieure in Paris and in geochronology in Geneva. She obtains a Ph.D. in Earth Sciences at the University of Firenze (2019).

ISSN 2612-8039 (print)
ISSN 2612-8020 (online)
ISBN 978-88-5518-419-9 (Print)
ISBN 978-88-5518-420-5 (PDF)
ISBN 978-88-5518-421-2 (XML)
DOI 10.36253/978-88-5518-420-5

www.fupress.com